

**ORIGIN AND OBDUCTION OF THE OPHIOLITIC REDFERN COMPLEX
ON THE OMINECA-INTERMONTANE BELTS BOUNDARY,
WESTERN CARIBOO MOUNTAINS, BRITISH COLUMBIA**

by

JUDITH KATHERINE RADLOFF

B.Sc., B.A., University of California, Santa Cruz

**A THESIS SUBMITTED IN PARTIAL FULFILMENT OF
THE REQUIREMENTS FOR THE DEGREE OF
MASTER OF SCIENCE**

in

THE FACULTY OF GRADUATE STUDIES

Department of Geological Sciences

We accept this thesis as conforming
to the required standard

THE UNIVERSITY OF BRITISH COLUMBIA

April, 1989

©Judith K. Radloff, 1989

In presenting this thesis in partial fulfilment of the requirements for an advanced degree at the University of British Columbia, I agree that the Library shall make it freely available for reference and study. I further agree that permission for extensive copying of this thesis for scholarly purposes may be granted by the Head of my Department or by his or her representatives. It is understood that copying or publication of this thesis for financial gain shall not be allowed without my written permission.

DEPARTMENT OF GEOLOGICAL SCIENCES

The University of British Columbia

2075 Wesbrook Place

Vancouver, Canada

V6T 1W5

Date: APRIL, 1989

ABSTRACT

The Redfern Complex is a klippe of a dismembered, metamorphosed ophiolite resting on top of the crystalline Snowshoe Group in east-central British Columbia. The Snowshoe Group belongs to the Barkerville terrane of the Omineca Crystalline Belt while the Redfern Complex, which is structurally overlain by the Triassic black phyllite, comprises the basement to Quesnel terrane rocks of the Intermontane Belt. The contiguous boundary between the two belts lies west of the Redfern Complex and is marked by the Crooked Amphibolite, a thin, highly sheared mafic amphibolite with blocks of ultramafic rock near its base.

The Redfern Complex and Crooked Amphibolite are correlative assemblages evidenced by similarities in lithology, whole rock and mineral chemistry, and structural position. Both assemblages are composed of variable amounts of hornblende-epidote-plagioclase amphibolite, dunites, cumulate layered peridotite, and serpentinite. Chemically the rocks are subalkaline, tholeiitic basalts or gabbros and depleted peridotite with relict forsteritic olivine (Fo_{83} and $\text{Fo}_{87-90.7}$), chromian diopside, and chromite spinel. Ultramafic rocks from both assemblages show evidence of plastic deformation under mantle conditions including dislocation glide on the high temperature (010):[100] slip system and glide climb in olivine, plus dynamic recrystallization and dynamic recovery. Although the structural succession of lithologies is best defined at the locality of the Redfern Complex, variably complete structural successions across the Crooked Amphibolite were observed which indicate that the two units occupy the same structural position on top of the Hadrynian to Paleozoic metasedimentary Snowshoe Group and that both units are structurally overlain by the Triassic black phyllite. The two assemblages differ in intensity of metamorphism and degree of hydration alteration related to their relative structural positions and their size and permeability. While the Crooked Amphibolite bears the chlorite-zone assemblage actinolite + chlorite + plagioclase and related ultramafic rocks are dominantly completely serpentinized, the Redfern amphibolite metamorphic assemblage of hornblende + albite + epidote belongs to the albite-epidote amphibolite facies. In addition the large, coherent Redfern peridotite body shows evidence of complete serpentinization only at its margins and also bears an amphibolite facies assemblage of tremolite + olivine

+ chlorite + talc. Thus the Redfern Complex experienced more intense metamorphism because it occupied a deeper structural level than the Crooked Amphibolite.

The local and regional setting of the Redfern Complex reflects a complex geologic history of multiple deformation episodes and syn-tectonic, locally intense metamorphism related to the emplacement of the Complex onto the Snowshoe Group along the east-vergent Redfern thrust. Prior to emplacement, the Snowshoe Group underwent one enigmatic phase of deformation and metamorphism. The intrusion of the felsic Redfern orthogneiss which has a poorly constrained U-Pb age of Devonian-Mississippian may be related to this deformation. A second orthogneiss which intrudes the Redfern amphibolite and contains ultramafic xenoliths probably intruded during or soon after emplacement. Tight, east-vergent folds and a pervasive second foliation developed in the Snowshoe Group while tight folds and a pervasive foliation developed in the Redfern amphibolite and Triassic black phyllite during emplacement. Microfracturing and grain sliding predominantly on the margins of the Redfern peridotite are the only structures developed during emplacement. Metamorphism peaked after emplacement stresses had relaxed, producing sillimanite in the Snowshoe metapelites, albite-epidote amphibolite assemblages in mafic lithologies, and possibly only kyanite in the black phyllites. Post-emplacement deformation accompanied sustained but decreased temperatures of metamorphism. Large-scale, west-vergent, overturned to the east buckles fold the Redfern thrust and refold earlier structures and produced the current map patterns and distribution of foliation. Kinked metamorphic porphyroblasts and an S_2 crenulation cleavage overgrown by staurolite in the Triassic black phyllite indicate that intense deformation and fluid enhanced retrograde metamorphic reactions were localised in a structurally lower "pocket" of this unit in the core of a post-emplacement synform on the east side of the map area.

TABLE OF CONTENTS

ABSTRACT	ii
LIST OF FIGURES	vii
LIST OF TABLES	ix
ACKNOWLEDGEMENTS	x
1. INTRODUCTION	1
1.1. Location	1
1.2. Previous work	4
1.3. Purpose of this study	6
2. STRATIGRAPHY	7
2.1. Introduction	7
2.2. Unit 1: Snowshoe Group	7
2.1.1. Pelitic Schist and Quartzite	9
<i>Pelitic Schist</i>	9
<i>Micaceous Quartzite</i>	10
2.1.2. Amphibolites	10
2.1.3. Marble Marker Layer	12
2.1.4. Trondhjemite Pegmatite	14
2.3. Redfern Gneiss	14
2.4. Redfern Complex	17
2.4.1. Unit 3A: Tectonized Dunite	18
2.4.2. Unit 3B: Layered Cumulates	19
2.4.3. Unit 3C: Ultramafic-mafic mixed subunit	20
2.4.4. Unit 4: Redfern Amphibolite	23
2.5. Crooked Amphibolite and Antler Formation	27
2.5.1. Crooked Amphibolite	28
<i>Crooked Lake Sites</i>	28
<i>Wolverine Lake Sites</i>	28
<i>MacKay River Sites</i>	30
<i>Bassett Creek Site</i>	30
2.5.2. Antler Formation	30
2.6. Triassic Black Phyllite	31
2.5.1. Unit 5A: Black phyllitic limestone	31
2.5.2. Unit 5B: Staurolite schist	31
2.7. Summary and Discussion	33
3. STRUCTURE	36
3.1. Introduction	36
3.2. Lower Plate: the Snowshoe Group	36
<i>Phase 1</i>	37
<i>Phase 2</i>	37
<i>Phase 3</i>	40
<i>Phase 4</i>	42
3.3. The Redfern Gneiss	44
3.4. Upper Plate: the Redfern Complex	46
3.4.1. Redfern Peridotite	48
<i>Mesosopic structures</i>	48
<i>Microscopic structures</i>	48
<i>Textures</i>	51
<i>Deformed Cumulate</i>	51
<i>Protogramular</i>	52

<i>Porphyroclastic</i>	53
<i>Mosaic</i>	53
<i>Application to the Redfern Peridotite</i>	57
3.4.2. Redfern Amphibolite and Triassic Black Phyllite	61
<i>Phase 1</i>	62
<i>Phase 2</i>	65
<i>Phase 3</i>	68
3.5. Discussion	68
4. METAMORPHISM	74
4.1. Introduction	74
4.2. Lower Plate: the Snowshoe Group	74
<i>Garnet</i>	75
<i>Staurolite</i>	75
<i>Kyanite</i>	78
<i>Sillimanite</i>	78
<i>Conditions of Metamorphism</i>	79
4.3. Redfern Gneiss	80
<i>Metamorphism and Timing to Deformation</i>	82
4.4. Upper Plate: the Redfern Complex	83
4.4.1. Redfern Peridotite	84
<i>Unit 3A: Tectonized Dunites</i>	85
<i>Unit 3B: Layered Cumulates</i>	87
<i>Metamorphism</i>	89
4.4.2. Contact Zones of Unit 3	91
4.4.3. Unit 4: Redfern Amphibolite	92
4.4.4. Triassic Black Phyllite	99
<i>Staurolite</i>	99
<i>Garnet</i>	99
<i>Kyanite</i>	103
<i>Summary</i>	103
4.4.5. Crooked Amphibolite	104
<i>Ultramafic Rocks</i>	105
<i>Amphibolite Rocks</i>	106
<i>Metamorphism</i>	107
4.5. Discussion	108
<i>Summary of Lower Plate Metamorphism</i>	108
<i>Summary of Upper Plate Metamorphism</i>	111
<i>Thermal History of the Redfern Complex</i>	112
5. GEOCHEMISTRY	114
5.1. Introduction	114
5.2. Major and Trace Element Geochemistry	116
5.2.1. XRF Analysis	116
5.2.2. Chemical Character	117
<i>Mafic Rocks</i>	117
<i>Ultramafic Rocks</i>	119
5.2.3. Tectonic Diagrams	119
5.2.4. Conclusions	123
<i>Effects of Alteration</i>	123
<i>Discussion</i>	125
5.3. Ultramafic Mineral Chemistry	126
5.3.1. Olivine	126
5.3.2. Pyroxene	128

5.3.3. Spinel	128
5.4. Pyroxene Thermobarometry	130
5.4.1. Theoretical Basis for the Thermobarometer	131
5.4.2. Results	132
5.4.3. Conclusions	134
5.5. Summary	135
6. DISCUSSION AND CONCLUSIONS	136
6.1. Introduction	136
6.2. Discussion	136
6.2.1. Summary of Stratigraphy and Chemistry	136
6.2.2. Structural and Metamorphic Synthesis	137
<i>Pre-emplacement</i>	137
<i>Emplacement</i>	138
<i>Post-emplacement</i>	139
6.2.3. The Redfern Complex as an Ophiolite	140
6.2.4. Tectonic Models	142
6.3 Conclusions	147
7. REFERENCES CITED	148
8. APPENDICES	154

LIST OF FIGURES

1.1.	Geologic map of the Dunford Lake area	(plate)
1.2.	Structural cross section	(plate)
1.3.	Five tectonic belts of the Canadian Cordillera	2
1.4.	General geology of the Quesnel Lake region	3
2.1.	Structural succession of lithologies	8
2.2.	Snowshoe Group, micaceous quartzite.	11
2.3.	Snowshoe Group, mafic amphibolite	12
2.4.	Snowshoe Group, marble marker unit	13
2.5.	Pegmatite cutting Snowshoe Group	15
2.6.	Gradational contact between Snowshoe Group and Redfern Gneiss	16
2.7.	Xenolith in the Redfern Gneiss	17
2.8.	Talc-serpentine vein in unit 3A	19
2.9.	Cumulate layering in unit 3B	21
2.10.	Mixed ultramafic-mafic subunit	22
2.11.	Gneissic layering in the Redfern amphibolite	24
2.12.	Metagabbro in Unit 4	24
2.13.	mullion outcrop style of lineated amphibolite	25
2.14.	Crooked Amphibolite	29
2.15.	Staurolite schist, Triassic Black phyllite	32
3.1.	Isoclinal F_1 in Snowshoe micaceous quartzite	38
3.2.	D_2 folds in Snowshoe	39
3.3.	Stereoplot of S_0/S_1 , S_2 and L_2 in the Snowshoe Group	41
3.4.	D_3 folds in Snowshoe	42
3.5.	Stereoplot of D_3 and D_4 structures in Snowshoe	43
3.6.	D_4 crenulations in Snowshoe pelitic schist	44
3.7.	Stereoplot for structures in the Redfern Gneiss	45
3.8.	Concordia diagram of U-Pb zircon age for the Redfern Gneiss	47
3.9.	Stereoplot for structures in the Redfern peridotite	49
3.10.	Photomicrograph of deformed cumulate texture	52
3.11.	Photomicrograph of protogranular texture	54
3.12.	Photomicrograph of porphyroclastic texture	55
3.13.	Photomicrograph of mosaic texture	56
3.14.	Summary of peridotite textures with conditions of formation	58
3.15.	Olivine deformation map.	59
3.16.	Peridotite microtextures in the structural succession	60
3.17.	D_1 fold in the Redfern amphibolite	62
3.18.	Photomicrograph of mylonites in the Redfern amphibolite	64
3.19.	Intrafolial D_1 folds in staurolite schist	65
3.20.	Cusate-lobate D_2 folds in Triassic black phyllite limestone	66
3.21.	Stereoplot of Redfern amphibolite and Triassic black phyllite	67
3.22.	Photomicrograph of S_2 crenulation cleavage in Triassic black phyllite	69
3.23.	Map of formlines showing trace of S_0/S_1 & S_2 (lower plate) and S_1 (upper plate)	70
3.24.	Diagrammatic unfolding of the Redfern thrust	72
4.1.	Map of regional metamorphic isograds	76
4.2.	Garnet in the Snowshoe	77
4.3.	Staurolite in the Snowshoe	77
4.4.	Kyanite and sillimanite in the Snowshoe	78
4.5.	Photomicrograph of the gneissosity in the Redfern Gneiss	81
4.6.	Poikilitic hornblende porphyroblasts, Redfern Gneiss	83
4.7.	Talc + chlorite replacing olivine	86
4.8.	Chlorite + magnetite replacing chromite	86

4.9.	Symplectic textured spinel inclusions in diopside	88
4.10.	Tremolite replacing diopside	90
4.11.	Metamorphic olivine	90
4.12.	Randomly oriented hornblende in the Redfern Amphibolite	93
4.13.	Hornblende in the Redfern amphibolite	94
4.14.	Garnet in the Redfern amphibolite	97
4.15.	Staurolite inclusions in the Triassic black phyllite	100
4.16.	Garnet cores replaced by chlorite, rims with folded inclusion trails, Triassic black phyllite	102
4.17.	Kinked kyanite, Triassic black phyllite	104
4.18.	Thin section negative of serpentinite from the Crooked Amphibolite	106
4.19.	Bathozones and AFM diagrams for pelitic lithologies	110
5.1.	Geochemical sample location map	115
5.2.	Oxide variation plot of major and minor oxides	120
5.3.	Total Alkalis versus silica	121
5.4.	Alkali-FM diagram	121
5.5.	Al ₂ O ₃ -FM diagram and TiO ₂ -P ₂ O ₅ -MnO diagram	122
5.6.	Variation in forsterite content of olivine with stratigraphy in the Redfern peridotite.	127
5.7.	Pyroxene quadrilateral for Redfern peridotite diopsides	129
5.8.	Cr number versus Mg number in chromites	130
6.1.	Tectonic model for evolution of the Redfern Complex	145

LIST OF TABLES

I.	Lithologic subtypes, mineralogy and textures, Redfern Amphibolite	26
II.	Summary of metamorphic grade for each map unit	109
III.	Percent LOI and percent alteration	124
IV.	Results from pyroxene thermobarometry	133
V.	Major and trace element analyses, ultramafics	154
VI.	Major and trace element analyses, amphibolites	158
VII.	Olivine compositions	164
VIII.	Spinel compositions	172
IX.	Pyroxene compositions	174
X.	Microprobe standards	180

ACKNOWLEDGEMENTS

Field and laboratory expenses were provided for by NSERC grant 5-82134 to Dr. John V. Ross who also provided the topic for this thesis, invaluable assistance in understanding ultramafic rocks, and continued inspiration. I would also like to thank Drs. J. Kelly Russell, William Barnes, and especially Hugh Greenwood for advice and multiple reviews of thesis drafts.

Technical advice and assistance were greatly appreciated from Stanya Horsky, Kelly Russell, Peter Michael, Maggy Piranian, Yvonne Douma, Gord Hodge, Fariyal Pirani, and John Knight.

Brilliant discussions on Cariboo geology were always forthcoming and appreciated from Steve Garwin, Peter Lewis, Jeff Fillipone, Dave McMullin, Don Murphy, and Mary Anne Bloodgood. Bruce James was always a cheerful source of computer wisdom.

Special thanks for their hospitality to Stuart and Joyce Maitlin of Forest Grove, B.C. and to Susan Taite for field assistance. Special thanks for the ongoing support and spiritual rejuvenation provided by Dean Wilson and the Vancouver Disc Sports Society.

1. INTRODUCTION

The Canadian Cordillera may be divided into five distinctive tectonic belts (see Fig. 1.3) which arrived at their present configuration during Mid-Jurassic to Mid-Cretaceous time (Monger and Price, 1979). The five belts are composed of numerous tectonostratigraphic terranes with allochthonous terranes comprising three western belts and paraautochthonous terranes comprising two eastern belts. The boundary between the cratonic Omineca Crystalline Belt (OMB) and the island arc-related Intermontane Belt (IMB) is well-exposed in the region around Crooked and Quesnel Lakes, east-central British Columbia, and represents the easternmost contact of accreted allochthonous terranes with the pre-Mesozoic North American craton. Hadrynian through Early-Paleozoic metasedimentary rocks and orthogneisses of the Snowshoe Group, Barkerville terrane (OMB) deposited on the trailing margin of the craton are structurally overlain by Permian(?) through Lower-Jurassic metaigneous and marine metasedimentary rocks of the Quesnellia and Slide Mountain terranes, Intermontane Belt. The study area straddles the OMB-IMB boundary south of Crooked Lake where it comprises a remnant thrust klippe east of the main boundary. The area is underlain by a structural succession of Snowshoe Group rocks overlain by a dismembered ophiolite sequence and Upper Triassic metasedimentary rocks of the Triassic black phyllite (Bloodgood, 1987a & b).

1.1 LOCATION

The Dunford Lake map area (Fig. 1.4) is 100 km due east of Williams Lake, British Columbia and is located within NTS map sheet 93A/1. Access to a dirt logging road at the base of the map area is from a well-maintained gravel logging road originating from 100 Mile House on the Cariboo Highway via Canim Lake. From the north, the same local logging road can be reached out of the town of Horsefly along an all-season road via Crooked Lake. From No-Name Lakes on Deception Creek an outfitter's pack trail traverses the map area and continues north toward Mica Mountain. Access to the main map area for the 1987 field season was by helicopter out of Williams Lake and for the 1988 season was by foot along the pack trail.

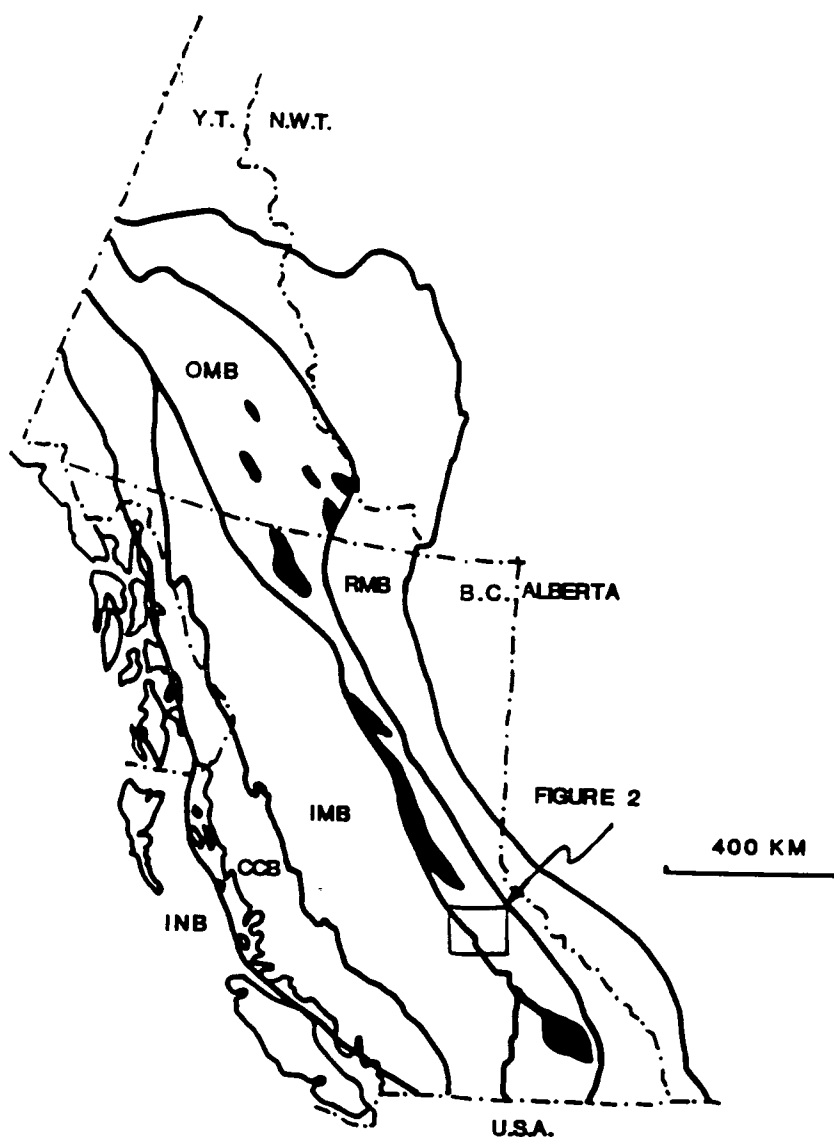


Figure 1.3: Five tectonic belts of the Canadian Cordillera. RMB = Rocky Mountain Belt, OMB = Omineca Belt, IMB = Intermontane Belt, CCB = Coast Crystalline Belt, INB = Insular Belt; Slide Mountain Terrane highlighted in black.

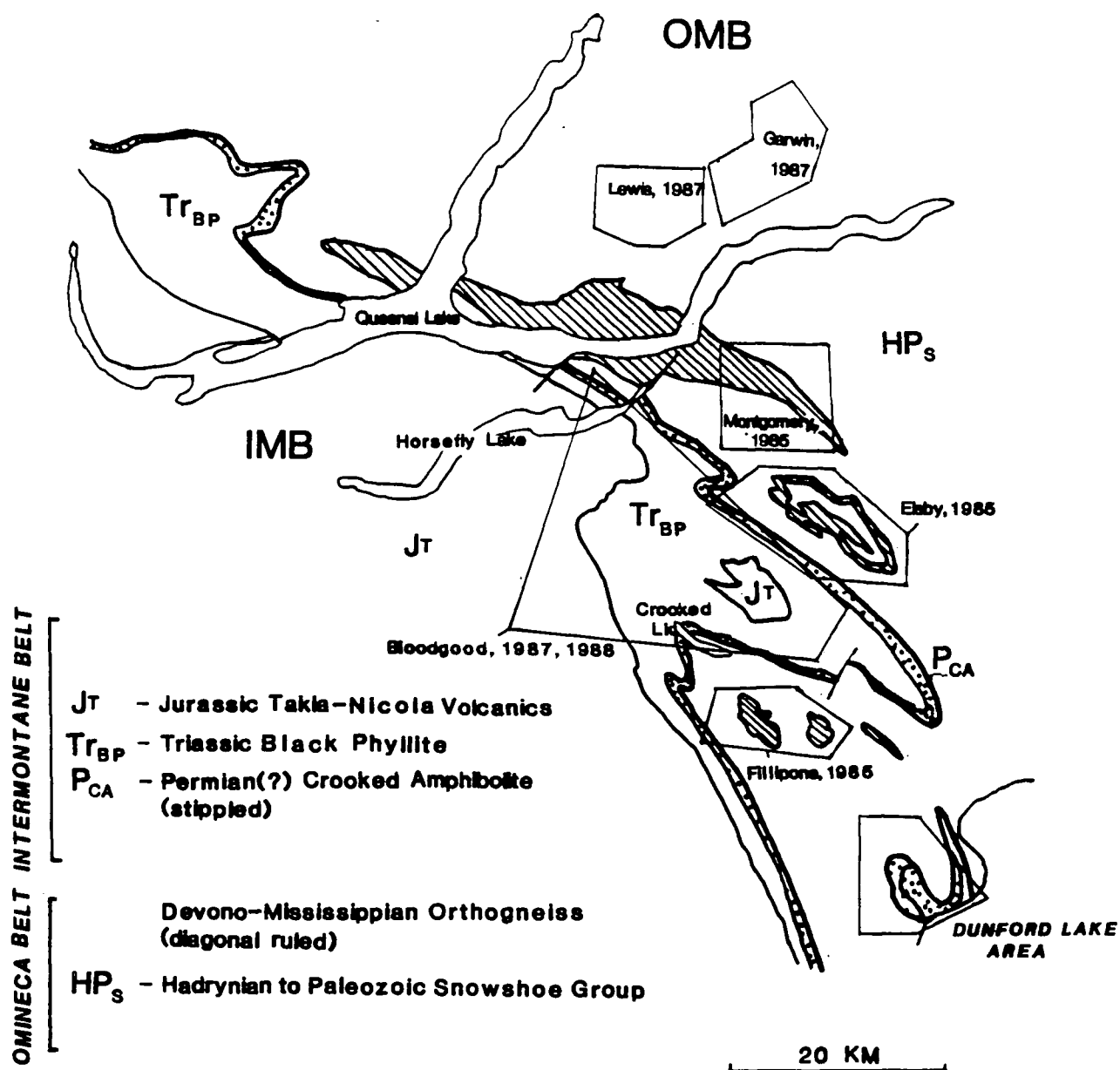


Figure 1.4: Generalized regional geology of the Quesnel Lake area. Other study areas and authors which are frequently referenced in the text are shown.

Exposure in the study area depends upon the physiography which consists of a high, sub-alpine plateau of moderate relief with steep, densely vegetated slopes and intervening low areas containing shallow, marshy lakes and swamps. Exposure in the swamps and meadows is poor and most of the rocks are rounded boulders, probably glacial erratics rather than bedrock outcrop. Exposure on the peaks, however, is excellent and on the slopes and in streamcuts varies from poor to excellent.

Additional areas in the Quesnel Lake region (NTS 93A) were mapped on a reconnaissance level and sampled for laboratory study. Targeted outcrops were the mafic Crooked Amphibolite and large pods of peridotite within the Crooked Amphibolite (for locations, see Figure 5.1).

Mapping of the Dunford Lake region at a scale of 1:15,840 and sample collection from three other sites was done between late June and late August, 1987. This work was supplemented by two additional weeks in July, 1988.

1.2 PREVIOUS WORK

The area was first mapped by R.B. Campbell as part of a regional study mapping central B.C. who found a large ultramafic-mafic body south of the Crooked Lake area (Campbell, 1963). In 1971, K.V. Campbell completed a detailed study of the Crooked Lake area including petrography and bulk rock geochemistry of the Antler Formation of the Slide Mountain Group to the north, the Fennell Formation to the south, and the mafic amphibolite of the Crooked Lake area which he also called Antler Formation (Campbell, 1971). He also mapped several large, elliptical ultramafic bodies within the Snowshoe Formation near its upper tectonic contact with the Antler Formation. In 1978, the Quesnel Lake map sheet was published as an Open File (O.F. 574, Campbell 1978) and included the work of both R.B. and K.V. Campbell. The large ultramafic-mafic complex south of Crooked Lake was named the Redfern Complex and assigned to the Omineca Belt (Campbell, 1978). In that year Montgomery also completed a master's thesis project studying the Redfern Complex which he informally named the Black Riders Complex, and the area the Dunford Lake area (Montgomery, 1978).

Since 1978, the amount and detail of work in the region has intensified with studies aimed at better documenting the stratigraphy and structure of rocks on both sides of the IMB-OMB boundary in order to

better understand the evolution of this suture. Struik of the Geological Survey of Canada, has mapped from Spanish Lake northward at a scale of 1:50,000 refining the stratigraphy of the Snowshoe Group. He also named the amphibolite unit of the Crooked Lake area which Campbell (1978) called Antler Formation the Crooked Amphibolite, including all occurrences of ultramafic rock and serpentinite. Struik (1988a) now equates it with the Slide Mountain Group (Struik, 1985; 1988a). South of the study area, Schiarizza and Preto (1987) mapped the Adams Plateau-Clearwater-Vavenby area and analysed both the Antler Formation equivalent Mississippian Fennell Formation and the Eagle Bay Formation of the Kootenay Terrane for major and trace elements.

Numerous thesis projects have complemented this regional work with detail on the stratigraphy structure, and metamorphism of rocks across the IMB-OMB boundary (see Fig. 1.3). In the OMB, studies by Engi (1984), Montgomery (1985), Getsinger (1985), Garwin (1987), Lewis (1987), and McMullin and Greenwood (1988) have delineated detailed stratigraphy, four phases of folding, and conditions of metamorphism in Snowshoe Group rocks. Studies by Bloodgood (1987a & b; 1988) have focussed on the stratigraphy and delineation of three fold phases in Triassic and Lower Jurassic rocks of the Triassic black phyllite (IMB). Studies which straddle the boundary by Carye (1986), Elsby (1985), Fillipone (1985), and Rees (1987) have illuminated the variation in structural succession and style along and across the boundary.

Current interpretation of the Quesnel Lake region involves Jurassic convergence normal to a west-dipping subduction zone. The IMB, is a composite of already amalgamated terranes including Quesnel and Slide Mountain terranes (Terrane I of Monger and Price, 1979), was thrust eastward over the OMB, burying Snowshoe Group rocks to depths sufficient for intense ductile deformation (Ross et al., 1985). Amphibolite grade metamorphism in the Snowshoe Group, which varies with time and space, peaked as this deformation event was waning. Lower sections of IMB rocks also experienced amphibolite grade metamorphism and the rocks directly on the contact were extensively mylonitized (Ross et al., 1985).

Tectonic models depicting the evolution of the entire Canadian and Alaskan Cordillera cite paleomagnetic evidence of northward paleolatitudinal shifts and Tethyan faunas in the Cache Creek Terrane, also part of "Terrane I", to support large scale, right-lateral translation accompanying the Mesozoic terrane accretion (Monger and Price, 1979). However, kinematic analysis of structures along the

IMB-OMB suture zone do not indicate a large component of lateral translation related to oblique subduction. Any large scale translation must have been taken up away from the suture or have taken place prior to accretion and evidence was obscured by later, convergence-related deformation (May and Butler, 1986).

1.3 PURPOSE OF THIS STUDY

The detailed study by Montgomery (1978) included many excellent observations and descriptions of the map units and their field relations. However, his subsequent lab analysis, particularly of the ultramafic rocks, was cursory and generalized. His descriptions indicate that the ultramafic rocks were sufficiently fresh to be studied in detail and deduce their original chemistry, igneous mineralogy and texture. Ideally, the temperature, pressure and depth of equilibration could also be determined, as has been done for many alpine ophiolite suites (for example, see Mercier et al., 1987).

The primary purpose of this study is to characterise, as fully and quantitatively as possible, the rocks of the Redfern Complex and observe the structural geometry of the complex itself and with respect to the surrounding Snowshoe Group. The second purpose is to compare chemically these rocks to the Crooked Amphibolite and similar, less deformed and lower grade rocks of the Antler and Fennell Formations in order to aid correlation attempts between the units. Finally, the evolution and deformational history of the complex is reinterpreted in the light of much new and detailed work completed in the immediate vicinity since Montgomery's work was completed in 1978.

2. STRATIGRAPHY

2.1 INTRODUCTION

Rocks exposed in the map area may be separated into three fault-bounded stratigraphic assemblages (see Fig. 2.1). From bottom to top, the assemblages are:

1. Hadrynian to Paleozoic (?) metasedimentary rocks of the Snowshoe Group, Barkerville terrane (Struik, 1987);
2. Ultramafic tectonites and cumulates and metamorphosed mafic volcanics of the Redfern Complex, (Slide Mountain or) Quesnel Terrane (Campbell, 1978);
3. Triassic metasedimentary rocks of the Triassic Black Phyllite, Quesnel Terrane (Bloodgood, 1987; McMullin and Greenwood, 1988).

A granitic orthogneiss intrudes assemblages 1 and 2 in the map area.

Primary igneous and sedimentary structures have been partly to completely obscured by amphibolite grade metamorphism and polyphase deformation. Present thicknesses reflect both thickening and thinning by structural processes such as folding, faulting, and cleavage formation. The map pattern and distribution of different lithologies is controlled by their position in the structural succession rather than a true stratigraphic sequence (see Figure 2.1).

The Redfern Complex and overlying Triassic Black Phyllite are believed to be a klippe (Montgomery, 1978) of the Crooked Amphibolite, the contiguous unit which traces the Omineca-Intermontane Belts boundary (Struik, 1987). The Crooked Amphibolite was examined in three locations in order to compare and contrast it with the Redfern Complex. In addition, the Antler Formation of the Slide Mountain Group was examined at one locality for comparison with published descriptions of the Antler Formation itself and with its tentative equivalents, the Crooked Amphibolite and the Redfern Complex.

2.2 UNIT 1: SNOWSHOE GROUP

There are four different lithologies in the Snowshoe Group in the Dunford Lake area: micaceous quartzite, staurolite-kyanite-garnet-quartz-mica schist, hornblende-quartz-plagioclase gneiss, and coarse grained marble. The two former rock types comprise the bulk of the group in the region with the latter two

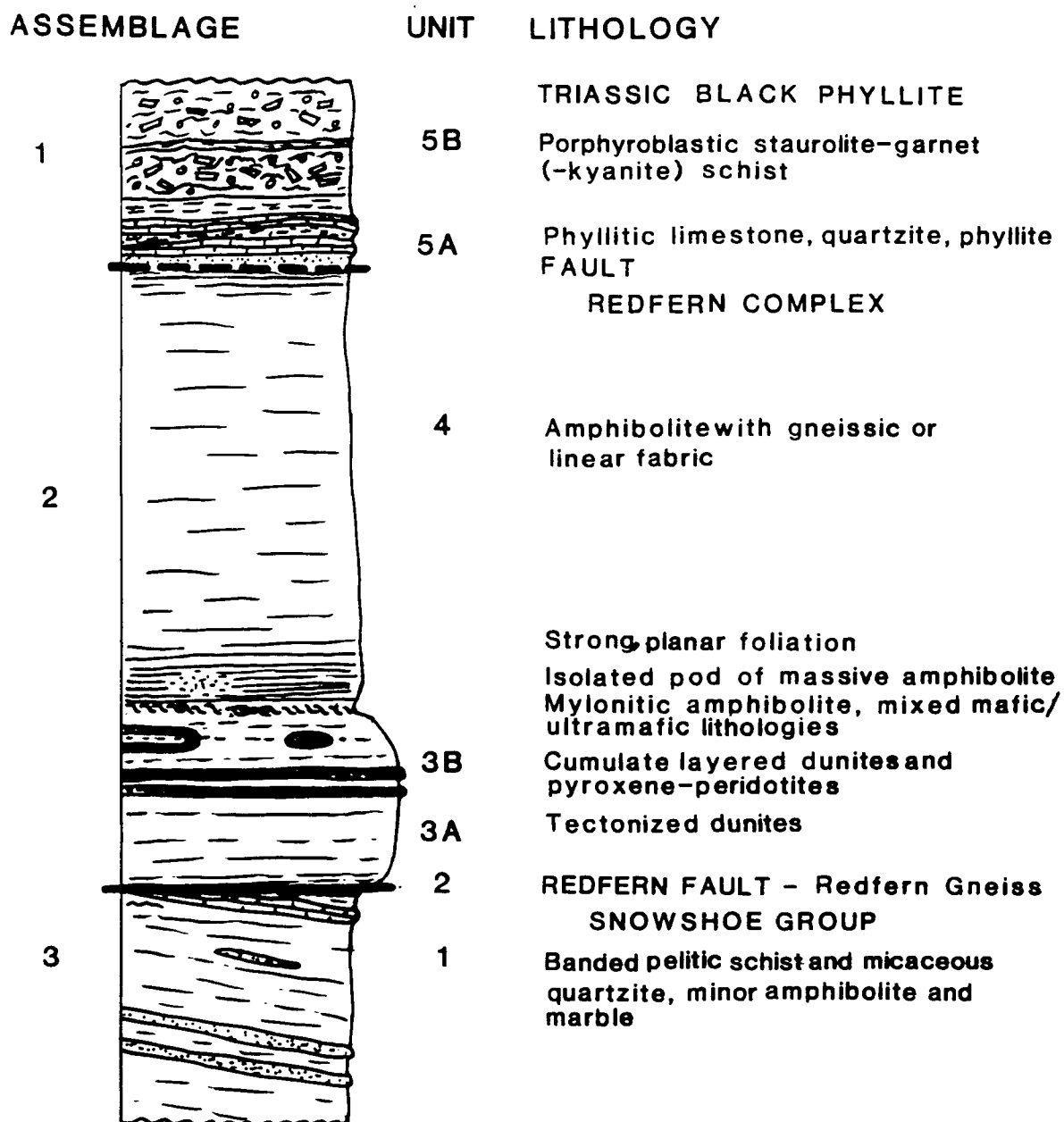


Figure 2.1: Structural succession of lithologies in the Dunford Lake Region. Not to scale but thickness of Redfern Complex is approximately relative to the true thickness.

occurring as minor yet distinctive irregular interlayers. In addition, trondhjemite pegmatites locally intrude the Snowshoe Group.

Quality of outcrop ranges from excellent on Orpheus Mountain (peak 6910') to good, poor or non-existent around Dunford Lake. Outcrops frequently are completely covered with moss or grey and brown lichen. Best exposures can be found where the root ball of a newly fallen tree has left the rock clean. Outcrops are elongate parallel to the prominent, usually planar, ubiquitous foliation. Bluish-grey, grey, and buff colored quartzite layers weather resistantly while the interlayered mica schists weather recessively. Veins of vitreous quartz with rectangular or tabular crystals also weather prominently. Large garnet and staurolite porphyroblasts protrude from the homogeneous micaceous matrix which erodes preferentially.

Montgomery (1978) called the rocks Kaza Group and separated them into two packages on the basis of metamorphic grade. He also described a marker sequence approximately 25 m thick consisting of a siliciclastic sequence and a distinctive marble marker unit. The type locality for the marker sequence is a small knoll dubbed "Marble Knob" by Montgomery. He traced the marker unit around the map area where it is offset by several faults (see Montgomery, 1978, Fig. 1). Montgomery's high-grade Kaza units are assigned here to the Triassic (see below).

2.2.1 Pelitic Schist and Quartzite

Pelitic Schist

This is the most abundant rock type observed within the Snowshoe Group. It consists of 20% to 80% muscovite and biotite with the remainder comprising quartz, plagioclase, and porphyroblasts of red garnet, staurolite, kyanite, and sillimanite. Micas are generally medium- to fine-grained elongate blades with muscovite at least twice as abundant as biotite. Quartz and minor plagioclase occur in four habits: 1) as small, evenly distributed grains and groups of grains separated by anastomosing mica layers, 2) as lenticular agglomerations 3 to 20 centimeters in length with about 2:1 length/width aspect ratios, 3) planar cross-cutting layers up to several grains wide composed of vitreous, tabular quartz, and 4) planar interlayers one to several grains wide consisting of tabular quartz and plagioclase, separated by planar mica layers.

The third habit constitutes veins formed by a hydraulic fracture mechanism early in the metamorphic and deformational history; the second habit may consist of rootless isoclinal fold hinges of veins (Fig. 2.2; c.f. Fillipone, 1985). Garnet porphyroblasts form euhedral dodecahedra, deep ruby red in color and up to 10 mm in diameter, although most are less than 5 mm. Staurolite porphyroblasts are dark brown to black with yellow streaks, and form small (< 2-5 mm) euhedral prisms that in rare instances reach 15 mm lengths with double crystal terminations. Kyanite occurs as very small crystals which may be confused with sillimanite and as blue blades up to 1 cm long. Sillimanite identification in the field was based upon the occurrence of small, needle-like crystals with vitreous luster and a purplish-pink sheen which may indicate the presence of fibrolite.

Micaceous quartzite occurs where the mica component of the schists diminishes and quartz becomes the dominant phase.

Micaceous Quartzite

This unit is made up of more than 80% quartz that occurs as thin to thick (5-50 cm) interlayers between pelitic schist layers. Individual layers weather out preferentially and are grey to bluish-grey on both fresh and weathered surfaces. Quartz is fine grained and tabular with fine biotite and muscovite flakes homogeneously distributed throughout the layers, aligned parallel to the long axes of quartz and the foliation. Small (< 5 mm), red euhedral garnets are dispersed throughout the matrix. No other porphyroblasts were observed. Lenses and stringers of coarse-grained transparent quartz, identical to the veins observed in the pelitic schists, are also common.

2.2.2 Amphibolites

Amphibolites occur as a minor rock type in rare, discontinuous interlayers. An exceptionally thick unit crops out on a cliff below the north slope of Orpheus Mountain where it is continuous for more than 100 m. The rocks comprise laminated and foliated gneisses of alternating mafic and felsic layers, from a few mm to several cm thick. Mafic layers are composed of up to 30% fine-grained green-black hornblende, biotite, red garnet, minor quartz, and plagioclase (Fig. 2.3). One layer about 25 cm thick

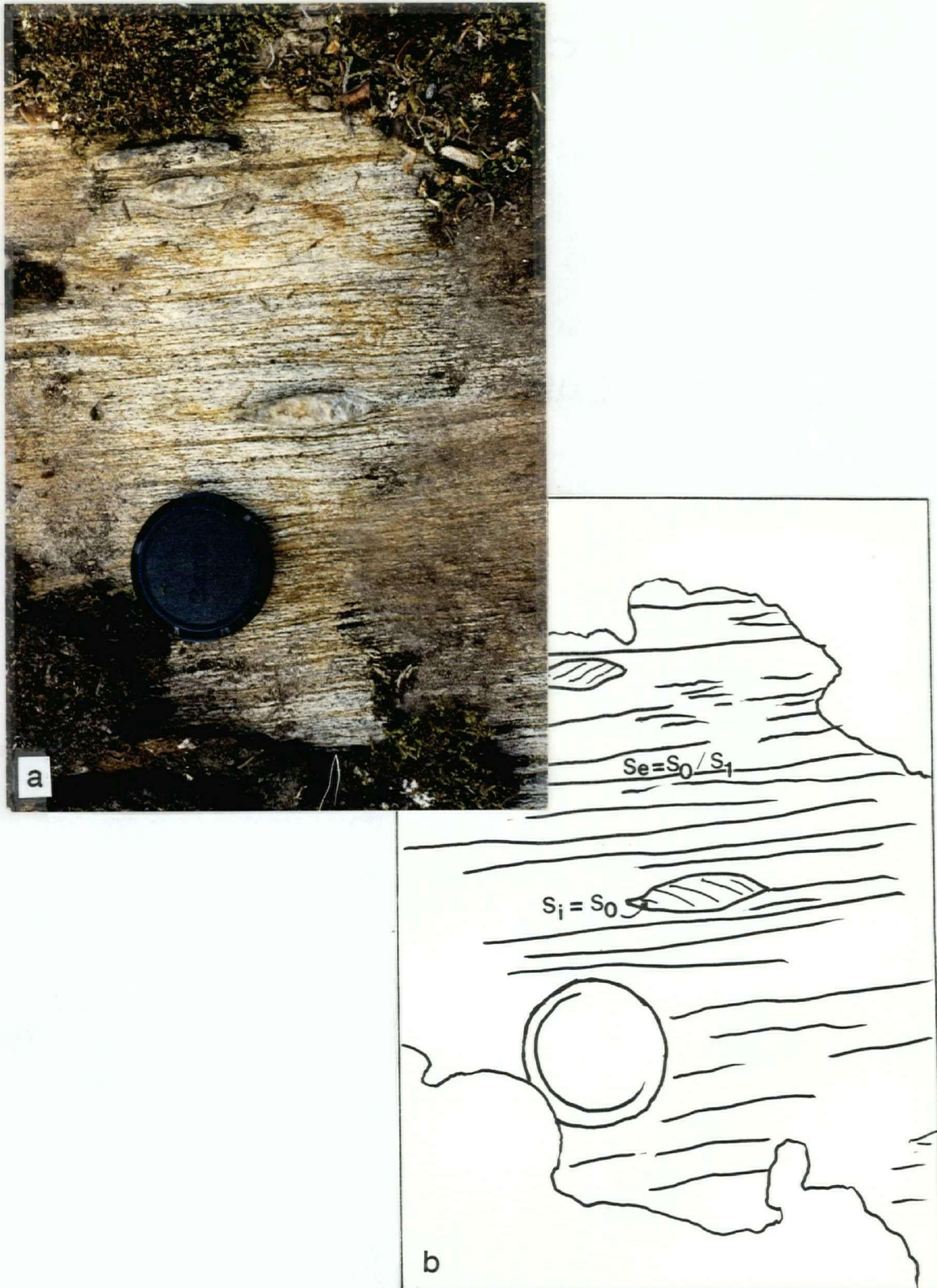


Figure 2.2: Snowshoe micaceous quartzite. a) Photograph of quartz vein lenses; b) sketch highlighting angular relationship between internal foliation (S_i) and external foliation (S_e) of quartz lenses, showing that the lenses are rootless fold hinges.



Figure 2.3: Interlayered hornblende amphibolite and micaceous quartzite in the Snowshoe Group.

composed of mostly garnet was observed. Felsic layers consist of fine-grained quartz and plagioclase. The marker unit on Orpheus Mtn. locally contains pyrite and/or chalcopyrite.

2.2.3 Marble Marker layer

An impure marble unit composed of several individual carbonate layers crops out in the western part of the map area. The best exposure occurs on "Marble Knob" where the unit is also at its thickest (Fig. 2.4). Calcite crystals are medium to coarse-grained and equant, yet still show a preferred orientation. Small, dark green equant minerals occur throughout the matrix and also as small agglomerations. Tremolite was not observed in hand specimen. Lenses and stringers of coarse crystalline quartz, similar to the veins in the quartzites and mica schists, lie within and parallel to the compositional layering.



Figure 2.4: Marble marker unit in Snowshoe Group, from location on "Marble knob."

The sequence on Marble Knob consists of 2 or 3 layers, 10-15 cm thick at the base of the carbonate unit (Fig. 2.4). This is overlain by 40-50 cm of thin (few mm to 3 cm) marble interlayered with mica schist laminae followed by several 15 cm thick layers. The sequence is capped by a similar sequence of interlayered marble and mica schist, with schist laminae up to 1 cm thick and less frequent between thicker marble layers. Alternating thin quartzites and mica schists comprise the remaining 20 m of the section, above which the Redfern Gneiss and the ultramafic unit are in fault contact.

The marble layer is most important since it is the only unique and distinctive lithology in the Dunford Lake region which can be used to outline transposed Snowshoe Group stratigraphy (see Fig. 1.1). The unit thins and becomes coarser grained towards the south before being covered by vegetation. Along strike to the north the unit is covered near Marble Knob but when projected along the same trend it would be truncated by the contact with the overlying ultramafics. A similar thin marble unit reappears from below the ultramafic contact just east of Dunford Lake. Additional exposures of marble in stream cuts can

be reasonably connected on the basis of structural trend (see Fig. 1.1) to form a continuous unit which traces out transposed Snowshoe stratigraphy.

Attempts were made to follow Montgomery's (1978) map trace of the marker unit but it was not found in his locations anywhere north of Marble Knob. One area where Montgomery shows it being offset by a fault has virtually no exposure and no marble was seen. Montgomery describes a fairly thick section of quartzites which he used to trace the unit northward away from Marble Knob. Since quartzites are variably abundant throughout the field area, the marble layers are the only truly distinctive feature of the marker unit and, thus the trace by Montgomery (1978) of the marker unit is herein considered to be incorrect north of Marble Knob.

2.2.4 Trondhjemite Pegmatite

Extremely coarse-grained quartz-plagioclase-K-feldspar-muscovite-tourmaline pegmatites intrude the Snowshoe Group variably throughout the field area. Quartz is white, K-feldspar is perthitic, plagioclase shows albite twinning, muscovite occurs in 10-20 cm diameter books and agglomerations, and tourmaline occur as black or pink euhedral prisms. Pegmatites are larger and more abundant in the cores of folds where they crosscut the S_0/S_1 foliation (Fig. 2.5).

The contact of the Snowshoe Group with the overlying Redfern Complex is never exposed and is discontinuously intruded by the Redfern Gneiss.

2.3 UNIT 2: REDFERN GNEISS

The Redfern Gneiss is a felsic orthogneiss whose occurrence is almost wholly restricted to the contact between the Snowshoe Group and the overlying Redfern Complex. The unit was informally named the Deucalion Gneiss by Montgomery (1978). It will here be renamed the Redfern Gneiss after Ruth Redfern Creek to the east and following the naming convention of Campbell (1978) since its occurrence seems to be related to the Redfern Complex.

The Redfern Gneiss weathers into very light grey, bouldery outcrops elongate parallel to its well-developed foliation. The gneiss consists of medium- to fine-grained quartz, plagioclase, potassium feldspar,

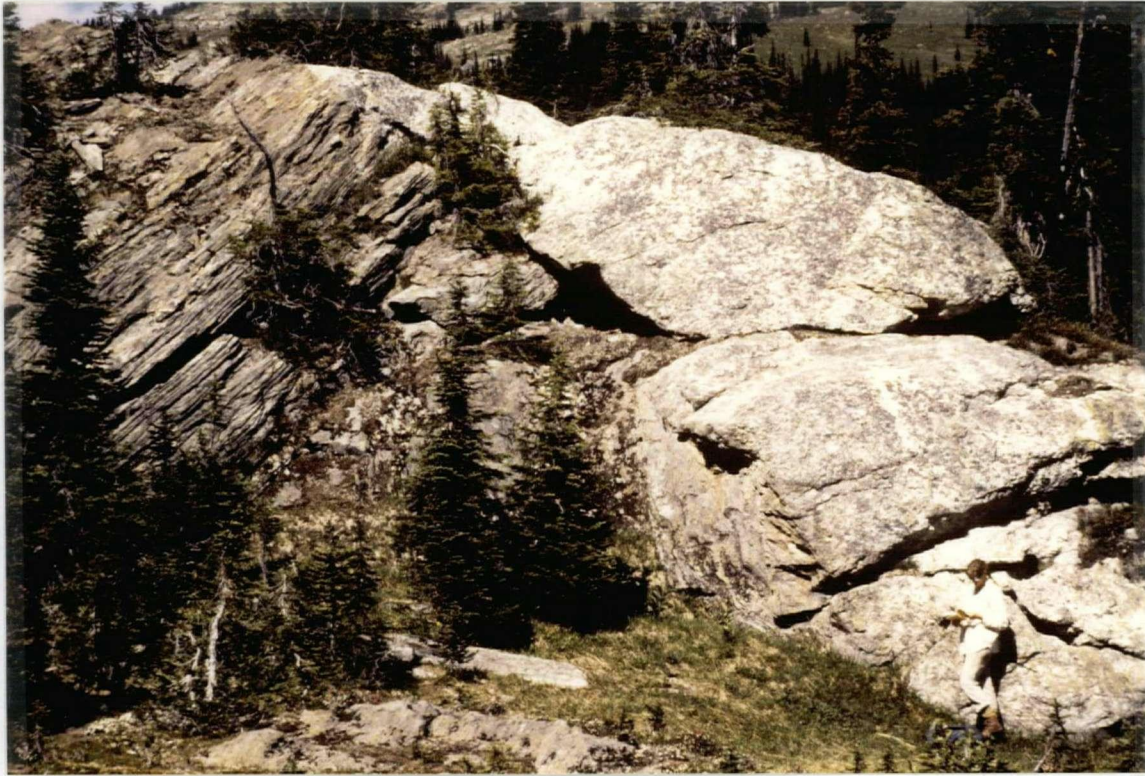


Figure 2.5: Trondjhemite pegmatite intruding Snowshoe Group in the core of a mesoscopic fold, cross-cutting S_0/S_1 at a high angle.

and biotite. All of the specimens examined are granodiorites to quartz monzonites, based on approximate modal analyses of rock slabs stained for feldspars with cobaltinitrate. Thickness of the unit varies from a few metres to about 25 m. In addition to biotite, muscovite and minor chlorite are present, the latter occurring in elliptical agglomerations up to 1 cm long. These agglomerations are larger than all other minerals in the rock; otherwise the rock is not porphyroblastic.

Contacts with unit 3 (ultramafic) are not exposed but, due to the close spacing of outcrops on either side of the contact and lack of mixed rock types, are presumed to be sharp. Contacts with unit 1 metasedimentary rocks are gradational over 0.5 to about 4 metres: foliations in the units 1 and 2 are parallel at their contact and the similar mineralogy and composition of the two units make them appear

very similar in outcrop (Fig. 2.6). Rare, ellipsoidal xenoliths of intact Snowshoe mica schist are found within the gneiss, elongate parallel to the foliation and containing a parallel foliation (Fig. 2.7). A xenolith composed almost entirely of tremolite was found near Dunford Lake and was likely derived from the Redfern ultramafics. In one location on the northeast slope below Anita Peak (see Fig. 1.1) a gneiss of identical lithology and appearance to the Redfern Gneiss intrudes unit 4 amphibolites immediately above its contact with unit 3. Xenoliths of amphibolite are found within the gneiss and the gneiss has a finer grained "chilled" margin at its contact.

An orthogneiss of similar composition occupying an equivalent structural position to the Redfern Gneiss was found by Elsby (1985) in the Mt. Perseus area north of Crooked Lake. The main difference between that unit and the Redfern Gneiss is the presence of variable size augen of potassium feldspar in a finer grained matrix in Elsby's study area. The two gneisses are probably coeval and formed by the same, syntectonic intrusive process.



Figure 2.6: Gradational contact between banded Snowshoe schist (left) and parallel foliated Redfern Gneiss.



Figure 2.7: Xenolith of biotite schist (Snowshoe) in the Redfern Gneiss, concordant and elongate with the foliation.

2.4 REDFERN COMPLEX

In 1978, R.B. Campbell (1978) named the Redfern Complex on the Open-File map sheet of Quesnel Lake, and Montgomery (1978) informally named it the Black Riders complex in his unpublished Master's thesis. Each recognised it as a fault-bounded klippe of ultramafic rock overlain by mafic amphibolite, both overlying the Snowshoe Formation (Kaza Group - Montgomery, 1978). Campbell (1978) suggested an Early Paleozoic to Mississippian age for the Complex, while Montgomery (1978) correlated it directly with the Permian to Mississippian Antler Formation. The published name, Redfern Complex (Campbell, 1978) is used here. This study attempts to address the problems of age, tectonic affinity and correlation of the Complex. In this section, field relations of the different lithologies are described with special attention given to observations which address these problems.

Redfern Peridotite

Ultramafic rocks crop out in a 2 km long, continuous northeast trending arcuate pattern underlying the topographically highest point in the field area. Their maximum possible stratigraphic thickness is 400 m. Montgomery (1978) separated the unit into three subunits which are, from bottom to top: a tectonized dunitic unit overlain by cumulate harzburgites with a generally more massive zone of dunites at the top. The lower two subunits are distinctive and easy to recognize and have been adopted here. The upper unit is discontinuous and poorly defined in the field, and is here replaced by a new subunit called the mixed ultramafic-mafic subunit. Dunites weather to a distinctive red-brown colour and show varied surface textures due to cumulate layering, a penetrative foliation, and later veining and metamorphism. Harzburgites, renamed pyroxene-bearing peridotites or layered cumulates, display alternating red-brown dunitic layers with black, coarser-grained pyroxene-rich layers.

2.4.1 Unit 3A: Tectonized Dunite

This unit ranges in thickness from approximately 50 to 100 m. Recognizable primary minerals are coarse to fine grained olivine and tiny granules (1 mm or less) of chromite which are rarely aligned into trains on the outcrop surface. White weathering elongate, coarse olivine or mimetic replacement minerals in a fine-grained red-brown coloured matrix define a penetrative tectonic foliation in the rock (Fig. 2.8). In some places the foliation is parallel to anastomosing fractures and the rocks are noticeably more altered. Serpentinization and steatization have also resulted in locally extensive veining and other replacement textures. Veins vary from a few grains to a maximum of 5 cm thick and are composed of white fibrous serpentine and/or talc (Fig. 2.8). The talc is locally green and coarse-grained. Evidence for several episodes of alteration include folded veins and cross-cutting vein sets. Vein orientations are highly variable and no attempt was made to recognize distinct vein generations. Serpentine also occurs as thin, black wisps in the dunitic matrix which bend around coarser relict grains. White replacement minerals are talc, carbonate, and tremolite/anthophyllite. Random sprays/sheafs of prismatic white amphibole up to 3 cm long are either tremolite or anthophyllite.



Figure 2.8: Talc-serpentine vein cross-cutting S_1 foliation, unit 3A.

The contact with the overlying cumulate layered subunit is sharp, marked by the first appearance of black, pyroxene-rich mesoscopic compositional layering (Fig. 2.9).

2.4.2 Unit 3B: Layered Cumulates

There are only three areas where these rocks occur as a continuous zone (see Fig. 1.1). The best exposures occur on the north facing slope immediately south of Dunford Lake and form a continuous outcrop for a length of about 750 m. The other two exposures are both along the north trending ridge south of Dunford Lake and west of Capacitor Lake.

Layering is defined by accumulations of black, equant medium to coarse grained pyroxene having good cleavage, within a finer-grained olivine matrix interlayered with red brown dunites (Fig. 2.9a).

Magnetite occurs within and between pyroxene grains, giving them a black colour; some of these rocks are

highly magnetic. Percentages of pyroxene in the layers range from nearly 100% in pyroxenite layers and veins to about 20-30% in pyroxene peridotites. Boundaries with interlayered dunitic layers are sharp but locally contacts grade upward where pyroxene grains become more disseminated within the matrix (Fig. 2.9b). Layers range from about 1 to 30 cm thick and are discontinuous over 100 metres or less. Irregular pods, lenses, and lensoid shapes with cusped offshoots are common. Primary cumulus flow structures such as recumbent, intrafolial slump folds and less common cross-bedding and layer truncation have been observed but are not abundant. Planar pyroxenite dikes 4-25 cm thick crosscut the cumulus layers may continue for 50 m or more but their occurrence is irregular.

Small, discontinuous outcrops of the layered subunit also crop out on the slope southwest of Dunford Lake and northwest of Capacitor Lake, cropping out to within 30 m or less below the base of the amphibolite unit. The cumulus layered subunit is truncated sharply above by the overlying mixed subunit contact.

2.4.3 Unit 3C: Ultramafic-mafic mixed subunit

The contact between mafic and ultramafic lithologies is neither sharp, nor planar, but rather is a transitional zone of mechanically intermixed slices and fragments of both rock types ranging from 3 to 50 m thick. The lowermost appearance of bright green weathering amphibolite defines the lower contact of the mixed zone. Likewise, the last appearance of the distinctive red-brown weathering of ultramafic lithologies defines the bottom contact. The zone weathers recessively and forms topographic benches and saddles at a nearly constant elevation.

Orientations of the contact between the two rock types are highly variable, from horizontal to vertical, and structural "mixing" occurs on all scales (Fig. 2.10). For example, on the slope south of Dunford Lake a lens 100 m by 50 m of mafic amphibolite is surrounded by ultramafics. Just east of this is a particularly wide occurrence of the mixed zone along a bench-like step in topography with alternating green and red weathering slices tens of centimetres to several metres wide (Fig. 2.10). Thus in this area the contact seems to be nearly flat-lying or, more likely, strike is parallel to the hillside and the contact dips gently to the south.

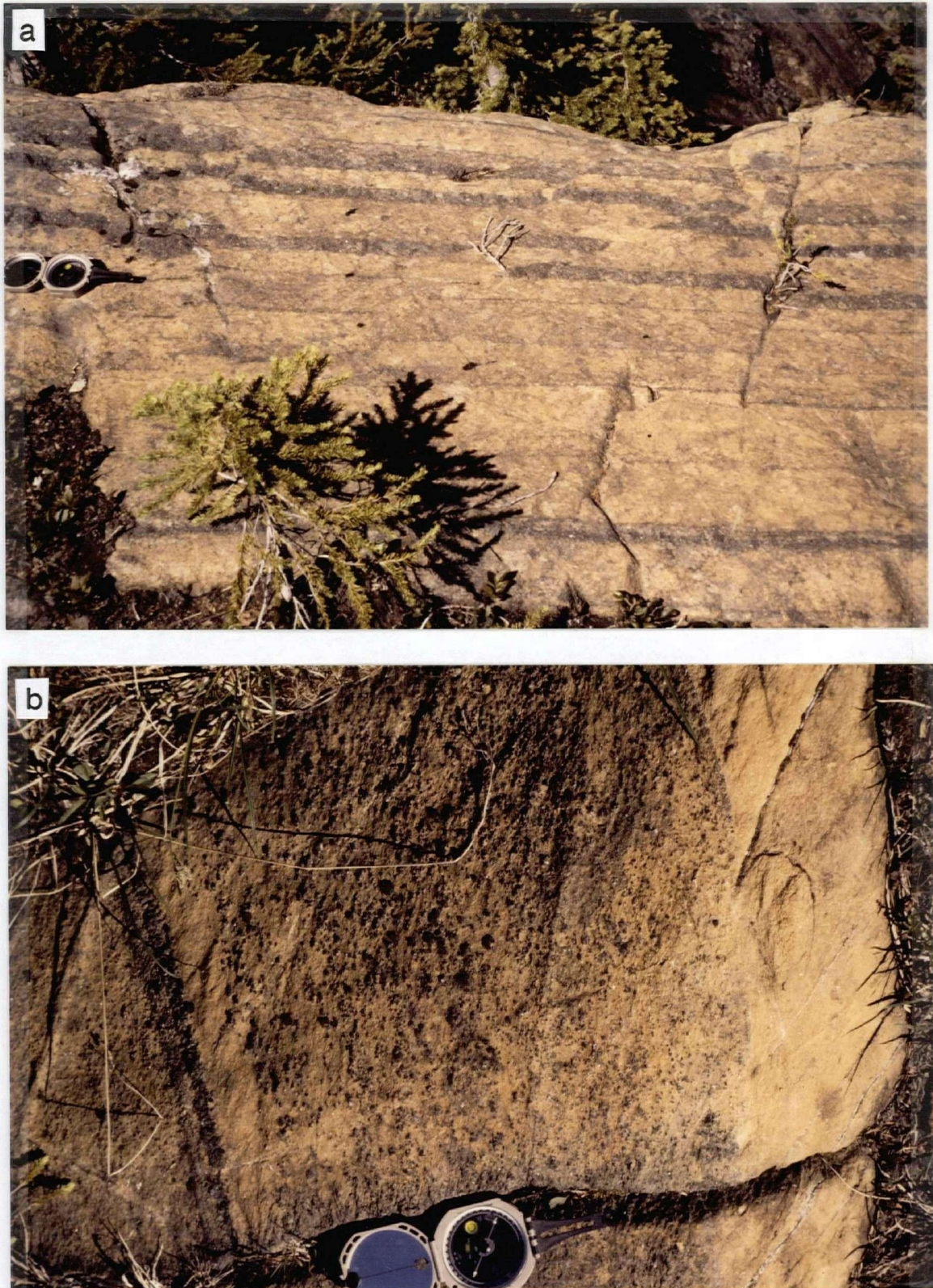


Figure 2.9: Pyroxene-bearing peridotite, unit 3B. a) Cumulate layering; b) disseminated pyroxene grains, close-up.

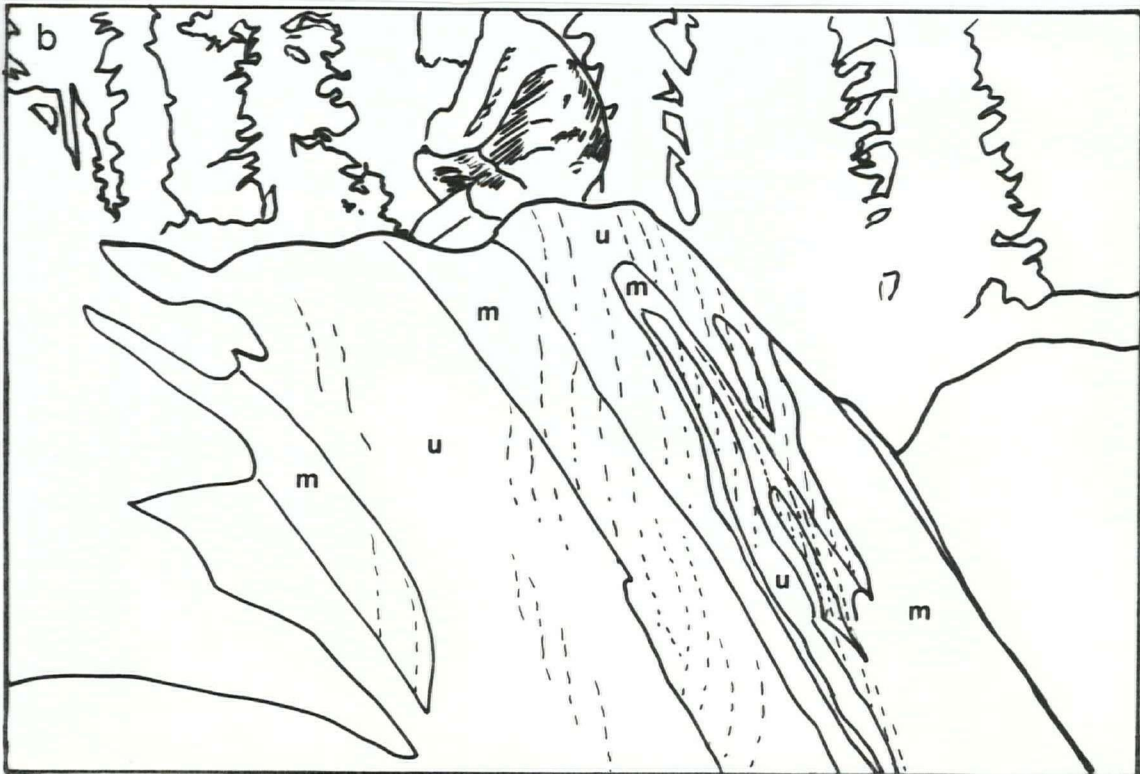
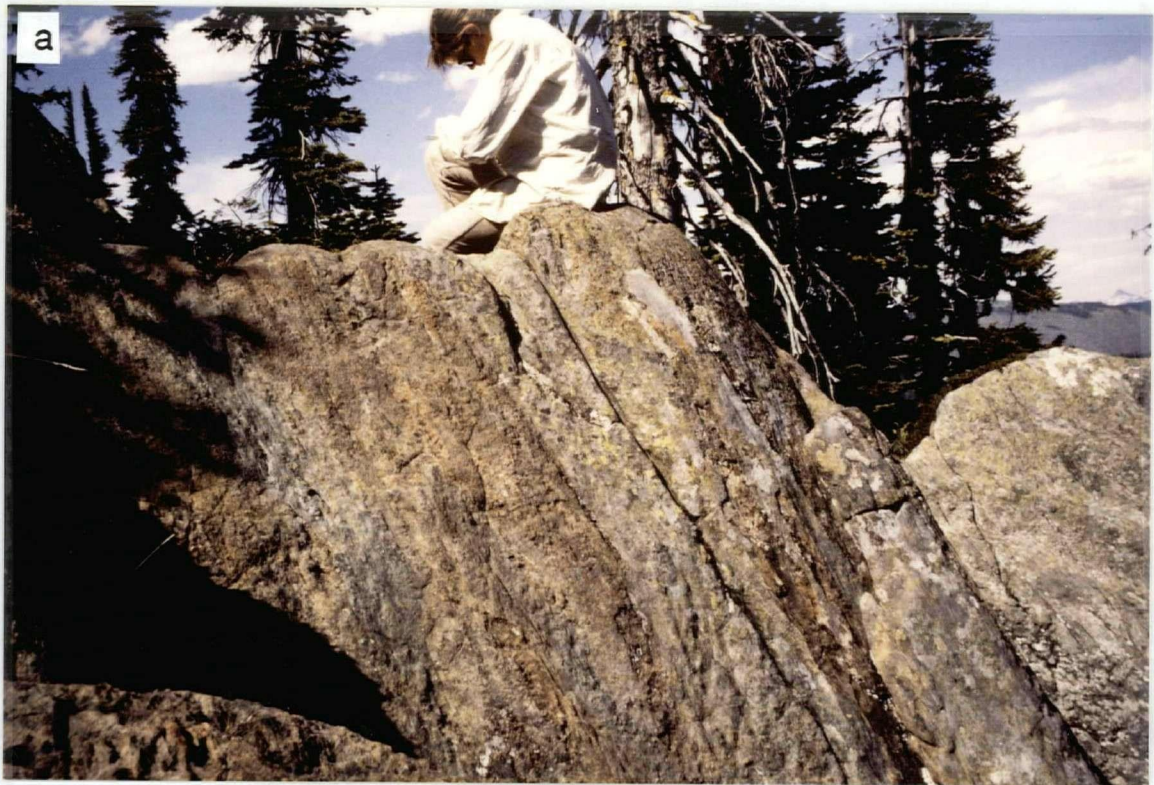


Figure 2.10: Mixed ultramafic-mafic subunit. a) Photograph; b) sketch highlighting low angle that layer contacts make with the foliation.

On the west side the contact also probably strikes parallel to the hillslope and dips gently into it. Overall, the contact is probably parallel to the local foliation within the mixed zone.

Rock types comprising this mixed zone appear to include both mafic and ultramafic original compositions which have been subsequently altered. Twenty to thirty metres above the contact zone the amphibolites are medium-grained, massive to well-foliated gneisses. As the zone is approached, gneisses give way to a bright green, fine-grained, talc or chlorite schist. Medium-grained green and white amphiboles displace original pyroxenes in both the gneiss and the schist. Schist layers range in thickness from 5 cm to 2 m and the schistosity is commonly crenulated. Ultramafic layers have similar size variations but overall tend to be thicker and comprise the majority of the mixed zone (Fig. 2.10). Dunitic and pyroxenitic "slices" are highly altered to monominerallic zones of talc, serpentine, tremolite/ anthophyllite, and magnetite. These minerals form an anastomosing foliation as well as interstitial fillings, mats, and radiating sheafs.

2.4.4 UNIT 4: REDFERN AMPHIBOLITE

Amphibolite in the map area is the thickest continuous exposure of this rock type in the Quesnel Lake region. It covers an area 2-3 km southwest by 4-5 km northwest and reaches a minimum thickness of nearly 1000 m, the top of the unit having been eroded away. A second exposure of this unit on the slope just west of the Spanish Creek valley is about 80 m thick and is probably continuous with the first (see Cross Section, Fig. 1.2). It occupies the same structural position and is part of a thinner, yet identical structural succession, including about 30 m of ultramafic rocks (massive dunites) and 5 m of Redfern Gneiss (see Fig 1.1). Most importantly, the upper contact of this amphibolite, with the purplish quartzite of proposed Triassic age, is exposed in a stream bed where it is sharp and concordant.

Variations in texture, more than composition, characterize the amphibolite lithology. Gneissic layering is defined either by changes in grain size or compositional segregation (Fig. 2.11) Locally the rock is massive with irregular compositional changes (Fig. 2.12) and has a dominant linear rather than planar fabric, frequently forming mullion-like outcrops (Fig. 2.13). In two locations a planar fabric is extremely

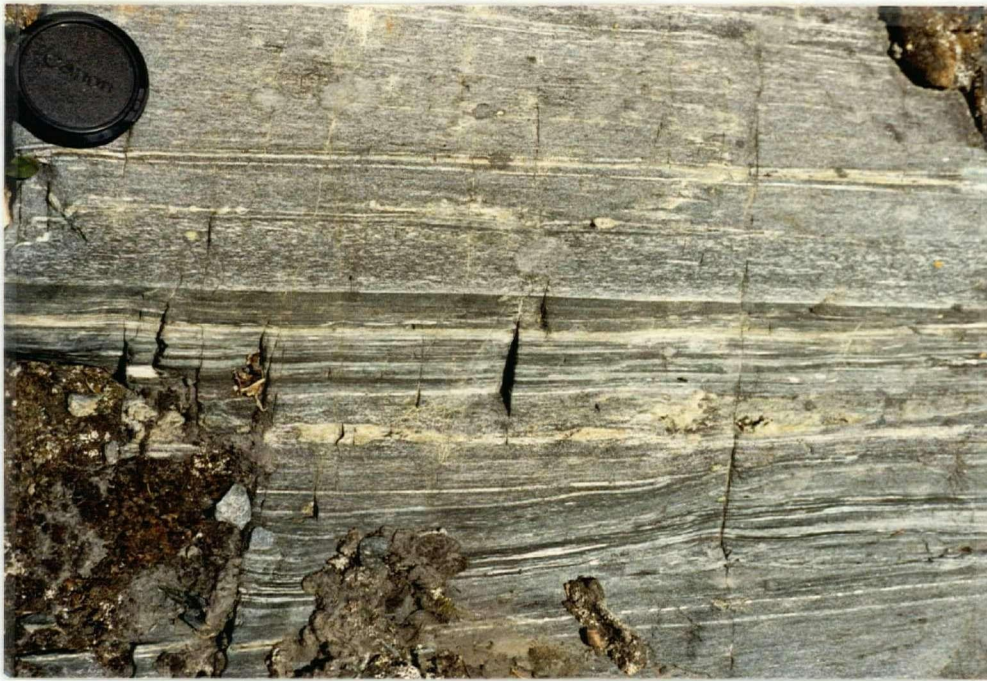


Figure 2.11: Gneissic layering in the Redfern amphibolite, unit 4. Both alternating compositional layers and changes in grain size comprise the fabric.



Figure 2.12: Metagabbroic lithologic subtype. Note linear fabric and lack of planar foliation.



Figure 2.13: Mullion outcrop style of Redfern amphibolite, controlled by dominantly linear fabric.

well-developed: along the unit's basal contact and in the Spanish Creek exposure. The colour of these rocks is a function of grain size, the darker being finer-grained.

Montgomery (1978) divides the amphibolite into two subunits, a gneiss and a schist. Campbell (1978) differentiates a more gabbroic unit at the base of the amphibolite. In this study, no gross compositional or textural change across the section was recognized on the basis of field observations and the unit is not formally subdivided. Layers are discontinuous over almost any distance and the occurrences of highly schistose or massive lithologies (perhaps more gabbroic) are small and localized.

However, seven lithologic subtypes have been recognized but not mapped and are described in Table I. Three have limited distribution related to their paragenesis; the other four comprise the bulk of the amphibolite unit and are primarily a textural distinction. Further discussion of these subtypes occurs in the Discussion section at the end of this chapter.

TABLE I

SUBTYPE	GRAIN SIZE	MINERALOGY	TEXTURES	DISTRIBUTION
Massive	0.5-7 mm	hb+plag+qtz	massive, homogeneous	near basal contact
Blasto-Mylonite	12 and 0.2 mm;	hg+plag+qtz+chlorite	pblastic w/ S-C fabric;	on basal contact;
Mylonite	<0.1 mm	same	very fg w/planar foliation	thin zones in upper section
Mafic, FG	<0.5 mm	80% hb, 20 % qtz + plag	wispy or parallel laminated, layers <0.5 m thick; lineated	random
Felsic, FG	<0.5 mm	80% qtz+plag 20% epidote	granoblastic phacoidal 5-20 cm layers	upper 50 m, increasing abundance upward
Mafic, MG	7-10 mm	60% hb, 40 % qtz+plag also qtz+plag aggloms in fg hb matrix	planar or linear fabric; 1-3 cm qtz+ plag+ep veins; garbenschiefer	random, common
Felsic, MG	7-10 mm	75% qtz+plag, 25% biotite+ hb, red-orange staining	layers 20 cm-1 m planar fabric w/ hb laths at an angle	upper 200 m
Coarse-grained	> 1 cm 7-10 mm	hb+qtz+plag± red garnet; red-orange stain	layers 10-40cm anastamosing fabric; hb garbenschiefer	random, rare; Spanish Ck

FG, fine-grained; MG, medium-grained; hb, hornblende;

2.5 CROOKED AMPHIBOLITE AND ANTLER FORMATION

The Crooked Amphibolite is a metamorphosed and well-foliated mafic amphibolite and serpentinite with ultramafic pods at the base (Struik, 1988a). It occurs along the Omineca-Intermontane Belts boundary, tectonically overlying the Snowshoe Formation. K.V. Campbell (1971) first described the unit as an amphibole-chlorite-plagioclase-epidote schist with pods of serpentinitized peridotite. Elsby (1985) describes it as a layered assemblage of various amphibole-chlorite schists with talc-bearing schists at the base. Struik (1988a) notes that northwest of the Cariboo River the unit is mostly serpentinite. McMullin and Greenwood (1988) also found a small, previously unrecognized meta-ultramafite associated with amphibolite on Mica Mountain in a structural position equivalent to the Crooked Amphibolite.

The Crooked Amphibolite is inferred to be the metamorphosed equivalent of the Antler Formation (Struik, 1988a; Rees, 1987; Campbell, 1978; Montgomery, 1978), which comprises the upper section of the Mississippian-Permian Slide Mountain Group (Sutherland-Brown, 1957; 1963). In the type section, it is composed mostly of unmetamorphosed basic volcanic rock and chert, and conformably overlies the Guyet Formation, a sequence of dominantly marine sedimentary rocks plus some volcanic flows and volcanoclastic rocks (Sutherland-Brown, 1963). Struik (1988a) found ultramafic rocks near Mount Murray in the Antler Formation occurring as pods and sheets mixed with other mafic lithologies. Although both mafic and felsic lithologies within the Crooked Amphibolite might have protoliths in the Antler Formation, the presence of ultramafic rocks at the base of the Crooked Amphibolite contrasts sharply with the sedimentary lithologies of the Guyet Formation found at the base of the Antler Formation.

The Crooked Amphibolite was examined at four locations for comparison and contrast with the tentatively correlative Redfern Amphibolite (see Fig. 5.1). The Antler Formation was also examined at one site near its type section locality along the Willow River. Field locations and observations are briefly described below but the main basis for comparison is the geochemical analysis, described and discussed in Chapter 3.

2.5.1. Crooked Amphibolite

Crooked Lake sites - The geology around Crooked Lake was examined and two ultramafic outcrops at the base of the Crooked Amphibolite were sampled. On the south shore of the lake, a short structural sequence on the south limb of the Boss Mountain antiform was examined. At this site the Crooked Amphibolite is a fine-grained, biotite-chlorite schist with more felsic interlayers. Ultramafic rocks are massive, fine-grained, red-weathering dunite found on and near the base of the Crooked Amphibolite. Structurally below the Crooked Amphibolite, a weakly foliated and lineated granitic augen-orthogneiss was found.

On the steep slopes above the northeast shore of Crooked Lake, one large body of peridotite about 20 m high by 75 m long was sampled. The site is on the south limb of the Eureka Peak Syncline at a structural level equivalent to the MacKay River sites (see below). The upper and middle portions are layered dunites and pyroxene-peridotites (Fig. 2.14a) and the base of the outcrop is a sheared serpentinite. Layers consist of disseminated relict pyroxene within an olivine matrix alternating with massive, red-weathering dunites. A 5 cm wide, coarse-grained talc vein cross-cuts the layering and is offset by later shear fractures. Contacts are not exposed and no other lithologies were seen at this site.

Wolverine Lake sites - Three localities of steatite and serpentinite were examined and sampled within the Antler Formation near Wolverine Lake north of Likely, B.C. Outcrops occur as elliptical bodies at most a few hundred metres long within poorly exposed Crooked Amphibolite. A few hundred metres east of the easternmost site another potassium feldspar augen gneiss is mechanically intermixed with the Crooked Amphibolite on its contact with the Snowshoe Group. At the easternmost site the rocks are brecciated and consist of angular and rounded blocks of tectonized and veined relict dunite and pyroxene peridotite in a talc + carbonate + serpentine matrix (Fig. 2.14b). Chromite and relict olivine are evident on weathered surfaces. At a second site about 1 km west of the first, the rock is dark green or grey to black fine-grained serpentinite with a well-developed foliation. Talc occurs in sheafs and the rocks are highly magnetic. At the westernmost site, rocks are similar to the easternmost site, breccia fragments with relict pyroxene grains weathering out.

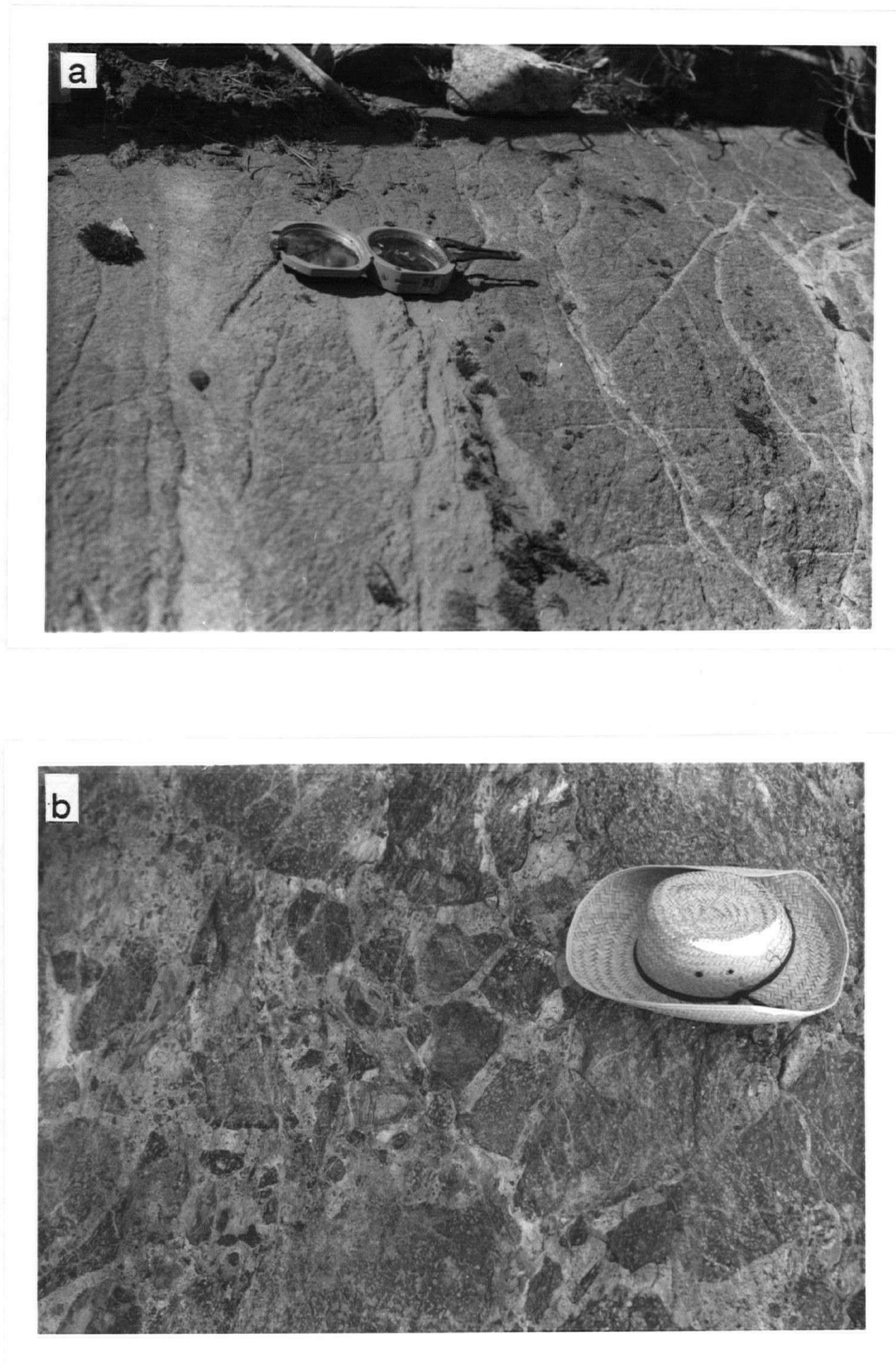


Figure 2.14: Outcrops of Crooked Amphibolite. a) Cumulate layering in peridotite at Crooked Lake site, north shore; b) peridotite breccia at Wolverine Lake site.

MacKay River sites - The Crooked Amphibolite was sampled in four different localities along the MacKay River valley north of Eureka Peak. The area was mapped in detail by Elsby (1985) and observations here are consistent with his. The sites rest on the steeply dipping, overturned north limb of the Eureka Peak syncline and structurally overlie a felsic augen gneiss and the Snowshoe Formation. The Crooked Amphibolite is a medium-fine grained to medium-coarse grained, banded, light to dark green amphibole-chlorite-biotite-plagioclase amphibolite. Pyrite is locally associated with biotite. Both quartz and calcite filled fractures were observed. The rock is extremely well-foliated but is locally massive. No ultramafic lithologies were identified in this area.

Basset Creek site - One site was observed in the Basset Creek valley along the northwest flank of the Boss Mountain antiform. The rock is a felsic, light green medium to medium fine-grained amphibolite. Minerals present include hornblende, plagioclase, quartz, chlorite, and epidote, with epidote veins locally abundant. In one large outcrop, quartz and plagioclase form elliptical agglomerations identical to some observed in the upper portion of the Redfern Amphibolite (felsic, medium-grained). No ultramafites were observed at this site.

2.5.2. Antler Formation

Willow River site - The only sample from the contiguous Antler Formation of the Slide Mountain Group was obtained from the Willow River site. This site is outcrop 3 in Struik's field trip guide through the Cariboo Mountains Gold Belt (Struik, 1985). The rocks consist of sheared pillows of the Antler Formation overlain by greenschist, with serpentinite at the base on the contact with the underlying Barkerville Terrane rocks (Struik, 1985). No serpentinite was found but a sample of greenschist was taken for geochemical analysis. The outcrop consists of fine-grained chlorite-epidote-plagioclase schist with a well-developed foliation parallel to compositional layering. Symmetrical boudins (pillows?) within the foliation plane and quartz filled fractures at a high angle to the foliation were also observed.

2.6 TRIASSIC BLACK PHYLLITE

Filippone (1985) was the first to recognize the Triassic black phyllite east of the contiguous Intermontane-Omineca belts boundary in cores of late synforms in the Boss Mountain area. McMullin and Greenwood (1988) also found black Triassic phyllite occupying the core of a synform on the east flank of Mica Mountain directly north along strike of the outcrops in Spanish Creek. Based on field observations and correlations with adjacent areas (Bloodgood, 1988, 1987; McMullin and Greenwood, 1988), the High Grade Kaza unit of Montgomery (1978) is here assigned to the Triassic section of the Triassic black phyllite. Two distinctive lithologies are recognized: high-grade metamorphic staurolite schist, and black phyllitic limestone. The occurrence of Triassic rocks is restricted to a synform on the east side of the area. Triassic rocks were not observed above unit 4 on top of Peak 6495'.

2.6.1 Unit 5A: Black phyllitic limestone

Unit 5A has a maximum structural thickness of about 75 m and consists of distinctive graphitic and pyritic limestone plus minor quartzite and phyllite. The limestone is black and fissile due to a well-developed, folded schistosity. Mica porphyroblasts up to 5 mm in diameter define a lineation within the cleavage plane. Porphyroblasts of rusty-weathering pyrite are also present. The base of the unit is locally marked by purplish, biotite-muscovite-garnet-kyanite-staurolite bearing quartzite, also with a well-developed schistosity. Minor interlaminated phyllites and psammitic phyllites, and one occurrence of mud rip-up clasts in a psammitic matrix were observed. In the northern part of the Dunford Lake region near Seahorse Lake, the black limestone is the first rock type encountered across the contact with unit 1 (Snowshoe Group), followed by the staurolite schist. Further to the south, directly east of Dunford Lake and above Spanish Creek, Triassic rocks are in sharp contact with underlying garnet-bearing amphibolites of unit 4 of the Redfern Complex (see Fig. 1.1).

2.6.2 Unit 5B: Staurolite schist

This unit consists of banded, porphyroblastic, graphitic schist with a well-developed, anastomosing schistosity. Large porphyroblasts of staurolite up to 5 cm long, garnet up to 2 cm in diameter, and some kyanite up to 3(?) cm long make the unit highly distinctive (Fig. 2.15a). The rock weathers silvery-grey and has dark and light compositional bands 2 to 10 cm thick (Fig. 2.15b) which represent transposed bedding (see Chapter 3). Staurolite porphyroblasts in the schist commonly have been extended in their long dimension and the broken partings are filled with fibrous quartz. Quartz pressure shadows also frequently form symmetrical tails around staurolite and kyanite. Garnet porphyroblasts have euhedral rims surrounding more anhedral cores. Minor green-black amphibolite layers 10-40 cm thick and rare milky quartz pegmatites 5 by 20 m occur parallel to the banding.

McMullin and Greenwood (1988) report the occurrence of a sequence of Triassic sedimentary rocks on Mica Mountain consisting of ultramafics overlain by quartzite, amphibolite, graphitic and pyritic phyllite, carbonate, and staurolite schist. They tentatively correlate the phyllite and carbonate (Unit 5, McMullin and Greenwood, 1988) with Unit 3 of Bloodgood (1987b) and the staurolite schist (Unit 6, McMullin and Greenwood, 1988) with her Unit 4. The Triassic black phyllite rocks described above are considered to be continuous with the rocks observed on Mica Mountain by McMullin and Greenwood. Unit 5A is correlated with Unit 5 of McMullin and Greenwood (1988) and unit 5B is correlate with their Unit 6.

2.7 SUMMARY AND DISCUSSION

The distribution of lithologies in the Dunford Lake area comprises the following structural succession, from bottom to top (Fig. 2.1): Hadrynian to Paleozoic Snowshoe Group metasedimentary rocks, a fault of unknown age (Late Paleozoic to Jurassic?) which is discontinuously followed by the granitic Redfern orthogneiss, a minimum 1400 metre succession of tectonized dunites, cumulate layered pyroxene-peridotites, and mafic amphibolite herein called the Redfern Complex, and phyllitic limestone and staurolite schist of the Triassic black phyllite. Thinner structural successions comprising identical



Figure 2.15: Triassic staurolite schist. a) Close-up of staurolite porphyroblasts; b) gneissic banding.

lithologies have been recognized in the Crooked Lake area, the Crooked Amphibolite being the structural and lithologic equivalent to the Redfern Complex.

The protoliths of the Snowshoe Group high-grade metamorphic schists and quartzites were probably siliciclastic sedimentary rocks belonging to a pericratonic, continental shelf sequence. In the Dunford Lake region, the abundance of schist and purity of quartzites indicate that protoliths were dominantly finer-grained sediments: shales, siltstone and fine, dominantly quartz with some feldspathic sandstone and lesser amounts of grit. The minor occurrence of mafic amphibolite and marble lithologies represent intersedimentation accumulations of volcanic rock(/dolomitic sandstone?) and limestone, respectively. Snowshoe Group rocks immediately adjacent to the Dunford Lake area are assigned to the Barkerville Terrane (Struik, 1982). Snowshoe Group rocks in the Dunford Lake area are south of a regional structural dome and are probably some of the structurally highest Snowshoe Group rocks in the region.

The Redfern Complex has characteristics of a dismembered ophiolite (Coleman, 1977): cumulate peridotites with a tectonized and more highly altered basal sequence, capped by polydeformed, metamorphosed mafic amphibolite. Several faults, along which portions of the ophiolite may have been removed, are recognizable from field evidence: the base of the Complex which juxtaposes ultramafic rock against presumably older, high-grade metasedimentary rocks; the contact between the units 3 and 4, which is marked by blastomylonites within the amphibolite and truncates primary cumulate layering in the underlying unit; and thin, very planar zones of ultrafine-grained, mylonitic amphibolite within unit 4. Lithologic subtypes within the amphibolite probably represent original variations within the upper portion of the ophiolite. Unit 3C, which appears to contain both mafic and ultramafic lithologies, may contain portions of a sheeted dike segment. The more massive amphibolite subtype near the base of unit 4 may represent an original intrusive phase texture such as massive gabbros. The occurrence of more felsic material within the amphibolite increases upward and could represent either more felsic extrusive phases, later intrusive sills and/or interlayer sedimentation such as chert accumulation. Grain size is partly a function of original grain size but mostly of conditions and duration of metamorphism, particularly the coarsest grain sizes and the garbenschiefer texture. The only occurrence of garnet within the amphibolite

on Spanish Creek may indicate an increase in metamorphic grade and it is associated with a very well-developed planar to mylonitic foliation, a thinner structural succession, and the highest metamorphic grade of Triassic rocks in the entire region.

The section of Triassic black phyllite rocks correlates well with Bloodgood's (1987a & b) lower stratigraphy in the Eureka Peak area and north. The difference in metamorphic grade - chlorite grade in Bloodgood's areas and sillimanite grade in this study - give the rocks a very different appearance. However, they also appear very different from local Snowshoe lithologies of the same metamorphic grade. McMullin and Greenwood (1988) noted the abundance (an excess) of staurolite and a "graphitic" quality to the siliciclastic rocks. Also, relict sedimentary structures as seen in these rocks have never been recognized in the highly deformed, western facies of the Snowshoe Group. The limestone in this unit, being highly graphitic and pyritiferous, is much less pure than the typical, very light grey calcite marbles of the Snowshoe Group in the Dunford Lake area. Finally, the structural position of the unit and the recognition of a continuous succession, from Snowshoe Group through Redfern Gneiss, ultramafics and amphibolites to staurolite schist, supports the Triassic interpretation of lithologic characteristics.

In summary, the field relations support correlation of the Redfern Complex with the Crooked Amphibolite on the basis of lithologic similarities, structural succession and position. Correlation of these units with the Antler Formation of the Slide Mountain Group is not tenable on the basis of field relations, although comparison was mostly made to published descriptions rather than first hand observation. Variations in stratigraphic facies obscured by metamorphism and multiple deformations events are commonly invoked to explain differences between the two rock suites. Therefore, correlation must be based upon other evidence or remain tentative.

3. STRUCTURE

3.1 INTRODUCTION

The structure of the Dunford Lake area is characterized by polyphase deformation of three mechanically heterogeneous lithologic assemblages. These assemblages comprise upper and lower plate packages separated by a major structural discontinuity, the Redfern thrust. The lower plate consists of the metasedimentary rocks of the Snowshoe Group. The upper plate is composed of the Redfern Complex mafic and ultramafic rocks capped by and in fault contact with metasedimentary rocks of the Triassic black phyllite (TBP).

Distinct structures are found in each lithology due to extreme contrasts in rheology as well as timing of development of different sets of structures. The geometry of each phase of deformation is first described locally for each unit and the geometrical elements found within the units are labelled and numbered separately. Deformation phases are denoted D_1 - D_4 for the lower plate and D_1 - D_3 for the upper plate. Planar and linear arrays of minerals are S and L respectively while F denotes fold axial trends. These local structural elements are then synthesized and related to the overall structural and regional deformation phases in the Discussion.

3.2. LOWER PLATE: THE SNOWSHOE GROUP

Minor structures such as folds from four deformation phases are readily seen within the finely layered Snowshoe Group metasedimentary rocks. However, partly due to poor exposure and lack of continuous map units, only one set of map scale features was found with which to relate one set of these minor structures. Combining field observations of superposed structural elements with work in adjacent, better exposed areas, the geometry of Snowshoe Group structures can be outlined and the remaining minor structures assigned to well-defined regional deformation events. The study areas of authors whose work is commonly referred to are located in Figure 1.4. All four phases are fold events but at least one phase is associated with faulting.

Phase 1

Snowshoe Group rocks exhibit a pervasive metamorphic foliation which is parallel to compositional layering. Upon close inspection of hand specimens and thin sections rootless hinges to isoclinal folds composed of tabular quartz are seen intrafolial within a pervasive schistosity (Fig. 3.1). This layer parallel foliation is a transposed foliation, is the earliest recognizable structure in the Snowshoe, and is referred to as S_0/S_1 . Other workers have documented similar-style (Class II of Ransay, 1967), isoclinal folds with mica growth across compositional layering and parallel to S_1 (Garwin, 1987) and isolated floating hinges of dismembered folds (Lewis, 1987). Many of the quartz hinges are derived from early quartz veins, reported by Fillipone (1985) and Garwin (1987) to locally comprise up to 60% of the rocks. Axial planes and F_1 fold axes were not observed, but other workers have shown axial planes to be variably inclined and have a generally indeterminate vergence. Fold axes are curvilinear (Garwin, 1987) and appear to be parallel to D_2 mineral lineations (Lewis, 1987). The original geometry of D_1 is unknown due to strong overprinting by later deformation.

Phase 2

Limited exposure and lack of marker units make it difficult to completely characterise D_2 . Minor folds with thickened hinges and attenuated limbs are fairly abundant (Fig. 3.2). They were also observed to have tight, rounded hinges and planar limbs with a high amplitude to wavelength ratio (Fig. 3.2). Other workers have determined that they are Class IC to II, depending upon lithology (Fillipone, 1985; Garwin, 1987; Lewis, 1987).

An axial planar cleavage, S_2 , is well-developed on both mesoscopic and microscopic scales and its style and orientation is strongly controlled by the previously existing planar fabric, S_0/S_1 . In schistose lithologies, S_2 comprises either an asymmetric crenulation cleavage at moderate angles to S_0/S_1 or the two foliations merge to form an anastomosing cleavage which deflects around metamorphic porphyroblasts. In more quartz-rich lithologies, micas growing perpendicular to S_0/S_1 in the hinges of minor folds define S_2 . The orientation of S_2 is generally reclined with a varying strike. Fillipone (1985) recognized the dominant schistosity in the Boss Mountain area to be S_2 . This is the case in the Dunford Lake area as well and

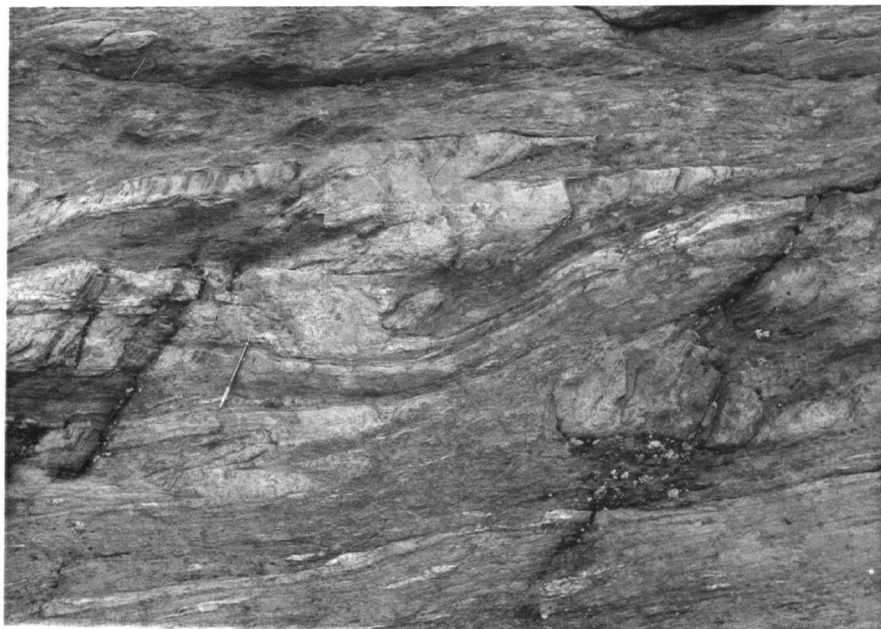


Figure 3.1: Intrafolial F1 isoclinal folds in micaceous quartzite of the Snowshoe Group, 2 scales.



Figure 3.2: Tight D_2 folds in micaceous quartzite (prominent) and pelitic schist (recessive), Snowshoe Group, 2 scales.

commonly, the two foliations cannot be distinguished from one another. On a stereonet plot, S_2 and S_0/S_1 show a similar spread of orientations (Fig. 3.3). Where the cleavage is anastomosing or the exposure does not allow separation of the two geometries, what is actually S_2 may have been labelled S_0/S_1 .

The intersection of compositional layering and S_2 axial planes has produced a pervasive mineral lineation. The lineation is defined by long dimensions of micas and quartzofeldspathic rods. Metamorphic porphyroblasts are not consistently aligned. This lineation is sub-parallel to F_2 fold axes (Fig. 3.3) but the centre of the cluster is askew to a calculated fold axis. This probably is due to the influence of both the earlier and later fold phases.

Map scale folds associated with the minor structures were not identified although they are almost certainly present based on work from adjacent areas. Large antiform-synform sets are recognized where compositional layering is well defined and fold orientations vary from west to east. Adjacent to the contiguous Omineca-Intermontane belts boundary (Fig. 1.4), folds are upright with steeply dipping axial planes and become recumbant as one moves eastward (Fillipone, 1985). Further east, D_2 folds are once again upright (Garwin, 1987; Lewis, 1987). On a regional scale, fold vergence is easterly and fold axes now plunge variably northward and southward. The Dunford Lake area lies south along the axial trend of the recumbant structures in the Boss Mountain area (Fillipone, 1985) and the reclined to recumbant orientations of minor folds suggest that they rest on shallowly dipping limbs of larger order folds.

Phase 3

Phase 3 folds are recognized on all scales. On the map scale, two westerly-verging antiform-synform pairs are defined by the trace of S_0/S_1 (see Fig. 1.1 and 3.23). Mesoscopic folds are upright and open with an interlimb angle greater than or equal to 90° and have tight, angular hinges which do not show any thickening (Fig. 3.4). Detachment surfaces separating folded from planar layers are common parallel to S_0/S_1 . This style of folding indicates that slip has only occurred between layers, ductility contrast was high between layers and that a buckle fold mechanism was operative (Ramsay, 1967). These mesoscopic folds are best developed within about 50 m of the Redfern fault where a spaced cleavage is also observed.

Snowshoe Group

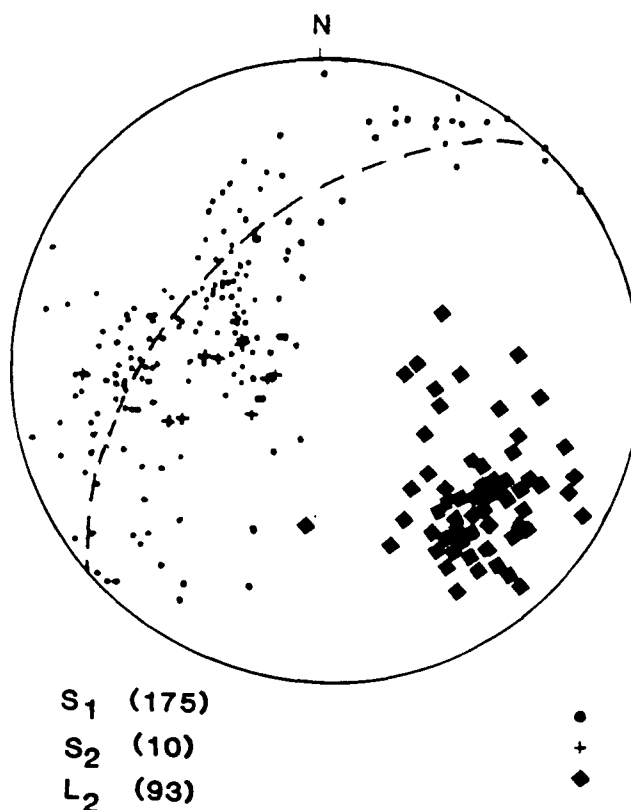


Figure 3.3: Equal-area stereonet plot of poles to S_0/S_1 and S_2 and mineral lineations, L_2 . The centre of the cluster of L_2 mineral lineations is parallel to P_1 -axis, the pole to the girdle containing poles to the foliations. Number of points in parentheses.

The orientation of F_3 is variable, both on regional and mesoscopic scales. The axial surface is not planar on a mesoscopic scale, as shown in Figure 3.4 and a stereonet plot of S_3 shows that it is not planar on a regional scale (Fig. 3.5). Minor fold hinges plunge to the east and southeast except along the Redfern Fault where they plunge shallowly east and west. Fold hinges are dominantly sub-parallel to L_2 , suggesting that F_3 coaxially refolds F_2 . However, the cluster of L_2 is askew with respect to the calculated F_3 and near the Redfern fault, angles between F_3 and L_2 are high. In thin section, micas are rarely kinked around F_3 folds and have mostly recrystallized with a few grains grown parallel to the F_3 axial trace.



Figure 3.4: D_3 folds in micaceous quartzite of the Snowshoe Group. Lens cap for scale, left centre (small).

On a regional scale F_3 folds are conical. Just north of this area is a regional structural culmination of F_3 folds marked by near horizontal lineations and very shallowly dipping S_0/S_1 surfaces. North of this culmination, F_3 fold axes plunge to the northwest (Campbell, 1978; Ross et al., 1985).

Phase 4

Phase 4 consists only of small scale crenulations (Fig. 3.6) with axial surfaces trending southwest-northeast at variable angles to F_3 (Fig. 3.6). It is pervasive on a regional scale and has been recognized by other workers (Fillipone, 1985; Bloodgood, 1987a; Garwin, 1987; Lewis, 1987) but has not been related to any larger order structures. A set of late fractures which are roughly parallel to this trend produce a strong structural grain observable on aerial photos. These fractures may be related to this fold phase.

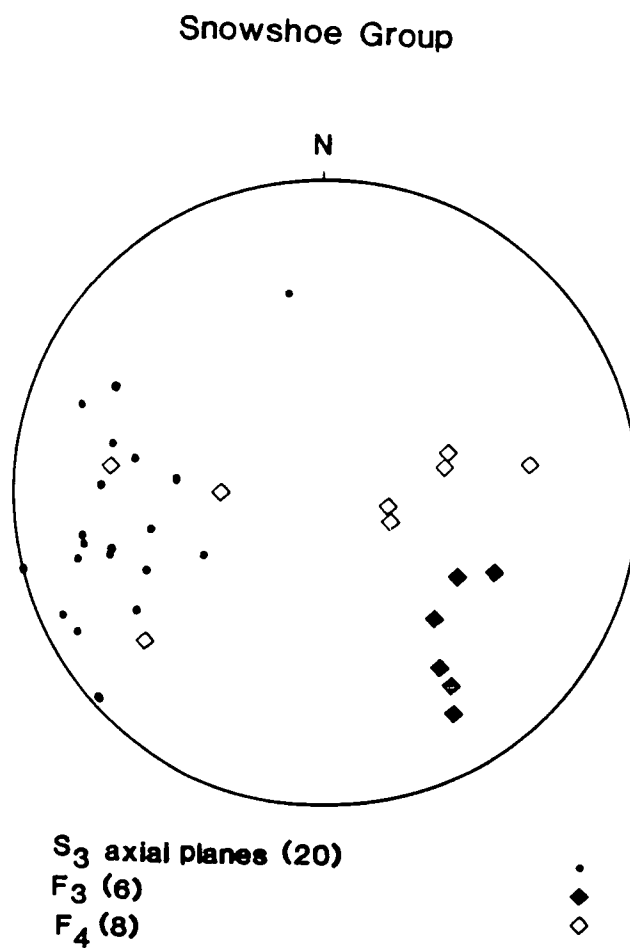


Figure 3.5: Equal-area stereoplot of D₃ and D₄ structures in the Snowshoe Group. Number of points in parentheses.



Figure 3.6: D_4 crenulations in pelitic schist, Snowshoe Group on Orpheus Mountain.

3.3. THE REDFERN GNEISS

The Redfern Gneiss consists of several very small, elongate bodies of deformed granitic rock which occur along the Redfern Thrust and in one other locality near the base of the Redfern amphibolite (see Fig. 1.1). The gneiss has a foliation, S_1 , and a lineation, L_1 , defined by the alignment of micas and elongate lenses of quartz and feldspar. Outcrops are elongate parallel to the trend of S_1 . Xenoliths of biotite schist (see Fig. 2.7) and tremolite schist concordant with the foliation are interpreted as fragments of Snowshoe Group and Redfern peridotite, respectively. Gentle folding of S_1 is demonstrated by the changing orientation of its map trace and the partial girdle distribution of poles to S_1 on a stereoplot (Fig. 3.7). L_1 is clustered around the pole to the girdle and the average orientation of L_1 and this calculated fold axis is $124/47$.

Montgomery (1978) hypothesized that since the Redfern Gneiss contains a foliation and xenoliths of Snowshoe Group while also cutting the Redfern amphibolite, its emplacement was effectively contemporaneous with emplacement of the Redfern Complex onto the Snowshoe Group. In this study the

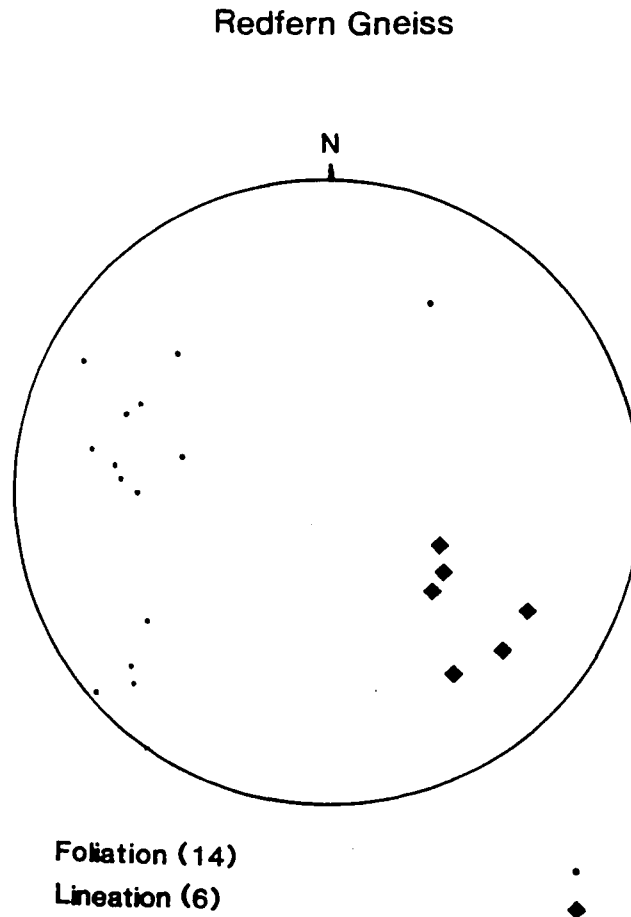


Figure 3.7: Equal-area stereonet plot of linear and planar structures in the Redfern Gneiss. Number of points in parentheses.

foliation, Snowshoe and ultramafite xenoliths were found, in agreement with Montgomery's (1978) observations and conclusions. The xenoliths of ultramafite and the cross-cutting relationship observed between the gneiss and the Redfern amphibolite clearly indicate that the gneiss intruded after the Redfern Complex was in contact with the Snowshoe. The contact between the gneiss and the amphibolite appears to be igneous and not a product of infolding and erosion: the gneiss bears a "flow foliation" and it appears to have a chilled margin.

However, a U-Pb zircon age recently obtained for the gneiss presents a paradox to this relationship. The age obtained is Devonian-Mississippian (J. Mortensen, pers. comm., 1989), much older than the inferred Jurassic age of thrusting, suggesting that the gneiss should be included with the Snowshoe Group in the lower plate and that it belongs to the intrusive series which produced the Quesnel Lake (QLG) and Boss Mountain Gneisses (BMG) (Mortensen et al., 1985). Zircons from one sample of the Redfern Gneiss (DL176; see Fig. 3.8) show scattered results and have quite a large error. The sample bears similar U-Pb systematics to the QLG and BMG, including a mid-Paleozoic crystallization age (338 ± 62 , -77 MY), zircon core inheritance of average Precambrian age, and Pb loss (J. Mortensen, pers. comm., 1989). The sill-like intrusion style of the QLG and BMG along pre-existing planar discontinuities in the Snowshoe may account for the fortuitous occurrence of the gneiss along the Redfern Thrust. The mineral foliation and lineation in the gneiss, S_1 and L_1 respectively, are defined primarily by the alignment of micas and probably developed during D_2 in the lower plate.

The simplest resolution to this paradox is that there are two different gneiss bodies, one mid-Paleozoic and one mid-Jurassic in age. Although there is no great difference in composition based on petrography, this possibility need not be ruled out. If all of the data is taken as correct and having equal weight, this interpretation is suggested to explain these observations.

3.4. UPPER PLATE: THE REDFERN COMPLEX

A maximum of four deformation phases are developed in the Redfern Complex. The first phase is only developed in the peridotite and consists of a macroscopic foliation and microfabrics related to mantle deformation. These fabrics are overprinted by a second, non-pervasive foliation in the peridotite. During the same event, the amphibolite and Triassic black phyllite were deformed for the first time, consisting of tight folds and pervasive planar and linear fabrics. Structural development was most intense along lithologic contacts where transposed and mylonitic foliations are recognized. A second phase of open, westerly verging folds produced minor folds mostly in the Triassic black phyllite and the girdle distribution of foliations and compositional layering in the amphibolite and peridotite.

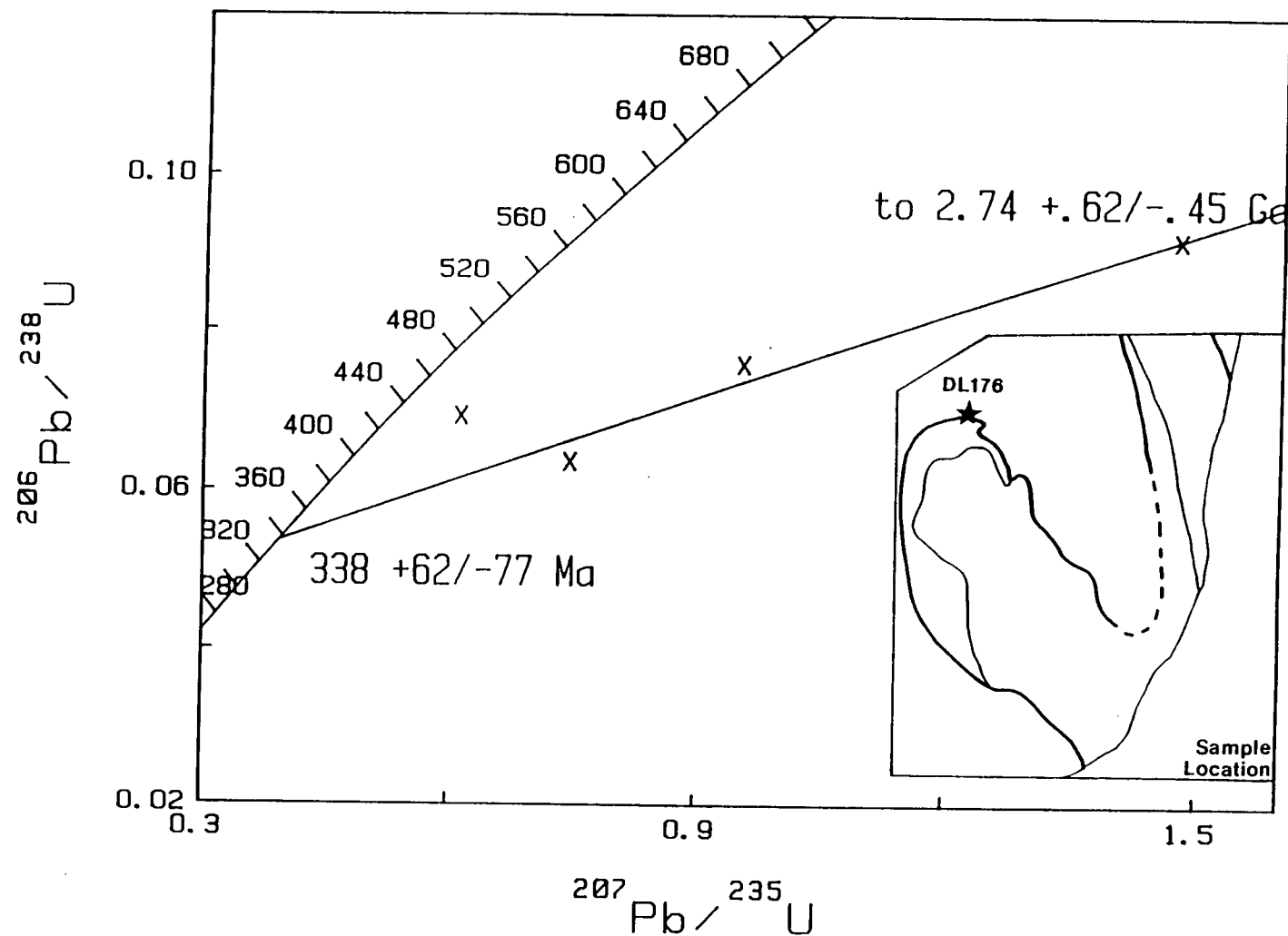


Figure 3.8: Concordia diagram for U-Pb age date on zircons in sample DL-176 of the Redfern Gneiss; sample location in inset. Plot courtesy of J. Mortensen, Geological Survey of Canada.

3.4.1. Redfern Peridotite

The Redfern peridotite bears 4 mesoscopic structural elements: compositional layering, minor folds, and two foliations, one pervasive and one developed only along the contacts. Three microtextures developed during accommodation of strain are associated with folding and the formation of the pervasive foliation. A fourth microtexture is associated with the non-pervasive foliation.

Mesoscopic structures

Mesoscopic, tight to isoclinal minor folds of compositional layering are present locally (Fig. 3.10). They have an axial planar foliation which is developed more pervasively than the minor folds themselves. Fold axes are difficult to observe due to outcrop style but a few were observed and were subhorizontal and curvilinear.

The macroscopic foliation defining axial surfaces of minor folds is defined by inequant olivine and its mimetic replacements with long dimensions contained within the foliation plane (see Fig. 2.8.). S_1 is more pervasive than minor folds and it was observed throughout the unit. The orientation of S_1 is subparallel to S_0 except in the hinges of early isoclinal folds and together they comprise a transposed foliation, S_0/S_1 (Fig. 3.9). A second foliation defined by fractures and aligned metamorphic minerals is developed along both upper and lower contacts. Poles to both S_0 and S_1 have a girdle distribution on a stereonet, indicating that they are folded. The calculated fold axis or P_1 axis to the girdle is parallel to the F_2 fold axis in the overlying Redfern amphibolites (compare Fig. 3.9 with Fig. 3.21a).

Microscopic structures

Deformation mechanisms operative in a peridotite are determined by investigating the respective mechanisms for the constituent phases, olivine, enstatite, and diopside. The mechanisms which are active are dependent upon the temperature, strain-rate, stress, confining pressure, and fluid state of the rock during deformation (Carter, 1976). Experiments can be extrapolated to natural strain rates in rocks which show similar microstructures to those developed during experiments to infer mechanisms and conditions of natural deformation.

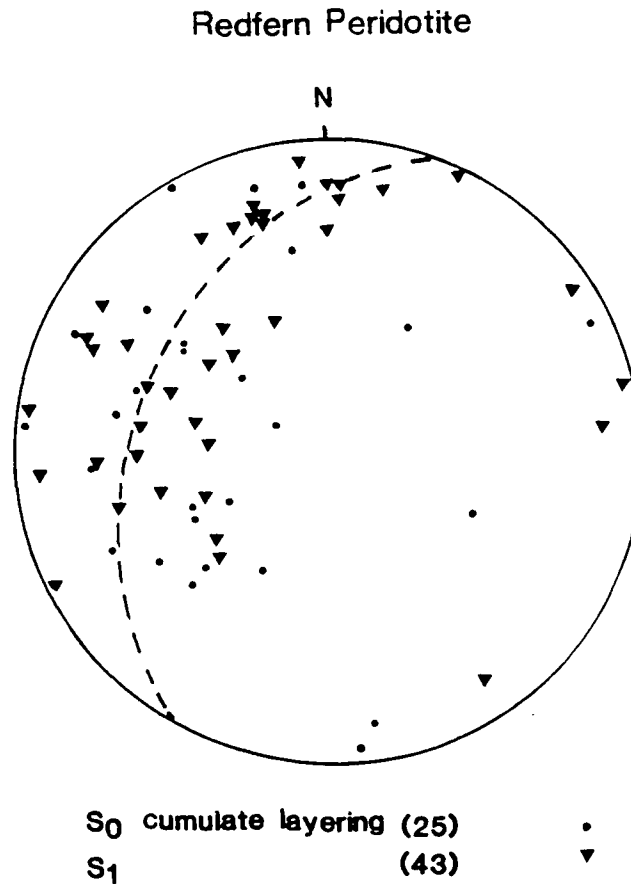


Figure 3.9: Equal-area stereoplot of poles to planar structures in the Redfern Peridotite. Number of points in parentheses.

Olivine deforms by translation glide along several independent slip systems dictated by its orthorhombic symmetry and crystallographic lattice parameters (Raleigh, 1968; Carter and Ave' Lallement, 1970). The most common slip system observed in natural rocks is the $(010):[100]$ system, and less commonly the $\{0kl\}: [100]$ and $(001):[100]$ (see, for example, Girardeau and Mercier, 1988). At laboratory strain rates of less than 10^{-7} sec^{-1} the first two systems are activated at $850\text{--}1000^\circ \text{C}$ or more and the last at much lower temperatures (see Figure 12, Raleigh, 1968; Carter and Ave' Lallement, 1970). However, Mercier (1985) argues that direct extrapolations of experimental data to natural conditions are not

warranted because experimental pressures are too low, most data do not represent steady-state creep, and the measured strain rates only apply to the highest temperature part of the sample. Therefore absolute pressures and temperatures must be determined independently for use in creep flow laws.

Large, permanent, ductile strains can only accumulate in a rock when deformation is accompanied by recovery. Recovery mechanisms in olivine include cross slip and glide-climb, producing neoblasts by dynamic recovery and dynamic recrystallization processes. Several recovery mechanisms can be active in a mineral at the same time but the fastest recovery mechanism will control the strain rate if the processes are independent. Cross slip and glide climb recovery operate by diffusion and require temperatures greater than approximately half the melting temperature of the mineral to be rate-controlling (Carter, 1976). Both mechanisms begin by the diffusion of dislocations out of their slip planes into sharp kink band boundaries, thereby concentrating the grain's dislocation density and strain energy. The crystal lattice is disorted across the kink band boundary by rotation about an external axis, perpendicular to both the kink band boundary and the slip direction (Carter and Raleigh, 1969; Nicolas and Poirier, 1975).

Dynamic recovery involves the progressive angular misorientation of subgrains separated by dislocation walls, a process known as polygonisation (Poirier and Nicolas, 1975). This is a recovery mechanism but it does not involve strain softening. Neoblasts formed by polygonisation can be recognized by local domains which have similar birefringence and close extinction angles, within 12^0 (Nicolas and Poirier, 1975). Sub-grain diameter is inversely proportional to total stress difference.

Neoblasts also form by dynamic recrystallization (Mercier, 1985). Dislocation pile-ups at grain and kink band boundaries produce high strain gradients which restructure themselves by the process of bulge nucleation into new grain boundaries. Once nucleated, the strain-free grains grow in the direction of the highest strain gradient, consuming the maximum number of dislocations and thus minimizing the rock's total strain energy. These neoblasts are recognized by their optical continuity and lack of undulose extinction, and slightly curved grain boundaries. This is a cyclic process which develops a foliation defined by a strong preferred crystallographic orientation of grains. The diameter of these neoblasts is also inversely proportional to stress (Ross et al., 1980).

Enstatite and diopside also deform by translation glide, both on the (100):[001] system above 1000⁰C (Raleigh, 1965; 1968). In addition, enstatite experiences a symmetry transformation to clinoenstatite below 1000⁰C with increasing strain rate and the mechanical exsolution of Ca atoms, producing diopside lamellae along (100) (see Nicolas and Poirier, 1975, p. 188). Diopside also undergoes mechanical twinning, with (100):[001] prevailing over (001):[100] at temperatures up to 1000⁰C, high stress difference, and low strain rates. Dynamic recovery mechanisms in the pyroxenes are inhibited by the presence of stacking faults, resulting in a high creep resistance and strain hardening in the higher temperature regimes where creep is climb-controlled (Nicolas and Poirier, 1975).

Experimentalists have observed that for a given strain rate, olivine has a viscosity 2-3 orders of magnitude less than enstatite or diopside (Nicolas and Poirier, 1975). Thus olivine will be the load bearing framework mineral of a peridotite and will control the rate of deformation.

Textures

Deformation textural terms are used to describe sets of microstructures developed by the activity of various combinations of deformation and recovery mechanisms under a particular set of conditions. Textural nomenclature was first developed to describe textures observed in mantle xenoliths within basalts (Mercier and Nicolas, 1975; Mercier, 1985). Because ophiolite peridotites formed in the mantle and then were deformed by crustal processes the xenolith mantle textures are useful for separating original textures from superimposed textures. Three textures were identified in the Redfern peridotite related to mantle deformation: deformed cumulate, protogranular and porphyroclastic. The last texture is called mosaic and is not formally described in the literature but is here used to describe a texture which overprints the other three. This texture formed later during crustal deformation.

Deformed cumulate textural type shows the most evidence of cumulate processes with little evidence of ductile deformation. It is characterized by large, subhedral grains of olivine and pyroxene and anhedral, interstitial chromite. The texture is homeoblastic with slightly curved grain boundaries. Large olivine grains are 0.4 to 10 mm in diameter, equant to slightly elongate and either display total optical

continuity or are slightly deformed, showing undulose or incomplete extinction produced by dislocation glide. Pyroxene grains are the same size or slightly smaller, display optical continuity and have straight cleavage planes with opaque inclusions (Fig. 3.10).

Protogranular texture (also called granoblastic, Mercier, 1985) is also homeoblastic and is described by Nicolas and Poirier (1976) as having a coarse grain size (4 mm) which has been reduced from a larger (10 mm) grain size through deformation. Olivine and enstatite typically have no preferred orientations (Mercier and Nicolas, 1975) and there is no foliation or lineation. However, groups of crystals with a close common orientation and straight mutual grain boundaries suggest that they evolved by continued rotation misorientation of subgrains (Nicolas and Poirier, 1976). Sharp (010) kink band

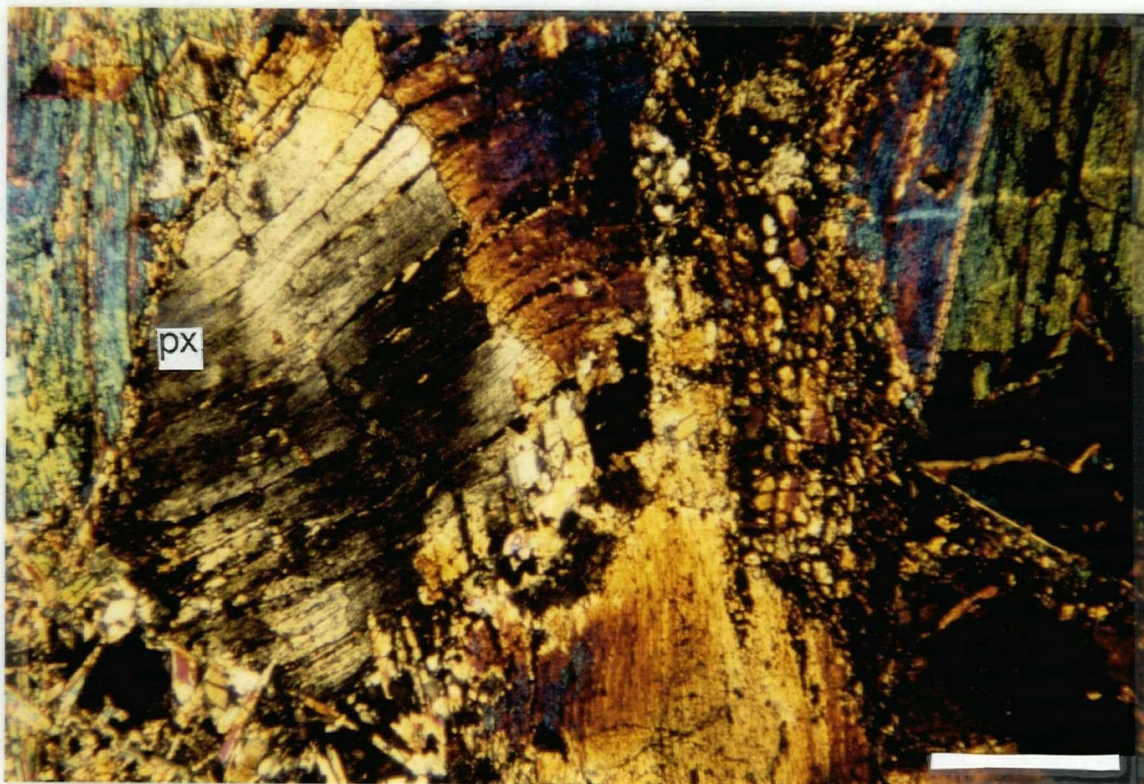


Figure 3.10: Deformed cumulate texture. Opaque inclusions in diopside show sweeping extinction, indicating the operation of translation glide DL019; scale bar is 2 mm.

boundaries and small dynamically recrystallized neoblasts along grain and kink band boundaries are moderately developed (Fig. 3.11).

Porphyroclastic texture is heteroblastic and generally has a bimodal grain size distribution. Large porphyroclasts are inequant (8x2 mm and smaller) and contain numerous subgrains having straight boundaries (Nicolas and Poirier, 1976). Neoblasts are abundant and form anastomosing zones of dynamic recrystallization resulting in a rock foliation. The foliation is enhanced by the preferred orientation of the new grains and the long dimension of porphyroclasts (Fig. 3.12). Many workers have noted the preferred orientations of neoblasts resulting in a crystallographic fabric of olivine with [010] perpendicular to the rock foliation and [100] parallel to the lineation (for example, see Ave' Lallement, 1967).

Mosaic texture is not formally described in the literature but is here used to describe a texture composed of the following features: large, equant olivine grains with undulose and irregular, patchy extinction (Fig. 3.13a); enhanced olivine mineral cleavage (Fig. 3.13b); a second rock cleavage, S_2 ; and rolling of small grains (Fig. 3.13a). These features are semi-brittle, formed by deformation mechanisms of both ductile and brittle nature. Low temperature ductile mechanisms include diffusion creep and translation glide on the low-temperature (001):[100] system without recovery producing the irregular extinction (see Figure 3.13a). Intragranular cracking along {010} cleavage planes and intergranular sliding are brittle and tend to develop along planes of previous weakness such as kink band boundaries, mineral cleavage planes, and S_1 planes marked by zones of neoblasts (Fig. 3.13b).

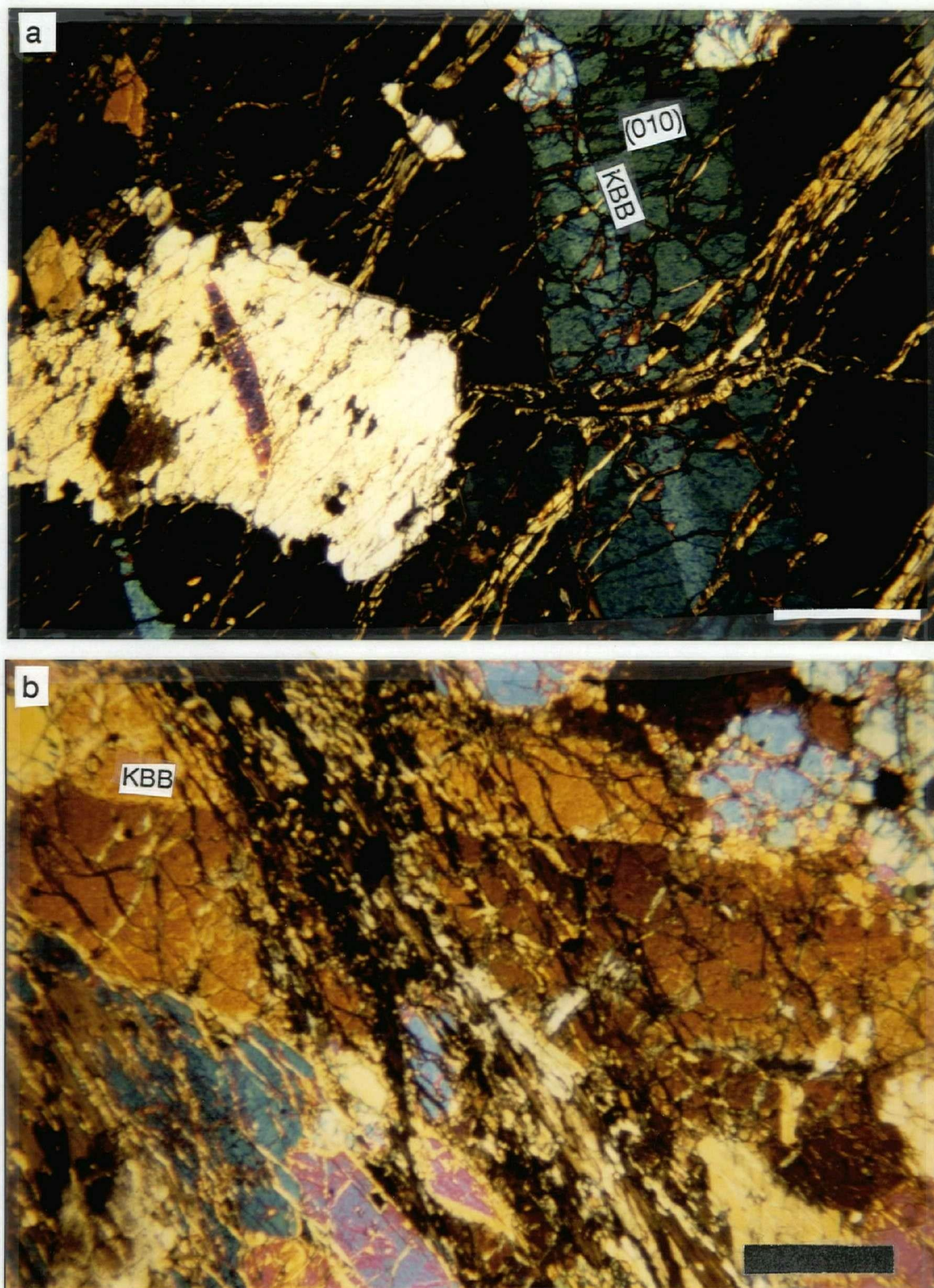


Figure 3.11: Protogranular texture. a) sharp kink band in olivine formed by translation glide along the $(010):[100]$ slip system, accompanied by climb perpendicular to the slip plane; b) kink band perpendicular to (010) slip plane in large olivine with neoblasts recrystallized along the kink band boundary (KBB), at right. Sample DL157, scale bars are 2 mm.

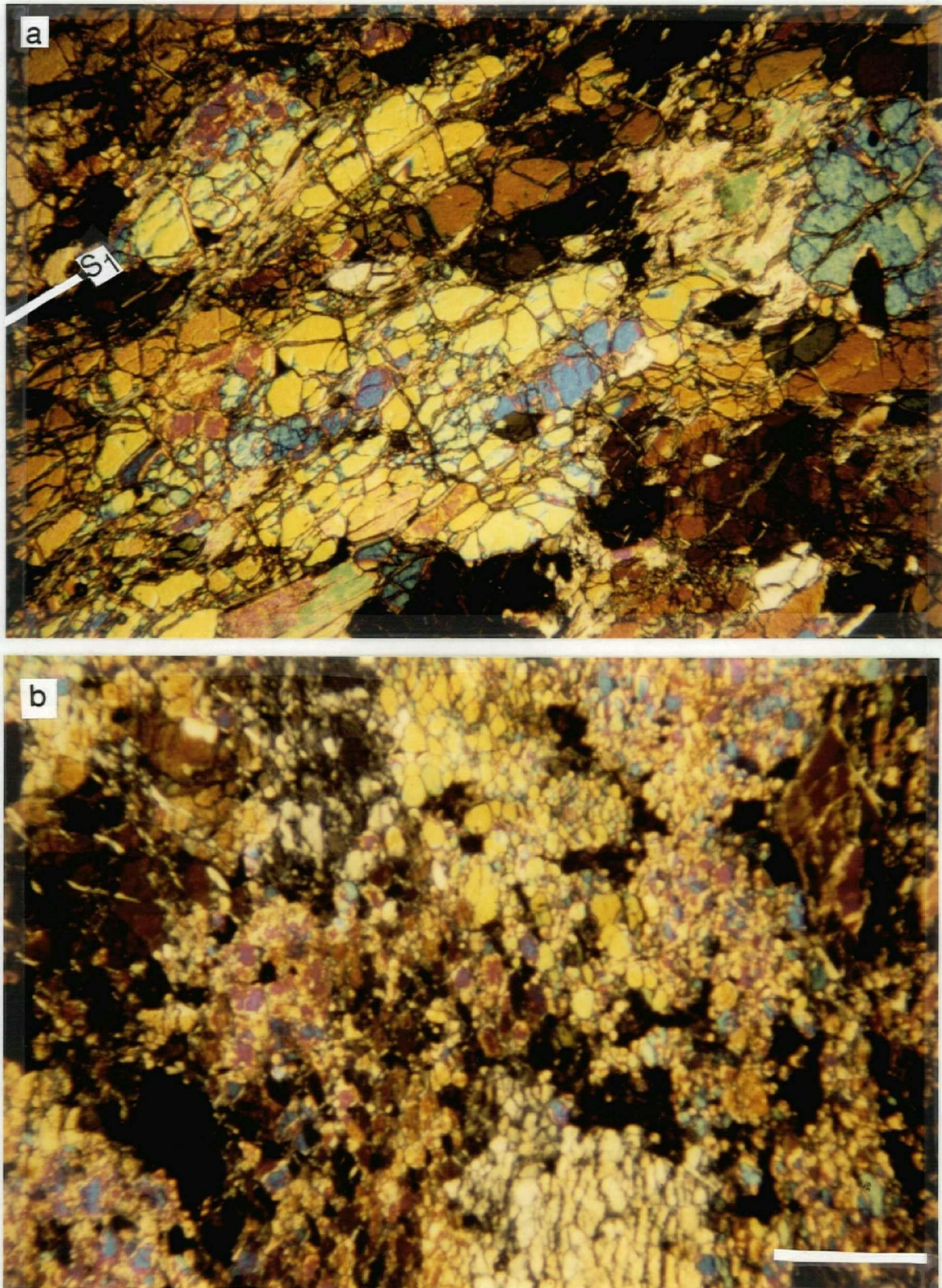


Figure 3.12: Porphyroclastic texture. a) strong dimensional orientation of olivine parallel to the trace of S_1 , DL014; b) deformed neoblasts of olivine, evidenced by differences in extinction position, DL116. Scale bars are 2 mm.

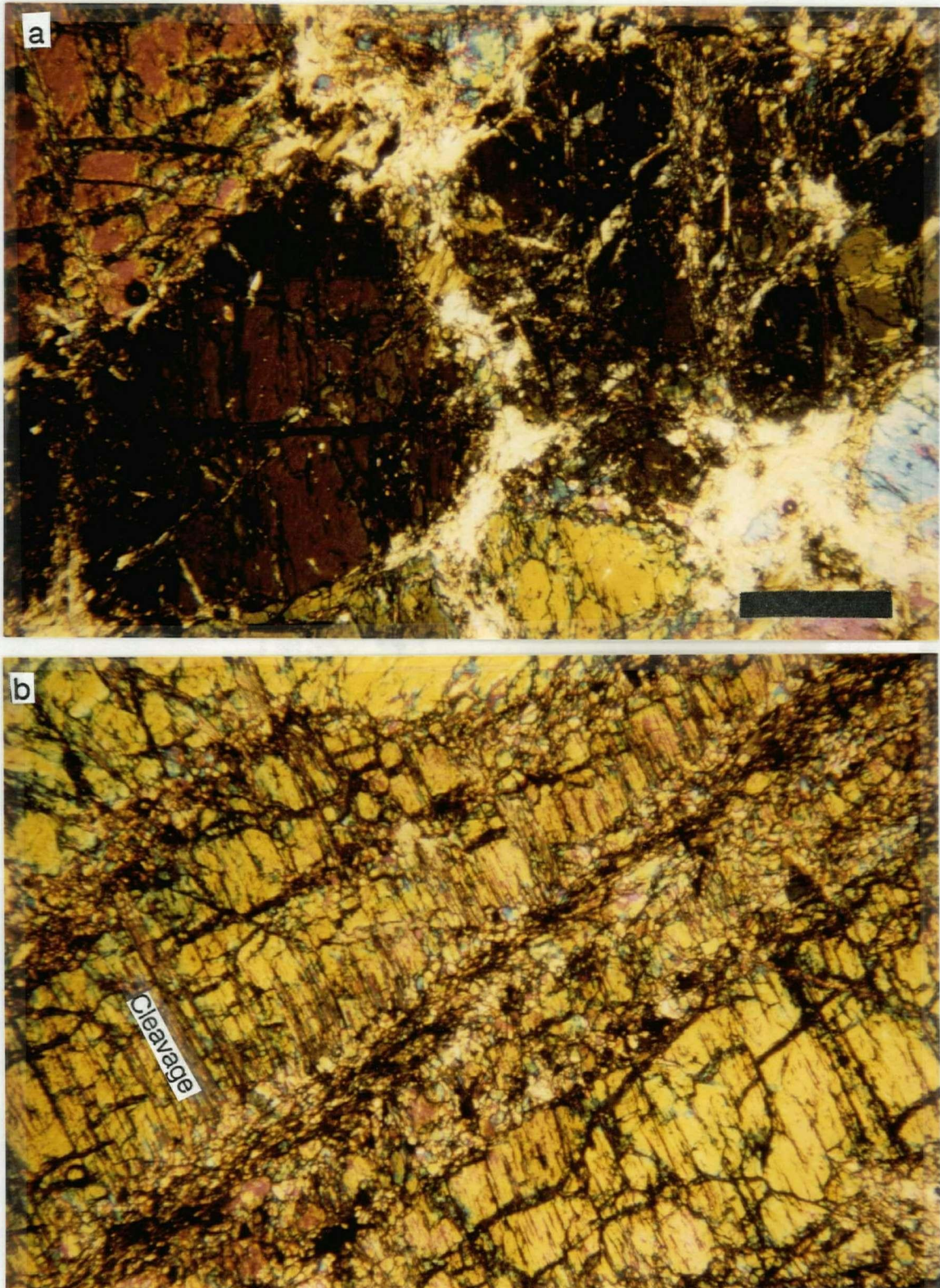


Figure 3.13: Mosaic texture. a) Patchy extinction produced by dislocation glide without recovery, indicative of low-temperature plasticity, DL088, scale bar is 2 mm; b) cleavage fracture along (010) and rigid rotation or rolling of neoblasts within microshear, sample DL088, scale bar is 0.5 mm.

Application to the Redfern Peridotites

The three mantle textures observed in the Redfern peridotite exhibit kink bands and neoblasts indicative of mantle conditions. The mosaic texture has fractures and rolled grains which indicate a crustal conditions. Figure 3.14 summarizes and illustrates the relative differences in temperature, pressure, stress, and strain rate for the dominant deformation mechanisms which formed each of the textures. Graphically these relative differences are shown on a deformation map, shown in Figure 3.15.

Both ductile and cataclastic flow in the upper mantle can be modelled by rate laws. During cataclastic flow two independent mechanisms may be operating: fracturing and rolling and sliding of granules (Ashby and Verrall, 1977). The stress necessary to initiate both mechanisms is simply a function of confining pressure and friction and the strain rate will be infinite if both mechanisms are operative (Ashby and Verrall, 1977). The flow law for ductile deformation of all rock types is a steady-state creep law of the form

$$\dot{\epsilon} = A \sigma^n \exp (-Q_c / RT)$$

where $\dot{\epsilon}$ is the strain rate, σ is the differential stress, T is the absolute temperature, n , Q_c , and A are essentially material constants (Kirby, 1985). The flow law constants and steady-state behaviour of olivine are well known, and strain rate is dominantly a function of temperature (for reviews see Kirby, 1985; Mercier, 1985; Carter, 1976).

Deformation within the Redfern peridotite is concentrated at the margins of the unit, shown by the distribution and development of deformation textures with respect to the structural stratigraphy (Fig. 3.16). Rocks with the deformed cumulate texture are the least strained and predominantly occur in the middle of the structural succession. With increasing ductile deformation rocks develop a protogranular texture and these are concentrated in the upper portions of both subunits 3A and 3B, and within dunites in unit 3B. The porphyroclastic and mosaic textures represent the most deformed rocks under any conditions and occur almost exclusively on the margins of the unit.

Evolution of the Redfern peridotite and the deformation textures within it are interpreted in the following way. The cumulate layered unit and possibly the basal dunite accumulated at the base of a magma chamber below a spreading axis. The depth of this chamber is not known but it was probably

a

TEXTURAL SUMMARY

Texture	T	P_c	σ_D	$\dot{\epsilon}$
MANTLE				
Deformed Cumulate	high	high	low	low
Protogranular	high	high	higher	low
EMPLACEMENT				
Porphyroclastic	lower	high	highest	higher
Mosaic	lowest	lower	highest	highest

b

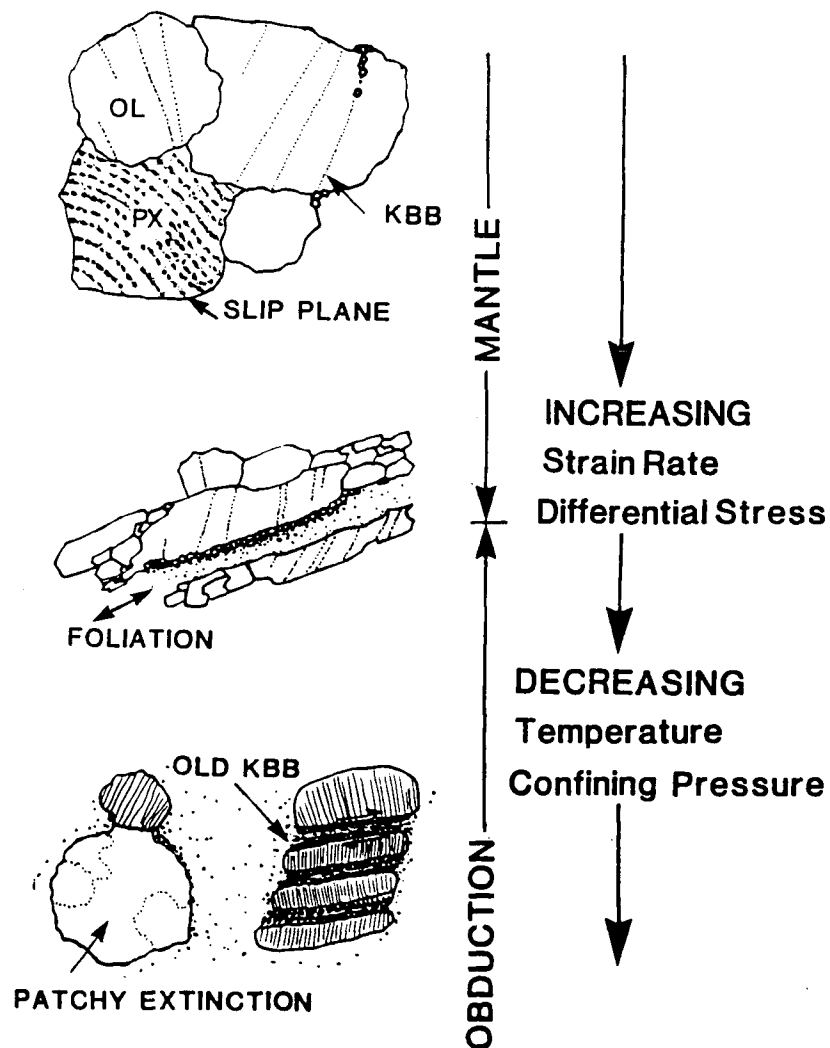


Figure 3.14: Summary of peridotite microtextures. a) Relative conditions of texture formation; b) schematic illustration of progressive textural development.

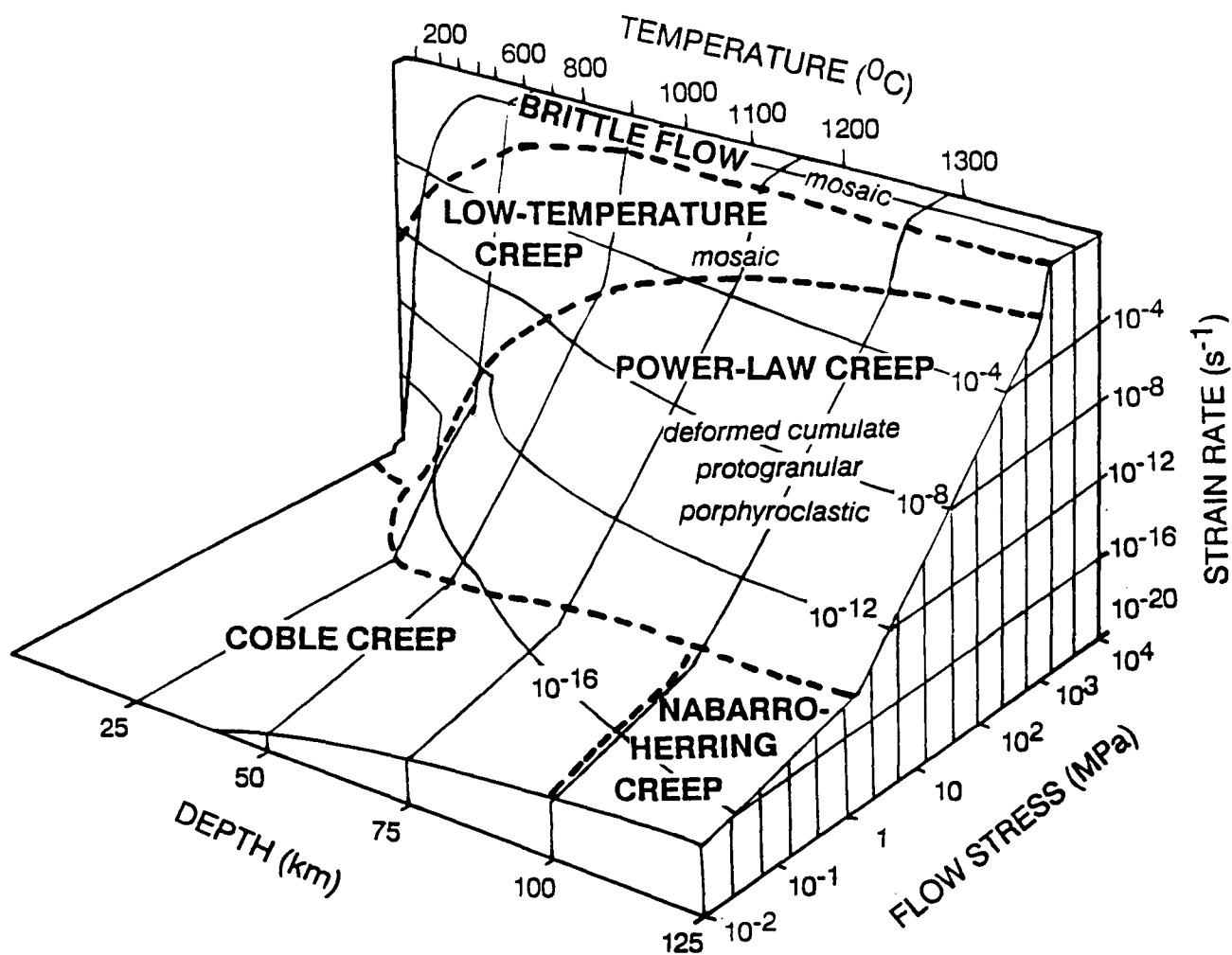


Figure 3.15: Deformation map for single crystalline wet olivine, diameter = 1 mm, and polycrystalline peridotites and dunites. Textures from the Redfern peridotite in italics under corresponding deformation regimes. After Tsenn and Carter, 1987; brittle flow field approximate, after Ashby and Verrall, 1977.

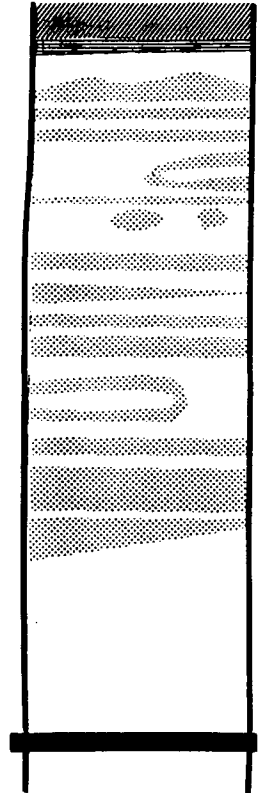
	LITHOLOGY	TEXTURE	TEXTURAL ORIGIN
	Amphibolite	Transposed Foliation	Emplacement
	Dunite	Mosaic on Cumulate	Emplacement on Mantle
	Dunite	Porphyroclastic	
	Px-Peridotite	Deformed Cumulate	
			Mantle
	Dunite- Px-Peridotite	Protogranular to Porphyroclastic	
	Dunite	Protogranular	
	Dunite	Mosaic on Protogranular	Emplacement on Mantle
	Snowshoe		

Figure 3.16: Peridotite microtextural distribution in the structural-stratigraphic succession, and inferred tectonic setting of textural genesis.

between 10 and 35 km, on or near the petrologic Moho (Coleman, 1977; Ashby and Verrall, 1977). Mantle conditions of high temperature (> 0.5 the melting temperature of olivine), high confining pressure, and low strain rate plus a low deviatoric stress mildly deformed the cumulates, producing the deformed cumulate and protogranular textures. Development of a porphyroclastic texture represents the localization of shear strain. The shear zone is at the base of the Redfern peridotite and may have resulted from the initiation of the thrust fault along which the peridotite was obducted. This is a common occurrence in ophiolites although the development of the porphyroclastic texture in the Redfern peridotite is not as extensive as that developed in mylonites at the base of other ophiolites (e.g. - Xigaze: Girardeau and Mercier, 1988; White Hills: Girardeau, 1982; Vourinos: Ross et al., 1980; Lanzo: Boudier, 1978). Prolonged shearing by ductile flow would be expected to produce a well-defined shear zone with a strong asymmetry and kinematic imprint (see Juteau et al., 1977; Ave' Lallement, 1976). This suggests that the shear zone at the base of the Redfern peridotite did not form under ductile conditions. This is supported by the strong overprint of the brittle mosaic texture on the weakly developed porphyroclastic, and in places protogranular, texture. In summary, a shear zone at the base of the Redfern peridotite may have initiated in the ductile regime but quickly was moved to the brittle state. An increase in shear stress and also probably a drop in both temperature and confining pressure due to uplift accompanied the ductile to brittle transition.

3.4.2. Redfern Amphibolite and Triassic Black Phyllite

The Redfern amphibolite and Triassic black phyllite metasedimentary rocks contain structural elements from three deformation phases, some pervasive while others are inhomogeneously developed. The development of the earliest phase structural elements S_1 and L_1 is pervasive but varies in intensity. The second phase consists of regional buckle folding of S_1 about an axis subparallel to L_1 and is accompanied by the limited development of S_2 , an axial planar crenulation cleavage in the metasedimentary rocks. Minor folds are rare in the amphibolite and more abundant in the metasedimentary rocks and where observed, F_2 fold axes parallel L_1 .

Phase 1

Phase 1 structures consist of a foliation, S_1 , a lineation, L_1 , and rarely observed minor folds (Fig. 3.17). Bedding is not inverted overall and the structural sequence represents a shortened and disrupted stratigraphic sequence. However, at the base of both units, S_0 becomes transposed parallel to S_1 and mylonites (Fig. 3.18) and blastomylonites are noted in the amphibolite. Both S_1 and mylonitic fabrics are folded by phase 2.

A planar foliation in the amphibolites, S_1 , consists of a preferred orientation of grain boundaries parallel to compositional layering and/or lenticular mineral aggregates. Long dimensions of hornblende, inequant quartz and plagioclase are contained within the foliation plane while short dimensions are



Figure 3.17: Very tight F_1 fold in the Redfern amphibolite. White layer may have been an early vein.

normal to the foliation. Planar arrays of hornblende-rich layers alternating with layers rich in quartzofeldspathic material define a gneissosity. Rarely, hornblende crystals are found growing at a low angle across compositional layering. On a microscopic scale, epidote and sphene-rich lenses one to a few grains thick also define the gneissosity. Thickness of gneissic layers is most commonly only several grains but ranges up to about 10 cm. A second common foliation type is defined by planar distributions of grain-size variations. Most commonly, thin layers 1-50 mm of very fine-grained hornblende occur between coarser-grained material. Structurally higher in the section closely spaced discontinuities are parallel to the axial plane of minor folds; some are filled with calcite. Microlithons between discontinuities are 1-5 mm wide and within them hornblende needles are strongly aligned parallel to the walls.

Where compositional or grain size segregations are absent the preferred orientations of hornblende prisms define a linear fabric. Quartz rods are also found parallel to the aligned hornblende and comprise an intersection lineation between S_1 and compositional layering. The lineation is always present on S_1 surfaces. Lineations consistently plunge southeast throughout the field area.

Extremely rare tight to isoclinal minor folds of bedding (?) or compositional layering and veins in the amphibolites have axial planes parallel to S_1 , suggesting that S_1 formed as an axial planar foliation to a regional fold set (Fig. 3.17). Structurally higher in the unit folds open up and they have a rounded hinge which shows considerable thickening with planar limbs. The paucity of minor folds may be attributed to the lack of primary layering in the starting material. The basal lithology, in which S_1 is best developed, was probably a gabbro with little or no layering which now bears a strong gneissosity inferred to have formed by metamorphic differentiation accompanied by shear and/or flattening. F_1 fold axes are parallel to the mineral lineation L_1 . As the base of the amphibolite is approached the strike of the foliation plane becomes sub-parallel to the trend of the contact. Extremely fine-grained layers interpreted as mylonites and porphyroblastic mylonites with an anastomosing foliation defined by lensoid aggregates of quartz and fine-grained hornblende pressure shadows of equant hornblende pseudomorphing pyroxene are common near the base. In the 80 m thick section on the slope west of Spanish Creek, the entire amphibolite unit bears a prominent, very planar mineral cleavage which is independent of grain size. Upwards from the basal contact the planar foliation becomes less pervasive. These features are interpreted

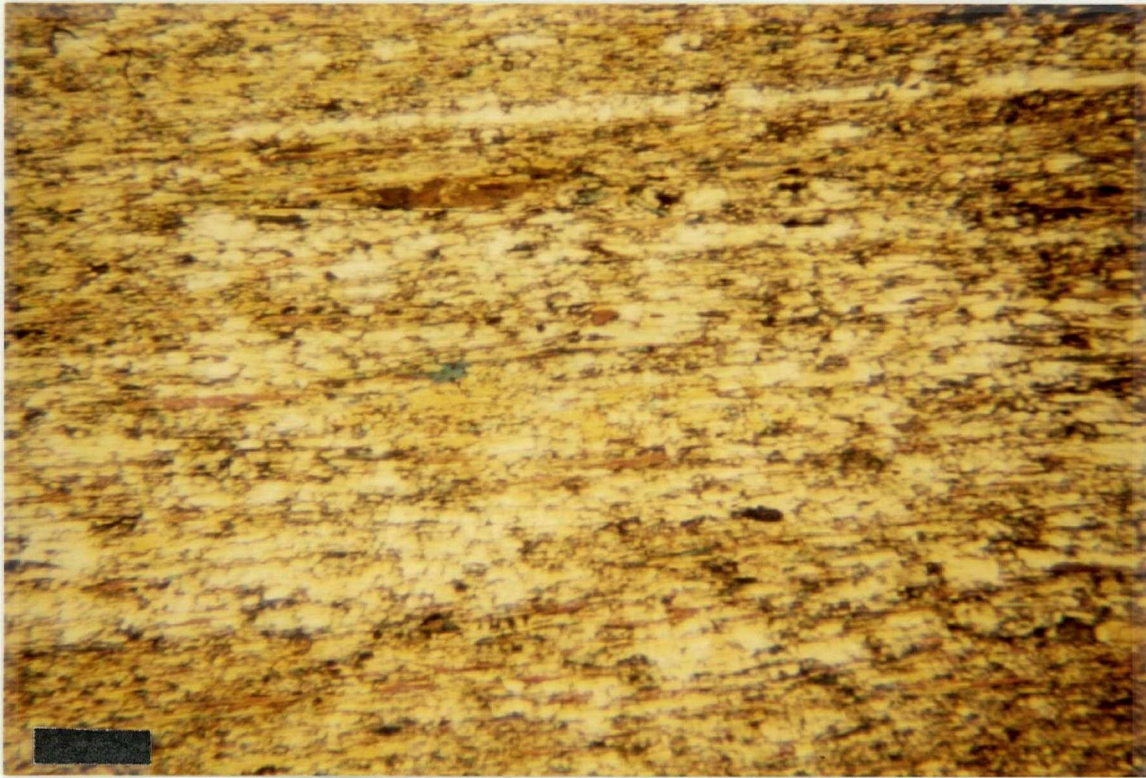


Figure 3.18: Extremely fine-grained Redfern amphibolite from the base of the unit, sample DL086: mylonite. Scale bar is 2.5 mm.

as marking an increase in shear and/or flattening strain near the base of the unit. This increase comprises a sharp strain gradient approaching the lower contact where the amphibolites become tectonically intercalated with ultramafic rock.

In the Triassic black phyllite phase 1 consists of tight to isoclinal folding of bedding with a well-developed axial planar schistosity. Bedding is defined by gross compositional banding outlined by micas and lenses of quartz-rich material. Although the rocks are extensively recrystallized, rare sedimentary structures such as silty laminae and rip-up clasts reveal the presence of relict bedding. An axial planar schistosity, S_1 , is defined by aligned micas and dimensional orientations of quartz and feldspar parallel with compositional layering. Within the staurolite schist, intrafolial hinges and foliation parallel compositional banding indicate that bedding has locally been transposed parallel to the foliation (Fig. 3.19). On a regional



Figure 3.19: Intrafolial D_1 folded quartz vein in Triassic black phyllite.

scale S_1 consistently strikes northwest and dips moderately steeply to the northeast (Fig. 1.1). Examination of hand samples and thin sections reveals that S_1 is pervasively folded.

Phase 2

Phase 2 consists primarily of folding of S_1 and the contacts and has produced the current map pattern of units. The amphibolite and TBP were the two structurally highest units prior to D_2 and consequently both occupy the cores of phase 2 synforms. The hinge is interpreted to be very tight as most orientations of S_1 are parallel to the limbs (see Fig. 1.1). No hinge orientations of S_1 were measured in the TBP and its synform is interpreted to have a cusate hinge (see Fig. 1.2). Minor D_2 folds of a limestone surrounded by phyllite have cusate-lobate hinges (Fig. 3.20). This indicates a large competency contrast between the two lithologies, the one occupying the core of the cusp being less competent (phyllites



Figure 3.20: Cusate-lobate D_2 folds in Triassic black phyllite. Matrix is fine-grained graphitic calc-silicate while prominent layers are more quartz-rich and competent. Coin is 19 mm in diameter.

and TBP) which is consistent with conditions of buckle folding (Ramsay, 1967). A stereonet plot of S_1 in both units reveals that it is folded about a phase 2 axis plunging 35° toward 125° (Fig. 3.21). Minor folds are more common in the metasedimentary rocks than in the amphibolites, and have variably dipping axial planes with southeast trending hinges. In the metasedimentary rocks two lineations are present in hand specimen. The first is defined by curvilinear crenulation axes and plunge gently to the southeast. The second is defined by recrystallized aggregates of commonly fibrous quartz, frequently in pressure shadows of large staurolite porphyroblasts. These are oriented generally downdip of the S_1 plane. A stereonet plot of L_1 lineations shows a spread of orientations about a calculated P_1 axis to the girdle containing poles to S_1

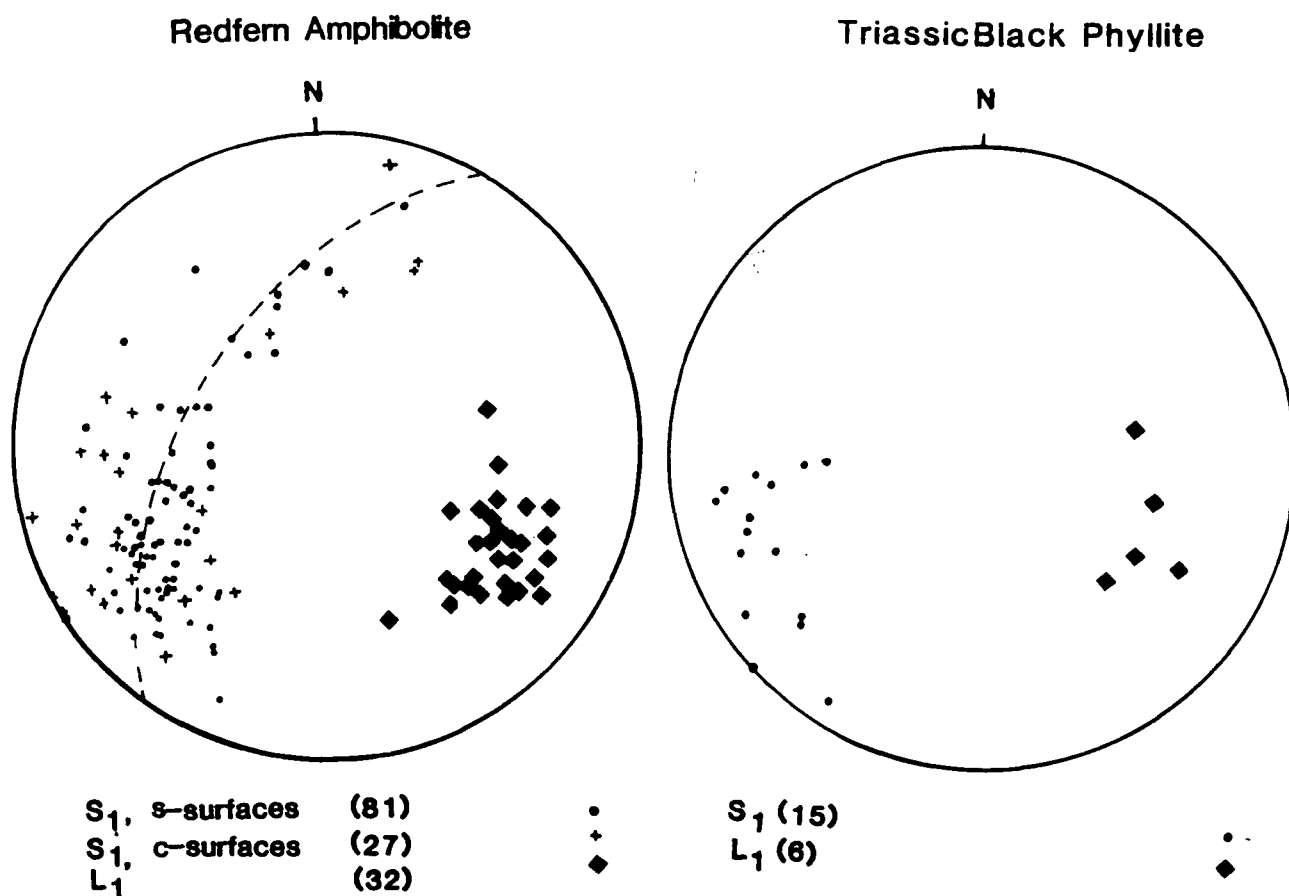


Figure 3.21: Equal-area stereoplots of D_1 planar and linear structures in the upper plate rocks; number of points in parentheses. a) Redfern amphibolite, Pi-girdle with orientation 215/35 NW; b) Triassic black phyllite.

(Fig. 3.21). They occupy a locus that appears to be part of a small circle, indicating that they have been folded by a buckle fold mechanism.

On a microscopic scale, folds are locally disharmonic within the porphyroblastic staurolite schist. An S_2 crenulation cleavage defined by micas at a moderate angle to S_1 (Fig. 3.22) is strongly deflected around early syn- D_2 porphyroblasts.

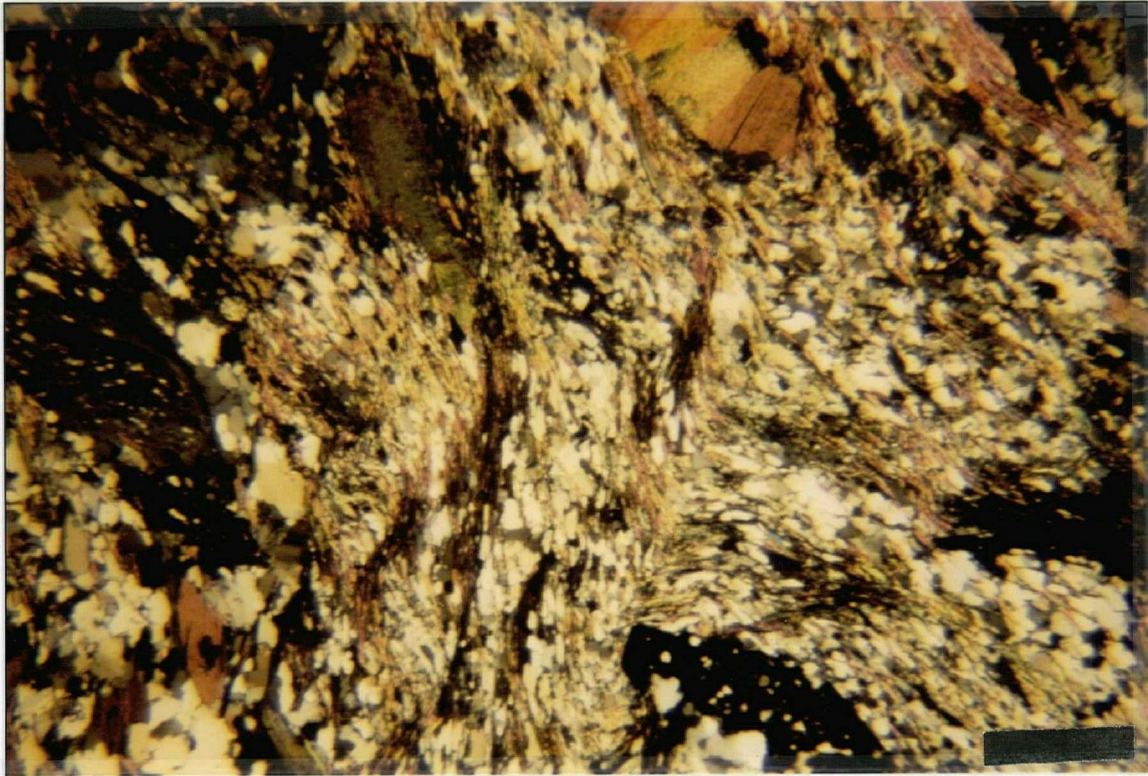


Figure 3.22: Photomicrograph of D_2 crenulation cleavage in Triassic black phyllite staurolite schist. Scale bar is 2 mm.

Phase 3

Local crenulations in both units distort earlier mesoscopic structures at a high angle to F_2 axes, and are believed to be associated with a phase 3 fold set. Within the staurolite schist it is difficult to distinguish the F_2 from F_3 axes as cross-folding relationships are unclear.

3.5. DISCUSSION

The upper and lower plate assemblages have between them a surface of separation which is interpreted as a fault, informally named here the Redfern fault or thrust. The fault is defined by contrasting structural geometries in the rocks above and below it, the geometry of the separation surface,

and strain patterns believed to be associated with its development. Structures associated with movement along the thrust are the first common phase between the two assemblages and the thrust is folded by the last large scale fold event which is D_3 in the lower plate and D_2 in the upper (see Fig. 1.2). Not only are the two assemblages believed to be different ages but the lower plate assemblage has experienced one earlier phase of crustal deformation absent in the upper plate, the development of the pervasive S_0/S_1 transposed foliation. The truncation of successively higher structural levels by the fault illustrates that the fault has a ramp structure. Examination of strain patterns, the distribution of strain within and between units, reveals that there is a sharp strain gradient perpendicular to the fault zone.

The geometry of the lower plate rocks consists of a transposed foliation which is refolded twice by coaxial NW-SE trending fold phases. The first refolding event was so intense that the axial planar cleavage developed makes a small angle with S_0/S_1 and the two first phases essentially act as one during the second refolding, D_3 . This refolded geometry is illustrated schematically in Figure 3.23 as form lines representing both S_0/S_1 and S_2 are shown tracing out the fold form of two antiform-synform sets in the Dunford Lake region. In contrast, the geometry of the upper plate rocks is defined by a single refolding of a pervasive foliation S_1 which becomes locally transposed in the amphibolite and metasedimentary lithologies. The foliation is sub-parallel to the Redfern thrust along the fault itself and at the contacts between units in the upper plate (Fig. 3.23). Elsewhere the foliation traces out the limbs of the same synform-antiform sets as do the fabrics in the lower plate rocks.

The trace of the Redfern thrust is best defined by the upper contact of the Snowshoe Group. As the trace of the fault is followed west to east, successively higher structural levels in rocks of the upper plate are juxtaposed against structurally higher levels within the lower plate (Fig. 3.23). Although local transposition of compositional layering is recognized in the upper plate, the gross succession of units shows no inversion and the sequence has been shown to young structurally upward. Therefore, the higher structural levels in the upper plate are represented by succeeding rock units as defined by the structural stratigraphy (Fig. 2.1). In the lower plate rocks, regional compositional layering has been regionally transposed, making the definition of succeeding structural levels dependent upon the delineation of marker layers. Only one suitable marker layer was found in the Dunford Lake area, the marble marker unit, and

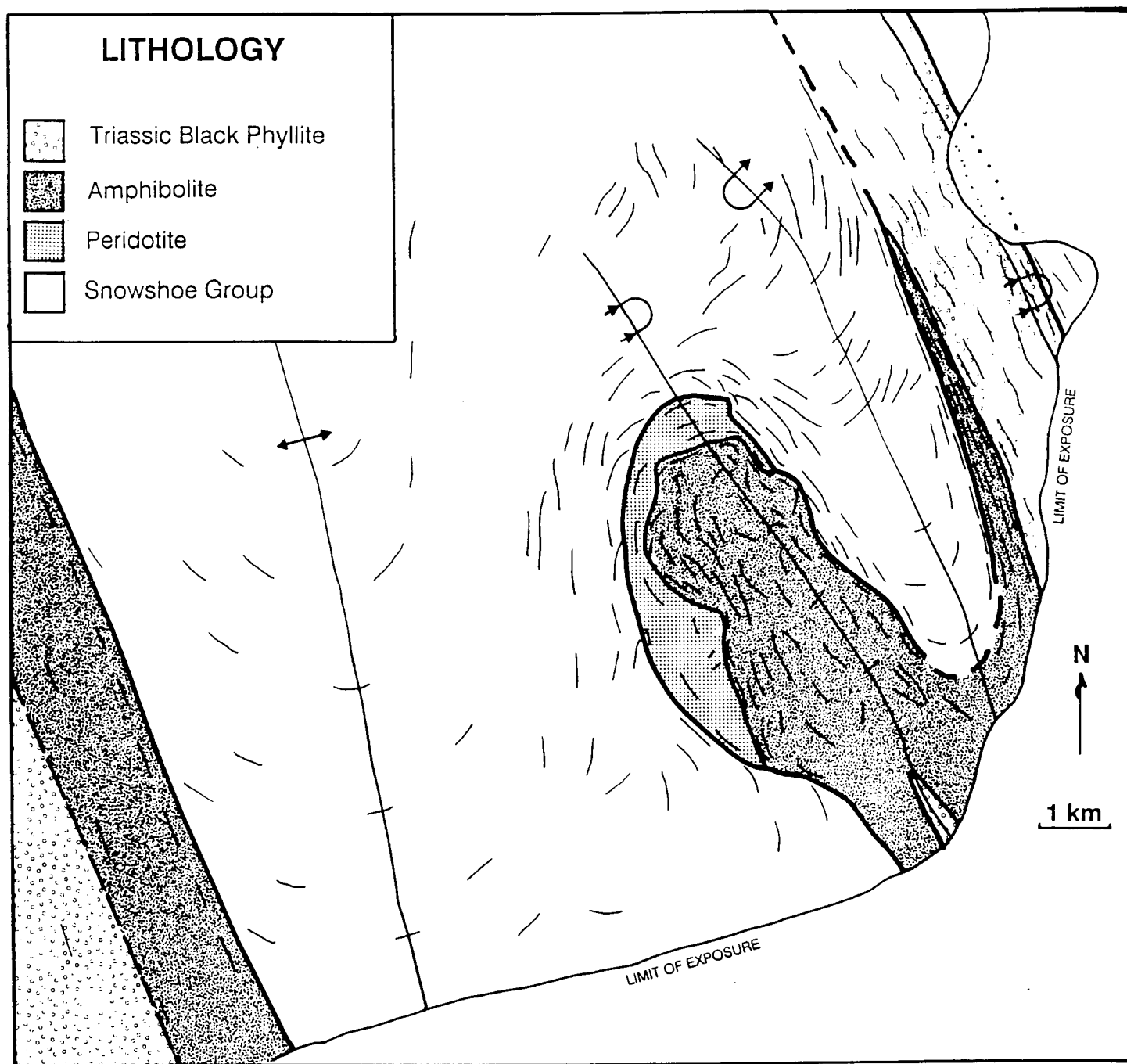


Figure 3.23: Map of formlines showing trace of S_0/S_1 and S_2 in the lower plate and S_1 in the upper plate. Additional data from Campbell, 1978, for Crooked Amphibolite and Triassic black phyllite on west side of map.

its trace which defines S_0/S_1 is shown on Figures 1.1 and 3.23. This marker unit illustrates both the truncation of S_0/S_1 by the Redfern thrust and the higher structural levels in the Snowshoe Group exposed as the fault is traced eastwards. Along the west side of the map area to the vicinity around Dunford Lake, the Redfern thrust places the Redfern peridotite on top of the Snowshoe Group at the level of the marble marker unit. Tracing the fault east of Dunford Lake, ultramafic rocks pinch out and the Redfern amphibolite contacts the Snowshoe Group above the marble layer. Further east, amphibolites also pinch out and the Triassic black phyllite contacts the Snowshoe. This successive upcutting of the Redfern thrust is illustrated schematically in Fig. 3.24 showing that when it is unfolded, the thrust comprises a west-dipping ramp structure in the Dunford Lake area. This ramp geometry implies an eastward vergence for the thrust, parallel to the inferred transport direction of the upper plate rocks.

The style and development of foliations and minor folds delineate the strain patterns related to the development of the fault and the partitioning of strain amongst the units during fault-related deformation. Foliations defined by aligned metamorphic minerals contained within axial planes of folds and/or planes of shear strain are variably developed in all rock units. Strain is interpreted to have been comparatively more concentrated where foliation planes are most closely spaced, metamorphic grain size is smallest, and the alignment of minerals is most pervasive.

Strain patterns related to thrusting comprise steep strain gradients perpendicular to contacts and partitioning of bulk strain preferentially to the least competent units. The thrust contact between the Snowshoe Group and the Redfern peridotite developed a steep strain gradient, reflecting the great competency contrast between the units. The Redfern peridotite was mechanically much stronger and only developed semi-brittle microstructures up to at most 30 m above its base. The conditions required to form semi-brittle microstructures in peridotites require elevated temperatures but mostly high shear stress (Fig. 3.15; Ashby and Verrall, 1977). In many areas along the contact ultramafic rocks have been extensively metasomatized and they exhibit obscure or chaotic fabrics. This is believed to indicate the presence of fluids along the contact during thrusting which gave rise to elevated pore pressures that facilitated and localized shear strain. In the Snowshoe Group near the thrust, only one planar foliation is seen, suggesting that S_0/S_1 and S_2 may have been rotated into parallelism as a result of highly advanced shear strain.

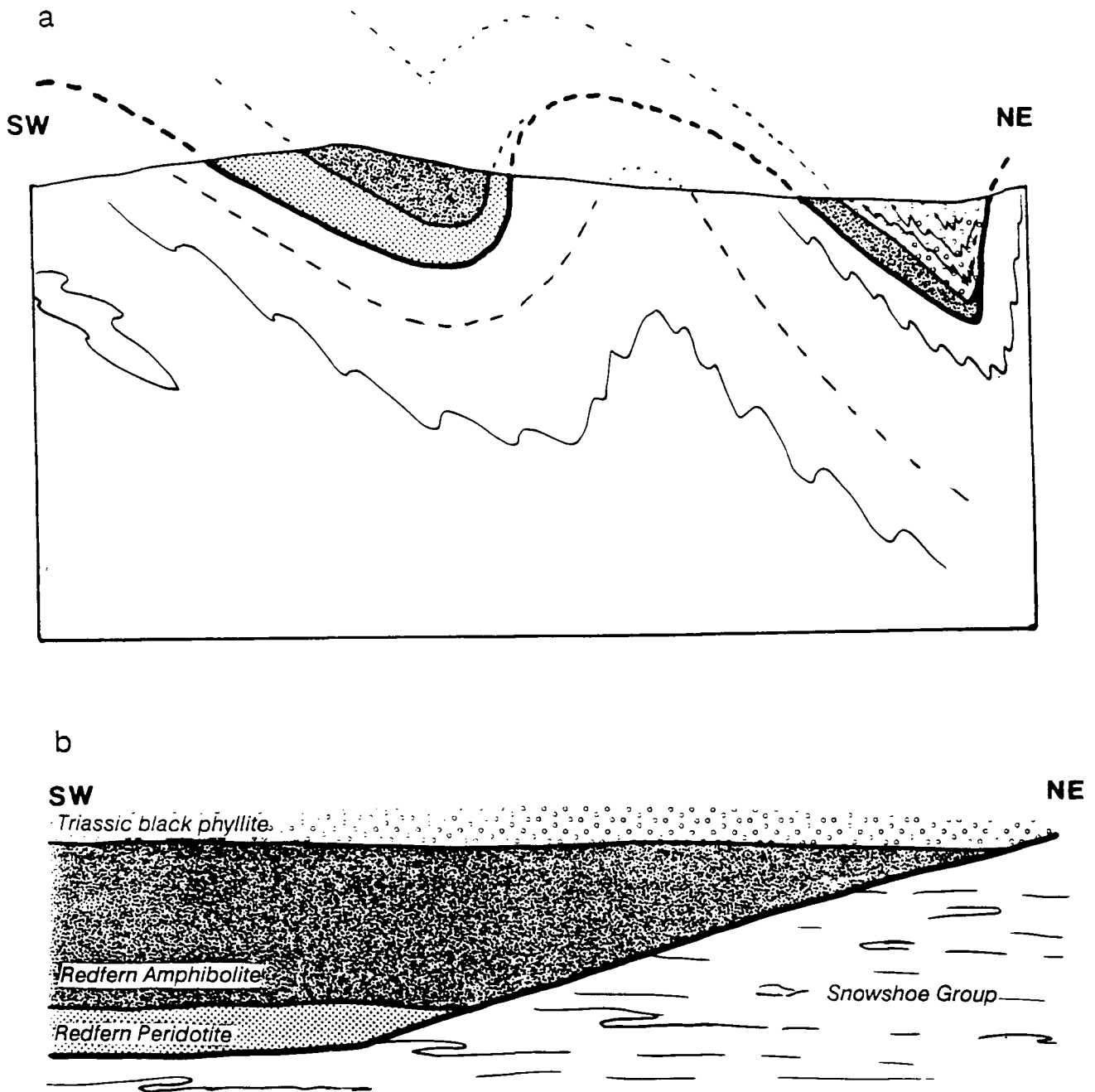


Figure 3.24: Schematic unfolding of the Redfern Thrust. Patterns same as Fig. 3.23. a) schematic reproduction of structural cross-section (Fig. 1.2); b) schematic restoration of cross-section after unfolding, showing eastward upcutting of thrust, comprising a ramp structure. True thickness of amphibolite will depend upon steepness of ramp.

Bulk strain was partitioned preferentially into the less competent units. The Snowshoe Group is relatively weaker than the Redfern peridotite which internally shows no structures related to emplacement. The overlying amphibolite was also much less competent than the peridotite and also shows a steep strain gradient across its contact with the peridotite, expressed in the intensity of foliation development. This contact is another metasomatized zone along which shear strain was concentrated, enhanced by elevated pore pressure. Overall, D_1 folding and the development of S_1 in the amphibolite in contrast to the essentially D_1 strain-free Redfern peridotite demonstrates that the bulk of D_1 strain was accommodated in the amphibolite. The Redfern peridotite body behaved like a large, competent boudin around which less competent material, amphibolite and Snowshoe schist, flowed during D_1 (D_2 in the Snowshoe).

Field observations suggest that slip along the thrust was reactivated during later folding. This fold event has been shown to comprise D_3 in the lower plate and D_2 in the upper plate. All of the units have a common fold axis but the axial plane is curved, consistent with buckle-style folding of an unconformity, the Redfern thrust. D_3 minor folds in the Snowshoe are most abundant and tightest immediately adjacent to the Redfern thrust, becoming less common and more open away from the fault, illustrated in Fig. 3.24. It is interpreted that these folds accommodated shortening during D_3 in the Snowshoe Group. Since the Redfern peridotite was essentially incapable of forming folds, the two units must have decoupled, presumably along the previously weakened slip surface of the Redfern thrust.

4. METAMORPHISM

4.1 INTRODUCTION

In terms of both structure and metamorphism, rocks of the study area comprise lower plate and upper plate assemblages separated by the Redfern thrust. All of the rocks in the study area were metamorphosed to middle-amphibolite facies corresponding to kyanite to sillimanite grade in the pelitic rocks. Subtle differences in the timing of growth of metamorphic minerals with respect to deformation phases exist between upper and lower plate assemblages. The peak metamorphic mineral assemblages and textures in the Redfern gneiss, amphibolites, and ultramafics indicate general conditions of deformation and metamorphism. The proto-igneous lithologies have ambiguous microtextures due to a lack of primary features and partial annealing by a post-deformational thermal event which obscures many of the textural relationships.

It is the two pelite bearing lithologies that contribute data which refines estimates of metamorphic conditions and places constraints on relative timing of deformation. The Snowshoe Group reached temperatures and pressures capable of crystallizing sillimanite during and after D_2 in the lower plate. Retrograde effects are minor. The metapelites of the Triassic black phyllite reached at least kyanite grade during and after D_1 . Temperatures dropped and staurolite completely recrystallized in the Triassic black phyllite during extensive during and following D_2 retrogression.

In comparison to the regional metamorphic history of the upper plate, rocks of the Redfern Complex experienced much more intense metamorphism. Rocks from the contiguous Crooked Amphibolite which are correlative with the Redfern Complex developed only D_1 chlorite zone assemblages during and after D_1 (Campbell, 1971; Campbell, 1978; Elsby, 1985).

4.2 LOWER PLATE: SNOWSHOE GROUP

One main phase of metamorphism is recognized in the Snowshoe Group rocks, beginning in D_1 and outlasting D_3 . Other workers have separated this into two distinct phases, M_1 and M_2 , plus a final retrograde stage (Ross et al., 1985). The first phase, M_1 , consisted of regional recrystallization of quartz,

muscovite, biotite, and plagioclase coincident with ductile deformation and the development of a transposed foliation, S_0/S_1 (Fillipone, 1985). Recrystallization associated with M_2 has obscured most of the evidence of M_1 . In this study the two phases are considered together.

The peak assemblage of sillimanite + garnet + staurolite + biotite + muscovite + quartz + plagioclase \pm kyanite formed during and after D_2 . The effect of retrogression was minimal. The most important new observation is the identification of sillimanite throughout the map area. The sillimanite isograd as mapped by Campbell (1978) previously excluded this region from the sillimanite zone. New isograds are proposed and presented in Figure 4.1.

Additional textural evidence for metamorphic reactions and results from garnet-biotite geothermometry are drawn from other work to augment inferences on the conditions of metamorphism.

Garnet

Garnet is ubiquitous, occurring in pelitic schists, quartzites and amphibolites. Grain size ranges from <0.5 mm fragments to 7 mm subidioblastic porphyroblasts. It is always poikilitic, containing inclusions of quartz, muscovite, plagioclase, and rarely sphene and zircon. These inclusions commonly trace out a planar or folded foliation and may be continuous with embayments of the external foliation into the garnet. The foliation S_2 commonly bends around garnets (Fig. 4.2). Other workers have documented two stages of garnet growth indicated by inclusion free, idioblastic rims around poikilitic cores (see Garwin, 1987; Fillipone, 1985; Engi, 1984). Although two stages of growth were not recognized here, long, continuous growth of garnet preceeding and spanning D_2 is evident.

Staurolite

Idioblastic staurolite prisms 0.25 to 2 mm in diameter contain arrays of inclusions with trends parallel to the matrix foliation. Crystal faces are common but long crystals are also broken. Staurolite is associated with post- D_2 porphyroblasts of kyanite and garnet, and also with sillimanite. It is absent in the only sample which contains sillimanite and not kyanite. Cross-sections of prisms may be seen in thin sections cut parallel to L_2 , indicating predominantly post- D_2 growth (Fig. 4.3).

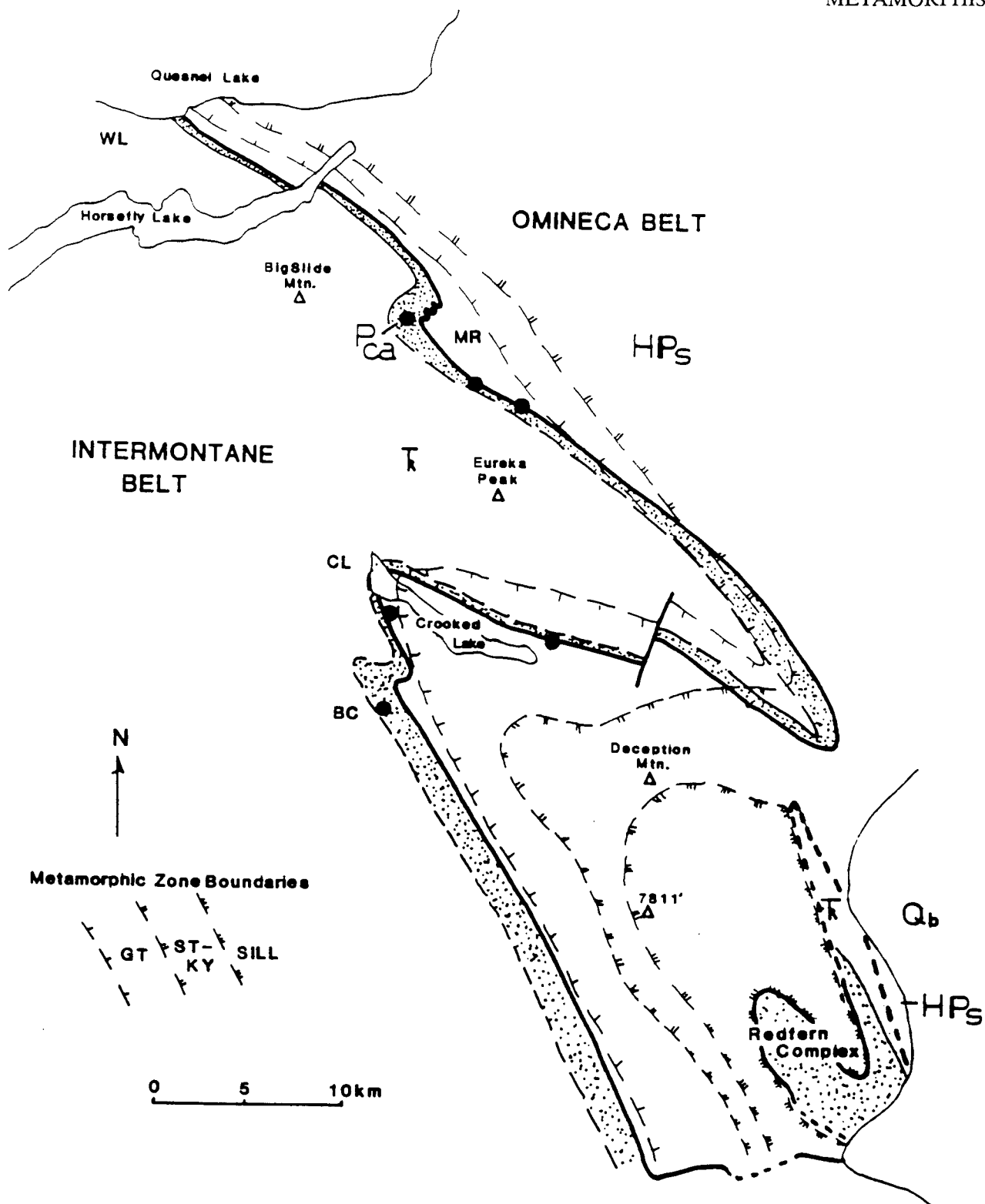


Figure 4.1: Metamorphic isograds of the southern Quesnel Lake region, after Campbell (1978) and modified after this study. Crooked Amphibolite stippled and sampling sites shown.

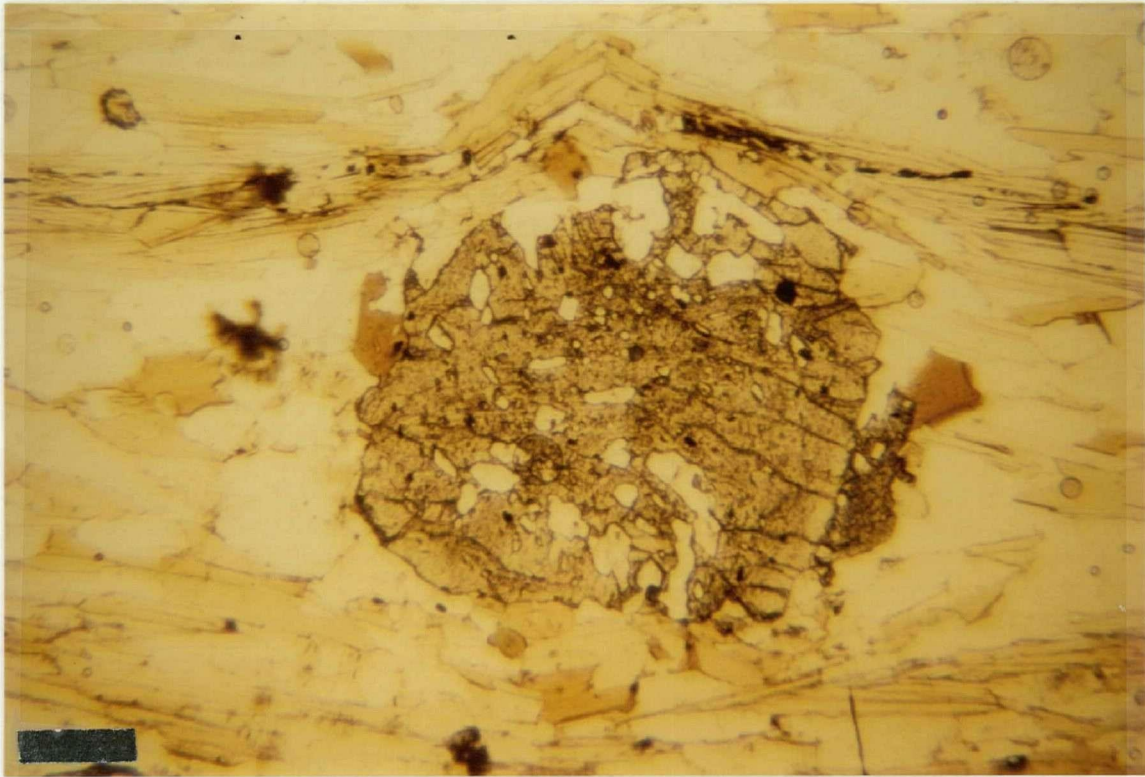


Figure 4.2: Garnet in Snowshoe Group; note curved inclusion trails and deflection of S_2 foliation defined by biotite, indicating garnet growth during early D_2 deformation. Scale bar is 2.5 mm, plane polarized light.

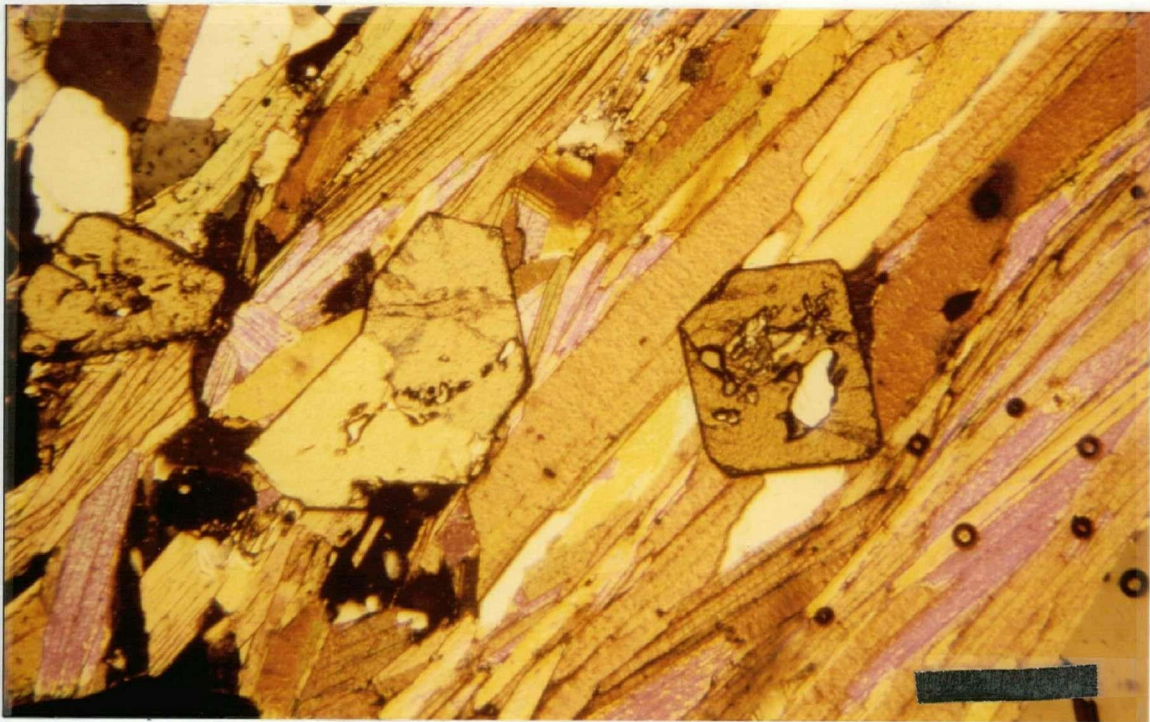


Figure 4.3: Post- D_2 staurolite in the Snowshoe Group, overgrowing the D_2 foliation. Scale bar is 2 mm, crossed nicols.

Kyanite

Porphyroblasts of kyanite range from 0.5 to 4 mm in length. Inclusions of quartz, plagioclase and muscovite are parallel to the S_0/S_1 and S_2 traces. These poikiloblasts are subidioblastic with serrated ends. They are uncommonly twinned. Orientations of kyanite are both parallel and oblique to the S_2 foliation, indicating that growth was syn- to post- D_2 deformation (Fig. 4.4).

Sillimanite

Small amounts of fibrolitic sillimanite are associated with biotite-rich zones, muscovite and quartz, commonly adjacent to garnet porphyroblasts. In sample DL098, sillimanite is in contact with kyanite, suggesting that it is directly replacing kyanite (Fig. 4.4). Other replacement textures for sillimanite are lacking and it only occurs within matrix phases, commonly adjacent to porphyroblasts.

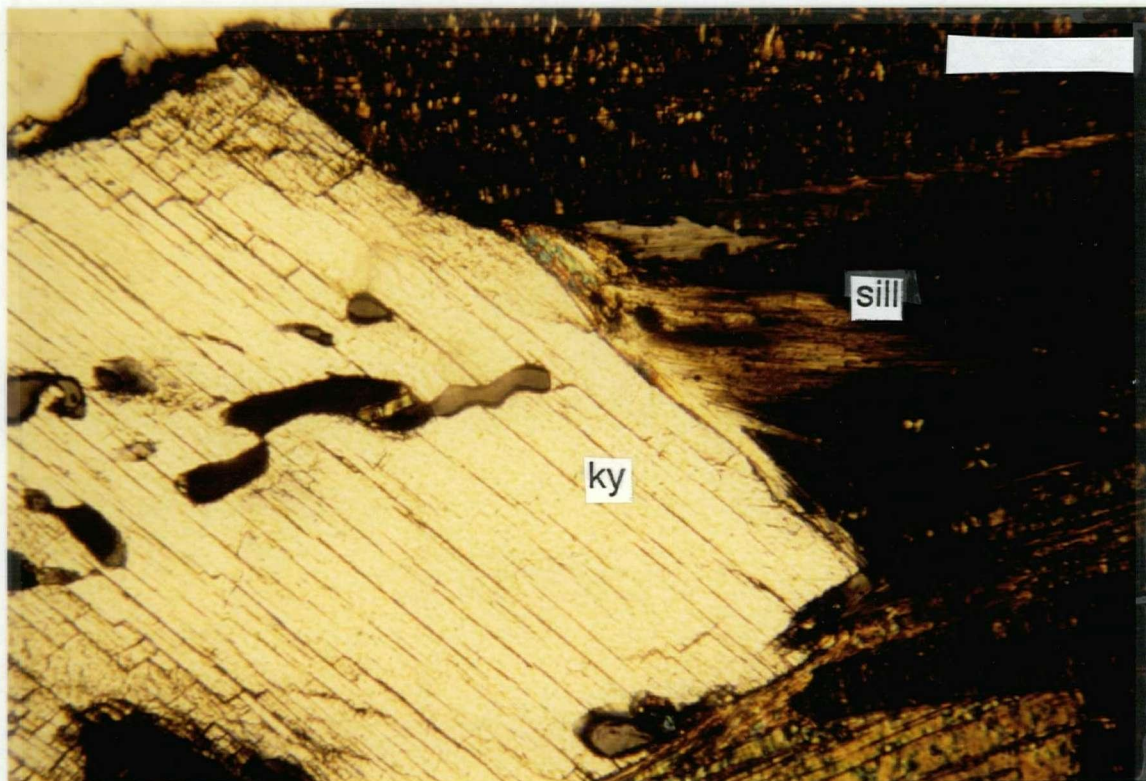


Figure 4.4: Fibrolite after kyanite, associated with biotite in Snowshoe Group, sample DL098. Scale bar is 0.5 mm, crossed nicols.

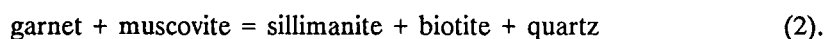
Randomly oriented sheaves of fibrolite suggest that growth took place statically during a post-D₂ lull in deformation. Fillipone (1985) and Garwin (1987) observed syn- and post-D₂ sillimanite which is folded by F₃.

Conditions of Metamorphism

All of the samples examined indicate that the entire study area lies within the sillimanite isograd. Prograde metamorphic reactions up to sillimanite grade of this metamorphic event are well-documented in the Quesnel Lake region for the Snowshoe Group metapelites (for a review, see McMullin and Greenwood 1988). The only metamorphic reaction of importance to this study is the formation of sillimanite. Two possible reactions based on textural observations model the formation of sillimanite. The first is the polymorphic transformation



The constant association of sillimanite with biotite suggests the operation of a second reaction producing biotite along with sillimanite. Textural evidence for the breakdown of either staurolite or garnet to produce sillimanite is lacking. Rocks just to the north on Mica Mountain are within the staurolite-kyanite-sillimanite zone (McMullin and Greenwood, 1988). There sillimanite may have formed as a result of the reaction

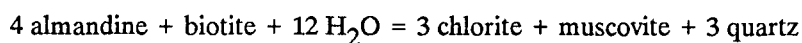


Garnet is still present since not all garnet is consumed by this reaction and it also may be generated by other reactions simultaneously (McMullin and Greenwood, 1988). Sillimanite in the study area may have formed as a product of reactions (1) and/or (2).

If the temperature of sillimanite formation is known then the pressure can be found using the known stability conditions of sillimanite (Holdaway, 1971). Temperatures determined using garnet-biotite thermometry by Fillipone (1985) and Garwin (1987) for Snowshoe rocks from the sillimanite and sillimanite-kyanite zones may be considered "typical" for this metamorphic event. Study areas of Fillipone and Garwin are shown in Figure 1.4. For the kyanite-sillimanite zone, Fillipone (1985) estimated 665⁰C and 5-6 kb while Garwin calculated lower temperature and pressure of 535⁰C and 4.5-5 kb. Garwin's

(1987) estimates may be taken as a minimum estimate for this study whereas Fillipone's (1985) results may be closer to the true value. This seems reasonable because Fillipone's area is closer to this study geographically and also is closer in terms of structural position and degree of retrograde alteration. Retrogression becomes significant in the western part of Garwin's area (Garwin, 1987), continuing into the adjacent area mapped by Lewis (1987). Conditions of metamorphism within the Snowshoe Group rocks beneath the Redfern Complex are thus considered to have exceeded 550⁰C and 5 kb.

Retrograde minerals and textures are minimal in the Snowshoe Group in the study area. As a regional trend, the most severe retrogression seems to have affected Snowshoe Group rocks within carbonate-rich stratigraphic sections (McMullin and Greenwood, 1988). The lack of carbonate lithologies in this region and the pristine appearance of peak assemblages is consistent with this observation. Minor chloritization of biotite associated with garnet suggests the reaction



(Fillipone, 1985). Minimal retrograde alteration also suggests that fluid mobility may have been restricted after the peak of metamorphism in this area.

4.3. REDFERN GNEISS

The Redfern gneiss contains the mineral assemblage plagioclase + quartz + K-feldspar + biotite + muscovite \pm hornblende with accessory apatite and zircon. Sphene, epidote (?), actinolite, and chlorite occur in some specimens. All of the specimens are fine-grained, many have a bimodal grain size, and all are gneissic (Fig. 4.5).

Plagioclase occurs as small (<0.5 mm), anhedral grains. Some grains are kinked and appear to be original and their composition is approximately An₃₀. Overall, twinned plagioclase comprises only about 5-15 modal percent of the rocks. If the presence of abundant untwinned plagioclase is ruled out, then the rock composition estimated from stained hand samples changes to a true granite, based on observation of stained thin sections.

Quartz and potassium feldspar comprise about 70-80% of the rock, with quartz being more abundant. Both commonly form medium-grained matrix minerals elongate parallel to the foliation trace.

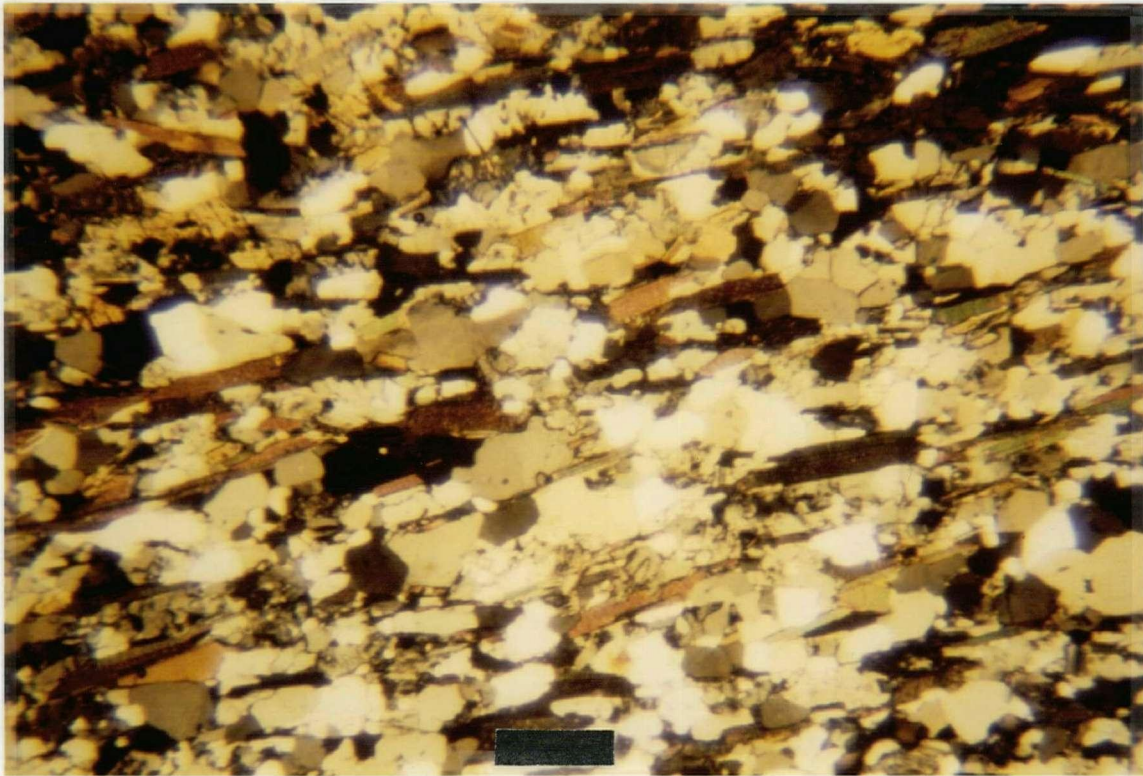


Figure 4.5: Typical Redfern gneiss, biotite-muscovite-plagioclase-quartz gneiss. Scale bar is 2.5 mm, crossed nicols.

Quartz is rarely seen without internal deformation such as subgrain development and healed microcracks. K-feldspar commonly has dusty overgrowths of clay encroaching from the grain boundaries, apparently along microcracks. The concentration of feldspar into layers, defines a weak gneissosity. Round mosaics of polycrystalline quartz composed of irregular-shaped quartz grains and subgrains appear to have recrystallized from rounded porphyroclasts. Layer parallel, lensoid domains of larger, elongate quartz up to 1.5 mm long may also have replaced porphyroclasts which were once elongate ribbon grains of highly strained original quartz.

Sheet silicates are small, commonly euhedral prisms of biotite, muscovite, and less commonly chlorite. Biotite is generally more abundant than muscovite (biotite 0-20%, muscovite 0-10%) but in one sample where muscovite is present biotite is absent. Biotite occurs as sub-idioblastic to xenoblastic porphyroblasts up to 2 mm long. Muscovite and biotite occur in two more habits, as disseminated grains growing on quartz grain edges and clustered into gneissic lenses and wisps. Strain-free and kinked grains occur in both habits. Chlorite occurs exclusively in association with biotite, most commonly along biotite cleavage planes and it appears to be a retrograde phase replacing biotite.

Poikilitic porphyroblasts of hornblende with associated sphene and epidote occur in two specimens (Fig. 4.6) Elongate, strained poikiloblasts have inclusions of aligned biotite and quartz. The poikiloblasts themselves are elongate within the foliation. Poikilitic to sieved cross sections of hornblende are mantled by thin hornblende needles which lie in the foliation.

Except for the presence of hornblende the Redfern gneiss is a fairly homogeneous, very felsic rock. The origin of the hornblende phase in the gneiss may be exotic. Xenocrysts or deformed and recrystallized xenoliths of mafic material may account for the origin of the amphibole. Although primary hornblende is not unreasonable, the presence of mafic xenoliths and the proximity of a source of xenoliths during intrusion (the Redfern Complex) suggest that at least some of the amphibole component may have been introduced.

Timing of Metamorphism and Deformation

Field relations suggest that the Redfern gneiss intruded syn-tectonically along the active Redfern thrust. The foliation within the gneiss is folded by the same phase which folds the Redfern thrust and refolds earlier structures in all other rock types. Thus constraints are placed on the timing of the growth of minerals that define the foliation. Primary grains that have not recrystallized during metamorphism may include large, highly strained quartz grains, inclusion-free biotite porphyroblasts, potassium feldspar, and strained, twinned plagioclase. Metamorphically recrystallized grains include poikilitic hornblende, idioblastic micas, and fine-grained quartz. The presence of abundant quartz which shows internal strain suggests that the rock has not been thermally annealed.

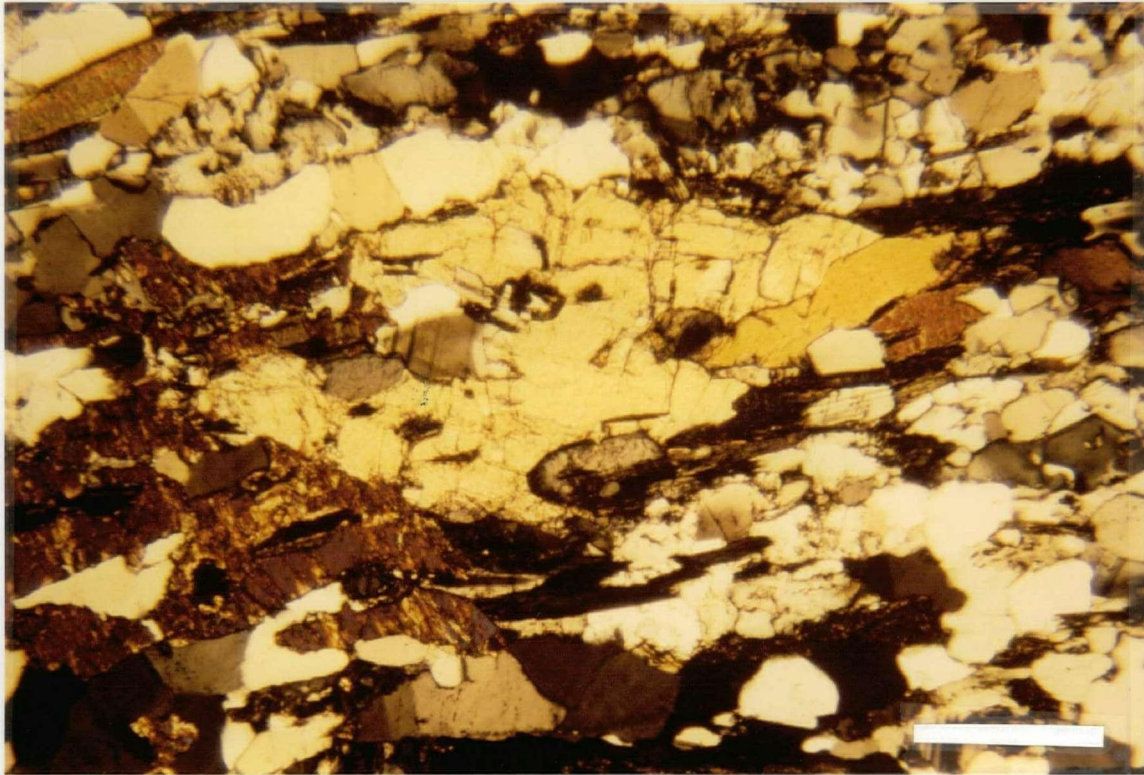


Figure 4.6: Poikilitic hornblende in the Redfern Gneiss, DL179. Scale bar is 2 mm, crossed nicols.

4.4 UPPER PLATE: THE REDFERN COMPLEX

Rocks of the upper plate underwent one protracted phase of prograde metamorphism and varying degrees of recrystallization during a retrograde event. Igneous minerals imprinted with textures related to mantle deformation are preserved in the Redfern peridotite. The peridotite body shows increasing effects of modification from the center outward to its margins which are intensely metasomatised. Each of the three diverse lithologies in the upper plate has a metamorphic mineral assemblage associated with the peak of metamorphism from which may be interpreted conditions of metamorphism. Retrograde

recrystallization was limited in the ultramafic and mafic rocks, but was much more extensive in the Triassic black phyllite.

4.4.1. Redfern Peridotite

Four distinct phases of recrystallization have affected the ultramafic rocks. They are, in chronological order:

- 1) Primary crystallization and accumulation of the igneous phases olivine, chrome spinel, and diopside;
- 2) "Mantle metamorphism" dynamic recrystallization of primary phases during ductile deformation in the upper mantle, without changes in phase composition;
- 3) One protracted phase of "alpine metamorphism", beginning with serpentinization and culminating in the formation of the amphibolite facies assemblage olivine + talc + tremolite + chlorite;
- 4) Limited retrograde recrystallization of the high-grade assemblage to serpentine and chlorite.

Petrographic observations allow recognition of three types of primary ultramafic rocks: dunites, pyroxene-bearing peridotites, and pyroxenites. Others have been altered beyond recognition as primary rock types and have been called serpentinites, amphibolites, and steatites. Olivine has been more resistant to alteration and metamorphism than has pyroxene. Fresh clinopyroxene was found in only four specimens and orthopyroxene has not been seen. However, textures can be used to infer prior existence of primary igneous minerals in many cases.

Petrographic descriptions have primary igneous mineralogy first, followed by the peak assemblage of "alpine-type" metamorphism. Retrograde minerals and textures are described last. Use of the term 'neoblast' is restricted to grains formed by dynamic recrystallization and recovery mechanisms. For a more detailed treatment of dynamic recrystallization structures and textures, see Structure, Chapter 3.

Unit 3A: Tectonized Dunites

Primary igneous minerals in the dunites are olivine (Fo_{90.5}) and chromite; evidence of original pyroxene was found in only one sample. Olivine has two grain sizes, coarse (0.5-15 mm) and very fine (< 0.1 mm). Coarse grains are generally elongate, subhedral, and strained. They exhibit undulose and incomplete extinction, have sharp kink band boundaries produced by dislocation glide and glide-climb along the (010):[100] and (100):[001] slip systems, and secondary development or enhancement of the weak {010} cleavage (for figures, see Chapter 3). Fine grains occur along grain and kink band boundaries, are dominantly equant, and where clustered commonly form a granoblastic mosaic having slightly curved grain boundaries subtending 120° at triple junctions. Where tabular, the fine grains still commonly form triple junctions at their terminations but have straight grain boundaries and are elongate parallel to the rock foliation. Chromite is anhedral with grain size 0.5-2 mm and commonly occurs as interstitial and poikilitic grains or as sub-spherical inclusions in olivine.

The metamorphic assemblage formed in the dunite at the peak of metamorphism is olivine + chlorite + talc + magnetite + tremolite ± chromite with accessory magnesite; chlorite and serpentine are retrograde. Overall, the metamorphic minerals are fine-grained, unstrained and unoriented except where associated with veins.

Talc + chlorite + magnetite partially replace primary forsteritic olivine and chromite. Patches of tiny olivine neoblasts are replaced preferentially over larger grains by a patchwork of talc and chlorite (Fig. 4.7). Larger grains are commonly mantled by talc and have grain boundary cracks filled with talc and chlorite. Chlorite tends to cluster in sheaves where replacing olivine; where replacing chromite, chlorite mantles the grains and is associated with magnetite and talc (Fig. 4.8). Magnetite occurs both as disseminated, idiomorphic cubes (<0.1 mm in diameter) and larger (up to 2 mm diameter) clusters of grains which nucleated on smaller grains and apparently grew as reactions proceeded. Talc around (primary?) magnetite cores suggest that talc replaced magnetite. Xenoblastic magnesite grains up to 2 mm in diameter and occur alone or in clusters or veins.

Anthophyllite and tremolite are uncommon in the dunites. The amphiboles occur as prismatic needles randomly growing across olivine; tremolite grains tend to cluster and are associated with talc.

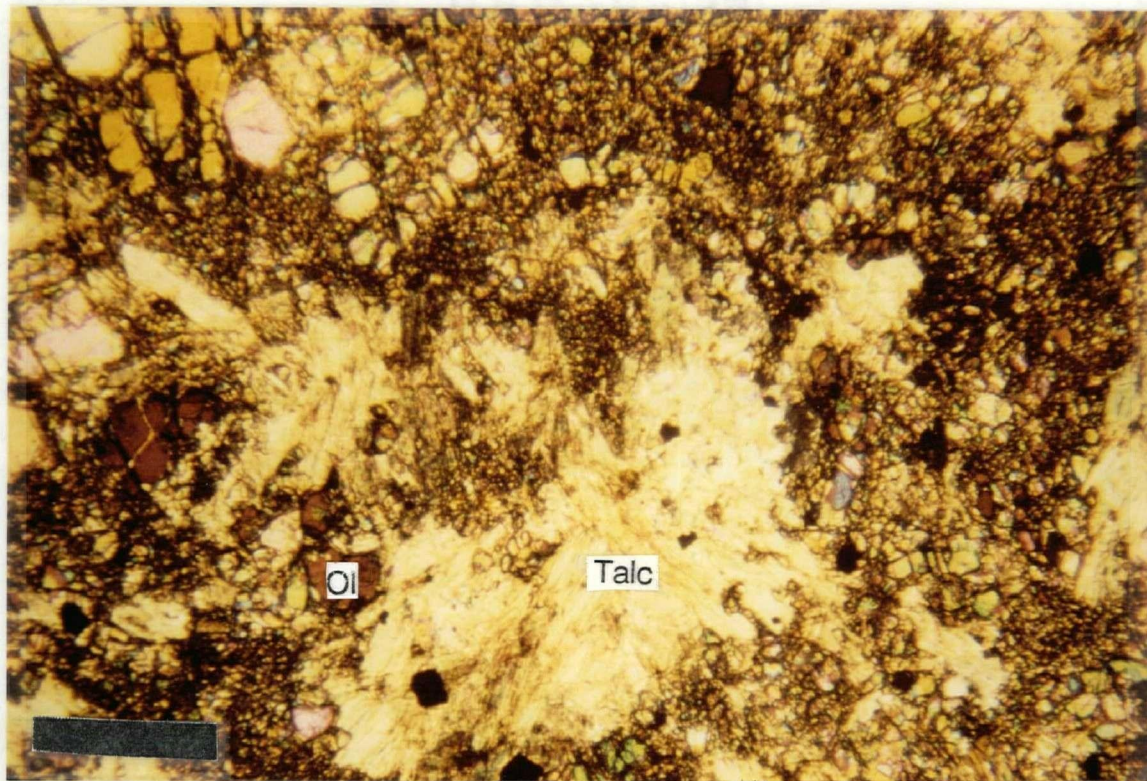


Figure 4.7: Preferential freplacement of olivine neoblasts by talc in dunite, sample DL026. Scale bar is 2 mm, crossed nicols.

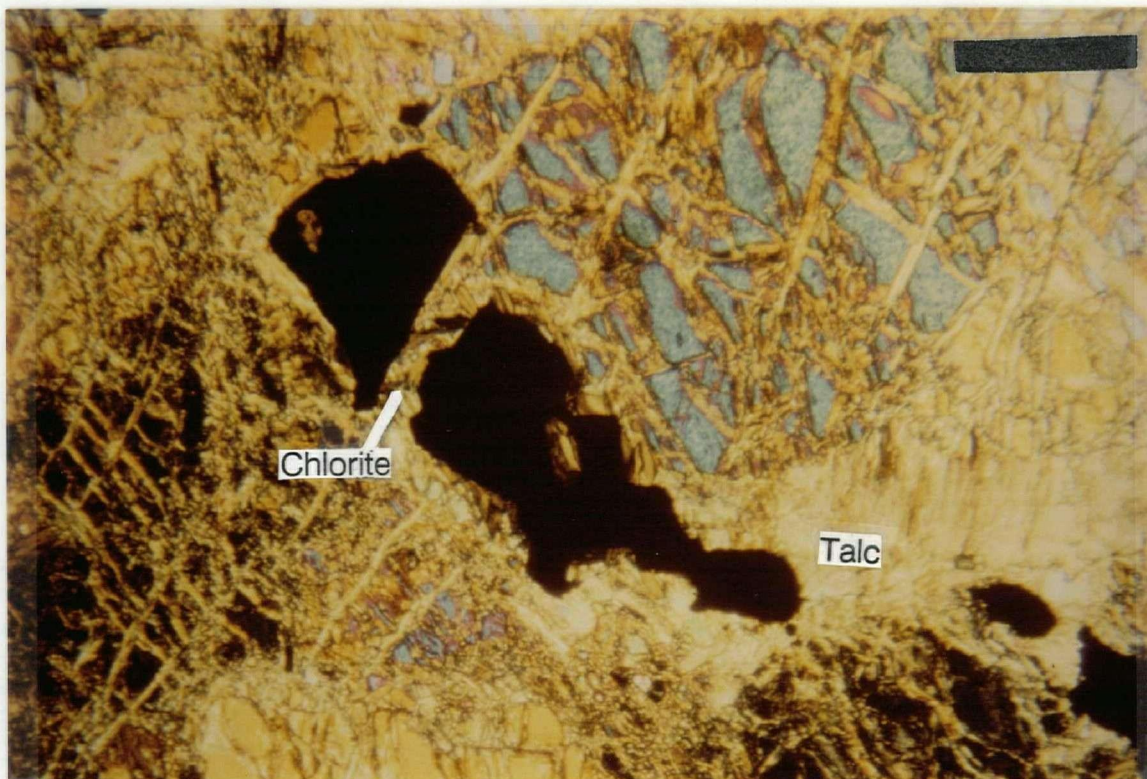


Figure 4.8: Chlorite + talc mantling chromite, sample DL037. Scale bar is 2 mm, crossed nicols.

Anthophyllite ranges from fine, fibrous needles to larger, random and oriented prismatic grains which may be twinned or have sweeping extinction.

Minerals with textures which either crosscut or overgrow earlier textures are believed to be retrograde in origin. Serpentine and talc veins are common although some samples completely lack serpentine. Serpentine is restricted to veins, intergranular and intragranular cracks, and has a fine-grained, fibrous habit. Anomalous brown birefringent chlorite needles commonly have anomalous blue birefringent tips, suggesting a later stage of Fe-chlorite growth. An orange-red iron-oxide stain also is commonly associated with magnetite and serpentine in veins. This is presumed to be a retrograde alteration/oxidation of the peak assemblage known as iddingsite.

Unit 3B: Layered Cumulates

This unit is characterized by the presence of pyroxene-bearing peridotites macroscopically interlayered with dunites. The dunites are very similar to unit 3A; the pyroxene peridotites contain between 10 and 95 modal percent pyroxene, now mostly pseudomorphed by tremolite.

Dunitic lithologies are very similar to those already described for unit 3A, but the grains tend to be more equant and are less deformed. Primary igneous textures and metamorphic mineralogy are the same as in subunit 3A. The exception is that olivine has a generally larger grain size (0.5-7 mm) and less development of kink bands, subgrains, and neoblasts.

Pyroxene-bearing lithologies have preserved relict cumulate textures and show the least amount of dynamic recrystallization. Relict pyroxene was found in only 4 of 20 samples, all chromian-diopside, determined either optically or by microprobe analysis (see below). Although orthopyroxene was never identified, the extent of amphibolitization in the majority of the samples warrants calling them pyroxene-bearing peridotites rather than wehrlites. Relict pyroxene grains and those pseudomorphed by tremolite are equant, squarish and range from 0.5 to 10 mm in diameter. Along cleavage and crystallographic planes, pyroxene contains magnetite inclusions or symplectic spinel (Fig. 4.9). This aids in the identification of pyroxene where it has been completely replaced by amphibole.

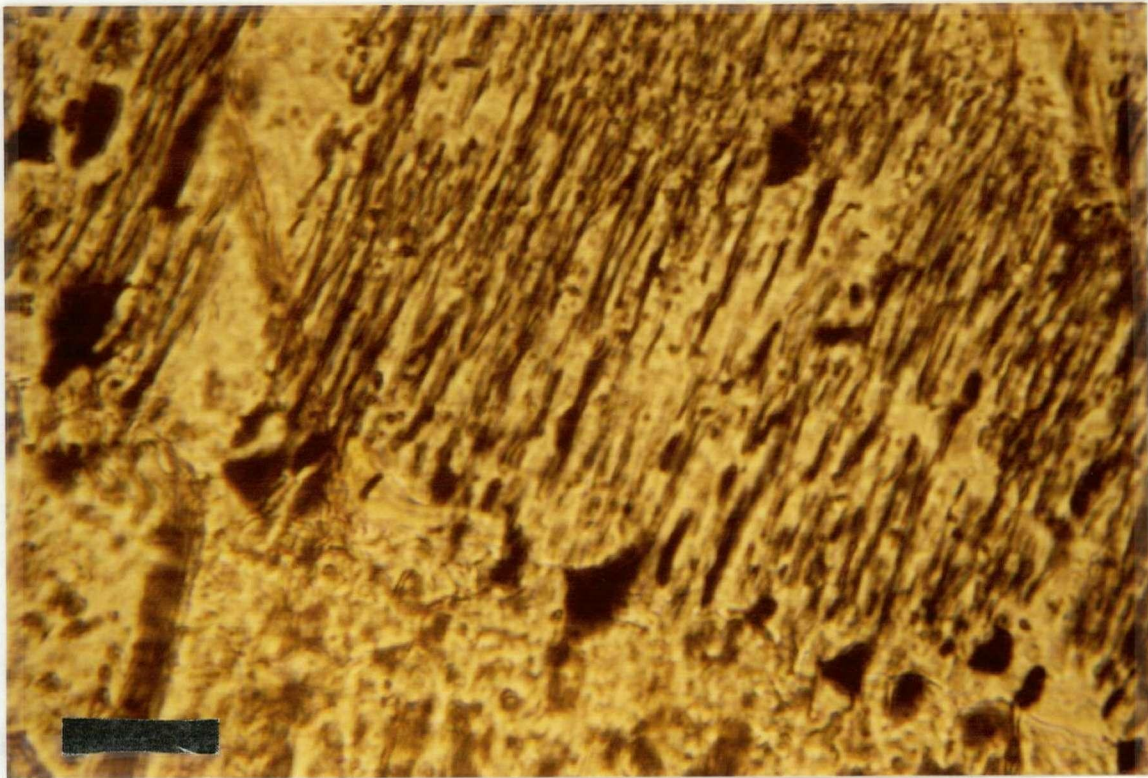


Figure 4.9: Symplectic texture spinel, plane polarized light, sample DL015. Scale bar is 0.1 mm.

Olivine is commonly finer-grained than the pyroxene, ranging from <0.1 mm (neoblasts) to 4 mm. Grain size generally increases with olivine abundance. Olivine neoblasts comprise irregularly shaped patches between pyroxene grains. It is unclear whether this is an igneous cumulate texture because it has been overprinted by mantle deformation textures. Larger grains of olivine are subhedral and appear to have a cumulate texture.

Primary chromite is less common than in unit 3A but exhibits the same textures and habits.

The major effect of metamorphism on pyroxene is its replacement by amphibole, most commonly tremolite. An originally continuous pyroxene grain now consists of an irregular patchwork of equant

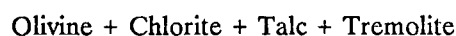
tremolite grains with prismatic terminations (Fig. 4.10). Idioblastic amphibole grows straight across relict pyroxene or already existing tremolite patchworks. Partially recrystallized pyroxene grains show two habits of amphibole nucleation and growth: 1) from the grain boundaries inward, or 2) originating within grains along crystallographic planes and spreading outward (Fig. 4.10). Tremolite pseudomorphs after pyroxene commonly have a lower internal density of opaque inclusions and a higher density along new grain boundaries. During recrystallization the inclusions may re-concentrate along new grain boundaries.

Other metamorphic minerals, talc, chlorite, anthophyllite, magnetite, and magnesite, exhibit the same textures as already described for unit 3A.

In one specimen from this unit a texture indicating the presence of metamorphic olivine was found. A patch of magnetite in a regular array resembling those found in pyroxenes pseudomorphed by amphibole is enclosed entirely within a nematoblastic olivine grain with interlocking grain boundaries (Fig. 4.11). This suggests the replacement of pyroxene first by amphibole and then by olivine. Textural evidence does not support the conclusion that all olivine is of metamorphic origin since relict mantle textures and structures exist in grains with compositions characteristic of upper mantle rocks (see Chapter 5).

Metamorphism

Metamorphism of the Redfern ultramafics during crustal deformation was a largely isochemical recrystallization of fresh to partly serpentized ultramafic rocks. This inference is based on the presence of multiphase, low-variance assemblages consisting of olivine, an additional Mg-phase, talc, an aluminous phase, chlorite, and a calcic phase, tremolite (Evans, 1982). Most of the samples observed appear to contain primary olivine (Fo_{90.5}) in apparent equilibrium with the metamorphic assemblage. Primary olivine is identified by having textures restricted to an upper mantle origin ((010) kink bands (Raleigh, 1965)). Some specimens in unit 3B have fresh olivine which lacks relict mantle textures and appears to have completely replaced primary pyroxene. Olivine in this unit which retains mantle textures has a lower forsterite component than those from unit 3A. Thus it appears that primary olivine with high forsterite content is in equilibrium with the peak assemblage,



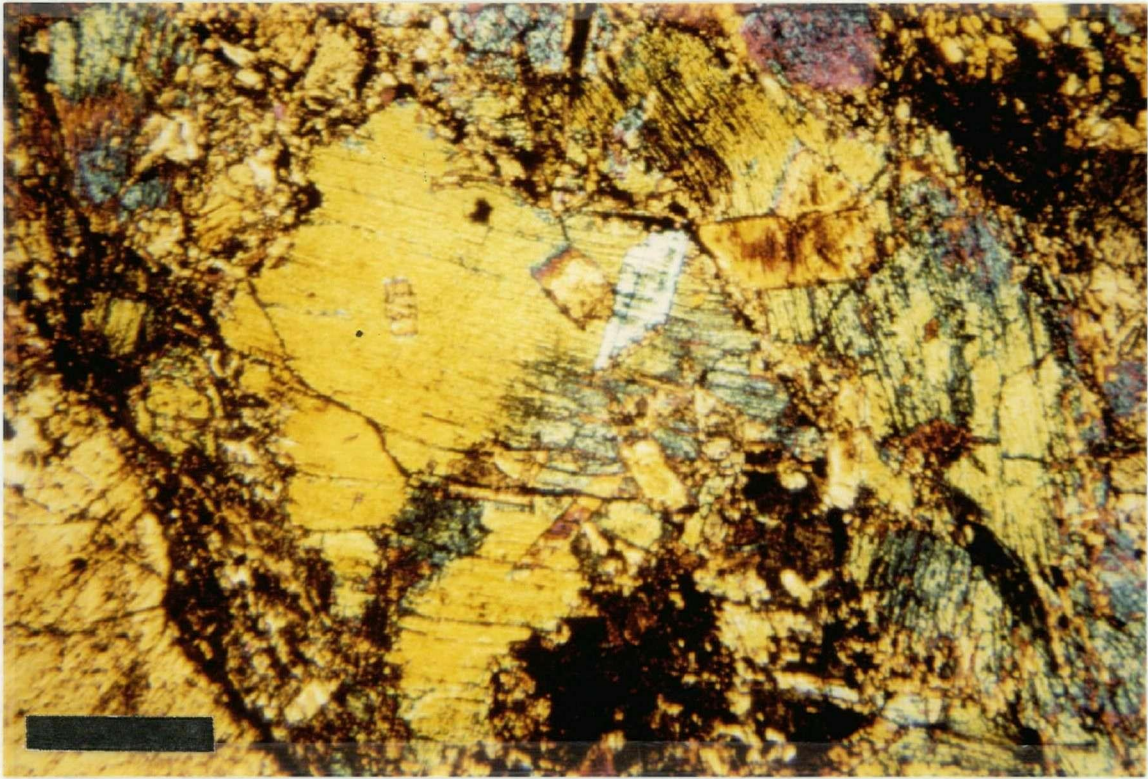


Figure 4.10: Diopside partially replace by tremolite, DL019. Scale bar is 2 mm, crossed nicols.

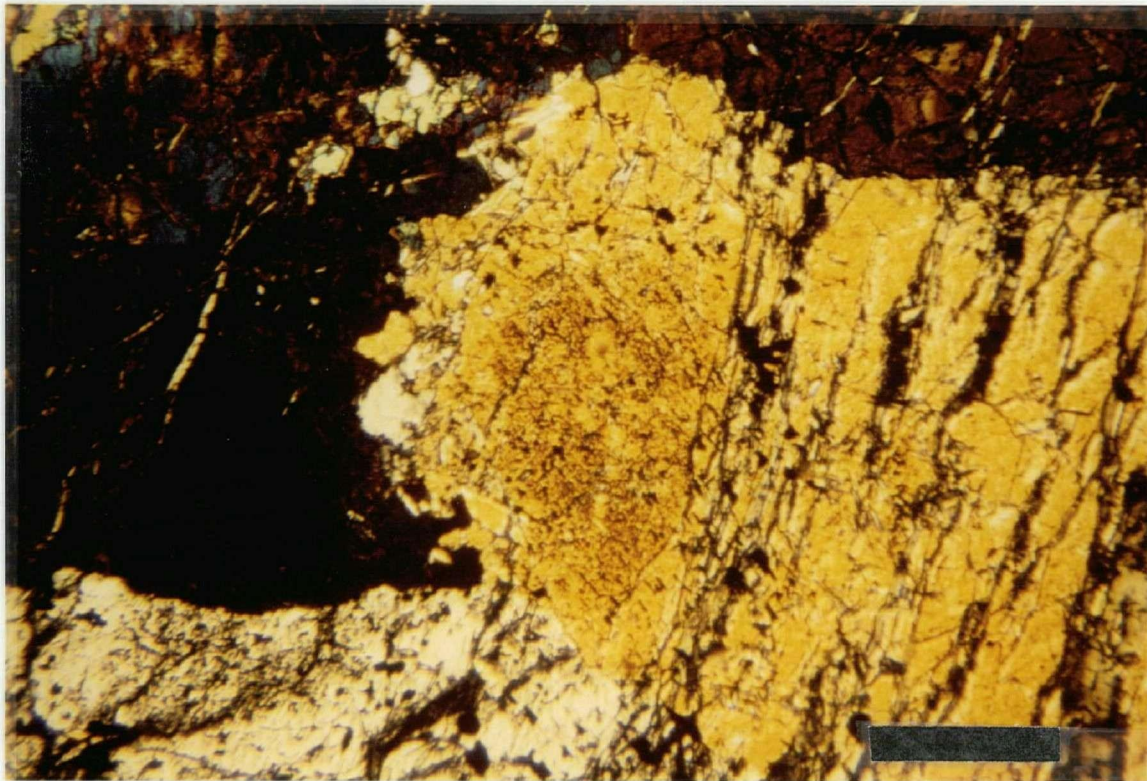


Figure 4.11: "Metamorphic olivine." Regular array of opaque inclusions in centre of photograph mark the replacement of pyroxene. Scale bar is 2 mm, crossed nicols.

This assemblage belongs to an intermediate metamorphic grade corresponding to the staurolite-kyanite zone of pelitic rocks (Trommsdorff and Evans, 1974). It is included in the correlation with the albite-epidote amphibolite facies of basic rocks (Wyllie, 1967). This is the same facies found in the overlying Redfern amphibolite (see below) but is slightly lower grade than the sillimanite-zone assemblage found in the structurally lower Snowshoe Group.

Several problems prevent further refinement of the pressure and temperature conditions attending the metamorphism. Relict primary assemblages suggest that the entire body of rock did not attain chemical equilibrium. The presence of preserved primary minerals indicates that the body was not completely serpentinized prior to the onset of metamorphism, as is commonly the case with alpine peridotites (Trommsdorff and Evans, 1974). A fluid phase was probably only present in discrete zones (see below) and in large portions of the peridotite its activity was lower, limiting reactions involving H_2O . The presence of CO_2 in the fluid phase, indicated by magnesite also may have had a complex affect on the equilibrium P-T conditions (Evans, 1982).

4.4.2. Contact Zones of Unit 3

Highly altered rocks occur along the margins of unit 3, both on its lower, fault-contact with unit 1 (Snowshoe Group) and on its upper contact with unit 4. Monomineralic zones of talc and tremolite with varying thickness are common within these zones (see Fig.2.10 and Chapter 2 for description) indicating that the rocks formed metasomatically (Evans, 1982).

The origin of these zones may be related to syn-deformational fluid migration along thrust faults. Monomineralic zones along thrust contacts have been described by Miller (1988) in a similar geological setting, the ophiolitic Ingalls Complex, Oregon. He recognized that fluid flow, deformation and metamorphism were complexly interrelated during imbrication of ultramafic thrust slices. Metasomatic fluids may have originated from dehydration reactions during amphibolite facies metamorphism of the Ingalls. Metamorphism was coincident with imbrication which focussed fluid flow along shear zones. Deformation of ultramafites was controlled by fluid pressure and concentrated in weaker metasomatic rocks of both marginal and internal mylonite zones (Miller, 1988).

A configuration similar to that of the Ingalls Complex may have existed within the Redfern Complex during emplacement onto the Snowshoe Group. Tremolite schist with a strong linear fabric and talc schist bearing a crenulation cleavage are found both on the upper and lower contacts of the Redfern ultramafics (see Structure, Ch. 5). The mineralogical zonation originated metasomatically and presumably reflects a chemical potential gradient that was present during reactions near the peridotite-amphibolite contact. The presence of a fluid phase either weakened the rocks or may have been introduced into zones already weakened by deformation. Either way, the zones evolved into shear zones, possibly as described by Miller (1988). Because these zones are much weaker than the surrounding crystalline rocks, they continued to localise succeeding movement as the Complex evolved to its present geometry.

4.4.3 Unit 4: Redfern Amphibolite

Mineralogic and textural evidence suggest one long phase of amphibolite grade metamorphism which began during the first phase of deformation and continued, outlasting the second phase. Excellent preservation of idioblastic, high-temperature mineral assemblages indicate that retrograde metamorphism was minimal.

The high grade mineral assemblage consists of common hornblende + albite + quartz + sphene + clinozoisite + ilmenite \pm garnet \pm biotite. Early veins of quartz and calcite, and one occurrence of a late serpentine (chrysotile?) vein were observed. Chlorite and possibly clinozoisite are retrograde; chlorite commonly replaces biotite. Textures indicate that thermal metamorphism outlasted deformation: random minerals of similar composition and grain size overgrow the metamorphic foliation; granoblastic polygonal textures are common (120° grain junctions) in quartz and plagioclase; and crystals are strain-free where they should show evidence of deformation consistent with surrounding structures.

Amphibole was identified optically as being mostly common hornblende. It has dark green to yellow-green to bluish-green pleochroism. Some grains with weak pleochroism and pale colour or colorless were identified as actinolite-tremolite.

Hornblende commonly displays two textural variants. The first has prismatic needles 0.1-0.5 mm long, either random or contained within the foliation plane, and the second has equant to elongate, post-kinematic poikilitic porphyroblasts. Random prismatic crystals either overgrow the foliation or form fine-grained, radiating sheaves (Fig. 4.12). These latter two textures indicate post-kinematic growth while the former was syn-kinematic. Larger poikiloblasts also show several crystal habits. In rocks with little or no foliation, randomly oriented, equant porphyroblasts with fine-grained opaque inclusions show incomplete extinction (Fig. 4.13a). These are probably pseudomorphs after primary pyroxenes and may have grown statically, prior to the main phase of metamorphism. In foliated specimens, porphyroblasts are poikilitic and are less typically equant. The poikiloblasts contain fine-grained quartz and feldspar inclusions which either define an internal foliation (Fig. 4.13b) or are randomly oriented, the foliation bending around the poikiloblasts. In the latter case the poikiloblasts are commonly composed of a patchwork of several grains.

Tremolite and actinolite are much less common than hornblende but have textures similar to those seen for hornblende. Most typically tremolite and actinolite occur as porphyroblasts, both poikilitic and free of inclusions. Tremolite mantles hornblende in one sample.

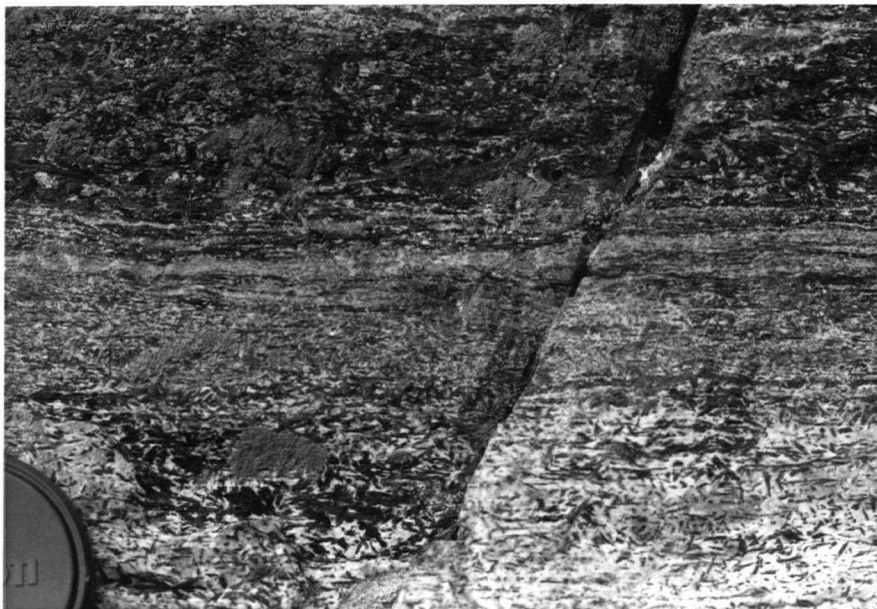


Figure 4.12: Randomly oriented hornblende in the Redfern amphibolite, indicating that metamorphism outlasted deformation.

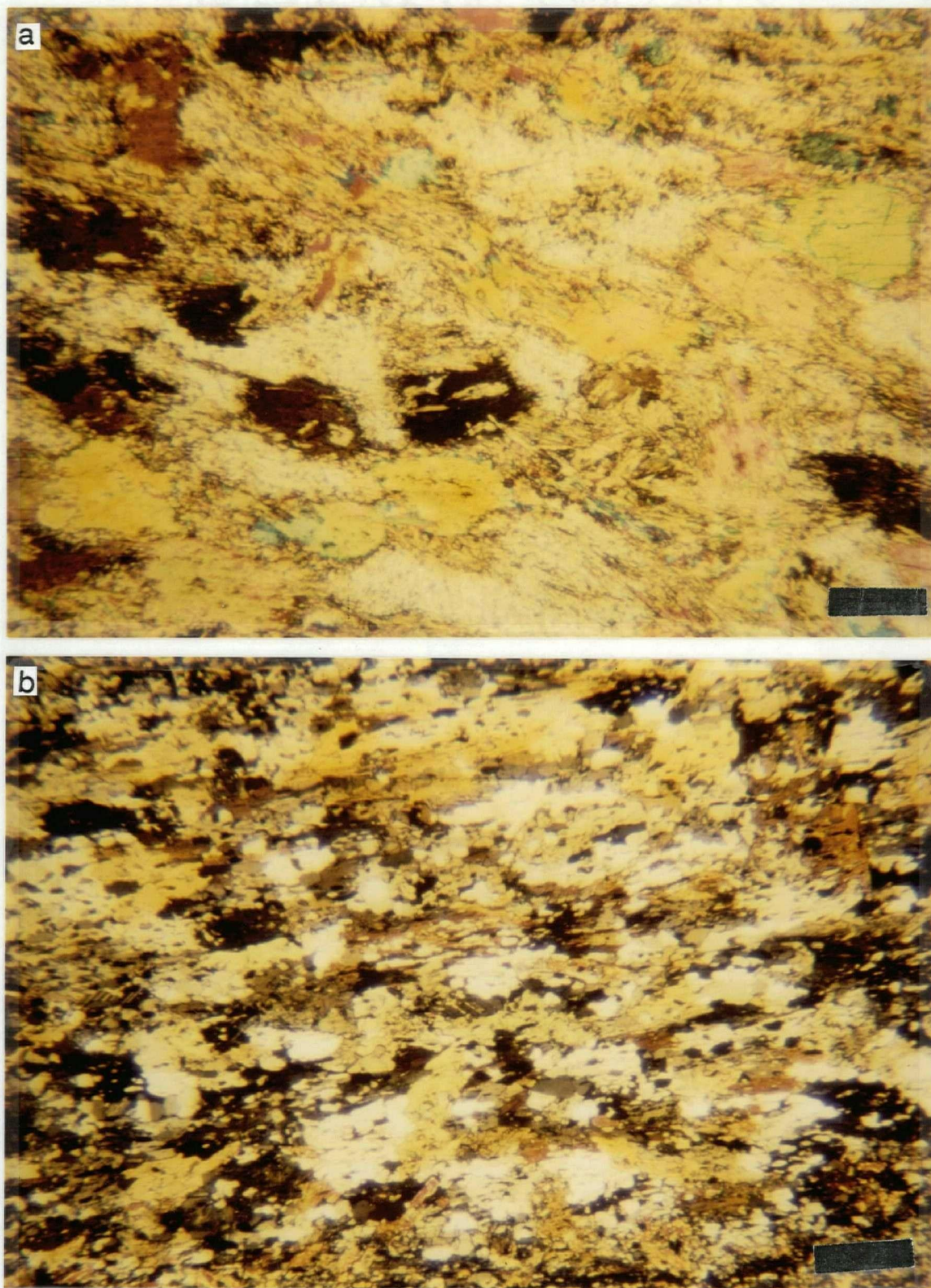


Figure 4.13: Hornblende in the Redfern amphibolite. a) Pre- D_1 equant hornblende mimetically after pyroxene, with smaller, prismatic, syn- D_1 hornblende growing around and across earlier grains; b) poikiloblasts with inclusion trails aligned parallel to S_1 trace, DL007. Crossed nicols, scale bar is 2.5 mm.

Together with quartz, plagioclase comprises leucocratic gneissic bands. Plagioclase rarely forms porphyroblasts and grain size ranges from <.01 to 0.5 mm. Smaller grains are syn-kinematic, commonly inequant and xenoblastic with long dimensions in the foliation plane. They are untwinned and typically have equilibrium grain boundary textures. Grains with albite twinning are mostly larger, equant, idioblastic, and occur within coarser-grained layers or else they are randomly oriented, indicating post-kinematic growth. One specimen contains a concentrically zoned, inequant plagioclase with its long axis parallel to the foliation. A few plagioclase compositions were obtained from simply twinned syn-to post-kinematic grains and range from albite (An_7) to oligoclase (An_{13}) (4-axis universal stage method of Turner, 1947).

Quartz is a xenoblastic, fine-grained, ubiquitous matrix constituent. Inequant, deformed grains with undulose extinction and subgrains are syn-kinematic and elongate parallel with the foliation plane. Post-kinematic recrystallization is indicated by strain-free, equant, equilibrium-textured mosaic patches. Two specimens contain extremely fine-grained quartz much less than 0.01 mm in diameter.

Epidote and sphene are both ubiquitous accessory minerals, their abundance varying with bulk composition. Epidote is the most abundant phase in the phacoidal, felsic or light coloured lithologic subtype which is common in the upper part of the unit. Sphene abundance increases along with epidote and is commonly associated with ilmenite and calcite. Both minerals are fine-grained, xenoblastic to subidioblastic, and occur interstitially within tabular plagioclase and quartz mosaics.

The most abundant opaque mineral is magnetite, which alters to hematite; ilmenite occurs irregularly with sphene. Magnetite has three common textures: 1) fine, tabular, subidioblastic and syn-kinematic grains with long axes parallel to the lineation trace; 2) larger, anhedral to subhedral post-kinematic poikiloblasts with matrix inclusions; and 3) fine- to very fine-grained inclusions within larger amphibole porphyroblasts, indicating a possible primary origin.

Biotite is notably rare in the Redfern amphibolites. It is present only in the felsic lithologic subtypes, forming small, (0.05-0.2 mm) idioblastic, syn-kinematic grains within the foliation. Rare, post-kinematic poikiloblasts reach up to 0.5 mm across.

Large (5-10 mm), sub-idioblastic poikiloblasts and fragments of garnet were found only in the thin, eastern section of unit 4. Its pale pink color and mineral association with hornblende, actinolite, epidote,

quartz, plagioclase and sphene suggest it is pyrope-almandine. Inclusion trails within the garnets consist of all of the matrix minerals and are typically subparallel to the rock foliation (Fig. 4.14). However, this foliation also bends around the garnets and form symmetrical amphibole "beards" around equant porphyroblasts. Garnet growth must have begun during D_1 but deformation must have continued, either a combination of the same phase or a later phase.

Calcite is relatively uncommon, occurring either in veins or as medium-grained (0.2-0.5 mm) porphyroblasts. It is always twinned and xenoblastic. As a porphyroblast it is associated with tremolite poikiloblasts, growing across and around large, sieved tremolite grains.

Early veins of quartz and calcite are parallel with the foliation. Calcite grains in veins are 0.3-0.5 mm across and mechanically twinned with irregular grain boundaries. Since S_1 parallel hornblende overgrows the calcite veins, they must have formed early in the deformational history of the rock.

Metamorphism

Textural relationships indicate that the peak metamorphic assemblage in the Redfern amphibolite is the assemblage hornblende + albite + quartz + epidote + sphene \pm magnetite/ilmenite \pm tremolite \pm calcite/dolomite. Using inferred and optically determined estimates of phase compositions, this assemblage may be assigned to the epidote-amphibolite facies.

Hornblende pleochroism is blue-green to green, corresponding to the garnet zone in pelitic rocks and the epidote-amphibolite facies (from James, 1955 in Miyashiro, 1973). The plagioclase composition is albite (An_7) to oligoclase (An_{13}).

The epidote phase is generally clinozoisite, determined from 2V and monoclinic dispersion. This composition indicates a lack of trivalent iron in favor of more aluminum and calcium. Epidote composition is strongly a function of oxygen fugacity up to the epidote-amphibolite/amphibolite facies boundary where it becomes unstable (Apted and Liou, 1983; Laird, 1980; Miyashiro, 1973). Therefore, without quantitative analyses of the phases, epidote details contribute nothing to the interpretation of metamorphic conditions other than its presence which indicates temperatures lower than epidote-out reaction conditions (Apted

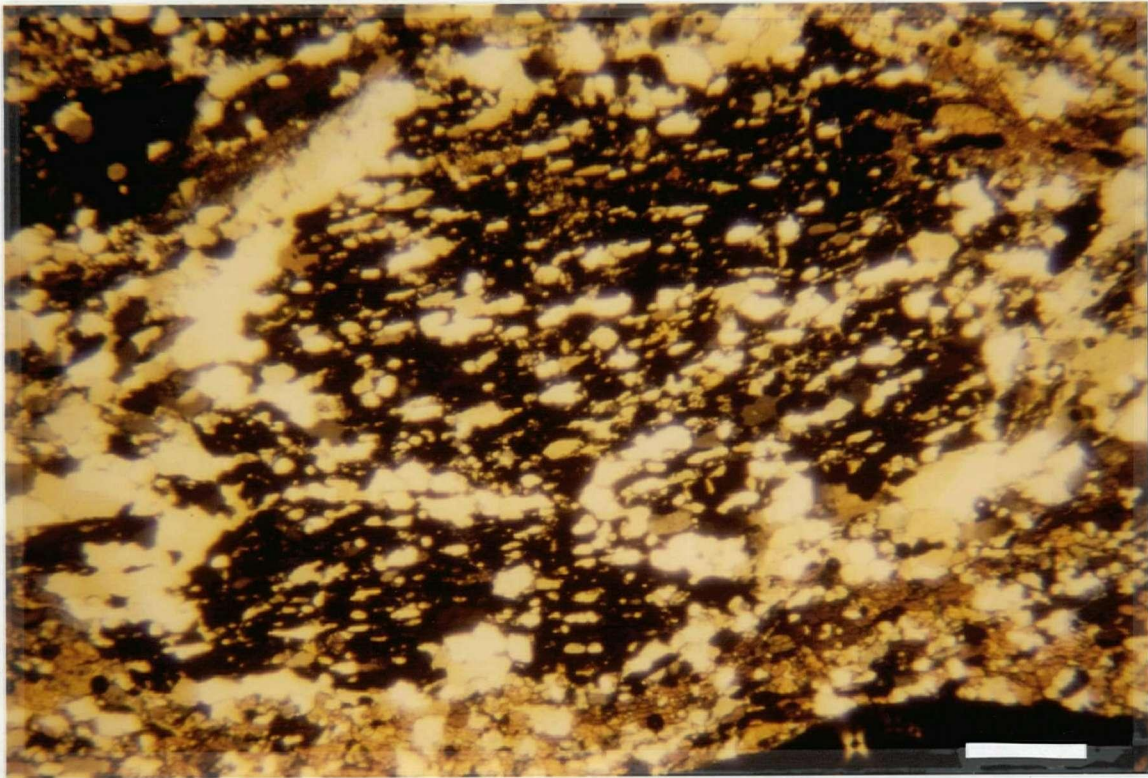


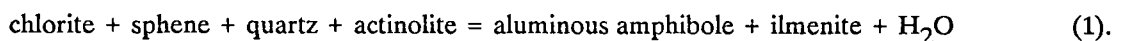
Figure 4.14: Garnet in the Redfern amphibolite, with inclusion trails continuous with external foliation. Scale bar is 2.5 mm, crossed nicols.

and Liou, 1983). The absence of epidote, most common in samples from the base of the unit and closer to an ultramafic composition, most likely reflects a change in bulk composition rather than metamorphic grade (e.g. sample DL086).

Absence of sphene may also reflect a difference in bulk composition rather than a reaction. Sphene is an important accessory phase which is present regardless of f_{O_2} (Moody et al., 1983). For example, sample DL041 contains no sphene or ilmenite and contains only 0.07% bulk rock weight percent TiO_2 (see Appendix A), which could easily be present in the hornblende. The occurrence of garnet is also

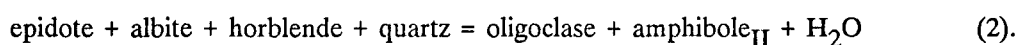
probably related to bulk rock composition. Garnet occurs within the epidote-amphibolite facies corresponding to the garnet-oligoclase and staurolite-kyanite-oligoclase pelitic zones in Fe-rich rocks (> 15% total FeO; Laird, 1980).

Determining the P and T conditions of metamorphism from an amphibolite is difficult without quantitative measurements of the phase compositions because of the continuous solid solution in most of the phases (Apted and Liou, 1983; Laird, 1980). Laird (1980) demonstrated empirically that metamorphism of basaltic rocks from greenschist to low-grade amphibolite involves primarily changes in mineral composition and modal abundance of the *common* five phase assemblage amphibole + chlorite + epidote + plagioclase + quartz which also includes a Ti-phase $\pm \text{Fe}^{3+}$ oxide \pm K-mica \pm carbonate. Metamorphic phase relations in a basaltic system have been investigated experimentally by Apted and Liou (1983). They determined the stability limits and transition controlling reactions of the greenschist, epidote-amphibolite, and lower amphibolite facies in natural basaltic glass as a function of temperature, pressure, and oxygen fugacity. Continuous reactions including increases in Al_2O_3 and TiO_2 in amphibole (actinolite to hornblende) and replacement of Na by Ca in plagioclase characterize progressive metamorphism and the formation of an epidote-amphibolite assemblage (Apted and Liou, 1983). They mark the lower amphibolite facies with a chlorite-out reaction:



They note, however, that rather than being a univariant reaction curve, this reaction is actually a divariant field due to the multi-component nature of the phases. Modal abundances and compositions of chlorite versus amphibole are used to gauge the progress of this reaction (Apted and Liou, 1983). For a given oxygen fugacity and 5-7 kb, chlorite is stable below about 500°C.

The upper limit of the epidote-amphibolite facies is marked by an epidote-out reaction at 650°C/5 kb and 675°C/7 kb (Apted and Liou, 1983):



Epidote stability increases markedly with fugacity of oxygen but decreases with lower total pressure (Apted and Liou, 1983). Pressure in the Redfern amphibolite is constrained by previous reactions discussed. Thus

the temperature and pressure conditions cited above are reasonable upper bounds for the Redfern amphibolite metamorphism, unless oxygen fugacity was unusually high.

4.4.4. Triassic Black Phyllite

Pelitic schists of the Triassic black phyllite which lie directly east of and in fault contact with the Snowshoe Group may have only attained kyanite grade. In addition, these rocks were more affected by retrogression than the Snowshoe Group and tiny fibrolite needles may be obscured or replaced by chlorite growth. Graphite is much more abundant than in the Snowshoe Group and accessory lithologies such as quartzite, calc-silicate, and amphibolite are distinct.

Staurolite

Staurolite has two grain sizes, small (0.05-0.5 mm) crystals in the matrix and very large porphyroblasts up to 20 mm long. The smaller grains are generally inclusion-free with common crystal terminations. They overgrow both the foliation and the D₂ crenulation cleavage (Fig. 4.15a). The larger porphyroblasts enclose earlier porphyroblast phases such as garnet (Fig. 4.15b), biotite, and kyanite (Fig. 4.15c) and have inclusions trails of dominantly quartz with some mica which are discordant with the external foliation. Inclusion trails are straight, folded or helycitic (Fig. 4.15d). Crystals are both poikilitic to their rims or have well-developed crystal faces with inclusions of graphite parallel to the faces.

These textures indicate several stages of staurolite growth. The large porphyroblasts grew syn- to post-D₂ as evidenced by their inclusions of both folded and helycitic foliations and metamorphic porphyroblasts. This is interpreted as prolonged retrograde growth and any prograde staurolite would have recrystallized during this event. Small, idioblastic crystals are post-D₂, commonly inclusion free or have more tightly folded inclusions.

Garnet

Garnet forms idioblastic porphyroblasts 1-5 mm in diameter. Many cores are corroded and embayed by chlorite, ilmenite, plagioclase and quartz (Fig. 4.16a). Some garnets have idioblastic rims with folded inclusion trails of quartz (Fig. 4.16b) and pressure shadows of biotite and quartz. Non-corroded

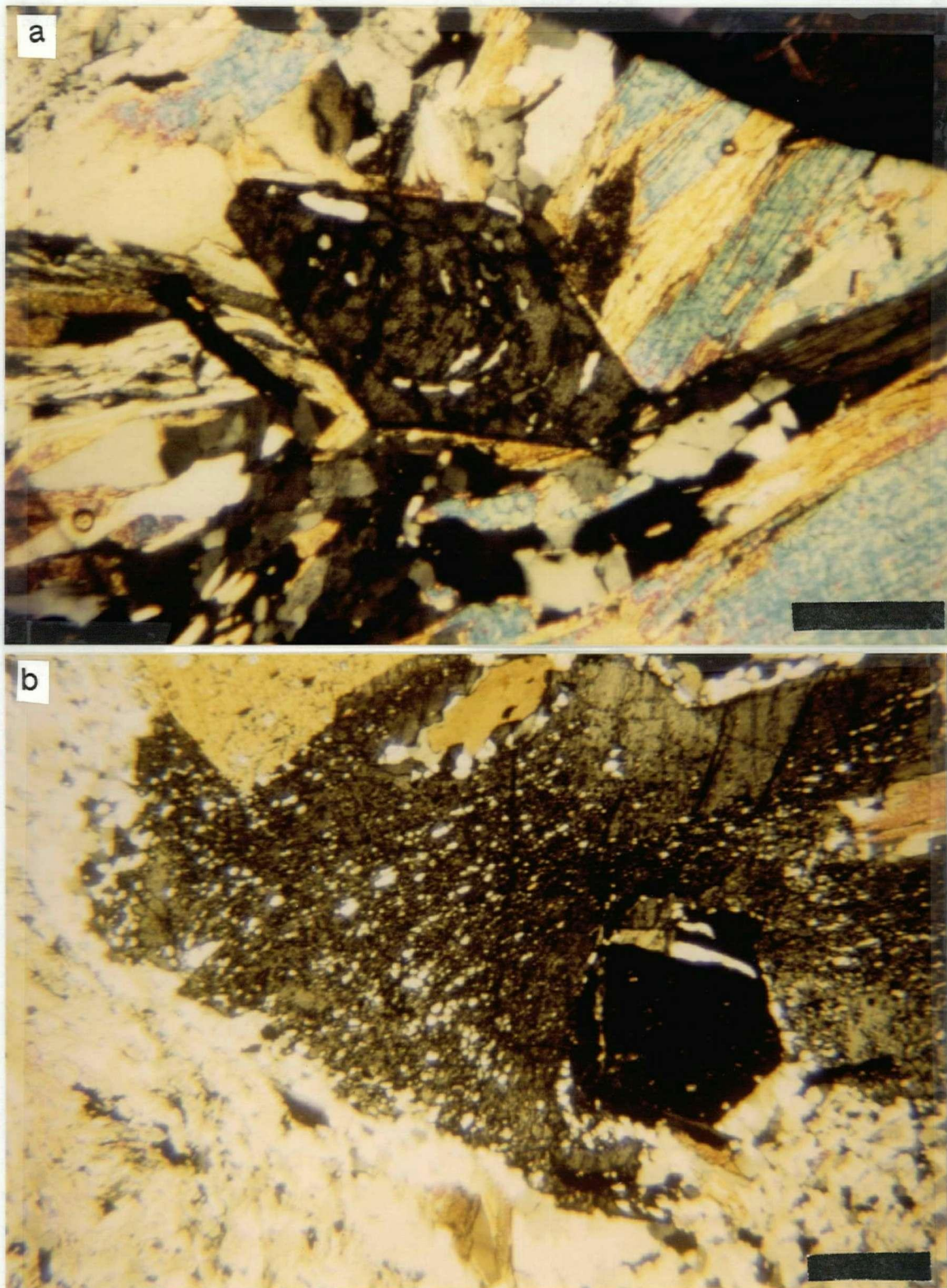
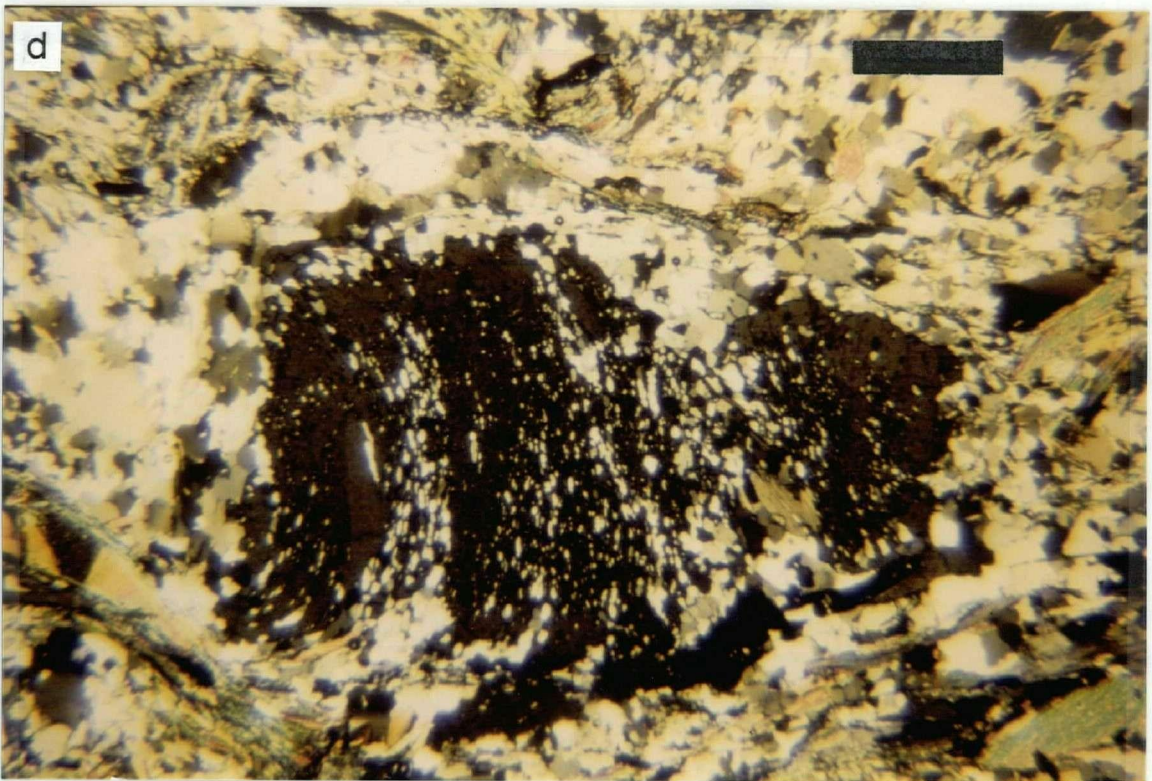
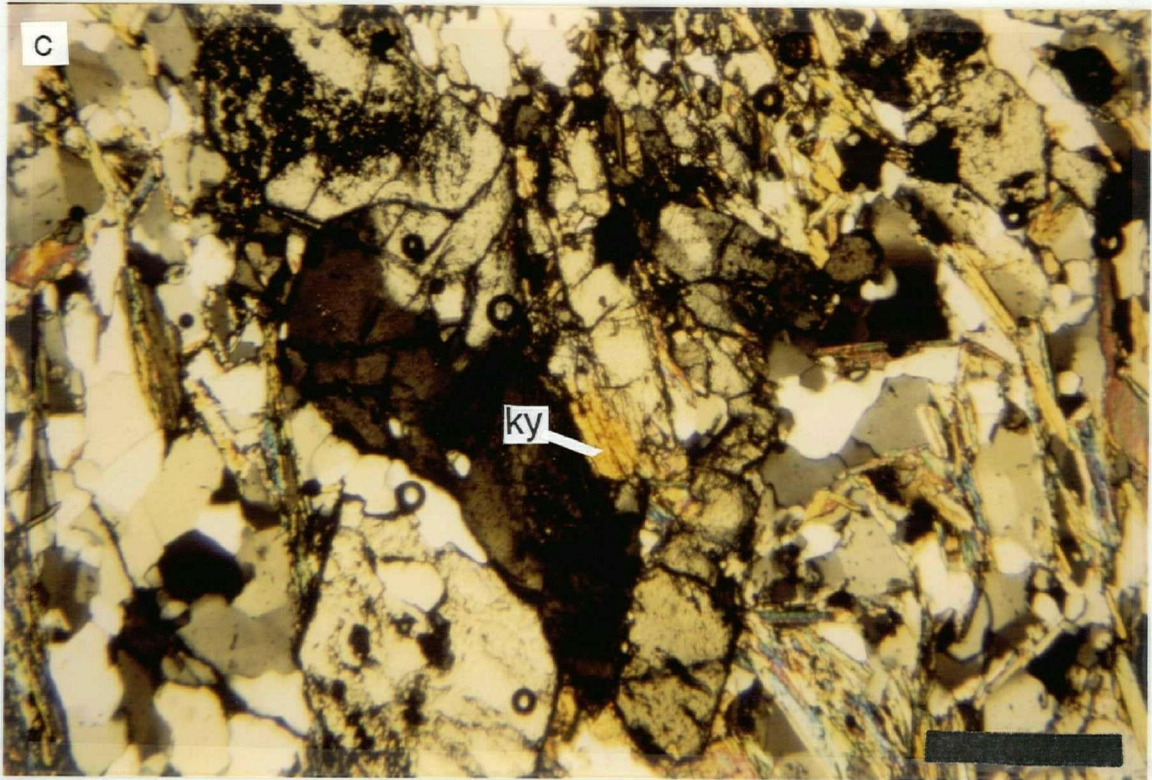


Figure 4.15: Staurolite in Triassic black phyllite, staurolite schist. a) Idioblastic staurolite with tightly folded inclusion trail, scale bar is 1 mm; b) poikiloblastic staurolite surrounding garnet, scale bar is 2 mm; c) cluster of staurolite enclosing kyanite, scale bar is 2 mm; d) . syn-D2, helycitic staurolite, inclusion trails are continuous with the external foliation, scale bar is 2 mm



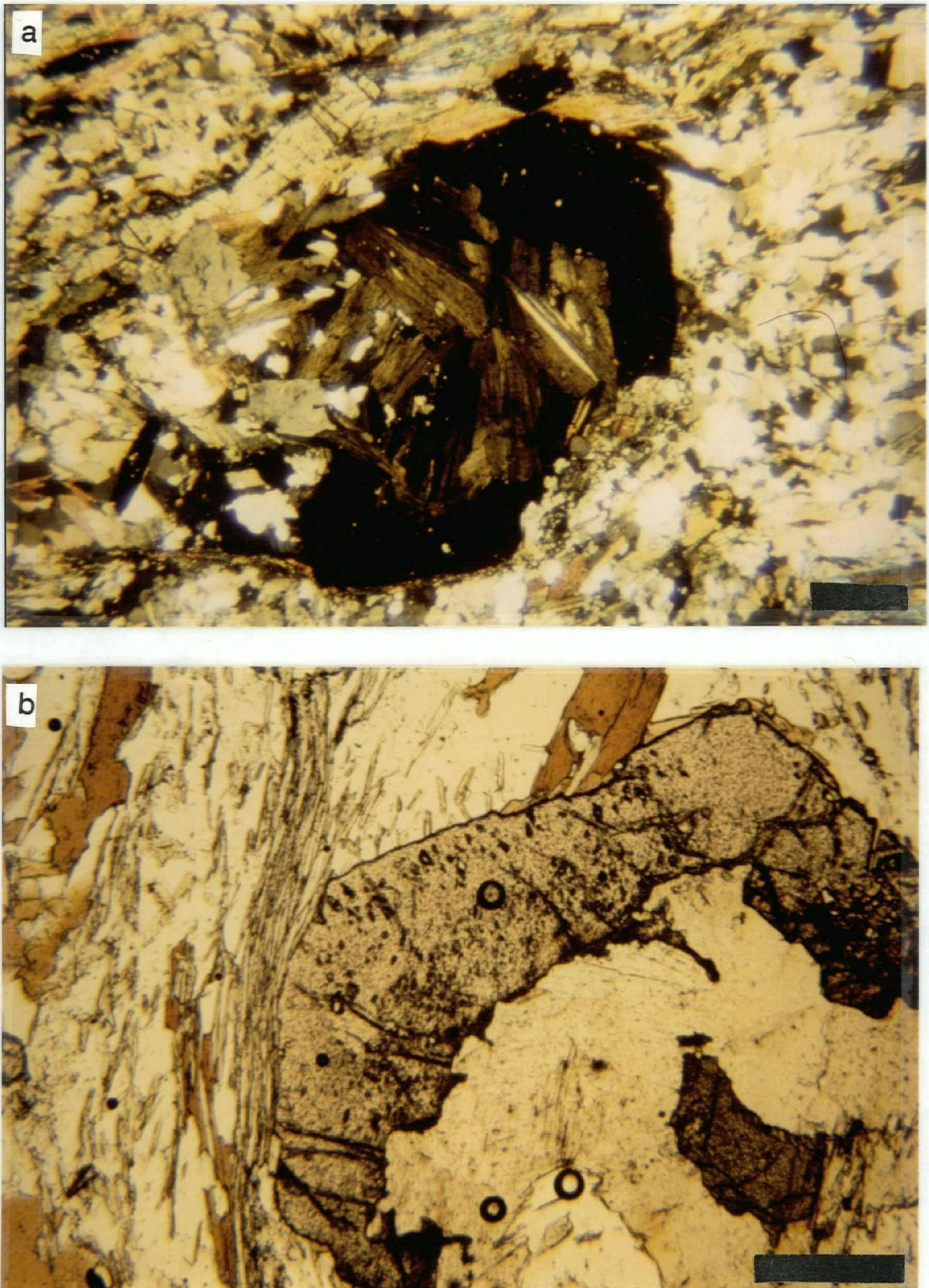


Figure 4.16: Garnet in Triassic black phyllite. a) core replaced by chlorite, scale bar is 2.5 mm, crossed nicols; b) core replaced by chlorite, rim with folded inclusion trails, scale bar is 2 mm, plane polarized light.

garnets show straight inclusion trails and have pressure shadows with large porphyroblasts of strained quartz and biotite. The D_2 crenulation cleavage bends around both types of porphyroblasts.

These textures suggest two stages of garnet growth. The earlier stage which composes some garnet cores has been altered by retrogression so the relationships to structures are unknown. The latter stage began post- D_1 and must have ceased sometime during D_2 prior to the development of the crenulation cleavage and is probably retrograde.

Kyanite

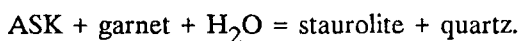
Porphyroblasts of kyanite are mostly inclusion-free. Crystals range from very small (0.1 mm) idioblastic grains to a few larger (up to 4 mm) poikiloblasts. All grains are kinked by S_2 and the smaller grains show undulose extinction (Fig. 4.17). Rare inclusion trails of quartz are parallel to the kinked external foliation.

Kyanite grew syn- to post- D_1 . Textures suggest that retrograde staurolite may be partially consuming kyanite. A small "ghost" kyanite grain in one thin section is completely surrounded by staurolite, having patches where the grain retains kyanite cleavage but has staurolite pleochroism (Fig. 4.15c).

Summary

Metamorphism accompanied D_1 folding of bedding and probably ceased sometime after D_2 had waned. Kyanite growth representing the peak of metamorphism occurred syn- to post- D_1 . A protracted retrograde event recrystallized garnet and large porphyroblasts of staurolite, beginning in D_2 . Late retrogression involving partial annealing and the replacement of garnet by chlorite and plagioclase outlasted D_2 .

The extensive retrograde metamorphism obscures earlier metamorphic and structural minerals and textures. Because of this the peak metamorphic assemblage is unknown. This assemblage may have consisted of kyanite-garnet-biotite but also staurolite and/or sillimanite may have been present. Retrogression began during D_2 and outlasted it, recrystallizing staurolite, garnet, quartz, muscovite and biotite. From textural evidence, retrograde staurolite seems to have formed by the reversal of the common staurolite-out reaction:



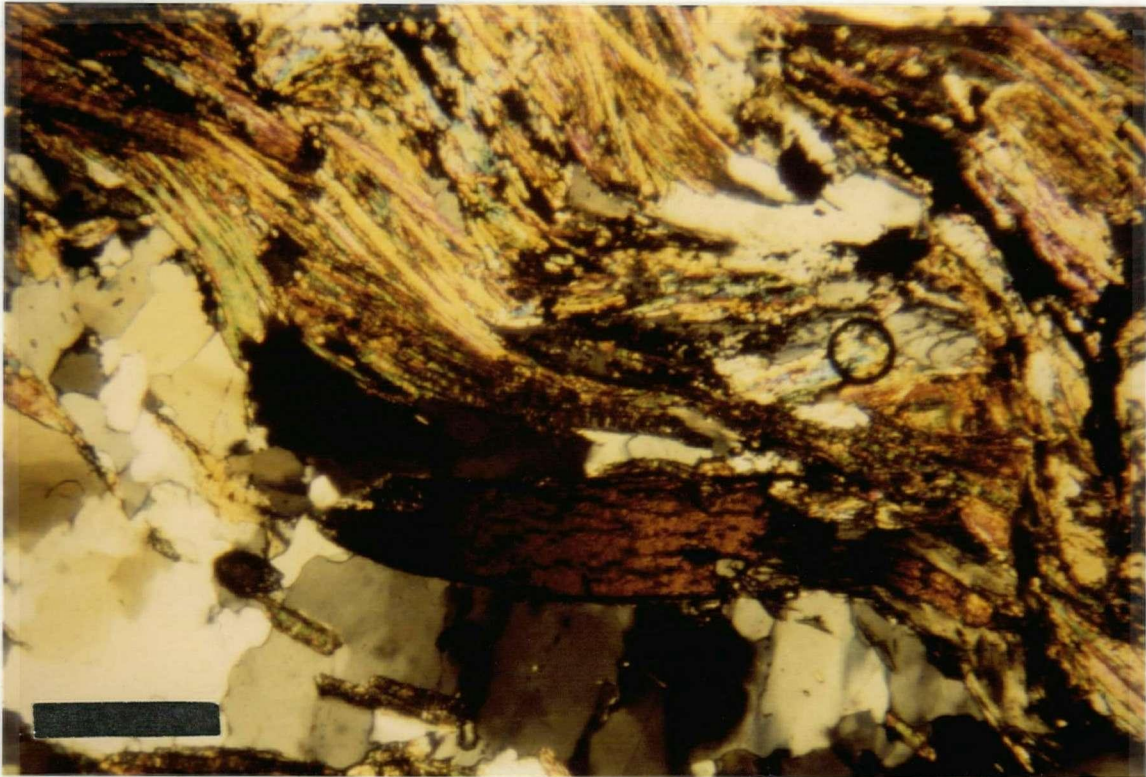
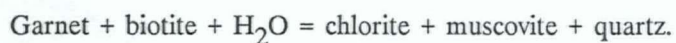


Figure 4.17: Kinked kyanite in Triassic black phyllite, concordant with folded S_1 foliation; scale bar is about 2 mm, crossed nicols.

Replacement of garnet by chlorite and quartz is described by the generalized reaction



Since water is a reactant in both, increased fluid activity would be expected during retrogression.

4.4.5 Crooked Amphibolite

The Crooked Amphibolite was defined and named by Struik (1988a) to include both mafic amphibolites and serpentinites directly above the Eureka Thrust. In this study, petrography and metamorphism of both rock types were determined to confirm correlation with the Redfern Complex.

Ultramafic Rocks

Olivine and chromite are the only primary phases left in the serpentinized Crooked Amphibolite suite and were found only in samples from the Crooked Lake site. Olivine occurs as 1-6 mm, equant grains which show the same evidence of strain including kink bands and neoblasts as the Redfern Ultramafics. A few neoblasts were observed as small (<0.1 mm) strain-free grains, between larger olivine "paleoblasts". Chromite occurs as anhedral, interstitial grains between olivine grains.

The metamorphic mineral assemblage consists of antigorite + magnetite \pm talc \pm magnesite \pm chlorite. Even where serpentinization is complete, relict primary grain outlines are preserved and original textures and mineralogies can be inferred (Fig. 4.18). Serpentine commonly forms oriented needles and needle clusters in an orthogonal grid pattern across the rock. It also forms coronas around olivine and veins with fine-grained magnetite on the walls and center seams of the veins. Magnesite forms xenoblastic, coarse-grained mats and appears to be associated with veins. Talc forms very fine-grained, randomly oriented patches and appears to be replacing primary pyroxene grains where patches are bounded by magnetite trains. Magnetite is disseminated throughout a rock, accumulating in wispy seams, within veins, and as a phase within complex coronas around olivine and pyroxene replacement assemblages.

Remanent grain outlines and metamorphic replacement textures in CL and WL rocks indicate primary phases and textures (Fig. 4.18). Both suites are characterized by a coarse-grain size and may have had cumulate and deformed cumulate textures. Samples from the Crooked Lake site appear to have been dominantly dunites, although mesoscopic cumulate layering was observed in one locality (see Fig. 16b). Primary olivine is replaced by serpentine + magnetite with wispy seams of magnetite outlining original olivine cleavage partings. Planar patches of talc separated by thinner planes of magnetite grains, all in a squarish array, characterize replacement of primary pyroxene. The Wolverine Lake sites, although completely serpentinized, appear to have been pyroxene-bearing peridotites (Fig. 4.18).

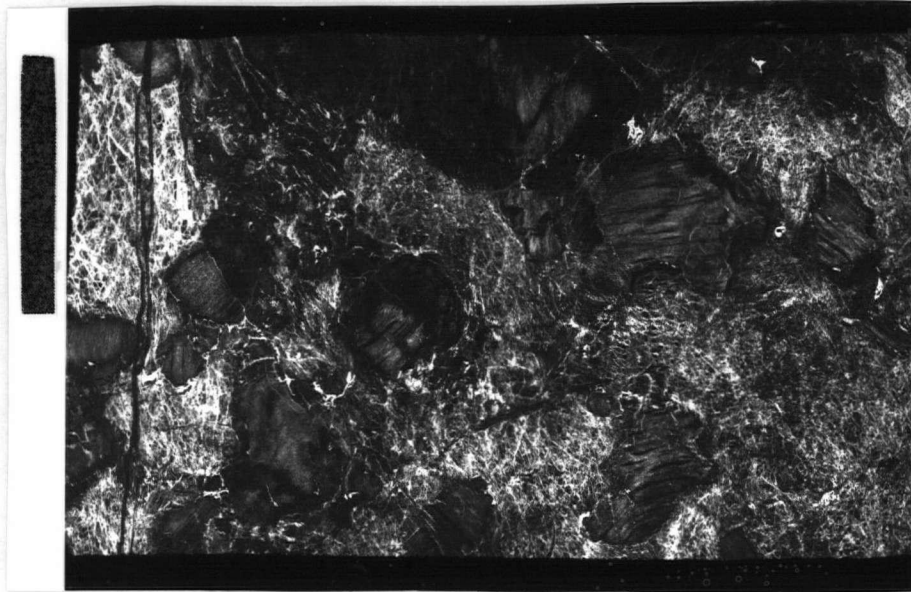


Figure 4.18: Negative image of serpentinite in thin section, WL18, Crooked Amphibolite. Equant darker grains with kinked cleavage traces were pyroxene, white veining is serpentine + magnetite replacing olivine. Scale bar is 1 cm.

Amphibolite Rocks

The amphibolite portion of the Crooked Amphibolite is a fine-grained, hornblende-plagioclase-epidote-chlorite-biotite schist with additional calcite, epidote, and magnetite. Dark green pleochroic hornblende occurs as idioblastic, commonly poikilitic, porphyroblasts (up to 2 mm) and idioblastic matrix-forming grains (0.1-0.5 mm). Two populations of biotite are recognized: 1) an older, sub-idioblastic group of porphyroblasts (0.3-0.6 mm) with bent (001) cleavage traces, and 2) fresh, idioblastic and lepidoblastic small grains (0.1-0.2 mm) which show little or no deformation. Chlorite is found either replacing older biotite grains along cleavage planes or as small, idioblastic grains similar in form to and associated with the younger biotite population.

Plagioclase forms xenoblastic, elongate to equant porphyroblasts (0.5-1 mm) and is also a dominant constituent of the matrix. Compositions were not attainable due to saussuritization which

obscures the albite twins. These larger grains may be paleoblasts or primary plagioclase out of chemical equilibrium with the metamorphic assemblage. Smaller, xenoblastic, untwinned plagioclase which forms the matrix, along with quartz, is probably recrystallized, metamorphic plagioclase. Xenoblastic epidote occurs both in clusters (up to 0.5 mm) of fine-grained (<0.2 mm) minerals and as larger (0.2-0.4 mm), cloudy isolated grains.

Calcite occurs as xenoblastic, larger matrix grains (up to 0.5 mm), porphyroblasts in sample MR05, and in veins associated with epidote.

Metamorphism

Metamorphism of dunitic lithologies resulted in the formation of the assemblage serpentine + magnetite \pm talc \pm magnesite \pm chlorite. This assemblage reflects the instability of forsterite (and enstatite) in the presence of excess water vapor at low temperatures and moderate pressures (Wyllie, 1971). At pressure < 8kb, antigorite is stable only below 600⁰C (Evans et al., 1976). Wyllie (1971) puts the upper limit of the serpentinite facies composed of serpentine + talc + brucite + chlorite + ?amphibole? + vapor at 500⁰C up to 20 kb.

Metamorphism of rocks of basaltic composition in the Crooked amphibolite resulted in the formation of the assemblage actinolite/hornblende, chlorite, biotite, calcite/dolomite, and epidote. This assemblage corresponds to conditions within the greenschist facies of metamorphism, below the chlorite-out reaction (Apted and Liou, 1983). The absence of relict pyroxene which only persists as a metastable phase under the metamorphic conditions implies that the period of metamorphism was long enough to attain chemical equilibrium (Apted and Liou, 1983). Igneous calcic plagioclase (An₆₅ to An₇₈) is less reactive. In experiments it remains as cores surrounded by an epitaxial growth of albite, showing only a small decrease in anorthite content (An₄₄ to An₆₃), up to 575⁰C at all pressures and oxygen fugacities (Apted and Liou, 1983). The presence of chlorite is indicative of greenschist facies conditions (Winkler, 1980; Miyashiro, 1973), below the chlorite-out reaction. Actinolite and actinolitic hornblende and epidote are also indicative of greenschist conditions, temperatures less than 550-575⁰C at pressures 5-7 kb, respectively.

The Crooked Amphibolite rocks exhibit textures and assemblages developed during low greenschist grade metamorphism of partially to extensively serpentinized ultramafites and hydrated mafic rocks. This contrasts with the Redfern Complex assemblage which reached middle amphibolite facies and appears to have been relatively much less hydrous than the Crooked Amphibolite.

4.5 DISCUSSION

Conditions of metamorphism are derived primarily from interpretations of observations of mineral assemblages and their textures with respect to deformation. The peak index mineral assemblages for each unit and their retrograde products are listed in Table II. Conditions are first summarized for "lower plate" and "upper plate" assemblages and then synthesized to describe a thermal history for the evolution of the Redfern Complex and surrounding rocks.

Summary of Lower Plate Metamorphism

The Snowshoe Group underwent an enigmatic deformation and metamorphism event prior to its involvement in the accretion of allochthonous Intermontane Belt terranes (Ross et al., 1985; Lewis 1987; Garwin 1987). The evidence of this event is obscured by later metamorphism which produced most of the minerals and textures now visible. This "second" metamorphism was syn-tectonic, and conditions for it are inferred from the following data:

- 1) Diagnostic mineral assemblages and inferred reactions of their formation;
- 2) Relationships to structures with styles that indicate ductile deformation conditions;
- 3) Temperature estimates and suggested pressures from garnet-biotite geothermometry studies by Phillipone (1985) and Garwin (1987).

The mineral assemblage sillimanite/kyanite-biotite-garnet belongs to bathozone 5 of Carmichael (1978) (Fig. 4.19). Over a range of temperatures greater than 500⁰ C, this zone exists at pressures above 4 kb.

TABLE II

UNIT	ASSEMBLAGE	GRADE/FACIES	RETROGRADE
1 - Snowshoe Group	ky/sill + gt + bi + st + ms + qz + il + pg <u>+to</u>	Kyanite/ sillimanite	chl
2 - Redfern gneiss	qz + plag + ms + bio <u>+act</u>	?	chl
3 - Redfern peridotite	tc + tr + ol + chl <u>+anth+mg</u>	Epidote- Amphibolite	tr,serp
4 - Redfern amphibolite	hb + ep + ab + qz + sp <u>+tr</u>	Epidote- Amphibolite	hb, chl
5 - Quesnel River Group	ky + gt + bi + qz + ms <u>+pg+st</u>	Kyanite	st, gt, chl
6 - Crooked Amphibolite	hb + ch + bi + pg + qz + ep	Lower Greenschist	--
7 - C.A., serpentinites	serp + mt + ch <u>+tc</u> <u>+mg</u>	Lower Greenschist	--

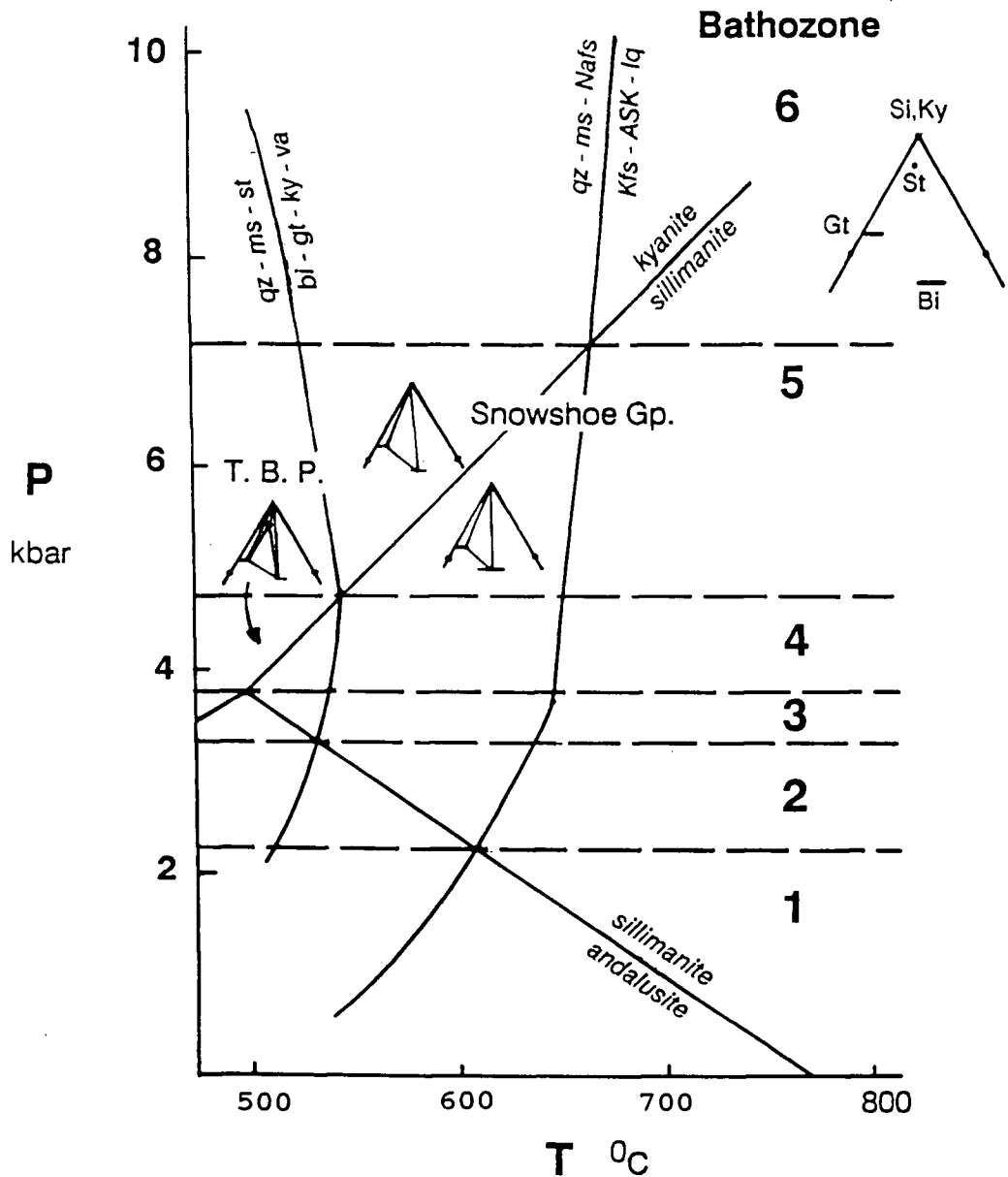


Figure 4.19: Conditions of metamorphism determined from pelitic rock assemblages. AFM diagrams, 2 for Snowshoe Group (kyanite and sillimanite zones) and 1 for Triassic black phyllite (TBP), are located on an idealized P-T diagram showing invariant points and bathograds; after Carmichael, 1978. Location of staurolite out curve approximate from calculations using GEOCALC software by R.B. Berman, T.H. Brown, E.H. Perkins, 1987 (see *Am. Min.* 72: 861).

Prograde metamorphism took place during D_2 of the Snowshoe Group. This deformation developed syn-metamorphic similar folds, cleavage, and shear fabrics, indicative of medium to high grade metamorphism.

Temperatures for the kyanite-sillimanite zone estimated by Fillipone (1985) and Garwin (1987) using garnet-biotite thermobarometry are inferred to be similar to temperatures for the kyanite-sillimanite zone rocks in this study. If this inference is correct then temperature exceeded about 550°C and pressure was greater than 5 kb.

Summary of "Upper Plate" Metamorphism

Rocks from the upper plate underwent one protracted phase of metamorphism, beginning during D_1 with a period of high-temperature retrograde outlasting D_2 . Pressure and temperature conditions are interpreted from the observed mineral assemblages in the three lithologies of the assemblage and correlations with structural fabrics. Comparison of the metamorphism of the Redfern Complex with that of the Crooked Amphibolite yields two important observations: 1) that the Redfern Complex is more intensely metamorphosed, and 2) that the volume and surface area of a body of ultramafic rock determines the permeability and fluid mobility which in turn controls the extent of its metamorphism.

Mineral assemblages developed in all three upper plate lithologies indicate conditions of epidote-amphibolite facies or kyanite grade metamorphism. Within the Redfern peridotite, the mineral assemblage of talc-tremolite-chlorite-olivine corresponds to the kyanite-staurolite zone (Trommsdorff and Evans, 1974) or middle-amphibolite facies (Wyllie, 1971). Two reactions bound the conditions of formation of the Redfern amphibolite mineral assemblage hornblende-albite-epidote-quartz. The chlorite-out and epidote-out reactions bracket temperatures between 500 and 650°C for reasonable geologic pressures of 5-7 kb (Apted and Liou, 1983). The mineral assemblage in the metapelites of the Triassic black phyllite is kyanite-biotite-garnet, corresponding to bathozone 5 (see Fig. 4.19; Carmichael, 1978). Conditions associated with this assemblage do not further refine the estimates made based on the amphibolite mineral assemblage.

Metamorphic minerals comprising the S_1 foliation in amphibolitic and pelitic lithologies of units 4 and 5, indicate that metamorphism began during D_1 . Fabrics related to D_2 are also defined by the growth

of metamorphic minerals along axial planes though much less extensively than those of D_1 . Randomly oriented minerals, primarily amphiboles in metaigneous rocks and staurolite in the metapelites, overgrow both D_1 and D_2 structures. This is interpreted as a syn- to post-deformation retrograde phase of the main metamorphic period.

The middle amphibolite facies/kyanite staurolite grade of the Redfern Complex contrasts with the lower greenschist facies/chlorite grade of the contiguous Crooked Amphibolite and overlying lithologies. This indicates that the peak metamorphic conditions attained in the entire upper plate were not the same throughout the region. The Redfern Complex must represent one of the structurally lowest levels of the upper plate which has not been eroded away.

Thermal History of the Redfern Complex

Metamorphism in both the upper and lower plate assemblages began prior to the emplacement of the Redfern Complex onto the Snowshoe Group. Development of upper plate D_1 and lower plate D_2 structures was initiated with the onset of convergence. Prograde metamorphism accompanied this deformation episode resulting in the formation of L_1 lineations and S_1 foliations in upper plate rocks and L_2 and S_2 in the lower plate. Metamorphic conditions peaked sometime after these foliations were well-developed, as many of the index minerals contain foliation-parallel inclusion trails. Importantly, porphyroblasts within the Snowshoe Group contain a folded foliation while the porphyroblasts in the Triassic black phyllite associated with the peak assemblage contain only straight inclusion trails.

A second thermal pulse during waning metamorphism resulted in a sustained retrograde phase, extensively recrystallizing the upper plate rocks. A second regional phase of buckle folding (third, lower plate) accompanied retrogression. Locally, shearing occurred subparallel to the steep axial planes of D_2 folds along the limbs of cusped synforms. Minerals were extended and new ones recrystallized both parallel to the F_2 fold axis and perpendicular to it, downdip on the limbs of folds. The Triassic black phyllite metasedimentary rocks rest within one of these D_2 cusped hinge zones and are the only rocks in the study area which have both of these lineations developed. Thus they are actually structurally lower than most of the Snowshoe Group rocks which remain relatively unaffected by the retrogression.

Both the amphibolites and ultramafics contain abundant post- D_1 , randomly oriented minerals, suggesting that they also partially recrystallized during the retrograde stage. Therefore the Snowshoe rocks must also have received some of the heat unless they were very far away at the time of retrogression. Diffusion, solid or fluid, must somehow have been inhibited.

Retrogression within the Snowshoe has been associated with the migration of fluids through the rocks, their source being prograde dehydration reactions (McMullin and Greenwood, 1988; Lewis, 1987; Garwin, 1987). The Redfern Thrust may have acted first as a barrier and then as a conduit for fluids driven off of the Snowshoe, directing them into overlying rocks. The ultramafic rocks themselves would have acted as an impermeable zone, inhibiting the flow into rocks directly overlying them. Fluids may have migrated along the thrust surface, moving upwards as they encountered thrust splays and eventually disseminating into more permeable rocks, such as the Triassic metasedimentary rocks. Thus a greater fluid content within the Triassic rocks prior to the onset of F_2 folding may have driven retrograde reactions. In addition, an influx of fluids along the Redfern thrust during D_2 would increase the pore pressure, once again localizing shear stress on the thrust surface and allowing renewed slip during buckle folding.

An alternative explanation is simply that the two assemblages were still separated during retrogression. This would require a large amount of movement on the Redfern thrust, on the order of tens of kilometres, during and perhaps after D_2 upper plate deformation. Some movement necessarily had to take place in order to accommodate buckle folding of the fault and rocks of high ductility contrast. A large amount of movement seems unreasonable and is not necessary to explain the differences in metamorphic textures and mineral assemblages in the upper and lower plates of the Redfern thrust.

5. GEOCHEMISTRY

5.1. INTRODUCTION

Geochemical analysis was undertaken in order to characterize the igneous rocks and minerals of the Redfern Complex and relate them through igneous and metamorphic/metasomatic processes. There were four objectives to the geochemical studies:

- 1) To ascertain the original composition of the rocks and minerals;
- 2) To determine the chemical affects of alteration;
- 3) To compare and contrast the Redfern Complex to the Crooked Amphibolite;
- 4) To derive the paleo-tectonic setting represented by these rocks from their geochemistry.

Samples of mafic and ultramafic rocks, altered and unaltered, were chosen from several different localities within the Redfern Complex and from the Crooked Amphibolite. Sample locations are illustrated in Figure 5.1. A suite of rocks representing the petrographically least altered was chosen to characterize the igneous chemistry. Rocks with greater than 50% alteration were used solely to evaluate the nature of alteration. Samples from the Crooked Amphibolite were collected at five localities along strike and compared to the Redfern Complex. Rocks of the Redfern Complex and Crooked Amphibolite are described together or referred to by their site names when described separately: Redfern Complex specimens are DL (Dunford Lake) and Crooked Amphibolites are CL (Crooked Lake), BC (Bassett Creek), MR (MacKay River) and WL (Wolverine Lake) (Fig. 5.1).

Previous work on the geochemistry of the Crooked Amphibolite was done by K. V. Campbell (1971; Antler Formation) and on the correlative Fennell Formation by Schiarizza and Preto (1987).

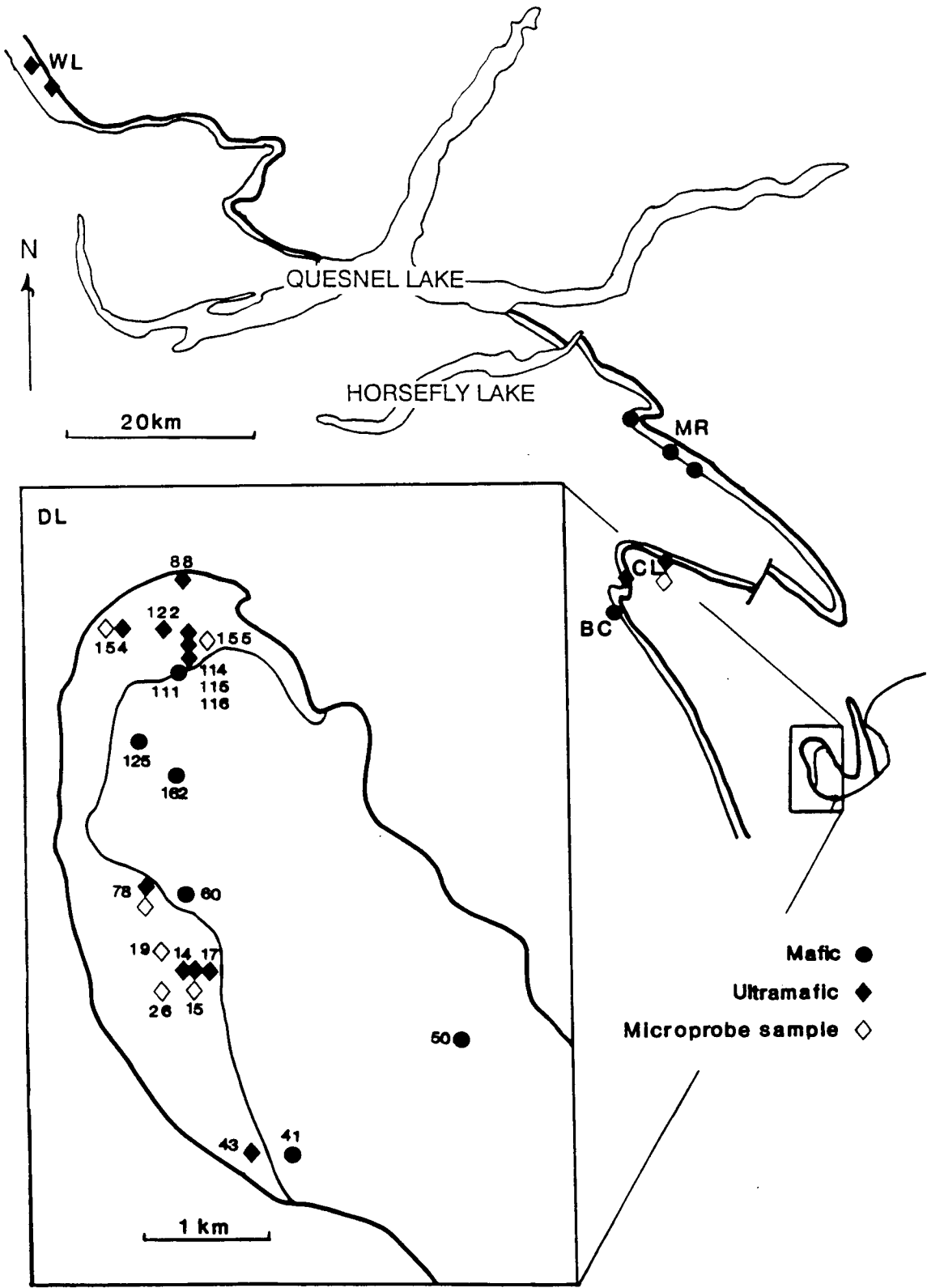


Figure 5.1: Location map for geochemical samples.

5.2. MAJOR AND TRACE ELEMENT GEOCHEMISTRY

Whole rock major and trace element geochemistry were determined for suites of ultramafic and mafic rocks from the Redfern Complex and the Crooked Amphibolite by XRF analysis. The purpose of determining the rock geochemistry is to characterise the rocks in the following ways:

- 1) To distinguish between alpine-type and stratiform/ concentric intrusion-types of ultramafic rocks;
- 2) To distinguish the tectonic setting of the amphibolite protolith as either oceanic or island arc;
- 3) To compare and contrast the chemical characteristics of the Redfern Complex and the Crooked Amphibolite.

The Redfern peridotite was sampled across stratigraphy and the Redfern amphibolite was sampled across structure. Samples from the smaller, tectonically disrupted Crooked Amphibolite were obtained where the unit is easily accessible by car or boat.

5.2.1. XRF Analysis

Sample preparation and analysis by X-ray fluorescence followed standard UBC procedure using fused-glass pellets for major element determination and 3-gm pressed powder pellets for the measurement of trace element concentrations. All pellets were prepared with dehydrated rock powder and loss on ignition was determined separately. Rock was ground to powder using a Cr-steel shatterbox and tungsten-carbide ring mill to minimize contamination of trace elements not already abundant in the rocks (Hickson and Juras, 1986).

XRF analysis was performed manually on a Philips 1140 W spectrometer. Counts for all standards and unknowns were collected on single peaks or in groups of peaks with similar two-theta angles to reduce machine drift, minimize analytical error, and maximize the quality of analysis. Raw counts were reduced using UBC software for major elements and using software or by hand for trace elements.

Analytical precision was estimated by running a monitor for major and trace elements during analysis. The monitor also provided an estimate of accuracy. The monitor for major elements is BCR-1 and the mean value obtained is accurate to within two standard deviations of the anhydrous value used for

calibration. Trace element analyses were subject to significant analytical error during count collection. To test the magnitude of the error, a set of 5 samples representing the range of compositions were run on the Philips automated XRF spectrometer in the Oceanography Department at UBC. As a result, analyses for Cr, Ni, and V are the only ones with relative errors within two standard deviations of the accepted value. The rest have been adjusted by a factor determined from the Oceanography results and are considered qualitative values only.

5.2.2. Chemical Character

Mafic Rocks

Mafic rocks from both the Redfern Amphibolite and the Crooked Amphibolite are grouped together. In a similar study, Campbell (1971) concluded that rocks from the Crooked Amphibolite were of similar origin. He based this on the fact that the variation in chemical compositions between rocks from different localities did not exceed the variations between rocks from the same site. Based on similarities between sample sets in hand specimen appearance, structural and stratigraphic setting, and a review of the chemical data, the same preliminary conclusion is drawn here. The major petrographic and petrologic differences between rocks from the Redfern and Crooked Amphibolites is metamorphic grade.

Major element ranges are displayed in Figure 5.2, a Harker-type oxide variation plot. All oxides are plotted against MgO, the major element which shows the greatest range over both the suite of amphibolites and the suite of ultramafic rocks. The weight percent SiO₂ range for the amphibolites is within and below that expected for basalts and comes very close to the upper limit of the range for the ultramafic rocks. It also shows little variation with respect to MgO, which varies greatly from 3.64 up to 23.23 %. Only TiO₂ and FeO show a consistent variation with respect to MgO, both decreasing with increasing MgO content. Aluminum is consistently high but drops drastically in the highest MgO rocks. Variations in calcium content tend to follow those in MgO, though neither is consistently higher than the other. The remainder are minor elements which are consistently low except in two anomalous Crooked Amphibolite samples, MR04 and MR05.

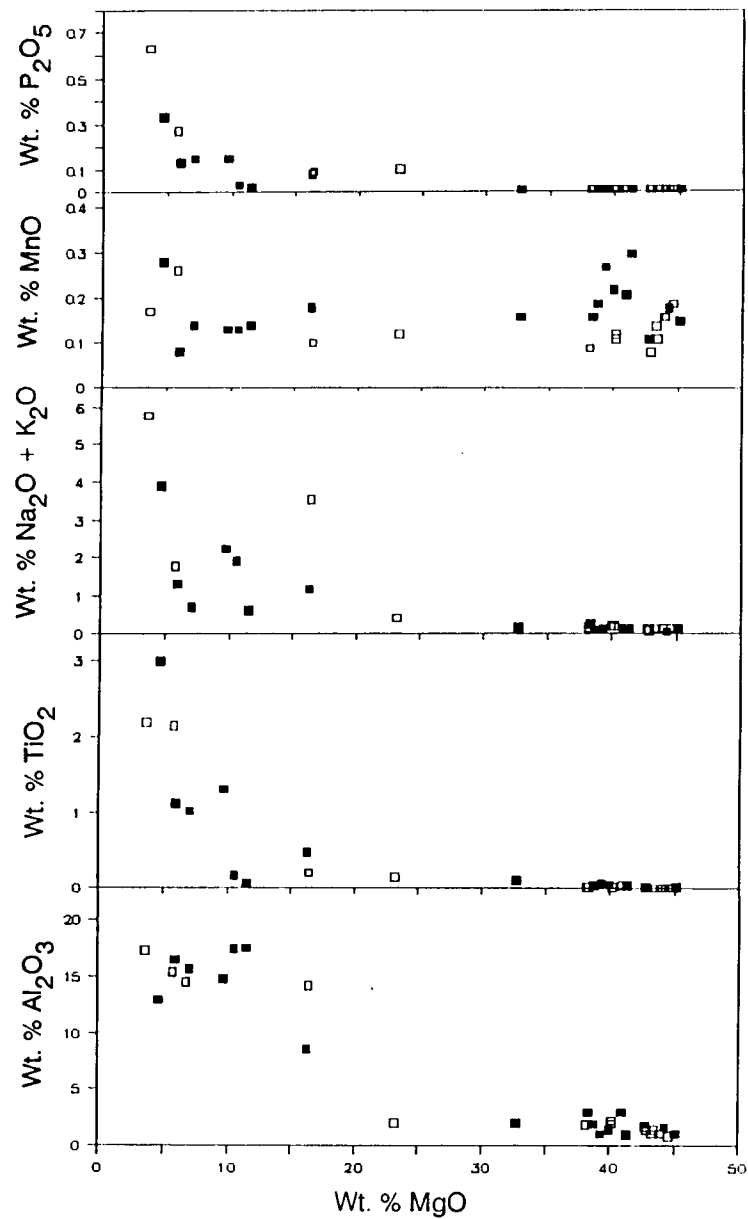
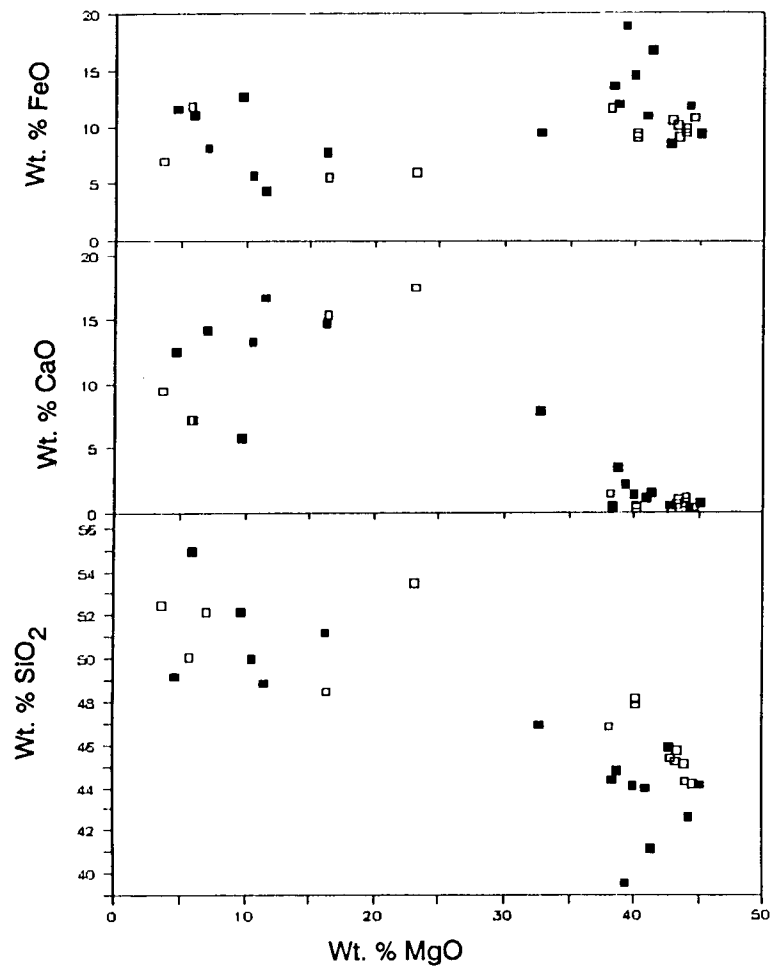


Figure 5.2: Harker-type oxide variation plot of major element oxides versus MgO. Redfern Complex filled symbols, Crooked Amphibolite open symbols.

Trace element analyses reveal high Ni and Cr contents compared to analyses of the Crooked Amphibolite by Campbell (1971) and of the Fennell Formation by Schiarizza and Preto (1987). Ranges of Zr are similar to those for Fennell Formation basalts and gabbros (Schiarizza & Preto, 1987).

Ultramafic Rocks

Ranges in chemical composition within the ultramafic rocks are much less than that observed in the mafic rocks (Fig. 5.2). Mafic and ultramafic rocks are well separated on the plot of MgO vs. SiO₂. Composition ranges within the Redfern ultramafics generally include all of the samples from Crooked Amphibolite sites; however, some distinctions can be made.

The content of SiO₂ ranges from 39.5 to 48 % with the Crooked Amphibolite rocks on the upper end of the range. This suggests that CL and WL serpentinites are equivalent to the upper portion of the DL rocks. The variations in MgO, FeO, and CaO are less with the DL rocks occupying both extremes of the ranges and CL and WL rocks clustered in the middle. Exclusion of the highest CaO value because it is from a layered (inhomogeneous) sample tightens the range considerably. The remainder of the major elements are present in only minor amounts, near detection, and their variations are not believed to be significant.

Two samples from unit 3B the Redfern Complex contain macroscopic igneous layering and display anomalies related to this inhomogeneity. Both samples contain various amounts of pyroxene blackened by opaque inclusions. Sample DL015 contains abundant clinopyroxene with symplectic intergrowths of spinel rather than magnetite. This is reflected in its high CaO, Al₂O₃, TiO₂, alkalis and phosphorous and lower MgO. Greater diopside content in samples DL114 and DL017 explain their high CaO content with respect to dunites composed of almost pure forsteritic olivine .

5.2.3. Tectonic Diagrams

The possibility of element mobility during amphibolite grade metamorphism must be considered when applying tectonic discriminant diagrams to rocks of that grade. However, plots on various

discriminant diagrams show that the sub-greenschist grade rocks of the Crooked Amphibolite tend to cluster just as well as the amphibolite grade Redfern Complex rocks.

Element ratios can be used to investigate element mobility versus immobility and conservation during a process (magmatic, metamorphic, or metasomatic) and thus to test the validity of applying discriminant diagrams based on primary igneous chemistry. Ratios comprising a denominator element which is hypothesized to represent a conserved element and a numerator element which is allowed to vary are plotted and their tendency to scatter or cluster gives an indication of true mobility of the denominator element. Not surprisingly, no elements were found to be conserved in the amphibolites even those thought to be relatively immobile such as MgO, Zr, or Nb. However, this could result simply from original chemical variations, including evolution from different magmas, much less different volcanic vents or intrusive versus extrusive rocks from a common parent magma. The failure of the amphibolite rock suites to pass this test indicates that they will also likely yield inconsistent and ambiguous results when plotted on tectonic discriminant diagrams.

The SiO_2 content and plot of alkalis versus silica indicate that the amphibolites have subalkaline basaltic compositions (Fig. 5.3). They plot mainly in the tholeiitic field on an A(total alkali)FM ternary diagram (Fig. 5.4). Two of the more altered Crooked Amphibolite samples fall in the calc-alkaline field. Most of the samples fall in the oceanic field of an A(Al_2O_3)FM diagram (Fig. 5.5a), again with highly altered and inhomogeneous samples falling in the island arc and intracontinental fields respectively. Pearce et al (1977; 1988) assert that the $\text{MgO-FeO}^*(\text{total Fe as FeO})\text{-Al}_2\text{O}_3$ diagram is as effective (75%) at discriminating tectonic environments as trace element diagrams. However, Erdman (1985) found that the field boundaries on this diagram are not sharp enough to adequately discriminate samples from known tectonic settings. Erdman (1985) recommends the $\text{TiO}_2\text{-P}_2\text{O}_5\text{-MnO}$ diagram of Mullen (1983) as more effective. The data from these suites, however, lie in almost every field on this diagram (Fig. 5.5b).

Trace element diagrams were not used for discrimination of tectonic environments as suggested by Pearce and Cann (1977) because of large analytical errors.

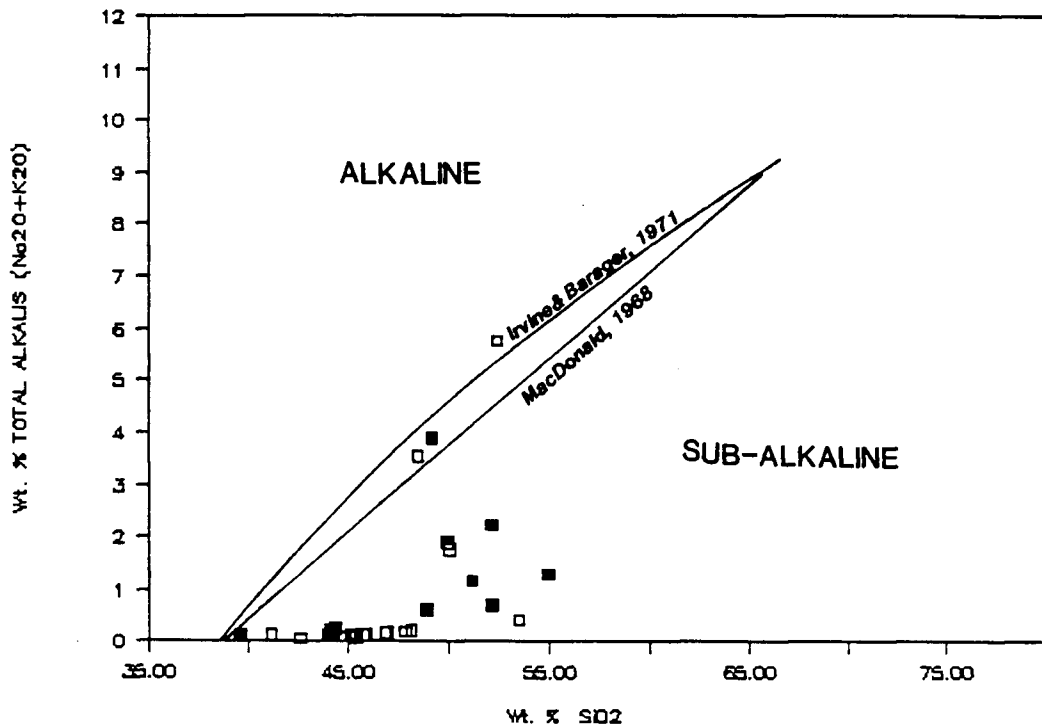


Figure 5.3: Plot of alkalis versus silica to discriminate alkaline versus subalkaline rocks. Filled symbols Redfern Complex, open symbols Crooked Amphibolite.

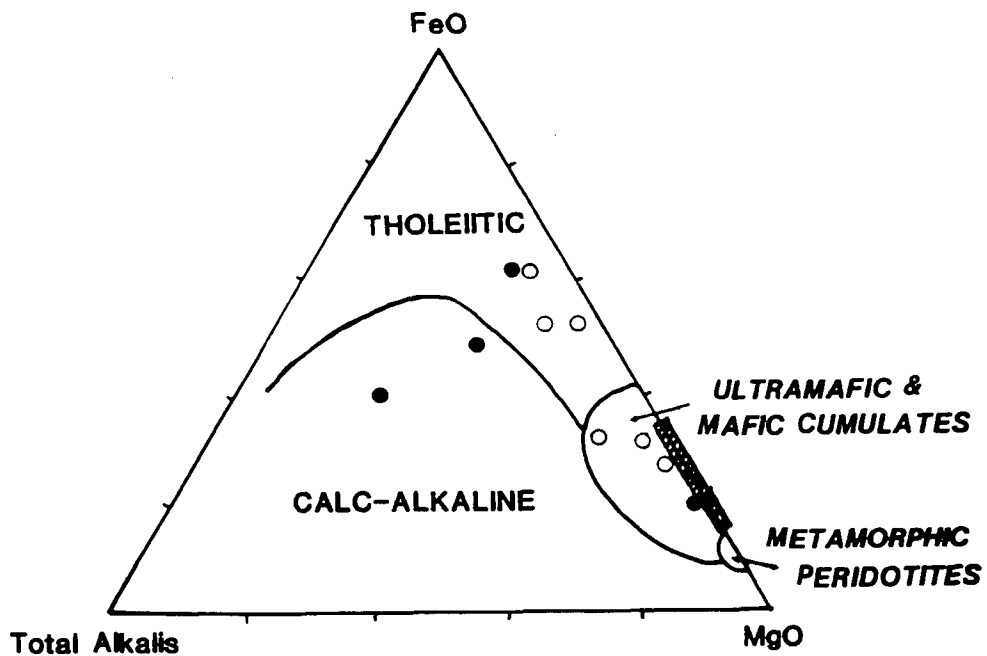


Figure 5.4: Ternary plot of FeO-Total Alkalies ($\text{Na}_2\text{O} + \text{K}_2\text{O}$)-MgO. Basaltic fields after Irvine & Barrager, 1971 and ultramafic fields after Coleman, 1978. Closed symbols Redfern amphibolites, open symbols Crooked Amphibolite, and hatched rectangular area is combined Redfern peridotites and Crooked Amphibolite serpentinites.

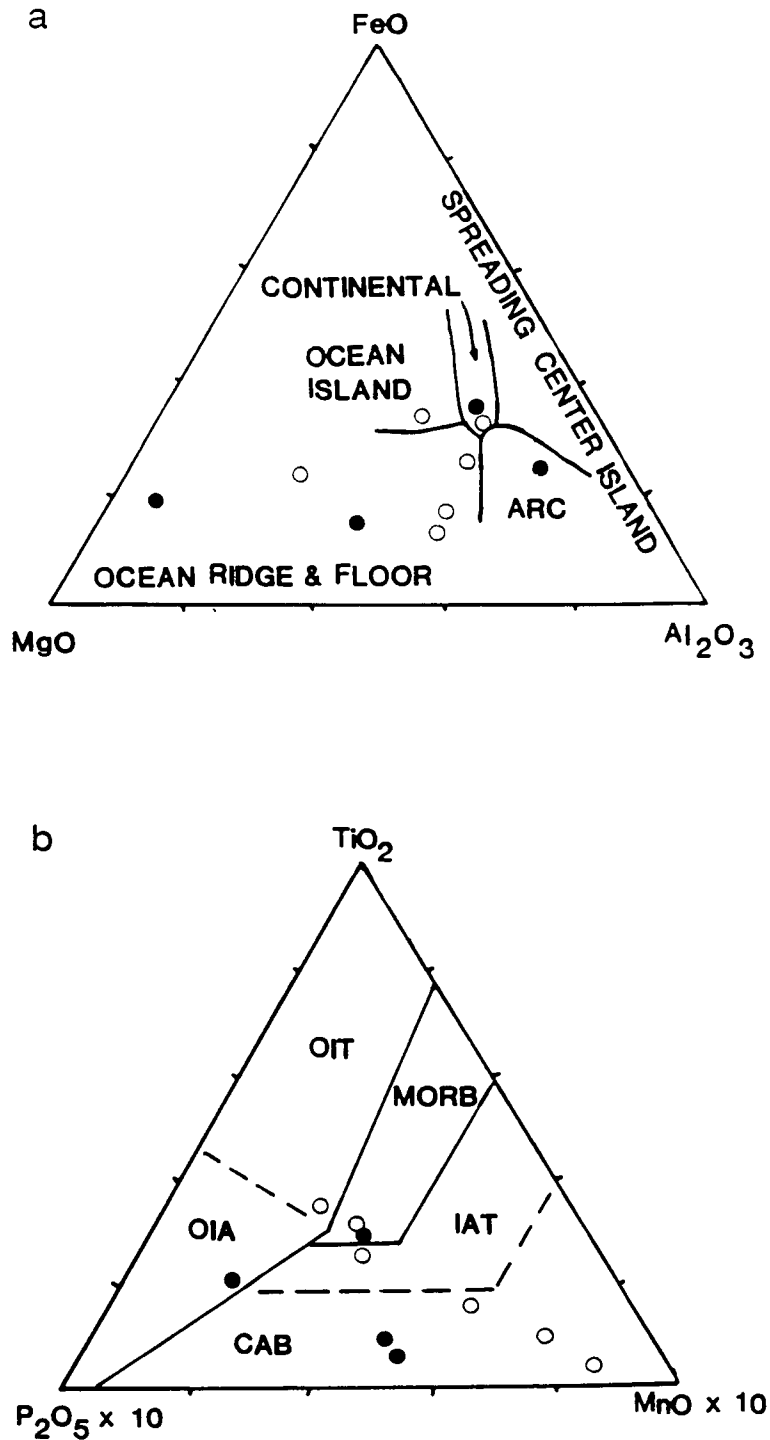


Figure 5.5: Ternary discriminant plots based on major and minor oxides. Filled symbols Redfern amphibolite, open symbols Crooked Amphibolite. a) FeO-MgO-Al₂O₃ plot, fields after Pearce et al., 1988; b) TiO₂-P₂O₅-MnO plot after Mullen, 1983.

5.2.4. Conclusions

Effects of Alteration

The degree of alteration affecting samples was estimated petrographically. Affects ranged from minor alteration in rocks where primary igneous minerals and textures are well-preserved to partial metamorphism (DL rocks) and complete metamorphism (WL13) and complete metasomatism (MR05). Major element variations are most easily explained by original compositional diversity (amphibolites) and sample inhomogeneity (layered ultramafics). The assumption that metamorphism was essentially isochemical is proved valid when partially and completely metamorphosed samples of the same lithology are compared. The two suites of ultramafic rocks from the Crooked Amphibolite, CL and WL rocks, perhaps illustrate this best. The CL suite consists of serpentinites which vary from partial to complete serpentinization and recrystallization of a dunite protolith at chlorite grade. All of the WL suite are magnetite-bearing serpentinites. Both of these suites show small compositional variations, both of individual oxides and totals, and are similar in composition to the less altered DL rocks. This indicates that the effects of total metamorphism have left the rocks' chemical composition essentially unchanged.

Percent loss on ignition, which primarily reflects loss of volatiles, may be used as an indicator of degree of alteration. Rocks which are mostly to completely serpentinized have much higher percent LOI than less serpentinized samples (see Table III). On the whole, DL rocks are least serpentinized, followed by the CL suite with the WL suite showing 100% serpentinization. This trend is reflected in the LOI values which are lowest in the DL rocks and highest in the WL rocks (Table III). Within the DL suite the same trend of increased alteration corresponding to increased LOI is observed. This trend in turn implies a correlation between percent alteration, which depends upon permeability and fluid penetration, and size of a peridotite body. Penetration of fluids into the peridotites must be accomplished through fracturing because of the rock's extremely low primary permeability (Coleman, 1977). The Redfern peridotite is the largest of the three peridotite bodies and the preservation of primary igneous minerals and textures is best in the DL rocks. Metamorphic minerals and textures also suggest a low amount of hydration prior to the onset of prograde alpine metamorphism (see above). Therefore, LOI may be used to indicate penetration of fluids and their alteration effects.

TABLE III

<u>SAMPLE</u>	<u>% LOI</u>	<u>APPROXIMATE % ALTERATION</u>
CL-04	7.2	65
CL-05	9.6	100
CL-16	6.5	35
CL-17	7.8	75
WL-13	11.3	100
WL-14	13.5	100
WL-15	12.5	100
WL-16	11	100
WL-18	4.6	100
DL-014	3.3	45
DL-015	1.5	25
DL-017	3.6	30
DL-043	4.0	45
DL-078	4.6	50
DL-088	2.8	15
DL-114	4	80
DL-115	3.5	25
DL-116	4.6	40
DL-122	7.5	50
DL-154	3.3	15

The Crooked Amphibolite rocks show large variations in major element concentrations which appear to be due to unknown amounts of several types of alteration. All of the Crooked Amphibolite samples have bad totals (either high or low) which are not related to systematic variations in any element or group of elements and the reason for the bad totals is unknown. In addition, some samples may have undergone carbonate metasomatism, such as sample MR05 which petrographically consists almost entirely of calcite and has the highest alkali content of any sample in the suite. Therefore, the Crooked Amphibolite rock suite probably has a complex history of alteration related to both metamorphism and metasomatism.

Discussion

Interpretations of chemical character including the use of tectonic discriminant diagrams involves comparison of the reference suite to other suites of fresh and altered rocks. Chemical classifications will thus be subject to errors arising inherently from the nature of the empirical data sets. Unknown variations in analytical procedures between labs and a lack of data on higher-grade metamorphic rocks are two problems which affect the interpretations. The necessary assumption that metamorphism is an isochemical process on the sampling scale may be erroneous.

Based on field and petrographic relations the Redfern peridotite appears to belong to the ultramafic cumulate portion of an ophiolite stratigraphy. Chemical characteristics of the peridotite support this interpretation. The ranges of major and minor element concentrations found in the Redfern peridotite defy simple classification as either primitive or depleted mantle. For example, while both MgO and SiO₂ overlap ranges for both primitive and depleted peridotite, FeO and CaO range much higher than either (Wyllie, 1971). The concentration of Ni and Cr is strongly dependent upon mineralogy, with Ni concentrated in olivine and Cr in spinel and diopside. Therefore, the chemical character of the "parent" material and the amount of melt extracted will determine the chemical character of each cumulate layer. Since many of the major elements reach similar values expected for underlying metamorphic harzburgites (Coleman, 1977), it is likely that the Redfern peridotite lies at the base of the cumulate section.

The wide and unsystematic variations in chemistry of the amphibolites suggests great heterogeneity of the protoliths. One sample with high MgO and Cr and low Al_2O_3 may be close to an ultramafic composition. The rest appear to have been low-K, tholeiitic basalts. Contamination of the igneous rocks by intersedimentation, metamorphism, and metasomatism probably significantly contributed to the wide variations in chemical concentrations of both major and minor elements.

The preliminary assumption that the Crooked Amphibolite and Redfern Complex had similar origins and source rocks seems to be born out by similarities in at least the ultramafic rocks. Mafic lithologies are more ambiguous and the Crooked Amphibolite appears to be more heterogeneous and probably more affected by alteration than the Redfern amphibolite suite.

5.3. ULTRAMAFIC MINERAL CHEMISTRY

The main objective for determining phase compositions was to evaluate the origin of the Redfern Complex, hence primary igneous minerals were analysed by electron microprobe. Compositions of olivine from four samples (three DL and one CL), clinopyroxene in four samples (all DL), and spinel in two (DL and CL) were measured. Sample locations are shown in Figure 5.1. Electron microprobe analyses and operating conditions are listed in Appendix B.

5.3.1. Olivine

Olivine from the Redfern Complex has a restricted composition range, $\text{Fo}_{82.4-83.7}$ and $\text{Fo}_{87-90.7}$. This range is consistent with the range for peridotite and ultramafic cumulate rocks from ophiolites (Coleman, 1977). Metamorphic olivine has a higher forsterite content, at least Fo_{95} , while stratiform ultramafic complexes are typically more iron-rich and show a greater range in forsterite content (Jackson and Thayer, 1972). Compositions of small (< 0.1 mm) dynamically recrystallized neoblasts have the same composition as larger "parent" grains. No compositional zoning was detected.

Composition varies systematically with stratigraphic position (Fig.5.6). Samples from unit 3A basal dunites have the highest forsterite content ($\text{Fo}_{90-90.7}$) and are also high in nickel (0.27-0.51 % NiO). These values are typical for metamorphic peridotites of ophiolites (Coleman, 1977). Olivine from unit 3B

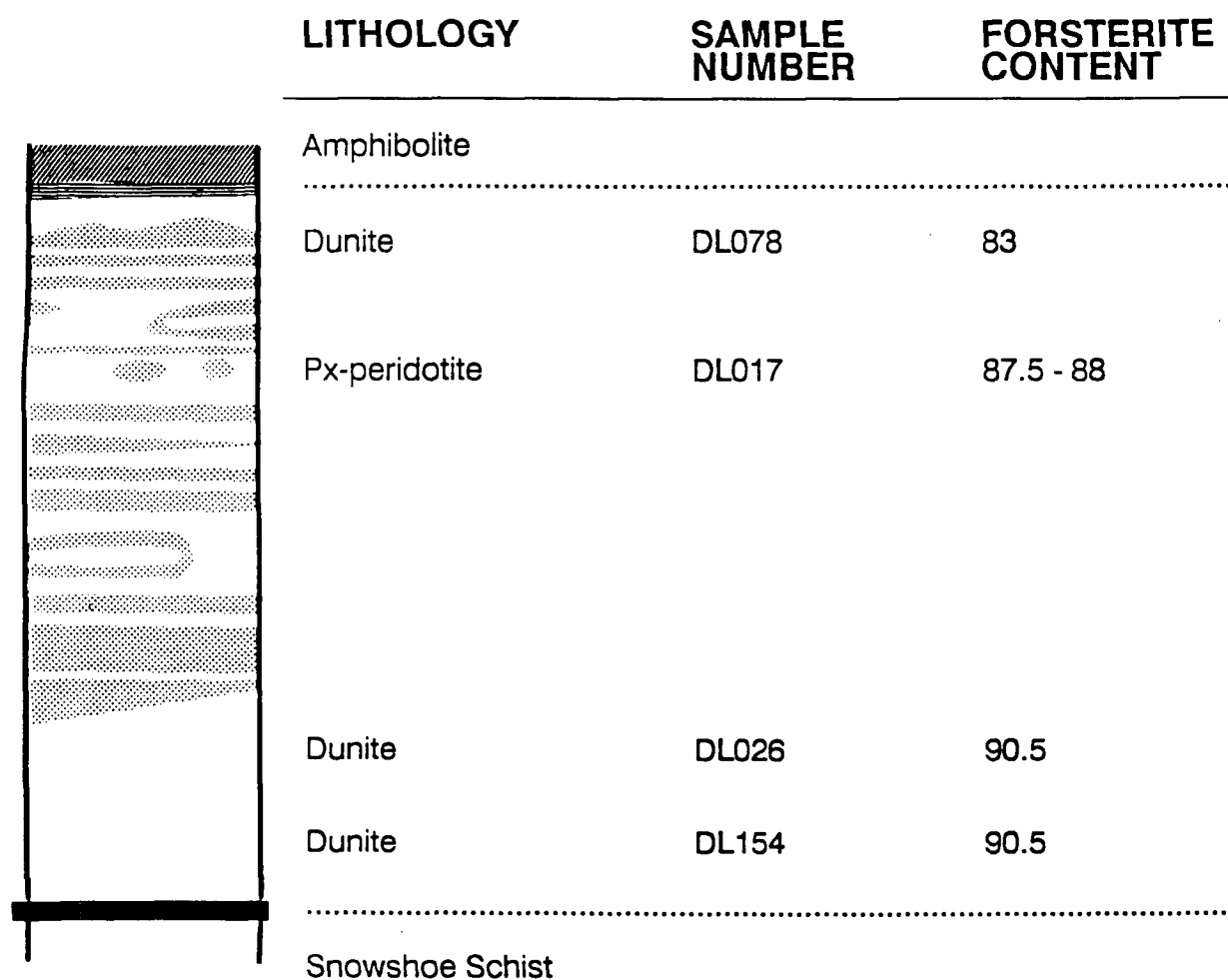


Figure 5.6: Variation in forsterite content of olivine with respect to the structural stratigraphy in the Redfern peridotite (sample location Fig. 5.1).

has both lower forsterite ($Fo_{87.5-88}$) and nickel (0.11-0.26%). The subunit has cumulate layering and cumulate textures and these values are more characteristic of ultramafic cumulates (Coleman, 1977). The lowest forsterite and nickel values are from a sample on the upper, tectonic contact of unit 3B. This contact shows evidence of metasomatism (see chapter 4) and may have been more severely altered than the others. Alternatively, the forsterite value is consistent with iron-enrichment associated with lithologies higher in the cumulate section (Coleman, 1977).

Relict olivine in one highly serpentinized CL sample was analysed. Grains are zoned, with lower Mg at rims and adjacent to serpentinized intergranular cracks, and the forsterite content ranges from $Fo_{87.4}$ to $Fo_{90.6}$ for different grains within the sample. Nickel contents are high for all the grains, ranging from 0.27-0.51 % NiO, the same as for the DL samples with forsterite values around $Fo_{90.5}$. This suggests that all of the olivine had an original composition of averaging $Fo_{90.5}$ and that Mg loss resulted from diffusion during serpentinization.

5.3.2. Pyroxene

Fresh pyroxene is preserved only in samples from the Redfern peridotite, unit 3B. It is a Cr-rich diopside (Fig. 5.7). Clinopyroxene also has a very restricted range of end-member compositions over the sampled area. However, minor and trace element concentrations have broader ranges in composition (see Appendix B.) which strongly affects the application of the pyroxene geothermobarometer (see below). The minerals are unzoned and optically they exhibit exsolution lamellae, although on the scale of electron microprobe analysis no chemical variation was found associated with these lamellae. Either they are too fine to be resolved at a 1-5 micron scale or they have re-equilibrated during metamorphism yet the optical effect remains.

A Cr-rich diopside is typical for clinopyroxene in metamorphic peridotites and ultramafic cumulates (Coleman, 1977). It is commonly in equilibrium with enstatite and together the two pyroxenes can be used to estimate temperature and pressure of equilibration based on the diopside-enstatite solvus. The empirical thermobarometer of Mercier (1980) was applied to the Redfern peridotite in an attempt to estimate temperature and pressure of formation of the peridotite (see below).

5.3.3. Spinel

Dunites from both the Redfern peridotite and the Crooked Amphibolite contain completely opaque spinel, chromite. No compositional zoning was measured with little variation between grains or between samples. Spinel composition is very sensitive to bulk rock composition and is also used as a petrogenetic indicator of degree of partial melting (Irvine, 1965; Dick and Bullen, 1984). Since Cr

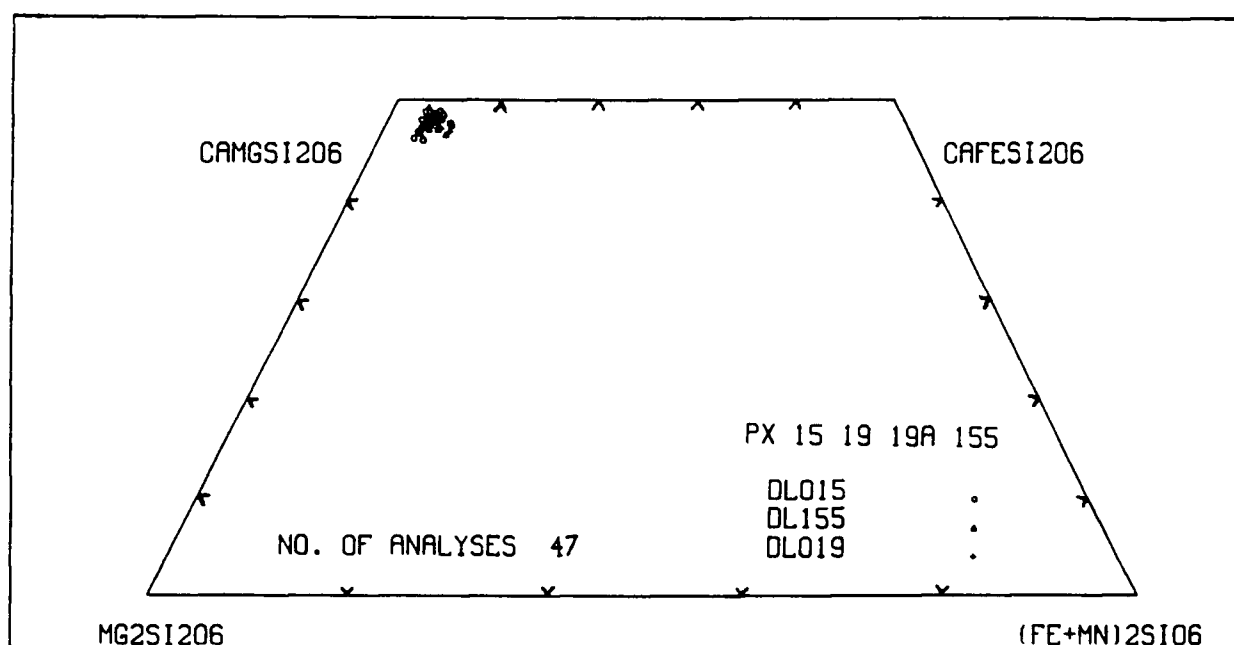


Figure 5.7: Pyroxene quadrilateral plot of electron microprobe analyses from diopsides within unit 3B, Redfern peridotite.

and Mg partition strongly into the solid while Fe and Al go into the melt, chromium enrichment in spinels may indicate depletion by extraction of a melt fraction. Dick and Bullen (1984) have empirically divided alpine-type peridotites into sub-oceanic and sub-volcanic petrogeneses based on their Cr# ($(Cr/Cr + Al)$ atomic fractions). Chromites from this study have a Cr# range of 0.63 - 0.73 which falls in the range of sub-volcanic spinels (Type III, Dick and Bullen, 1984). On a plot of $Cr/(Cr + Al)$ versus $Mg/(Mg + Fe)$ (Fig. 5.8) the samples fall within a range containing several overlapping fields including alpine-type, layered and Alaskan intrusion peridotites. Spinels from layered cumulates of the Samail Ophiolite (Type II: composite oceanic and island origin) and the Twin Sisters Dunite (Type III) have similar ranges of compositions as the study spinels. One major inconsistency is the presence of clinopyroxene in the rock suites which seems to negate the highly refractory nature indicated by the spinels. That the diopside is chromium rich and the bulk chemistry indicates greater than 0.5 % Cr suggests that the bulk composition was originally very chromium rich regardless of the tectonic setting.

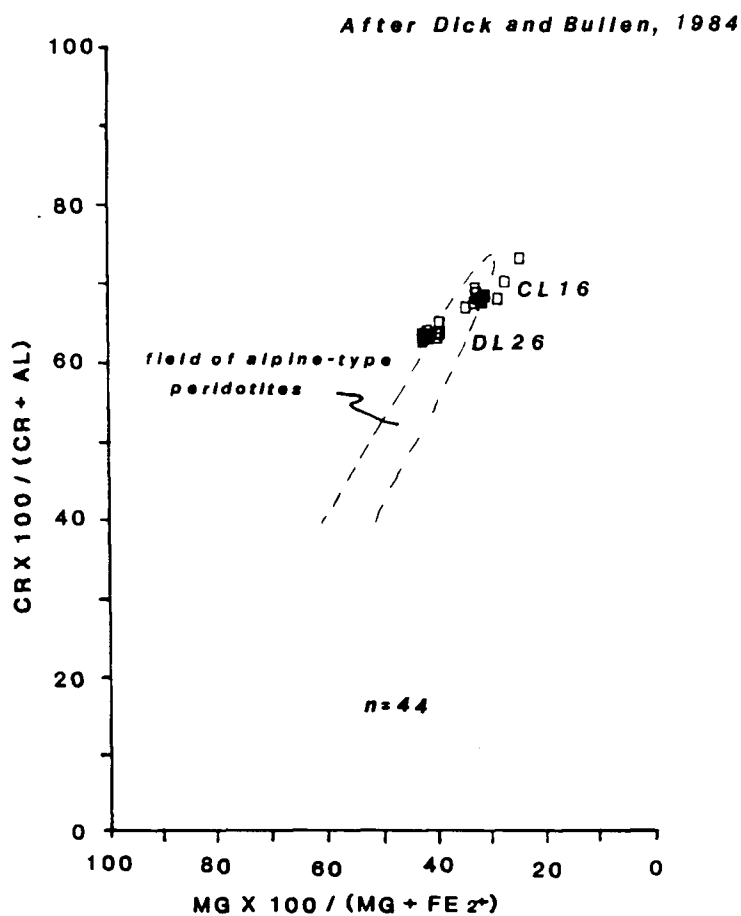


Figure 5.8: Chromites from Redfern peridotite and serpentinite in Crooked Amphibolite, more chromium-rich cluster is CL sample. After Dick and Bullen, 1984.

5.4. PYROXENE THERMOBAROMETRY

To estimate temperature, pressure and depth of origin for the Redfern ultramafics, the single pyroxene thermobarometer of Mercier (1976; 1980; Mercier et al., 1984) was used. The thermobarometer is based on experimentally derived thermodynamic parameters and a set of empirically derived partition

coefficients from natural assemblages applicable to equilibrium reactions in a four-phase peridotite. The thermobarometer requires equilibrium between two pyroxene phases, enstatite and diopside, in the presence of olivine and an alumina-rich phase, spinel or garnet. When the thermobarometer is applied to natural rocks, this equilibrium must either be demonstrated or assumed. If equilibrium is not established, the values obtained by the method are approximate with temperatures being a minimum and pressures a maximum. The single pyroxene thermobarometer was primarily developed for use on less than fresh, alpine-type peridotites (especially ophiolites) where it may not be possible to demonstrate original chemical equilibrium. Therefore equilibrium must be assumed when the method is applied to partially altered assemblages such as the Redfern Complex. Although this assumption is probably valid and can often be partially supported by relict textural relations, it is also a possible source of a fundamental error.

5.4.1. Theoretical Basis for the Thermobarometer

Temperature is usually estimated from Ca content of diopside and pressure from Al in enstatite. Corrections using isopleths which represent the slight pressure dependence of Ca and temperature dependence of Al solubility in pyroxenes are made from experimental data. Additional corrections for natural system element substitution/solid solution allow Mg, Fe^{2+} , and Mn to replace some of the Ca and Na and Cr some of the Al. The Fe^{3+} is believed to be present in insignificant amounts and to be independent of pressure and is thus ignored and all Fe is treated as Fe^{2+} (Mercier and Carter, 1975). Mercier (1976) derived a set of thermodynamic parameters to define Ca solubility for each pyroxene phase (En or Di) in each facies (spinel or garnet). This thermobarometer can be used on a single pyroxene analysis which is inferred to be in equilibrium with a second pyroxene and an Al-rich phase. He tested the resulting temperature and pressure equations on natural rocks for both internal consistency (i.e. - confirmation of original equilibrium) and precision of the method. The result was a satisfactory estimate of temperature plus or minus 30 degrees C, pressure plus or minus 3 kb and geotherms for the upper mantle section represented by the rock suites.

In a later review of his own and other thermobarometers Mercier et al. (1984) state that his empirical geobarometer consistently

"gives depths in the range 60-80 km, apparently implying a considerable shortening of the entire ophiolitic section and, in particular, of its basal lherzolites." (p. 397)

He states alternatively that these depth estimates are unrealistic and proposes a new barometer based on empirical relations which reduces the 60-80 km depths to as low as 13 km. Corrections of the thermodynamic parameters and geobarometry calculations based on this review were not obtained for this study. The lack of this correction must be considered in the interpretation of the estimates of pressure, temperature, and depth discussed below.

5.4.2. Results

The results obtained when this thermobarometer is applied to Redfern ultramafics using electron microprobe determined compositions of diopside are listed in Table IV. Temperatures vary between 850-1100 °C and pressures indicate depths between 60 and 100 km. Although the temperatures appear reasonable compared to an expected value, pressures (and depths) are much greater than expected. From field relations, petrologic and chemical characteristics, the Redfern ultramafics appear to represent the base of the cumulate portion of an ophiolite sequence near the petrologic Moho between 5 and 8 km depth (Coleman, 1977; Mercier et al., 1984). The sequence does not appear to be structurally shortened enough to account for large depth differences between samples. A reasonable depth expected for their formation would not exceed about 10 km. The discrepancy can be explained in several ways:

- 1) Failure of the original assumption that two pyroxenes were in equilibrium with olivine and spinel;
- 2) The necessity for the new geobarometry parameters for accurate pressure estimate;
- 3) Analytical errors in microprobe analysis;
- 4) The effects of metamorphism on the composition of pyroxenes.

The first possibility is a real one. If possible, chemical equilibrium between the two pyroxenes should be proven using correlation diagrams for coexisting minerals (e.g.- Mercier et al., 1984; Girardeau and Mercier, 1988). Petrographic evidence from the Redfern Complex suggests that orthopyroxene may never

TABLE IV

Averages and ranges of results from thermobarometry, Redfern peridotite. Number of analyses in parentheses.

SAMPLE	TEMPERATURE (⁰ C)	PRESSURE (kilobars)	DEPTH (kilometers)
=====			
DL015-1(5)			
AVG	1054.5	23.8	76.38
RANGE	979-1111	21-26	68-83.5
DL015-2(8)			
AVG	943.39	19.69	63.92
RANGE	867.5-1005	15-22.5	50.5-72.7
DL015-3(5)			
AVG	922.47	22.87	73.54
RANGE	892-955	17.3-29.1	56.5-92.5
DL015-4(9)			
AVG	990.61	24.87	79.62
RANGE	842.7-1122.7	18.5-29.8	60.2-98.9
DL155-1(4)			
AVG	939.83	25.49	81.5
RANGE	900.7-976.6	19.8-31.7	64.2-100.25
DL155-2(5)			
AVG	982.5	23.34	74.96
RANGE	921-1025	18.5-28.6	60.3-90.8
DL155-3(5)			
AVG	920.04	21.45	69.25
RANGE	788.7-1091.9	17.5-24.1	57.3-77.2
DL019-1(11)			
AVG	935.5	15.77	52.04
RANGE	887.8-1018.8	13.8-17.7	46.4-57.9
DL019-2(13)			
AVG	909.53	14.58	48.43
RANGE	838.1-960.5	9.7-19.3	33.6-62.8
DL019-3(32)			
AVG	928.13	18.2	59.39
RANGE	850.8-1031	11.95-24.65	40.5-79
DL019-4 (33)			
AVG	947.2	20.89	67.55
RANGE	829.4-1134.7	10.26-35.29	35.35-111.2

have been present and there is no way for the assumption of equilibrium to be tested. Therefore this may alone account for the discrepancy observed between the calculated and expected depth and pressure values.

It is probable that the revised K_f value of Mercier et al (1984) would produce a more reasonable pressure and thus depth value for the barometer calculations. Cr-diopsides from lherzolites of the Xigaze ophiolite have a similar composition to the Redfern Complex and yielded pressures of 4 ± 1 kb, corresponding to a depth of 13 km. Revision of the current program and a rerun of the data may result in a more reasonable pressure/depth estimate.

Analytical errors during microprobe analysis are discussed in Appendix B.

Re-equilibration as a result of metamorphism also affects the precision of data. Mercier et al (1984) found that in qualitatively comparing the partitioning of Tschermak's and binary diopside molecules in coexisting enstatites and diopsides, the fresher minerals from the younger Xigaze ophiolite showed less scatter than those from the Bay of Islands, Newfoundland (Mercier et al., 1984). Experiments of the prograde metamorphism of natural basalts by Moody et al (1983) showed that relict pyroxenes changed their compositions progressively with increasing temperature. Even the major element oxides, thought to be immobile up to very high grades, showed considerable changes throughout the experiments. Both the pressure and temperature results for the Redfern diopsides show a great deal of scatter and the ranges from single grains exceed the method errors ($\pm 30^{\circ}\text{C}$, ± 3 kb; Table IV) which can be attributed to large variations in minor element concentrations (Table IX). The thermobarometric calculations are very sensitive to small changes in Al, Cr, Na, and Ti, all of which have relatively large ranges within samples and even within grains (see Appendix B.)

5.4.3 Conclusions

Unreasonable values for pressure and depth and excessive ranges in temperature for a single sample obtained when applying Mercier's (1977; 1980; et al 1984) empirical thermobarometer indicate that primary assumptions of the model are incorrect for this application. The hypothesis that diopside has retained its primary composition which was originally in equilibrium with enstatite is not satisfied by the available data. The independent determination of temperature and pressure of formation of the Redfern

ultramafics would yield valuable information about the state of the mantle and overlying crust at the time of formation of the ophiolite.

5.5. SUMMARY

Major and trace element chemical data support field and petrographic evidence that the Redfern Complex and the Crooked Amphibolite are correlative. Ultramafic rocks and mafic amphibolites from the two suites likely comprised, from bottom to top, the base of an ultramafic cumulate section, upper level ultramafic and mafic cumulates, massive gabbros, and tholeiitic lavas with intersedimentary layers. The Redfern Complex and ultramafic rocks from the Crooked Amphibolite show little chemical variation due to the affects of alteration other than an increase in LOI with increasing alteration.

Nearly identical compositions of olivine and spinel reinforce the correlation between the Redfern Complex and the Crooked Amphibolite. Olivine retains an igneous composition and shows decreasing forsterite content at higher structural/stratigraphic levels. Metamorphism appears to have sufficiently altered the composition of diopside so as to yield unreasonable results when used in thermobarometric calculations. Both spinel and Cr-rich diopside compositions are Cr-rich, reflecting a Cr-rich bulk composition for the residual liquid which crystallized the cumulates.

Discrimination of tectonic environment based on bulk rock and mineral chemistry is treated with caution. Coleman (1977) states that using chemistry to tectonically discriminate ophiolites is dubious since ophiolites have a polygenetic history involving complex igneous, metamorphic and structural processes. This is certainly the case for the Redfern Complex and the Crooked Amphibolite. However, conservative application of a few of the most reliable discriminant diagrams yield consistent results suggesting a sub-oceanic origin for the peridotites and sub-alkaline tholeiite protoliths for the amphibolites.

6. DISCUSSION AND CONCLUSIONS

6.1 INTRODUCTION

The stratigraphy, chemistry, structural geometry and metamorphism of the Redfern Complex are consistent with an interpretation of the Complex as a dismembered ophiolite which was tectonically emplaced onto the Snowshoe Group during accretion-related compressional deformation. Comparison of the Redfern Complex with the Crooked Amphibolite reveals that the two rock assemblages have similar lithologies, bulk and mineral chemistries, and that they both occupy the same structural position within a well-defined regional structural geometry and show evidence of having the same tectonic history. This suggests, though not unequivocally, that they are correlative fragments which originated from the same ophiolite. In addition, the ophiolite assemblage appears to have a continuous structural-stratigraphic relationship with and the same structural history as the overlying Triassic black phyllite which is part of the allochthonous terrane Quesnellia (Fig. 1.4). Although the age of the ophiolite assemblage is not known, it is here proposed to be the basement to the Quesnellia arc. Previously the Crooked Amphibolite and related rocks have been correlated with the Antler Formation of the Slide Mountain Group (Campbell, 1971; Struik, 1986; 1988a) and was not considered to be the basement to the island-arc related Quesnellia. The basis of this correlation and its tectonic implications is discussed in the presentation of a tectonic model for the evolution of the region surrounding the Redfern Complex.

6.2 DISCUSSION

6.2.1. Summary of Stratigraphy and Chemistry

The stratigraphy of the Dunford Lake areas has been demonstrated to consist of three fault bounded assemblages: the lowest is the Snowshoe Group, overlain by the Redfern Complex which is in turn overlain by the Triassic black phyllite. The Redfern Complex is divided into three units, a basal, tectonized dunite which grades into cumulate-layered, pyroxene-bearing peridotites, capped by a heterogeneous sequence of mafic amphibolites. The chemistry of the Redfern Complex shows a general trend from its base to top of decreasing mafic character, but the majority of the samples studied are more

mafic than tholeiitic basalts, including several of the amphibolite samples. Similar trends are observed in the Crooked Amphibolite samples.

6.2.2. Structural and Metamorphic Synthesis

Designation of deformation episodes as pre-, syn-, and post-emplacement of the Redfern Complex into the Snowshoe Group facilitates the synthesis of upper and lower plate structural assemblages. The growth of metamorphic porphyroblasts constrain the relative timing of each episode within each unit.

Pre-emplacement

Structures developed prior to emplacement of the Redfern Complex are recognized only in the Snowshoe Group and the Redfern peridotite. The two sets of structures are unrelated and the two rock bodies were widely separated in space and probably time during their development.

The Redfern peridotite bears microtextural evidence of having undergone ductile deformation in the uppermost mantle. Without an age of crystallization for the unit no further constraints can be placed on the timing of this deformation other than that it is pre-emplacement. Typically during mantle deformation strain is concentrated in discrete zones which bound large volumes of less deformed rocks (Ross, 1983). Strain rates are 2-4 orders of magnitude higher in these zones than in the bulk of the mantle rocks (Ross et al., 1980). Strain is concentrated by strain softening mechanisms and it is an easier way to accommodate strain by concentration than through evenly distributed bulk rock strain (Kirby, 1985). Thus the Redfern peridotite is a block derived from a larger volume of mantle material which was little strained, but may have been near a ductile shear zone, facilitating its detachment from the upper mantle.

The Snowshoe Group also underwent ductile deformation and metamorphism prior to its involvement in emplacement related deformation, resulting in the growth of at least biotite and muscovite which define a foliation. Few constraints exist for this deformation either, although it is believed to be a pervasive event possibly related to the intrusion of several large mid-Paleozoic granitic bodies which occur throughout the Quesnel Lake area (Mortensen et al., 1985).

Emplacement

Emplacement related structures are the most penetrative and pervasive structures recognized in all units. The first planar and linear foliations in the Redfern amphibolite and the Triassic black phyllite are equivalent to S_2 and L_2 in the Snowshoe Group. These fabrics are ductile, defined by the growth of prograde metamorphic minerals and geometric elements of similar-style folds, axial planes and fold hinge lines. Within the Redfern peridotite, a semi-brittle microtexture and fracture cleavage developed in competent, unaltered ultramafites, and an anastomosing to crenulated cleavage formed in the highly altered ultramafites at both the upper and lower contacts. The Redfern gneiss also bears a metamorphic foliation which most likely formed during this event.

Similar style folds, metamorphic assemblages, foliations and lineations indicate high temperatures and decreased viscosity contrast between layers during deformation. The peak of metamorphism was achieved under hydrostatic conditions, probably just after emplacement related stresses had waned, indicated by the textures from index minerals. Investigation of the metamorphic conditions shows that temperatures exceeded about 550°C just after deformation ceased and were probably approaching that range during the last stages of deformation (Fillipone, 1985; Garwin, 1987).

However, the Redfern peridotite did not deform plastically during this deformation episode. Brittle and semi-brittle deformation mechanisms were active and only at the margins of the unit, showing that deformation did not penetrate into the core of the body. This is consistent with the conditions expected to produce the structures within the other units and emphasizes the great rheological contrast between the mantle peridotite and crustal rocks. The mantle rocks require even higher temperatures, approaching half the melting temperature of olivine ($T_m > 1700^{\circ}\text{C}$ at atmospheric pressure, increasing with pressure; Kirby, 1985) to flow plastically.

As a result of this continued competency contrast between the peridotite and its surrounding rocks, strain was partitioned unequally between units and lithologic contacts were the locus of steep strain gradients. The lack of structures in the peridotite indicate that it accommodated very little bulk rock strain during this event. Bulk strain was accommodated in the other units by tight folding and shear parallel to the axial planes of folds. Bloodgood (1987a) and Elsby (1985) also noted bulk strain accommodated by

internal shearing and shearing along lithologic contacts. The latest increments of strain appear to have been a flattening perpendicular to axial planes (Taite, written comm., 1988). Contacts also probably experienced an early component of shear strain with a superposed flattening component, not only at the margins of the peridotite but also probably between the amphibolite and overlying metasedimentary rocks. Highly altered rocks along contacts and intensified fold and foliation development support this conclusion. Thus a competency contrast probably still existed between the amphibolite and metasedimentary rocks, but less so than between the peridotite and other rocks.

The role of fluids during deformation was probably important, especially regarding the initiation and enhancement of shearing. Prograde metamorphic reactions commonly produce water at the same time deformation is reducing pore space. Concentration of fluids along lithologic contacts is likely since not only were steep strain gradients present but also likely diffusional and permeability gradients as well. Increased pore pressure would decrease the effective stress and greatly increase the tendency of the rock to shear. Evidence for an increase in fluids and shearing along contacts, particularly of the Redfern peridotite include the increase in alteration, evidence of metasomatism, and shear fabrics (see Fig. 2.10).

In summary, first phase structures in the upper plate rocks and second phase structures in the lower plate formed during emplacement of the Redfern Complex and Triassic black phyllite onto the Snowshoe Group. Strain was partitioned into shear zones at lithologic contacts and bulk rock folding of all units except the Redfern peridotite and possibly the Redfern Gneiss. Flattening is believed to have replaced shearing along fold axial planes during the late stages of deformation.

Post-emplacement

Post-emplacement deformation is regionally pervasive but its distribution is domainal on mesoscopic and microscopic scales. All of the units are gently folded about a common axis and the main expression of this fold phase is the regional map pattern. Minor folds are common and locally a crenulation cleavage is developed, predominantly only in schistose lithologies.

This fold event constitutes phase 3 in the lower plate Snowshoe Group and also the Redfern peridotite, phase 2 in the Redfern amphibolite and gneiss and the Triassic black phyllite, and folds the

Redfern Thrust. It is the first truly common phase of deformation for all of the structural packages, indicated by the folding of their mutual contacts. At higher structural levels, buckle folds formed, indicating a renewed competency contrast and a flexural slip folding mechanism. At deeper structural levels, such as in the lower limbs and cores of synforms, shortening gives rise to locally intense shearing parallel to fold axial planes. This is illustrated in the eastern synform where the weaker Triassic black phyllite rocks which show extension down dip on their limbs are infolded with the stronger, crystalline Snowshoe Group. Although the hinge is not exposed, it is believed to have a cusate form as seen on both the small scale (see Fig. 3.20) and in similar structural settings in the region (Fillipone, 1985; Ross et al., 1985). The cusate synformal hinge is absent in the western synform where the more competent Redfern peridotite occupies the core of the fold.

Late crenulations with axes parallel to the trends of fractures may be extensional features related to the relief of compressional stresses.

6.2.3. The Redfern Complex as an Ophiolite

An ophiolite as defined by the participants at the GSA Penrose Conference on ophiolites (Geotimes 17, pp. 24-25, 1972) is an assemblage of mafic to ultramafic rocks which, if completely developed, consists of an ultramafic complex consisting of harzburgite, lherzolite, and dunite tectonites, a gabbroic complex including cumulate peridotites, pyroxenites and gabbros, a mafic sheeted dike complex, and a mafic volcanic complex, commonly pillowed. Sedimentary rocks such as limestone and chert and felsic igneous rocks are considered to be associated rock types but not necessary constituents of the complete sequence. Contacts between units are commonly faulted and when large sections are missing, an ophiolite should be called a partial, dismembered, and/or metamorphosed ophiolite.

The Redfern Complex is a dismembered, metamorphosed ophiolite, according to the definition by the Penrose conferees. The bulk of the Complex probably is derived from the gabbroic complex, including ultramafic cumulates and massive (and layered?) gabbros. The upper portion of the ultramafic complex may also be present, represented by the dunite subunit, 3A. The upper portion of the Redfern Complex constitutes a mafic complex, probably derived from a volcanic rather than sheeted dyke complex protolith.

The contacts, both between the ultramafic/gabbroic units and the mafic unit and at the margins of the ophiolite, are faulted. Portions of the complete sequence may have been removed tectonically along these faults. The ophiolite is also metamorphosed to amphibolite grade but no remanent evidence of a dynamothermal aureole exists at the base of the complex, suggesting that it may have been equilibrated to surrounding temperatures at the time of its final emplacement. Brittle to semi-brittle deformation textures at the base of the peridotite related to emplacement also support the assertion that the complex no longer retained mantle temperatures at the time of emplacement.

Although the Redfern Complex superficially satisfies the model of a dismembered, metamorphosed ophiolite, some of its anomalous characteristics may have important implications. Even for a disrupted ophiolite sequence, the total rock exposed is very small compared to other collision-related ophiolites (e.g., Oman ophiolite). This suggests that the original crustal sheet may have been quite small; or, alternatively, the conditions simply were not conducive to obduction of a large fragment (e.g., deep level obduction). The complex also lacks a dynamothermal aureole or blueschist terrane commonly associated with large subduction/obduction complexes. These types of metamorphism could easily have been obscured by late- to post-emplacement amphibolite/sillimanite grade metamorphism. The observed variations in chemistry of the Redfern Complex and Crooked Amphibolite such as high chromium and nickel contents may be explained by a deviation from the classical MORB interpretation of ophiolites. For example, Hawkins (1979) suggests that volcanic arc-back arc basin pairs should be considered potential source terranes for ophiolites, based on work comparing samples from the Marianas Trench with the Zambales Range ophiolite. He postulates that back arc basins, which are chemically distinct from MORBs, are situated in a tectonic setting which facilitates their incorporation in orogenic belts, especially if continued plate convergence after the halt of subduction produces shortening of the arc region (Hawkins, 1979). The termination of subduction with continued plate convergence may be caused by blocking of the subduction zone by the attempted subduction of buoyant lithosphere such as seamounts or microcontinents. This obduction mechanism combined with the tectonic model presented below provide a simple and reasonable interpretation of the evolution of the Redfern Complex.

6.2.4 Tectonic Models

The simplest tectonic model which is consistent with the observed stratigraphy, structural geometry, and tectonic correlations for the units for a given region eventually emerges as the most favoured one from the plethora of models presented by workers of the region. For the case of the accretion of Late Triassic through Middle Jurassic island-arcs of the Quesnellia terrane to the North American craton, no single model has yet surfaced as the "best" interpretation as new data continues to proliferate along with new models. Coeval island-arc assemblages resting on basement of differing and commonly hypothetical ages and affinities, some with associated subduction-related or basin assemblages, occur along the entire length of the North American Cordillera. These arcs are represented in part by assemblages of the Nicola, Takla, and Stuhini Groups (Late Triassic to Jurassic) and the Hazelton and Rossland Groups (Jurassic; Monger and Price, 1979). The following models have been proposed for the tectonic setting of the island arcs prior to accretion to the craton: the arc above an east-dipping subduction zone separated from North America by a deep water trough (Davis et al., 1978 in Monger and Price, 1979); above a west-dipping subduction zone separated from North America by a fore-arc and ocean basin (Templeman-Kluit, 1979); above an east-dipping subduction zone separated from North America by an ocean basin wholly built upon rifted continental margin (Struik, 1988a; 1988b; 1987); and above a (polarity?) subduction zone separated from North America by a rifted marginal basin (Nelson and Bradford, 1989; Nelson, et al., 1989a & b). The possibility that one or more of these models is correct, or that each one is correct for the region which it models is supported by the discontinuity of the assemblages and "collage" nature of the Canadian Cordillera. The signature of the basement and upper mantle beneath each region is, ideally, the best discriminant of paleotectonic settings.

In the Quesnel Lake region, arc rocks of Quesnellia are grouped in the Late Triassic-Early Jurassic Takla-Nicola Group (Struik, 1988a; Tipper et al., 1981). These overlie the Triassic black phyllite which has been correlated with the Middle to Late Triassic Quesnel River Group (Bloodgood, 1987a after Tipper, 1978 and Campbell, 1978) and the Triassic Slocan-King Salmon assemblage (Struik, 1988b; Tipper et al., 1981). The Triassic black phyllite crops out beneath the island arc rocks both on the east side of the arc in the Quesnel Lake region and on the west side in the Hydraulic and Swift River areas (Bailey, 1989; 1988).

Beneath these two assemblages lies the Crooked Amphibolite-Redfern Complex assemblage which is here proposed to comprise fragments of the basement to the overlying Quesnellia rocks. As has been shown, these rocks appear to have oceanic and not island arc affinities, suggesting that the island arc was built upon oceanic crust. In addition, central British Columbia, including the Quesnel Lake region, appears to be currently underlain by oceanic upper mantle (Ross, 1983). This would require the subduction of presumably a large amount of oceanic crust and possibly a spreading ridge (Ross, 1983) beneath the Quesnellia arc along a west-dipping subduction zone, since no arc rocks are known east of this region. A model for this configuration has been proposed by Templeman-Kluit (1979; Fig. 20 pp. 22-23) for the Slide Mountain Group in the Yukon and by Ross et al. (1985; Fig. 5, p. 296) for the Quesnel Lake region. This model requires a change in transport direction and reversal of subduction polarity after the accretion of Quesnellia to North America (Ross et al., 1985).

Alternatively, Struik (1988a; 1988b) asserts that the Slide Mountain Terrane in the McBride map area is underlain by North American cratonic crust, based on the presence of inherited Precambrian zircon cores in the Antler Formation (Struik, 1988a) and the Fennell Formation to the south (P. Van der Heyden, pers. comm., 1989). The Crooked Amphibolite has been called the deformed and metamorphosed equivalent of the Antler Formation since they have common oceanic affinities and both occupy the same structural position, directly overlying autochthonous North American rocks (Campbell, 1971; Campbell, 1978; Tipper et al., 1981; Struik, 1988a). Therefore, Struik (1988a) separates the Slide Mountain Terrane entirely from Quesnellia, invoking large scale thrusting, transport, and erosion of the Slide Mountain Terrane ahead of the obducting island arc. The concept that a large ocean basin would rest entirely on top of rifted continental basement contradicts the known processes of seafloor spreading. A marginal basin with a small rift or spreading center which deposited pillow basalts on top of the edge of a rifted continent is much more plausible.

Such a model has been recently proposed by Nelson, Ferri, and Schiarizza (1989a), drawing upon work on the Slide Mountain Group from the Sylvester allochthon and the Fennell Formation in the Adams-Clearwater area. They hypothesize a series of marginal basins immediately adjacent to the North American craton for Slide Mountain terrane rocks. Initially this basin began (Permian and earlier?) as an

incipient rift basin adjacent to attenuated North American crust. This would account for craton-inherited zircons with Precambrian cores in some Slide Mountain Group exhalites (Struik, 1988a; P. van Der Heyden, pers. comm. 1989). Later it evolved to a back-arc basin behind the growing Quesnellia arc, under which an east-dipping subduction zone consumed oceanic crust. The oceanic affinity to the current upper mantle signature beneath central British Columbia (Ross, 1983) may be introduced by the subduction of a large oceanic component directly east of thinned cratonic crust, an additional rift basin, and an island arc built upon the margin of the rift basin. Deposition of the Triassic black phyllite probably began prior to the initiation of subduction in a deep water, anoxic basin (Bloodgood, 1988b) and continued after the arc began to form which became a sediment source for the phyllite basin, both to the east and west. Even further east, rocks of the Cache Creek Group may represent a fore-arc subduction complex (Wheeler and McFeeley, 1987). Finally, Nelson et al. (1989a, 1989b) propose that the "obduction" of Slide Mountain terrane related rocks (the Redfern Complex) simply comprised shortening caused by inter-plate collision outboard of the locus of the Slide Mountain terrane. A "cartoon" sketch of the evolution of the Redfern Complex according to this model is presented in Figure 6.1.

Two additional factors make this model particularly attractive. First, the configuration of a series of marginal basins along the continental edge would allow local rock ages and timing of structural events to differ somewhat throughout the Cordillera, depending upon the size of the basin and local tectonic forces. Secondly, a back-arc basin spreading centre would constitute a zone of weakness in the crust, beneath which the upper mantle would be very near the earth's surface. During shortening, the rift zone would be a likely zone of detachment along which a sliver of mantle material could be splintered and "obducted" or emplaced eastwards onto the continental rocks. Additionally, the proximity of upwelling mantle during shortening deformation (emplacement) would be a heat source for metamorphism. In the model of obduction of a back arc ophiolite, Hawkins (1979) suggests that the subduction zone be blocked by buoyant material, thus telescoping convergence inboard to the zones of weakness behind and within the arc. The docking of the Stikine block would suffice to halt subduction while convergence continued and shortened the arc assemblage, as proposed by Nelson et al. (1989a; 1989b).

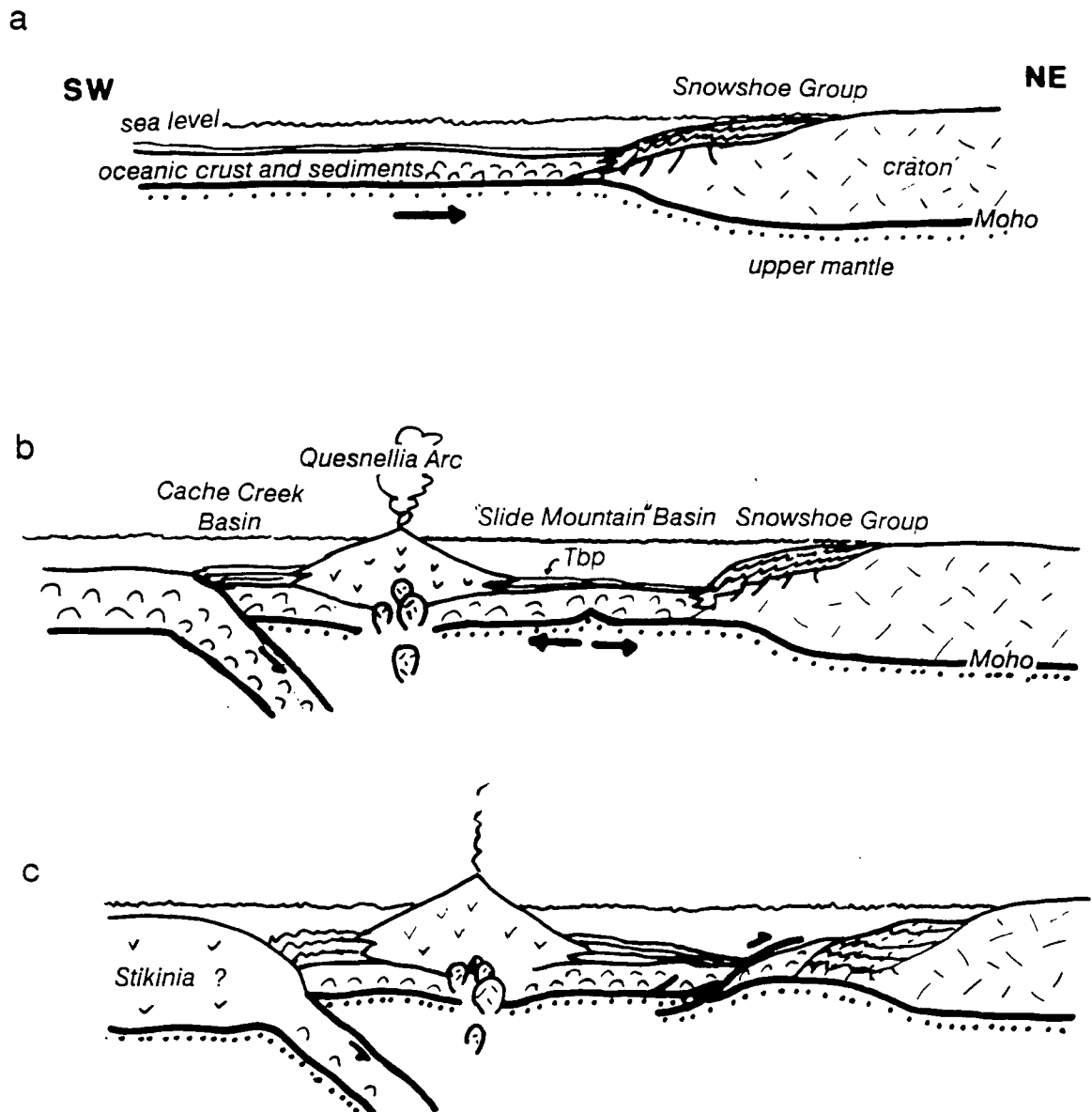


Figure 6.1: Tectonic model for the evolution of the Redfern Complex. a) Pre-Mesozoic: an ocean basin forms adjacent to rifted North American craton, depositing pillow basalts and cherts; Snowshoe Group has already experienced one phase of deformation; b) earliest Mesozoic: subduction is initiated outboard of the continent and the Quesnellia arc is born while the Slide Mountain basin becomes a back-arc environment; sedimentation of Triassic black phyllite receives volcanic influx; c) Early Jurassic: subduction ceases, possibly precipitated by the docking of the Stikine block to the west; east-vergent thrusting accommodates shortening caused by continued plate convergence and "obduction" of the ophiolite is initiated along a back-arc rift;

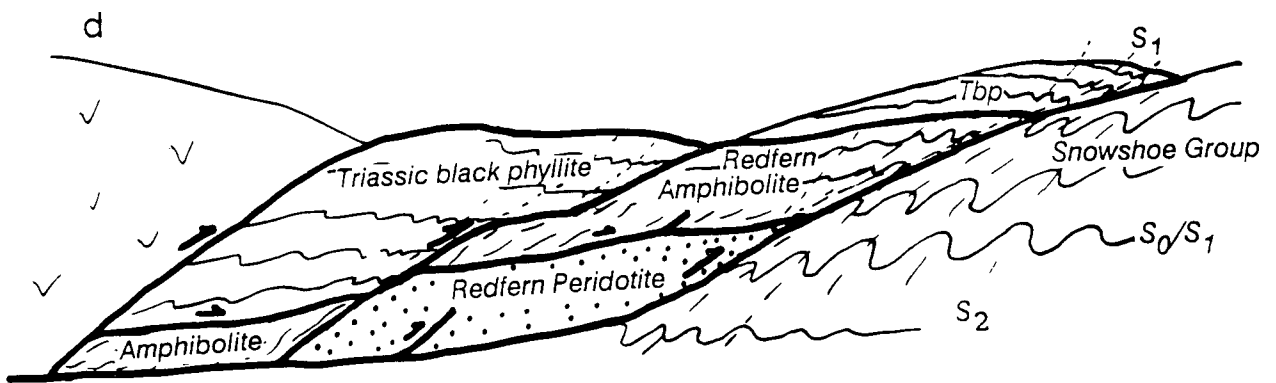


Figure 6.1: (continued) d) Middle Jurassic, enlarged scale: continued shortening instigates internal thrust imbrication and dismemberment of the ophiolite sheet. Emplacement foliations are formed, S_1 in the upper plate and S_2 in the lower plate.

6.3 CONCLUSIONS

The conclusions of this study may be summarized in point form:

1) The Redfern Complex comprises a dismembered, metamorphosed ophiolite, including dunites and interlayered dunites and peridotites from the ultramafic cumulate section near the petrologic Moho and the metamorphosed equivalent of a portion of the mafic section, possibly including gabbros and some basalt flows.

2) The Redfern Complex is a klippe that correlates with the Crooked Amphibolite which occurs along the contiguous IMB-OMB boundary. The two assemblages had a similar tectonic genesis and were derived from the same oceanic basin which probably comprised the basement to allochthonous island-arc terrane Quesnellia.

3) Both units are concordantly overlain by deformed metasedimentary strata of the Quesnellia terrane and all three rock assemblages bear the same structural history. If this association is correct, then the arc was built upon oceanic floor.

4) A tectonic model for the obduction of the Redfern ophiolite and the overlying island-arc, Quesnellia, involves east-directed subduction beneath Quesnellia adjacent to the rifted North American margin, and the formation of a tholeiitic back arc basin. Ophiolite obduction was initiated along a rift zone in the back arc, probably in the early mid-Jurassic as it must have been completed by the peak of mid-Jurassic metamorphism.

7. REFERENCES CITED

- Apted, M.J. and Liou, J.G., 1983. Phase relations among greenschist, epidote-amphibolite, and amphibolite in a basaltic system. *American Journal of Science*, **283-A**: 328-354.
- Ashby, M.F. and Verrall, R.A., 1977. Micromechanisms of flow and fracture, and their relevance to the rheology of the upper mantle. *Phil. Trans. R. Soc. Lond. A* **288**: 59-95.
- Ave' Lallement, H.G., 1967. Strutural and petrofabric analysis of an 'alpine-type' peridotite: the lherzolite of the French Pyrenees. *Leidse Geol. Meded.*, **42**: 1-57.
- , 1976. Structure of the Canyon Mountain (Oregon) ophiolite complex and its implication for sea-floor spreading. *Geogological Society of America Special Paper* 173.
- , Mercier, J-C.C., Carter, N.L., and Ross, J.V., 1980. Rheology of the upper mantle: inferences from peridotite xenoliths. *Tectonophysics* **70**: 85-113.
- Bailey, D.G., 1988. Geology of the central Quesnel Belt, Hydraulic, south-central British Columbia. In B.C.M.E.M.P.R. Geological Fieldwork, 1987, Paper 1988-1: 147-153.
- , 1989. Geology of the central Quesnel Belt, Swift River, South-central British Columbia. In B.C.M.E.M.P.R. Geological Fieldwork, 1988, Paper 1989-1: 167-172.
- Bloodgood, M.A., 1987a. Geology of the Triassic black phyllite in the Eureka Peak area, Central British Columbia (93A/7). In B.C.M.E.M.P.R. Geological Fieldwork, 1986, Paper 1987-1: 135-142.
- , 1987b. Deformational history, stratigraphic correlations and geochemistry of eastern Quesnel Terrane rocks in the crooked Lake area, east central British Columbia, Canada. Unpublished M.Sc. thesis, University of British Columbia, 165 p.
- , 1988. Geology of the Quesnel Terrane in the Spanish Lake area, Central British Columbia (93 A/11). In B.C.M.E.M.P.R. Geological Fieldwork 1987, Paper 1988-1: 139-145.
- Boudier, F., 1978. Structure and petrology of the Lanzo peridotite massif (Piedmont Alps). *Geological Society of America Bulletin* **89**: 1574-1591.
- Campbell, K.V., 1971. Metamorphic petrology and structural geology of the Crooked Lake area, Cariboo Mountains, British Columbia. Unpublished Ph.D. thesis, University of Washington, 192 p.
- Campbell, R.B., 1963. Quesnel Lake, east half, British Columbia. Geological Survey of Canada, Map 1-1963.
- , 1978. Quesnel Lake map area, British Columbia. Geological Survey of Canada, Open File map 574.
- , Mountjoy, E.W. and Young, F.G., 1972. Geology of the McBride map area, British Columbia. Geological Survey of Canada Paper 72-35, 104 p.
- Carmichael, D.M., 1978. Metamorphic bathozones and bathograds: a measure of the depth of post-metamoprhc uplift and erosion on the regional scale. *American Journal of Science* **278**: 769-797.
- Carter, N.L., 1976. Steady state flow of rocks. *Reviews of Geophysics and Space Physics*, **14**, No. 3: 301-360.

- and Raleigh, C.B., 1969. Principal stress directions from plastic flow in crystals. *Geological Society of America Bulletin*, 80: 1231-1264.
- and Ave' Lallement, H.G., 1970. High temperature flow of dunite and peridotite. *Geological Society of America Bulletin* 81: 2181-2202.
- Carye, J.A. 1986. Structural geology of part of the Crooked Lake area, British Columbia. Unpublished MSc. thesis, University of British Columbia, 185 p.
- Coleman, R.G., 1977. *Ophiolites*. New York: Springer-Verlag. 229 p.
- Deer, W.A., Howie, R.A., and Zussman, J., 1977. *An introduction to the rock forming minerals*. Longman, London, 528 p.
- Dick, H.J.B. and Bullen, T., 1984. Chromian spinel as a petrogenetic indicator in abyssal and alpine-type peridotites and spatially associated lavas. *Contrib. Mineral. Petrog.* 86: 54-76.
- Elsby, D.C., 1985. Structure and deformation across the Quesnellia-Omineca terrane boundary, Mt. Perseus area, east-central British Columbia. Unpublished M.Sc. thesis, University of British Columbia, 178 p.
- Engi, J.E., 1984. Structure and metamorphism north of Quesnel Lake and east of Niagara Creek, Cariboo Mountains, British Columbia. Unpublished MSc. thesis, University of British Columbia, 137 p.
- Erdman, L.R., 1985. Chemistry of Neogene basalts of British Columbia and the adjacent Pacific Ocean floor: a test of tectonic discrimination diagrams. Unpublished M.Sc. thesis, University of British Columbia, 294 p.
- Evans, B.W., 1982. Amphiboles in metamorphosed ultramafic rocks. In: *Review in Mineralogy*, 9A, *Amphiboles and Other Hydrous Pyroxenes - Mineralogy* (edited by Veblen, D.R. & Riblee, P.H.), 98-112.
- Fillipone, J.A., 1985. Structure and metamorphism at the Intermontane-Omineca boundary, near Boss Mountain, east central British Columbia. Unpublished M.Sc. thesis, University of British Columbia, 156 p.
- Garwin, S.L., 1987. Structure and metamorphism in the Niagara Peak area, western Cariboo Mountains, British Columbia. Unpublished M.Sc. thesis, University of British Columbia, 177 p.
- Getsinger, J.S., 1985. Geology of the Three Ladies Mountain/Mount Stevenson area, Quesnel Highlands, British Columbia. Unpublished Ph.D. thesis, University of British Columbia, 239 p.
- Girardeau, J., 1982. Tectonic structures related to thrusting of ophiolite complexes: the White Hills peridotite, Newfoundland. *Canadian Journal of Earth Sciences*, 19, No. 4: 709-722.
- and Mercier, J.-C.C., 1988. Petrology and texture of the ultramafic rocks of the Xigaze ophiolite (Tibet): constraints for mantle structure beneath slow-spreading ridges. *Tectonophysics* 147: 33-58.
- Hawkins, Jr., J. W., 1979. Petrology of back-arc basins and island arcs: Their possible role in the origin of ophiolites. In A. Panayiotou (ed.) *Ophiolites Proceedings, International Ophiolite Symposium, Cyprus*, pp 244-254.
- Hickson, C.J. and Juras, S.J., 1986. Sample contamination by grinding. *Canadian Mineralogist* 24: 585-589.

- Holdaway, M.J., 1971. Stability of andalusite and the aluminum silicate phase diagram. *American Journal of Science* 261: 97-131.
- Irvine, T.N., 1965. Chromian spinel as a petrogenetic indicator; Part 1, Theory. *Canadian Journal of Earth Sciences* 2: 648-671.
- and Baragar, W. R. A., 1971. A guide to the chemical classification of the common volcanic rocks. *Canadian Journal of Earth Sciences* 8: 523-546.
- Jackson, E.D. and Thayer, T.P., 1972. Some criteria for distinguishing between stratiform, concentric and alpine peridotite-gabbro complexes. *Intern. Geol. Congr. Sect. 2*: 289-296.
- Juteau, T., Nicolas, A., Dubessy, J., Fruchard, J.C., Bouchez, J.L., 1977. Structural relationships in the Antalya ophiolite complex, Turkey: possible model for an oceanic ridge. *Geological Society of America Bulletin* 88: 1740-1748.
- Kirby, S.H., 1985. Rock mechanics observations pertinent to the rheology of the continental lithosphere and the localization of strain along shear zones. *Tectonophysics* 119: 1-27.
- Laird, J., 1980. Phase equilibria in mafic schist from Vermont. *Journal of Petrology* 21, No. 1: 1-38.
- Lewis, P.D., 1987. Polyphase deformation and metamorphism in the western Cariboo Mountains near Ogden Peak, British Columbia. Unpublished M.Sc. thesis, University of British Columbia, 146 p.
- MacDonald, G.A., 1968. Composition and origin of Hawaiian lavas. *Geological Society of America Memoir* 116: 477-522.
- May, S.R., and Butler, R.F., 1986. North American Jurassic apparent polar wander: implications for plate motion, paleogeography, and cordilleran tectonics. *Journal of Geophysical Research* 91, No. B11: 11519-11544.
- McMullin, D.W.A. and Greenwood, H.J., 1988. Metamorphism in and near the northern end of the Shushwap Metamorphic Complex, south-central British Columbia. in *Current Research, Part E*, Geological Survey of Canada, Paper 88-1E, pp. 57-64.
- Mercier, J.C., 1976. Single pyroxene geothermometry and geobarometry. *American Mineralogist* 61: 603-615.
- , 1985. Olivines and Pyroxenes. In H.R. Wenk (ed.), Preferred Orientations in Deformed Metals and Rocks: an introduction to modern texture analysis. Academic Press, New York, N.Y. pp 407-430.
- , Benoit, V. and Girardeau, J., 1984. Equilibrium state of diopside-bearing harzburgites from ophiolites: geobarometric and geodynamic implications. *Contrib. Mineral. Petrol.* 85: 391-403.
- and Carter, N.L., 1975. Pyroxene Geotherms. *Journal of Geophysical Research* 80, No. 23: 3349-3362.
- and Nicolas, A., 1975. Textures and fabrics of upper mantle peridotites as illustrated by xenoliths from basalts. *Journal of Petrology* 16, No. 2: 454-487.
- Miller, R.B., 1988. Fluid flow, metasomatism and amphibole deformation in an imbricated ophiolite, North Cascades, Washington. *Journal of Structural Geology* 10, No. 3: 283-296.

- Miyashiro, A., 1973. Metamorphism and Metamorphic Belts. London: Allen and Unwin, 479 p.
- Monger, J.W.H., and Price, R.A., 1979. Geodynamic evolution of the Canadian Cordillera progress and problems. *Canadian Journal of Earth Sciences* 16: 770-791.
- Montgomery, J.R., 1985. Structural relations of the southern Quesnel Lake Gneiss, Isocoles Mountain area, central British Columbia. Unpublished M.Sc. thesis, University of British Columbia, 96 p.
- Montgomery, S.L., 1978. Structural and metamorphic history of the Dunford Lake map area, Cariboo Mountains, British Columbia. Unpublished M.S. thesis, Cornell University, 170 p.
- Moody, J.B., Meyer, D., and Jenkins, J.E., 1983. Experimental characterization of the greenschist/amphibolite boundary in mafic systems. *American Journal of Science* 283: 48-92.
- Mortensen, J.K., Montgomery, J.R., Fillipone, J., 1986. U-Pb zircon, monazite and sphene ages for granitic orthogneiss of the Barkerville terrane, east-central British Columbia. *Canadian Journal of Earth Sciences* 24, No. 6: 1261-1266.
- Mullen, E.D., 1983. $MnO/TiO_2/P_2O_5$: A minor element discriminant for basaltic rocks of oceanic environments and its implication for petrogenesis. *Earth and Planetary Science Letters* 62: 53-62.
- Nelson, J.L. and Bradford, J.A., 1989. Geology and mineral deposits of the Cassiar and McDame map areas, British Columbia. In B.C.M.E.M.P.R. Geological Fieldwork, 1988, Paper 1989-1, pp. 323-338.
- , Ferri, F., and Schiarizza, P., 1989a. Emplacement of the Slide Mountain Terrane: obduction or shortening? Abstracts of Papers, American Geophysical Union Pacific Northwest Region, 35th Annual Meeting, 1988, in EOS 70, No. 9.
- , Bradford, J.A., Ferri, F., Schiarizza, P., 1989b. Marginal basin and island arc elements in the Slide Mountain terrane: evidence for North American affinities. Abstracts with programs, Geological Society of America Cordilleran/Rocky Mountain Sections Annual Meeting, p. 121.
- Nicolas, A. and Poirier, J.P., 1976. Crystalline Plasticity and Solid State Flow in Metamorphic Rocks. John Wiley and Sons, London. 444 p.
- Pearce, J.A. and Cann, J.R., 1973. Tectonic setting of basic volcanic rocks determined using trace element analyses. *Earth and Planetary Science Letters* 19: 290-300.
- Pearce, T.H., Stimac, J. and Drobe, J., 1988. Why are major elements as effective as trace elements in diagnosing volcanic regimes? Geological Association of Canada-Mineral Association of Canada Joint Annual Meeting Programs with Abstracts 13: A96.
- Poirier, J.P. and Nicolas, A., 1975. Deformation-induced recrystallization due to progressive misorientation of subgrains, with special reference to mantle peridotites. *Journal of Geology* 83: 707-720.
- Raleigh, C.B., 1965. Glide mechanisms in experimentally deformed minerals. *Science* 150: 739-741.
- , 1968. Mechanisms of plastic deformation of olivine. *Journal of Geophysical Research* 73, No. 14: 5391-5406.
- Ramsay, J.G., 1967. Folding and Fracturing of Rocks. McGraw-Hill Book Company, 568 p.

- Rees, C.J., 1987. The Intermontane-Omineca Belt boundary in the Quesnel Lake area, east-central British Columbia: tectonic implications based on geology, structure and paleomagnetism. Unpublished Ph.D. thesis, Carleton University, 421 p.
- Ross, J.V., 1983. The nature and rheology of the Cordilleran upper mantle of British Columbia: inferences from peridotite xenoliths. *Tectonophysics* 100: 321-357.
- , Ave Lallement, H.G., Carter, N.L., 1980. Stress dependence of recrystallized grain and sub-grain size in olivine. *Tectonophysics* 70: 39-61.
- , Fillipone, J., Montgomery, J.R., Elsby, D., Bloodgood, M.A., 1985. Geometry of a convergent zone, central British Columbia, Canada. *Tectonophysics* 119: 285-297.
- Schiarizza, P. and Preto, V.A., 1987. Geology of the Adams Plateau-Clearwater-Vavenby Area, B.C.M.E.M.P.R. Paper 1987-2, 88 p.
- Struik, L. C., 1982. Snowshoe Formation (1982), central British Columbia. In Current Research, part B. Geological Survey of Canada, Paper 82-1B: 117-124.
- , 1985. Thrust and strike-slip faults bounding tectonostratigraphic terranes, central British Columbia. In Field Guides to Geology and Mineral Deposits in the Southern Canadian Cordillera, D.J. Templeman-Kluit, editor, Geological Society of America Cordilleran Section Meeting, Vancouver.
- , 1986. Imbricated terranes of the Cariboo gold belt with correlations and implications for tectonics in southeastern British Columbia. *Canadian Journal of Earth Sciences* 23: 1047-1061.
- , 1987. The ancient western North American margin: an alpine rift model for the east-central Canadian Cordillera. Geological Survey of Canada Paper 87-15, 19 p.
- , 1988a. Structural geology of the Cariboo gold mining district, east-central British Columbia. Geological Survey of Canada Memoir 421, 100 p.
- , 1988b. Regional imbrication within Quesnel Terrane, central British Columbia, as suggested by conodont ages. *Canadian Journal of Earth Sciences* 25, No. 10: 1608-1617.
- Sutherland Brown, A., 1957. Geology of the Antler Creek area, Cariboo District, British Columbia. British Columbia Department of Mines, Bulletin 38.
- , 1963. Geology of the Cariboo River area, British Columbia. British Columbia Department of Mines and Petroleum Resources, Bulletin 47.
- Templeman-Kluit, D.J., 1979. Transported cataclite, ophiolite and granodiorite in Yukon: evidence of arc-continent collision. Geological Survey of Canada Paper 79-14, 27 p.
- Tipper, H.W. Woodsworth, G.J. and Gabrielse, H., 1981. Tectonic assemblage map of the Canadian Cordillera and adjacent parts of the United States of America. Geological Survey of Canada Map 1505A.
- Trommsdorff, V. & Evans, B.W., 1974. Alpine metamorphism of peridotitic rocks. *Schweiz. miner. petrog. Mitt.* 54: 333-352.
- Tsenn, M.C. and Carter, N.L., 1986. Upper limits of power law creep of rocks. *Tectonophysics* 136: 1-26.

Wheeler, J.O., and McFeeley, 1987. Assemblage map of the Canadian Cordillera. Geological Survey of Canada Open File 1565.

Winkler, H.G.F., 1976. Petrogenesis of Metamorphic Rocks. 4th edition. New York: Springer-Verlag, 334 p.

Wyllie, P.J. (ed.), 1967. Ultramafic and Related Rocks. New York: Wiley, 464 p.

-, 1971. The Dynamic Earth: Textbook for the Geosciences. John Wiley and Sons, New York, N.Y. 416 p.

8. APPENDIX A: XRF ANALYSES

Table V: Major and Trace Element Analyses, Ultramafics

Oxide / Name	CL04	CL05	CL16	CL17	WL13
SiO ₂	44.28	45.10	44.15	45.20	47.84
TiO ₂	0.01	0.01	0.01	0.01	0.02
Al ₂ O ₃	1.07	1.06	0.87	1.07	2.24
Fe ₂ O ₃	0.00	0.00	0.00	0.00	0.00
FeO	9.88	9.51	10.79	10.11	9.44
MnO	0.16	0.16	0.19	0.14	0.11
MgO	43.99	43.95	44.55	43.26	40.18
CaO	1.11	0.77	0.45	0.60	0.57
Na ₂ O	0.08	0.05	0.09	0.09	0.08
K ₂ O	0.07	0.07	0.06	0.06	0.10
P ₂ O ₅	0.01	0.01	0.01	0.01	0.01
Total	100.66	100.70	101.17	100.55	100.59
LOI %	7.2	9.6	6.5	7.8	11.3
Fe ₂ O ₃	10.98	10.57	11.99	11.23	10.50
+ or -	1.10	1.06	1.20	1.13	1.05
ZBar	11.89	11.84	12.01	11.88	11.82
Ni ppm	2522	2591	2751	2448	2703
Cr	2961	2655	2424	3133	2651
V	41	35	21	49	38
Cu	4	5	5	5	5
Zn	54	49	55	48	39
Th	6	6	6	6	6
Zr*	8	8	8	8	8
Nb*	2	2	2	2	2
Y*	2	2	2	2	2
Rb*	0.4	0.4	0.4	0.4	0.4
Sr*	13	13	13	13	13

* - Values strictly qualitative.

Table V - continued

Oxide / Name	WL14	WL15	WL16	WL18	DL014
SiO ₂	45.74	45.38	48.11	46.85	44.09
TiO ₂	0.01	0.01	0.02	0.02	0.05
Al ₂ O ₃	1.46	1.40	1.94	1.88	1.47
Fe ₂ O ₃	0.00	0.00	0.00	0.00	0.00
FeO	9.09	10.62	9.08	11.62	14.54
MnO	0.11	0.08	0.12	0.09	0.22
MgO	43.40	42.88	40.15	38.19	39.97
CaO	1.00	0.39	0.38	1.44	1.36
Na ₂ O	0.05	0.01	0.12	0.09	0.13
K ₂ O	0.07	0.08	0.08	0.07	0.07
P ₂ O ₅	0.01	0.01	0.01	0.01	0.01
Total	100.93	100.85	99.98	100.27	101.91
LOI %	13.5	12.5	11.0	11.0	3.3
Fe ₂ O ₃	10.11	11.80	10.09	12.91	16.16
+ or -	1.01	1.18	1.01	1.29	1.62
ZBar	11.82	11.95	11.70	12.08	12.59
Ni ppm	2917	5289	2377	3080	1570
Cr	2814	2851	3831	2835	2274
V	35	32	42	47	70
Cu	4	116	26	30	26
Zn	37	84	62	40	73
Th	6	93	6	6	6
Zr*	8	8	8	8	8
Nb*	1	1	1	1	2
Y*	2	2	2	2	4
Rb*	0.3	0.3	0.3	0.3	2
Sr*	10	10	10	10	10

* - Values strictly qualitative.

Table V - continued

Oxide / Name	DL015	DL017	DL043	DL078	DL088
SiO ₂	49.17	44.81	43.97	44.37	42.61
TiO ₂	2.98	0.04	0.04	0.02	0.01
Al ₂ O ₃	12.89	1.94	3.00	2.98	1.67
Fe ₂ O ₃	0.00	0.00	0.00	0.00	0.00
FeO	11.54	11.98	11.00	13.60	11.83
MnO	0.28	0.19	0.21	0.16	0.18
MgO	4.66	38.73	40.95	38.38	44.27
CaO	12.52	3.48	1.15	0.51	0.39
Na ₂ O	3.34	0.04	0.06	0.18	0.00
K ₂ O	0.55	0.06	0.06	0.07	0.06
P ₂ O ₅	0.33	0.01	0.01	0.01	0.01
Total	98.27	101.29	100.45	100.27	101.03
LOI %	1.5	3.6	4.0	4.6	2.8
Fe ₂ O ₃	12.82	13.32	12.22	15.11	13.15
+ or -	1.28	1.33	1.22	1.51	1.32
ZBar	12.81	12.36	12.01	12.25	12.11
Ni ppm	521	1483	1998	1937	2733
Cr	2771	2602	5048	4792	3043
V	176	65	57	43	40
Cu	5	31	30	106	5
Zn	53	67	84	74	53
Th	23	6	21	21	6
Zr*	8	8	8	8	8
Nb*	2	2	2	2	2
Y*	4	4	4	4	4
Rb*	2	2	2	2	2
Sr*	11	11	11	11	11

* - Values strictly qualitative.

Table V - continued

Oxide / Name	DL114	DL115	DL116	DL122	DL154
SiO ₂	46.92	41.14	39.56	45.86	44.13
TiO ₂	0.10	0.04	0.07	0.02	0.02
Al ₂ O ₃	2.06	0.99	1.05	1.71	1.07
Fe ₂ O ₃	0.00	0.00	0.00	0.00	0.00
FeO	9.50	16.82	18.92	8.53	9.40
MnO	0.16	0.30	0.27	0.11	0.15
MgO	32.76	41.33	39.33	42.79	45.12
CaO	7.83	1.50	2.20	0.53	0.76
Na ₂ O	0.09	0.06	0.08	0.05	0.07
K ₂ O	0.08	0.06	0.06	0.07	0.06
P ₂ O ₅	0.01	0.01	0.01	0.01	0.01
Total	99.51	102.26	101.55	99.66	100.79
LOI %	4.0	3.5	4.6	7.2	3.3
Fe ₂ O ₃	10.56	18.69	21.03	9.48	10.45
+ or -	1.06	1.87	2.11	0.95	1.05
ZBar	12.16	12.89	13.10	11.60	11.83
Ni ppm	960	1853	1880	2463	2675
Cr	2946	1669	3633	2914	3499
V	124	61	133	20	36
Cu	30	104	32	5	4
Zn	49	142	83	61	55
Th	6	85	22	6	6
Zr*	8	8	8	8	8
Nb*	2	2	2	2	2
Y*	4	4	4	4	4
Rb*	2	2	2	2	2
Sr*	11	11	11	11	11

* - Values strictly qualitative.

Table VI: Major and Trace Element Analyses, Amphibolites

Oxide / Name	BC1	MR02	MR04	MR05	DL041
SiO ₂	53.46	48.46	50.06	52.09	48.86
TiO ₂	0.15	0.21	2.14	2.20	0.07
Al ₂ O ₃	2.04	14.10	15.33	17.11	17.46
Fe ₂ O ₃	0.00	0.00	0.00	0.00	0.00
FeO	6.01	5.58	11.73	6.93	4.42
MnO	0.12	0.10	0.26	0.17	0.14
MgO	23.23	16.42	5.79	3.42	11.51
CaO	17.45	15.34	7.23	9.43	16.71
Na ₂ O	0.33	3.43	0.38	4.55	0.52
K ₂ O	0.08	0.09	1.39	1.12	0.08
P ₂ O ₅	0.10	0.09	0.27	0.63	0.02
Total	102.98	103.82	94.57	97.67	99.79
LOI %	7.3	4.2	0.9	5.9	0.7
Fe ₂ O ₃	6.68	6.20	13.03	7.70	4.91
+ or -	0.67	0.62	1.31	0.77	0.49
ZBar	12.74	12.65	12.13	12.02	12.19
Ni ppm	31	268	116	48	139
Cr	1.4	998	219	91	279
V	482	140	226	435	137
Cu	32	32	58	84	27
Zn	116	48	110	116	39
Th	5	6	22	5	6
Zr*	20	20	20	20	20
Nb*	2.5	2.5	2.5	2.5	2.5
Y*	8	8	8	8	8
Rb*	3.5	3.5	3.5	3.5	3.5
Sr*	100	100	100	100	100

* - Values strictly qualitative.

Table VI - continued

Oxide / Name	DL050	DL060	DL111	DL125	DL162
SiO ₂	52.15	49.96	51.17	54.95	52.13
TiO ₂	1.31	0.18	0.48	1.12	1.02
Al ₂ O ₃	14.70	17.34	8.51	16.43	15.64
Fe ₂ O ₃	0.00	0.00	0.00	0.00	0.00
FeO	12.64	5.76	7.77	11.06	8.16
MnO	0.13	0.13	0.18	0.08	0.14
MgO	9.71	10.60	16.27	5.98	7.10
CaO	5.78	13.24	14.70	7.20	14.25
Na ₂ O	2.10	1.77	1.02	1.22	0.60
K ₂ O	0.12	0.13	0.14	0.08	0.11
P ₂ O ₅	0.15	0.03	0.08	0.13	0.15
Total	98.79	99.15	100.329	8.25	99.30
LOI %	1.0	0.5	0.6	1.2	0.6
Fe ₂ O ₃	14.05	6.40	8.64	12.29	9.07
+ or -	1.41	0.64	0.87	1.23	0.91
ZBar	12.44	12.07	12.53	12.29	12.49
Ni ppm	10	104	188	48	78
Cr	123	100	1489	137	309
V	362	145	331	348	331
Cu	33	27	92	30	28
Zn	99	61	63	54	40
Th	20	6	6	6	6
Zr*	20	20	20	20	20
Nb*	2.5	2.5	2.5	2.5	2.5
Y*	8	8	8	8	8
Rb*	3.5	3.5	3.5	3.5	3.5
Sr*	100	100	100	100	100

* - Values strictly qualitative.

Precision of Analyses on 18 Runs on the Monitor BCR-1

<u>Oxide / Name</u>	<u>BCR1</u>
SiO ₂	55.01 ± 0.11
TiO ₂	2.35 ± 0.01
Al ₂ O ₃	13.26 ± 0.05
FeO	12.52 ± 0.09
MnO	0.18 ± 0
MgO	3.56 ± 0.02
CaO	6.92 ± 0.04
Na ₂ O	3.56 ± 0.04
K ₂ O	1.76 ± 0.01
P ₂ O ₅	0.37 ± 0.01
Total	99.49 ±
Cr	490 ± 13
V	525 ± 8

Remaining trace element concentrations calculated by hand or qualitative.

APPENDIX B - ELECTRON MICROPROBE ANALYSES

Electron microprobe analyses of primary igneous phases of olivine, diopside and spinel in the ultramafic rocks were performed on a four spectrometer, automated Cameca SX-50 scanning electron microprobe at the University of British Columbia. Average and ranges of or representative results are presented in the following tables, followed by tables of the standards used, Table X.

Instrument operating conditions were an acceleration potential of 15 kV, beam intensity of 30 nanoamps, beam diameter of 1 micron, and peak counting times of 10 seconds. Data reduction, formula calculations, and end member assignments were produced automatically by Cameca GEO software.

For olivine, calcium is below detection and Mg number reported was calculated by GEO using mole fraction of $Mg / Mg + Fe$. Detection limit was calculated based on background counts on unknowns and peak counts on standards. Precision was calculated as sample variance determined from repeated runs on check standard P1569 which has a very similar composition to the unknown. Both figures are listed in the first set of data in Table VII.

Spinel data reduction was also done by GEO which partitions Fe into both ferrous and ferric states. Mole fractions of Cr and Al produced by GEO used for calculation of Cr # (times 100). Precision was not determined but detection limits calculated the same as done for olivine are listed in the first entry of Table VIII.

Pyroxene data was reduced using GEO which partitions Fe into ferrous and ferric states based on the concentration of other six-fold coordination atoms (dominantly Al). For thermobarometry calculations, Fe_2O_3 was converted back to FeO and then the formulae based on six oxygens were recalculated, using a LOTUS spread sheet and the method in Deer, Howie, and Zussman (pg. 515). Calcium was below detection in olivine. Precision of analyses was determined by statistical analysis of repeated standard runs throughout analyses; detection limit was calculated the same as for olivine and spinel. Both are listed with the first entry in Table IX.

Complete data sets including mole fractions used for thermobarometry calculations are available on diskette through the U. B. C. Geological Sciences Library.

Table VII: Olivine Compositions

SAMPLE: CL016			GRAIN NO. 2A			NO. ANALYSES: 17		
	SiO ₂	MgO	CaO	MnO	FeO	NiO	TOTAL	Mg #
Detection Limit	0.034	0.014	0.022	0.047	0.063	0.065		
Analysis Precision	0.0711	0.137	0.0002	0.0008	0.0137	0.002		
Most Forsteritic	40.96	49.21	-	0.16	9.98	0.35	100.67	89.65
Least Forsteritic	40.7	47.77	-	0.22	11.88	0.4	100.97	86.7
Average	40.95	48.3	-	0.18	10.72	0.4		
Standard Deviation	0.52	0.96	-	0.03	0.67	0.06		

SAMPLE: CL016			GRAIN NO. 2B			NO. ANALYSES: 8		
	SiO ₂	MgO	CaO	MnO	FeO	NiO	TOTAL	Mg #
Most Forsteritic	40.9	49.39	-	0.17	9.58	0.4	100.44	90
Least Forsteritic	40.87	47.49	-	0.22	11.92	0.37	100.86	87.45
Average	40.88	48.22	-	0.2	10.71	0.39		
Standard Deviation	0.17	0.76	-	0.03	0.86	0.06		

SAMPLE: CL016			GRAIN NO. 2C			NO. ANALYSES: 18		
	SiO ₂	MgO	CaO	MnO	FeO	NiO	TOTAL	Mg #
Most Forsteritic	40.92	49.75	-	0.13	9.0	0.39	100.2	90.7
Least Forsteritic	40.2	46.82	-	0.2	12.19	0.44	99.86	87.1
Average	40.7	48.71	-	0.15	10.19	0.39		
Standard Deviation	0.37	1.01	-	0.03	1.13	0.04		

SAMPLE: CL016		GRAIN NO. 3A				NO. ANALYSES: 17		
	SiO2	MgO	CaO	MnO	FeO	NiO	TOTAL	Mg #
Most								
Forsteritic	41.37	49.41	-	0.13	9.36	0.39	100.69	90.3
Least								
Forsteritic	40.63	47.43	-	0.18	11.62	0.41	100.26	87.75
Average	41.0	48.73	-	0.17	10.08	0.38		
Standard								
Deviation	0.29	0.62	-	0.04	0.76	0.06		

SAMPLE: CL016		GRAIN NO. 1A				NO. ANALYSES: 4		
	SiO2	MgO	CaO	MnO	FeO	NiO	TOTAL	Mg #
Most								
Forsteritic	41.1	50.22	-	0.11	9.21	0.41	101.05	90.6
Least								
Forsteritic	40.97	48.93	-	0.14	10.05	0.52	100.62	89.6
Average	41.16	49.53	-	0.14	9.65	0.44		
Standard								
Deviation	0.17	0.46	-	0.02	0.32	0.05		

SAMPLE: CL016		SUBGRAINS				NO. ANALYSES: 9		
	SiO2	MgO	CaO	MnO	FeO	NiO	TOTAL	Mg #
Most								
Forsteritic	40.4	47.84	-	0.22	11.32	0.48	100.25	88.1
Least								
Forsteritic	40.49	47.41	-	0.2	12.01	0.4	100.51	87.4
Average	40.59	47.63	-	0.21	11.61	0.41		
Standard								
Deviation	0.15	0.17	-	0.02	0.2	0.05		

SAMPLE: DL015		GRAIN NO. 5A				NO. ANALYSES: 8		
	SiO2	MgO	CaO	MnO	FeO	NiO	TOTAL	Mg #
Most								
Forsteritic	40.35	47.54	-	0.47	11.35	0.14	99.84	88.1
Least								
Forsteritic	40.35	47.31	-	0.45	11.93	0.23	100.27	87.2
Average	40.43	47.48	-	0.45	11.5	0.18		
Standard								
Deviation	0.11	0.15	-	0.03	0.21	0.04		

SAMPLE: DL015		GRAIN NO. 5B				NO. ANALYSES: 8		
	SiO ₂	MgO	CaO	MnO	FeO	NiO	TOTAL	Mg #
Most								
Forsteritic	40.23	48.06	-	0.44	11.26	0.23	100.22	88
Least								
Forsteritic	40.38	47.22	0.04	0.51	11.74	0.12	100.01	87.3
Average	40.31	47.55	-	0.46	11.54	0.18		
Standard								
Deviation	0.1	0.23	-	0.04	0.17	0.06		

SAMPLE: DL026		GRAIN NO. 1A				NO. ANALYSES: 5		
	SiO ₂	MgO	CaO	MnO	FeO	NiO	TOTAL	Mg #
Most								
Forsteritic	41.13	49.69	-	0.11	9.36	0.4	100.72	90.4
Least								
Forsteritic	40.93	49.21	-	0.14	9.65	0.45	100.37	90
Average	40.98	49.51	-	0.15	9.52	0.36		
Standard								
Deviation	0.09	0.18	-	0.04	0.14	0.07		

SAMPLE: DL026		GRAIN NO. 1B				NO. ANALYSES: 5		
	SiO ₂	MgO	CaO	MnO	FeO	NiO	TOTAL	Mg #
Most								
Forsteritic	41.1	49.62	-	0.14	9.37	0.42	100.64	90.3
Least								
Forsteritic	40.79	49.42	-	0.2	9.87	0.46	100.75	89.8
Average	40.98	49.45	-	0.16	9.61	0.42		
Standard								
Deviation	0.1	0.1	-	0.02	0.17	0.05		

SAMPLE: DL026		GRAIN NO. 1C				NO. ANALYSES: 5		
	SiO ₂	MgO	CaO	MnO	FeO	NiO	TOTAL	Mg #
Most								
Forsteritic	41.33	49.33	-	0.16	9.34	0.4	100.56	90.25
Least								
Forsteritic	41.4	49.42	-	0.17	9.67	0.4	101.07	89.9
Average	41.18	49.48	-	0.16	9.47	0.41		
Standard								
Deviation	0.18	0.1	-	0.01	0.12	0.01		

SAMPLE: DL026			GRAIN NO. 1, NEOBLASTS				NO. ANALYSES: 12	
	SiO ₂	MgO	CaO	MnO	FeO	NiO	TOTAL	Mg #
Most								
Forsteritic	41.00	49.99	-	0.12	9.07	0.37	100.55	90.65
Least								
Forsteritic	41.02	49.13	-	0.16	9.67	0.33	100.32	89.9
Average	40.96	49.65	-	0.16	9.31	0.35		
Standard								
Deviation	0.4	0.54	-	0.03	0.18	0.03		

SAMPLE: DL026			GRAIN NO. 1D				NO. ANALYSES: 19	
	SiO ₂	MgO	CaO	MnO	FeO	NiO	TOTAL	Mg #
Most								
Forsteritic	41.02	49.32	-	0.18	9.39	0.37	100.27	90.2
Least								
Forsteritic	40.82	48.84	-	0.14	9.98	0.29	100.06	89.6
Average	40.93	49.0	-	0.16	9.78	0.38		
Standard								
Deviation	0.12	0.29	-	0.03	0.17	0.06		

SAMPLE: DL026			GRAIN NO. 1E				NO. ANALYSES: 19	
	SiO ₂	MgO	CaO	MnO	FeO	NiO	TOTAL	Mg #
Most								
Forsteritic	40.9	49.96	-	0.15	9.16	0.39	100.57	90.6
Least								
Forsteritic	40.78	49.55	-	0.44	9.55	0.41	100.43	90.1
Average	40.99	49.56	-	0.15	9.36	0.4		
Standard								
Deviation	0.16	0.25	-	0.07	0.14	0.04		

SAMPLE: DL026			GRAIN NO. 2A				NO. ANALYSES: 5	
	SiO ₂	MgO	CaO	MnO	FeO	NiO	TOTAL	Mg #
Most								
Forsteritic	41.15	49.18	-	0.15	9.46	0.41	100.35	90.1
Least								
Forsteritic	41.04	49.02	-	0.15	9.97	0.45	100.65	89.6
Average	40.97	49.06	-	0.14	9.74	0.41		
Standard								
Deviation	0.12	0.17	-	0.02	0.18	0.04		

APPENDIX B

SAMPLE: DL026		GRAIN NO. 2B				NO. ANALYSES: 5		
	SiO ₂	MgO	CaO	MnO	FeO	NiO	TOTAL	Mg #
Most								
Forsteritic	40.94	49.29	-	0.13	9.26	0.39	100.01	90.35
Least								
Forsteritic	41.21	49.22	-	0.18	9.61	0.35	100.59	90
Average	41.04	49.36	-	0.17	9.44	0.38		
Standard								
Deviation	0.1	0.15	-	0.02	0.12	0.03		

SAMPLE: DL026		GRAIN NO. 2, NEOBLASTS				NO. ANALYSES: 10		
	SiO ₂	MgO	CaO	MnO	FeO	NiO	TOTAL	Mg #
Most								
Forsteritic	40.88	50.00	-	0.1	9.25	0.35	100.58	90.5
Least								
Forsteritic	41.00	49.54	-	0.17	9.72	0.34	100.81	90
Average	41.09	49.72	-	0.16	9.36	0.35		
Standard								
Deviation	0.15	0.17	-	0.03	0.15	0.04		

SAMPLE: DL026		GRAIN NO. 3A				NO. ANALYSES: 21		
	SiO ₂	MgO	CaO	MnO	FeO	NiO	TOTAL	Mg #
Most								
Forsteritic	40.94	49.7	-	0.13	9.24	0.39	100.42	90.5
Least								
Forsteritic	41.07	48.86	-	0.17	9.85	0.42	100.37	89.7
Average	41.02	49.29	-	0.15	9.6	0.39		
Standard								
Deviation	0.22	0.31	-	0.02	0.24	0.04		

SAMPLE: DL026		GRAIN NO. 3B				NO. ANALYSES: 11		
	SiO ₂	MgO	CaO	MnO	FeO	NiO	TOTAL	Mg #
Most								
Forsteritic	41.04	49.69	-	0.17	8.94	0.4	100.22	90.7
Least								
Forsteritic	41.01	49.47	-	0.14	9.46	0.38	100.46	90.2
Average	41.1	49.53	-	0.15	9.2	0.37		
Standard								
Deviation	0.17	0.18	-	0.02	0.15	0.03		

SAMPLE: DL078		GRAIN NO. 1				NO. ANALYSES: 3		
	SiO ₂	MgO	CaO	MnO	FeO	NiO	TOTAL	Mg #
Most Forsteritic	40.09	45.37	-	0.16	15.4	0.11	101.13	83.9
Least Forsteritic	40.06	45.43	-	0.17	15.03	0.18	100.87	84.2
Average	40.11	45.39	-	0.16	15.2	0.16		
Standard Deviation	0.05	0.03	-	0.01	0.15	0.03		

SAMPLE: DL078		GRAIN NO. 2				NO. ANALYSES: 4		
	SiO ₂	MgO	CaO	MnO	FeO	NiO	TOTAL	Mg #
Most Forsteritic	40.11	44.74	-	0.2	15.38	0.26	100.7	83.7
Least Forsteritic	40.22	44.85	-	0.17	16.19	0.18	101.61	83
Average	40.14	44.91	-	0.2	15.65	0.15		
Standard Deviation	0.13	0.14	-	0.02	0.32	0.08		

SAMPLE: DL078		GRAIN NO. 3				NO. ANALYSES: 4		
	SiO ₂	MgO	CaO	MnO	FeO	NiO	TOTAL	Mg #
Most Forsteritic	40.12	44.71	-	0.23	15.74	0.1	100.91	83.3
Least Forsteritic	40.11	45.36	-	0.2	15.45	0.14	101.26	83.8
Average	40.07	44.82	-	0.21	15.87	0.1		
Standard Deviation	0.13	0.39	-	0.02	0.36	0.02		

SAMPLE: DL154		GRAIN NO. 1A				NO. ANALYSES: 3		
	SiO ₂	MgO	CaO	MnO	FeO	NiO	TOTAL	Mg #
Most Forsteritic	41.28	49.66	-	0.13	9.25	0.34	100.67	90.4
Least Forsteritic	41.13	49.68	-	0.14	9.44	0.3	100.69	90.2
Average	41.13	49.76	-	0.13	9.34	0.32		
Standard Deviation	0.12	0.13	-	0	0.08	0.02		

SAMPLE: DL154		NEOBLASTS				NO. ANALYSES: 9		
	SiO ₂	MgO	CaO	MnO	FeO	NiO	TOTAL	Mg #
Most								
Forsteritic	40.89	50.03	-	0.15	9.15	0.37	100.6	90.6
Least								
Forsteritic	41.28	49.53	-	0.14	9.44	0.35	100.74	90.2
Average	41.18	49.81	-	0.15	9.3	0.35		
Standard								
Deviation	0.16	0.19	-	0.02	0.12	0.04		

SAMPLE: DL154		GRAIN NO. 2A				NO. ANALYSES: 4		
	SiO ₂	MgO	CaO	MnO	FeO	NiO	TOTAL	Mg #
Most								
Forsteritic	41.19	49.63	-	0.13	9.24	0.32	100.51	90.4
Least								
Forsteritic	41.28	49.66	-	0.13	9.41	0.36	100.86	90.3
Average	41.38	49.74	-	0.17	9.34	0.33		
Standard								
Deviation	0.15	0.11	-	0.04	0.06	0.02		

SAMPLE: DL154		GRAIN NO. 2B				NO. ANALYSES: 8		
	SiO ₂	MgO	CaO	MnO	FeO	NiO	TOTAL	Mg #
Most								
Forsteritic	40.92	49.9	-	0.16	9.95	0.4	100.33	90.7
Least								
Forsteritic	40.25	49.61	-	0.16	9.24	0.37	100.63	90.4
Average	41.18	49.8	-	0.15	9.32	0.35		
Standard								
Deviation	0.19	0.11	-	0.02	0.26	0.04		

SAMPLE: DL154		GRAIN NO. 3A				NO. ANALYSES: 6		
	SiO ₂	MgO	CaO	MnO	FeO	NiO	TOTAL	Mg #
Least								
Forsteritic	41.13	49.76	-	0.13	9.56	0.43	101.01	90.2
Most								
Forsteritic	41.1	49.44	-	0.16	8.95	0.36	100.01	90.6
Average	41.27	49.8	-	0.14	9.29	0.4		
Standard								
Deviation	0.14	0.28	-	0.02	0.2	0.04		

SAMPLE: DL154			GRAIN NO. 3B			NO. ANALYSES: 5		
	SiO ₂	MgO	CaO	MnO	FeO	NiO	TOTAL	Mg #
Most								
Forsteritic	41.45	49.5	-	0.13	9.29	0.44	100.81	90.4
Least								
Forsteritic	41.04	49.63	-	0.15	9.46	0.35	100.63	90.2
Average	41.28	49.62	-	0.15	9.41	0.37		
Standard								
Deviation	0.17	0.07	-	0.01	0.09	0.05		

SAMPLE: DL154			GRAIN NO. 4A			NO. ANALYSES: 3		
	SiO ₂	MgO	CaO	MnO	FeO	NiO	TOTAL	Mg #
	41.11	49.51	-	0.1	9.5	0.43	100.65	90.2
Average	41.14	49.71	-	0.14	9.46	0.38		
Standard								
Deviation	0.02	0.14	-	0.03	0.03	0.03		

Table VIII: Spinel Compositions

Representative analyses, average and standard deviations.

SAMPLE: CL016		GRAIN NO. 1				NO. ANALYSES: 7			
	SiO ₂	TiO ₂	Al ₂ O ₃	Cr ₂ O ₃	Fe ₂ O ₃	MgO	FeO	TOT	100 Cr#
Detection Limit	0.30	0.057	0.03	0.073	0.081	0.019	0.081		
	0.05	0.06	15.26	51.56	1.51	6.54	24.22	99.2	69.39
Average	0.03	0.04	15.64	50.75	1.26	6.28	24.41		
Standard Deviation	0.01	0.02	0.28	0.58	0.27	0.27	0.33		

SAMPLE: CL016		GRAIN NO. 2				NO. ANALYSES: 5			
	SiO ₂	TiO ₂	Al ₂ O ₃	Cr ₂ O ₃	Fe ₂ O ₃	MgO	FeO	TOT	100 Cr#
	0.02	0.04	15.77	51.51	1.05	6.36	24.63	99.4	68.66
Average	0.02	0.03	15.82	51.14	0.99	6.31	24.550		
Standard Deviation	0.01	0.01	0.1	0.25	0.2	0.06	0.1		

SAMPLE: CL016		GRAIN NO. 3				NO. ANALYSES: 8			
	SiO ₂	TiO ₂	Al ₂ O ₃	Cr ₂ O ₃	Fe ₂ O ₃	MgO	FeO	TOT	100 Cr#
	0	0.04	16.33	50.85	0.97	6.32	24.73	99.25	67.64
Average	0.03	0.06	15.18	50.35	2.23	5.98	24.89		
Standard Deviation	0.02	0.02	1.38	0.79	2.02	0.57	0.63		

SAMPLE: DL026		GRAIN NO. 4A				NO. ANALYSES: 4			
	SiO ₂	TiO ₂	Al ₂ O ₃	Cr ₂ O ₃	Fe ₂ O ₃	MgO	FeO	TOT	100 Cr#
	0.05	0.01	18.82	48.04	2.27	8.25	22.32	99.76	63.14
Average	0.04	0.02	17.83	47.69	3.48	7.94	22.55		
Standard Deviation	0.01	1.65	0.72	2.2	0.75	0.84			

SAMPLE: DL026		GRAIN NO. 4B				NO. ANALYSES: 5			
	SiO ₂	TiO ₂	Al ₂ O ₃	Cr ₂ O ₃	Fe ₂ O ₃	MgO	FeO	TOT	100 Cr#
	0.04	0.05	18.09	47.46	3.84	8.13	22.47	100.09	63.76
Average	0.04	0.05	17.96	47.74	3.53	8.22	22.210		
Standard									
Deviation	0.01	0.01	1.33	0.75	1.84	0.66	0.77		

SAMPLE: DL026		GRAIN NO. 4C				NO. ANALYSES: 5			
	SiO ₂	TiO ₂	Al ₂ O ₃	Cr ₂ O ₃	Fe ₂ O ₃	MgO	FeO	TOT	100 Cr#
	0.03	0.03	18.92	49.19	1.6	8.91	21.46	100.14	63.56
Average	0.03	0.02	18.86	48.77	1.73	8.8	21.47		
Standard									
Deviation	0.01	0.01	0.19	0.39	0.08	0.12	0.19		

SAMPLE: DL026		GRAIN NO. 5A				NO. ANALYSES: 5			
	SiO ₂	TiO ₂	Al ₂ O ₃	Cr ₂ O ₃	Fe ₂ O ₃	MgO	FeO	TOT	100 Cr#
	0.02	0.03	18.93	48.43	2.17	8.6	21.9	100.07	63.18
Average	0.04	0.03	18.64	48.44	2.14	8.64	21.64		
Standard									
Deviation	0.02	0.02	0.17	0.17	0.1	0.07	0.24		

SAMPLE: DL026		GRAIN NO. 5B				NO. ANALYSES: 5			
	SiO ₂	TiO ₂	Al ₂ O ₃	Cr ₂ O ₃	Fe ₂ O ₃	MgO	FeO	TOT	100 Cr#
	0.05	0.02	18.51	47.83	2.75	8.44	21.89	99.47	63.42
Average	0.03	0.03	18.37	47.86	2.72	8.41	21.84		
Standard									
Deviation	0.01	0.02	0.58	0.1	0.52	0.28	0.36		

SAMPLE: DL078		GRAIN NO. 4				NO. ANALYSES: 3			
	SiO ₂	TiO ₂	Al ₂ O ₃	Cr ₂ O ₃	Fe ₂ O ₃	MgO	FeO	TOT	100 Cr#
	0.01	0.94	0.12	11.51	55.25	1.64	27.89	97.36	98.48
Average	0.02	0.65	0.35	19.08	47.9	1.62	28.24		
Standard									
Deviation	0.02	0.21	0.17	5.65	5.52	0.04	0.25		

Table IX: Pyroxene Compositions

Representative analyses showing ranges in Ti, Al, Cr, and Na plus average and standard deviations.

SAMPLE NO. DL015			GRAIN NO. 2					NO. ANALYSES 6		
SiO ₂	TiO ₂	Al ₂ O ₃	Cr ₂ O ₃	Fe ₂ O ₃	MgO	CaO	MnO	FeO	Na ₂ O	TOTAL
Detection Limit										
0.032	0.04	0.013	0.042	0.03	0.02	0.0335	0.05	0.03	0.005	
Precision										
52.94	0.17	2.5	0.37	0.11	16.89	23.11	0.13	2.47	0.25	98.93
2C										
52.6	0.21	1.47	0.33	0.28	16.22	23.38	0.16	3.68	0.08	98.41
2GR										
53.07	0.11	2.34	0.36	0.21	17.55	22.99	0.1	2.16	0.12	99.01
Average										
53.19	0.14	2.06	0.32	0.09	16.67	23.35	0.14	2.83	0.13	
Standard Deviation										
0.32	0.05	0.31	0.03	0.11	0.43	0.25	0.03	0.58	0.07	

SAMPLE NO. DL015			GRAIN NO. 1					NO. ANALYSES 5		
SiO ₂	TiO ₂	Al ₂ O ₃	Cr ₂ O ₃	Fe ₂ O ₃	MgO	CaO	MnO	FeO	Na ₂ O	TOTAL
1ARIM										
53.53	0.15	2.2	0.48	0.31	17.44	23.31	0.17	1.99	0.22	99.82
1B										
51.7	0.14	4.0	0.53	1.46	18.75	21.03	0.09	0.8	0.15	98.68
1E										
51.49	0.12	3.37	0.28	1.94	17.91	21.72	0.1	1.53	0.06	98.53
Average										
52.62	0.15	2.9	0.44	0.86	17.79	22.28	0.14	1.73	0.18	
Standard Deviation										
0.89	0.02	0.7	0.08	0.73	0.51	0.82	0.04	0.52	0.07	

SAMPLE NO. DL015			GRAIN NO. 3					NO. ANALYSES 5		
SiO ₂	TiO ₂	Al ₂ O ₃	Cr ₂ O ₃	Fe ₂ O ₃	MgO	CaO	MnO	FeO	Na ₂ O	TOTAL
3D										
53.67	0.2	1.78	0.30	16.4	23.9	0.07	3.31	0.08	99.71	
3ER										
53.25	0.07	0.54	0.28	1.416.74		24	0.2	2.9	0.01	99.37
Average										
53.61	0.11	1.34	0.21	0.3	16.89	23.91	0.14	2.78	0.2	
Standard Deviation										
0.41	0.06	0.49	0.08	0.55	0.36	0.2	0.05	0.41	0.3	0.41

SAMPLE NO. DL015				GRAIN NO. 4				NO. ANALYSES 10		
SiO ₂	TiO ₂	Al ₂ O ₃	Cr ₂ O ₃	Fe ₂ O ₃	MgO	CaO	MnO	FeO	Na ₂ O	TOTAL
4B										
52.37	0.09	1.25		0.3	3.17	17.17	23.31	0.16	1.66	99.56
4G										
51.67	0.07	2.63	0.28	2.91	18.3	221.96	0.14	0.68	0.05	98.71
4I										
51.17	0.2	1.38	0.57	5.5	16.59	23.19	0.18	1.51	0.09	100.37
Average										
52.34	0.11	2.22	0.35	2.18	17.81	22.62	0.16	1.82	0.1	
Standard Deviation										
1.85	0.05	1.92	0.12	2.67	1.72	2.31	0.03	0.95	0.04	

SAMPLE NO. DL115				GRAIN NO. 2				NO. ANALYSES 5		
SiO ₂	TiO ₂	Al ₂ O ₃	Cr ₂ O ₃	Fe ₂ O ₃	MgO	CaO	MnO	FeO	Na ₂ O	TOTAL
DL155-2										
2A										
54.16	0.07	0.93	0.33	0	17.29	23.38	0.13	2.83	0.13	99.26
2ER										
53.07	0.04	1.93	0.78	0.62	17.44	23.33	0.07	1.71	0.16	99.14
Average										
53.37	0.05	1.23	0.58	0.82	17.17	23.4	0.1	2.4	0.13	
Standard Deviation										
0.63	0.01	0.37	0.18	0.9	0.2	0.23	0.03	0.52	0.02	

SAMPLE NO. DL15				GRAIN NO. 3				NO. ANALYSES 5		
SiO ₂	TiO ₂	Al ₂ O ₃	Cr ₂ O ₃	Fe ₂ O ₃	MgO	CaO	MnO	FeO	Na ₂ O	TOTAL
3A										
50.96	0.09	0.99	1.09	5.88	16.89	22.92	0.09	0.99	0.1	100.01
3C										
53.39	0.11	1.67	0.36	0	16.85	23.61	0.09	2.8	0.1	98.98
3E										
54.22	0.03	0.45	0.05	0	17.11	24.76	0.1	2.21	0.02	98.95
Average										
53.16	0.07	1.05	0.44	1.18	16.96	23.86	0.1	2.24	0.08	
Standard Deviation										
1.14	0.03	0.39	0.35	2.35	0.09	0.63	0.03	0.67	0.03	0.45

SAMPLE NO. DL019				GRAIN NO. 1				NO. ANALYSES 10		
SiO ₂	TiO ₂	Al ₂ O ₃	Cr ₂ O ₃	Fe ₂ O ₃	MgO	CaO	MnO	FeO	Na ₂ O	TOTAL
DL019										
52.85	0.07	2.15	0.67	0.55	16.95	23.49	0.08	2.28	0.13	99.21
DL019										
51.26	0.12	1.34	1.14	5.08	16.55	23.75	0.05	1.02	0.09	100.39
Average										
52.65	0.09	1.6	0.83	1.96	16.95	23.81	0.11	1.6	0.13	
Standard Deviation										
0.85	0.02	0.25	0.16	1.74	0.23	0.59	0.04	0.61	0.02	0.63

SAMPLE NO. DL019				GRAIN NO. 2				NO. ANALYSES 7		
SiO ₂	TiO ₂	Al ₂ O ₃	Cr ₂ O ₃	Fe ₂ O ₃	MgO	CaO	MnO	FeO	Na ₂ O	TOTAL
DL019										
52.6	0.08	1.76	0.81	1.47	17.08	23.88	0.14	1.25	0.12	99.18
DL019										
52.92	0.18	1.69	0.87	1.13	17.13	23.9	0.09	1.46	0.16	99.53
DL019										
51.75	0.13	1.28	1.06	4.43	17.06	23.92	0.07	0.41	0.1	100.21
Average										
52.68	0.11	1.58	0.91	1.66	17.03	23.8	0.08	1.57	0.13	
Standard Deviation										
0.44	0.04	0.14	0.08	1.17	0.2	0.25	0.03	0.62	0.02	0.55

SAMPLE NO. DL019				GRAIN NO. 3				NO. ANALYSES 12		
SiO ₂	TiO ₂	Al ₂ O ₃	Cr ₂ O ₃	Fe ₂ O ₃	MgO	CaO	MnO	FeO	Na ₂ O	TOTAL
DL019-3										
51.86	0.11	2.13	0.82	1.91	17.33	23.43	0.13	0.43	0.14	98.3
DL019-3										
53.46	0.05	1.28	0.78	0.81	17.09	24.4	0.03	1.68	0.12	99.7
DL019-3										
52.810	1.43	0.73	1.1	17.31	23.75	0.13	1.39	0.08	98.72	
Average										
52.81	0.09	1.52	0.77	1.14	17.13	23.99	0.09	1.35	0.12	
Standard Deviation										
0.44	0.05	0.25	0.04	0.62	0.23	0.28	0.04	0.58	0.03	0.4

SAMPLE NO. DL019				GRAIN NO. 4				NO. ANALYSES 5		
SiO ₂	TiO ₂	Al ₂ O ₃	Cr ₂ O ₃	Fe ₂ O ₃	MgO	CaO	MnO	FeO	Na ₂ O	TOTAL
DL019-4										
53.28	0.12	1.5	0.75	0.12	16.94	24.12	0.05	2.24	0.09	99.21
DL019-4										
51.86	0.13	2.22	0.98	2.78	17.5	23.35	0.06	0.21	0.16	99.24
Average										
52.19	0.14	1.84	0.91	1.91	16.96	23.76	0.08	1.13	0.14	
Standard Deviation										
0.64	0.03	0.23	0.1	1.17	0.3	0.28	0.04	0.8	0.03	

SAMPLE NO. DL019				GRAIN NO. 5				NO. ANALYSES 7		
SiO ₂	TiO ₂	Al ₂ O ₃	Cr ₂ O ₃	Fe ₂ O ₃	MgO	CaO	MnO	FeO	Na ₂ O	TOTAL
DL019-5										
52.39	0.03	1.53	0.78	1.98	16.93	24.09	0.09	0.74	0.18	98.74
DL019-5										
52.43	0.14	1.69	0.96	1.45	17.13	23.23	0.07		1.8	0.14 99.03
DL019-5										
53.59	0.08	0.79	0.28	0.36	17.21	24.22	0.05	2.13	0.06	98.76
Average										
52.68	0.08	1.31	0.69	1.43	17.04	24.01	0.07	1.3	0.12	
Standard Deviation										
0.8	0.03	0.34	0.25	0.68	0.14	0.46	0.03	0.58	0.05	

SAMPLE NO. DL019				GRAIN NO. 6				NO. ANALYSES 14		
SiO ₂	TiO ₂	Al ₂ O ₃	Cr ₂ O ₃	Fe ₂ O ₃	MgO	CaO	MnO	FeO	Na ₂ O	TOTAL
DL019-6										
51.79	0.11	1.86	0.93	2.79	17.34	23.0	0.05	0.98	9.13	98.94
DL019-6										
53.79	0.05	0.82	0.33	0.43	17.12	24.65	0.08	1.96	0.05	99.28
Average										
52.67	0.08	1.28	0.57	1.84	17.11	23.97	0.07	1.33	0.10	
Standard Deviation										
0.56	0.03	0.32	0.2	0.87	0.14	0.52	0.04	0.6	0.02	

SAMPLE NO. DL019A				GRAIN NO. 1				NO. ANALYSES 6		
SiO ₂	TiO ₂	Al ₂ O ₃	Cr ₂ O ₃	Fe ₂ O ₃	MgO	CaO	MnO	FeO	Na ₂ O	TOTAL
DL019A-1										
53.09	0.07	1.11	0.31	1.14	17.59	23.84	0.17	1.33	0.04	98.66
DL019A-1										
53.26	0.03	0.69	0.28	2.17	17.27	24.58	0.11	1.07	0.06	99.51
DL019A-1										
51.42	0.08	2.04	0.78	2.92	17.72	22.9	0.10	0.15	98.1	
Average										
52.61	0.06	1.35	0.52	1.64	17.34	23.87	0.09	1.07	0.08	
Standard Deviation										
0.59	0.03	0.42	0.2	0.69	0.26	0.51	0.04	0.53	0.04	

SAMPLE NO. DL019A				GRAIN NO. 2				NO. ANALYSES 7		
SiO ₂	TiO ₂	Al ₂ O ₃	Cr ₂ O ₃	Fe ₂ O ₃	MgO	CaO	MnO	FeO	Na ₂ O	TOTAL
DL019A-2										
50.02	0.17	1.29	1.12	7.97	16.41	22.57	0.09	1.24		0.1 100.99
DL019A-2										
52.41	0.12	1.14	0.67	3.19	17.71	23.33	0.03	0.95	0.07	99.63
DL019A-2										
52.44	0.13	1.73	0.89	1.74	17.18	23.72	0.15		1.1	0.12 99.19
100.05										
Average										
52.35	0.09	1.36	0.73	2.98	17.47	23.54	0.08	0.9	0.10	
Standard Deviation										
0.98	0.06	0.2	0.23	2.09	0.68	0.51	0.04	0.43	0.03	

SAMPLE NO. DL019A				GRAIN NO. 3				NO. ANALYSES 8		
SiO ₂	TiO ₂	Al ₂ O ₃	Cr ₂ O ₃	Fe ₂ O ₃	MgO	CaO	MnO	FeO	Na ₂ O	TOTAL
DL019A-3										
51.32	0.15	1.19	1.01	4.73	16.72	23.47	0.08	0.99	0.12	99.78
DL019A-3										
53.82	0.03	0.83	0.36	0.79	17.67	24.7	0.08	0.88	0.07	99.2
Average										
52.81	0.1	1.28	0.64	1.67	17.28	24.06	0.1	1.09	0.10	
Standard Deviation										
1.06	0.03	0.35	0.19	1.33	0.31	0.78	0.06	0.47	0.03	

SAMPLE NO. DL019A				GRAIN NO. 4				NO. ANALYSES 8		
SiO ₂	TiO ₂	Al ₂ O ₃	Cr ₂ O ₃	Fe ₂ O ₃	MgO	CaO	MnO	FeO	Na ₂ O	TOTAL
DL019A-4										
51.69	0.06	1.68	0.83	1.65	17.21	23.29	0.1	0.8	0.1	97.42
DL019A-4										
53.79	0.12	1.29	0.77	0.09	16.99	24.18	0.13	2.18	0.18	99.72
DL019A-4										
53.53	0.01	0.83	0.46	0.92	17.49	24.29	0.06	1.35	0.07	99.01
DL019A-4										
52.71	0.05	1.6	0.71	1.75	17.7	23.38	0.07	0.75	0.16	98.9
Average										
52.96	0.06	1.32	0.68	1.05	17.31	23.84	0.08	1.34	0.12	
Standard Deviation										
0.62	0.03	0.26	0.1	0.54	0.21	0.38	0.03	0.48	0.03	

SAMPLE NO. DL019A				GRAIN NO. 5				NO. ANALYSES 8		
SiO ₂	TiO ₂	Al ₂ O ₃	Cr ₂ O ₃	Fe ₂ O ₃	MgO	CaO	MnO	FeO	Na ₂ O	TOTAL
DL019A-5										
53.16	0.07	1.02	0.31	1.91	17.99	24.1	0.02	0.39	0.06	99.02
DL019A-5										
53.08	0.11	0.78	0.47	2.51	17.31	24.07	0	1.32	0.12	99.78
DL019A-5										
52.34	0.1	0.28	0.2	4.22	17.43	24.29	0.06	0.37	0.02	99.31
Average										
52.89	0.07	0.86	0.3	2.37	17.81	23.8	0.08	0.85	0.06	
Standard Deviation										
1.01	0.03	0.58	0.1	1.13	0.62	1.2	0.05	0.6	0.04	

SAMPLE NO. DL019A				GRAIN NO. 6				NO. ANALYSES 4		
SiO ₂	TiO ₂	Al ₂ O ₃	Cr ₂ O ₃	Fe ₂ O ₃	MgO	CaO	MnO	FeO	Na ₂ O	TOTAL
DL019A-6										
52.36	0.1	1.7	0.84	2.62	17.21	23.93	0.08	0.65	0.14	99.62
DL019A-6										
55.37	0.04	0.03	0.0	10.0	17.77	25.8	20.0	0.63	0.02	99.69
Average										
53.17	0.08	0.94	0.46	2.17	17.23	24.57	0.1	0.81	0.08	
Standard Deviation										
1.33	0.02	0.62	0.3	1.35	0.33	0.75	0.07	0.28	0.05	

TABLE X: Microprobe Standards Used

STANDARD NO.	ELEMENT	MINERAL	LOCATION
<u>OLIVINE ANALYSES</u>			
O275	Si, Mg	Olivine Fo ₉₀	San Carlos, Arizona
O233	Fe	Olivine	Springwater meteorite
P245	Mn	Pyroxmangite	Shidara-Machi, Japan
P379	Ca	Diopside	Wakefield, N.J.
O241	Ni	Nickel olivine	synthetic
<u>SPINEL ANALYSES</u>			
O13	Ti	Rutile	synthetic
O383	Al, Mg	Spinel	synthetic
O382	Cr	Chromite	synthetic
O130	Fe	Magnetite	?
P379	Si	Diopside	Wakefield, N.J.
<u>PYROXENE ANALYSES</u>			
P379	Si, Ca	Diopside	Wakefield, N.J.
P381	Mg	Orthopyroxene	?
P246	Fe	Aegerine	?
A229	Al, Ti	Hornblende	Kakanui, New Zealand
P245	Mn	Pyroxmangite	Shidara-Machi, Japan
O222	Cr	Chromite	New Caledonia